Univerzita Karlova v Praze

Přírodovědecká fakulta, katedra biochemie

studijní program Biochemie

Mgr. Kateřina Pavlásková

Hmotnostní spektrometrie v proteomice: strukturní biologie a klinické aplikace

Disertační práce

Školitel: Doc. RNDr. Miroslav Šulc, PhD.

Praha 2011

Prohlášení:

„Prohlašuji, že jsem disertační práci zpracovala samostatně a že jsem uvedla všechny použité informační zdroje a literaturu. Tato práce ani její podstatná část nebyla předložena k získání jiného nebo stejného akademického titulu.“

V Praze dne: Podpis:

Poděkování:

Mé poděkování patří školiteli Doc. RNDr. Miroslavu Šulcovi, PhD. za cenné rady a dlouhodobé přátelství.
Děkuji všem kolegům z Laboratoře charakterizace molekulární struktury na MBÚ AV ČR v.v.i. za pomoc a příjemnou pracovní atmosféru.
Děkuji také své rodině za jejich podporu a trpělivost.

Tato práce byla finančně podpořena grantovými agenturami GAUK (258179), GAČR (303/06/0928), MŠMT (LC07017 a LC545) a institucionálním záměrem MBÚ AV ČR v.v.i. (AVOZ50200510), kterým tímto děkuji.

Abstrakt

Hmotnostní spektrometrie (MS) je rychlá, specifická, citlivá a experimentálně variabilní metoda, kterou lze s úspěchem použít v celé řadě proteomických aplikací, např. při identifikaci a řešení primární struktury proteinů nebo pro studium terciární struktury a protein-proteinových interakcí. Zavedení tzv. měkkých ionizačních technik na konci 80. let minulého století umožnil ionizovat bez nežádoucí fragmentace biologické makromolekuly jako jsou proteiny, oligosacharidy nebo nukleové kyseliny, a tak nejvíce ovlivnil využití hmotnostní spektrometrie na poli proteomiky.

Cílem této práce bylo použití současných přístupů hmotnostní spektrometrie při řešení několika proteomických otázek. První část práce je zaměřena na studium terciární struktury a protein-proteinových interakcí pomocí kombinace techniky chemického zesítění s MS analýzou ve třech modelových systémech: (1) homodimeru lidského regulačního proteinu 14-3-3ζ, (2) systému proteinu 14-3-3ζ s regulační doménou tyrosinhydroxylasy, a (3) systému dvou membránových proteinů účastnících se biotransformace xenobiotik – cytochromu P450 2B4 a cytochromu b_5. Tento metodický přístup pracuje s proteiny ve vodných roztocích za fyziologických podmínek a zachovává tak jejich nativní struktury.

Ve druhé části práce byly pomocí MS studovány proteinové profily houbových spór kmenů *Aspergillus* a *Pseudallescheria*. Byly hledány peptidové/proteinové diagnostické znaky, které by bylo možné využít pro včasnou detekci invazivních mykóz způsobovaných těmito plísněmi.

Třetí část práce představuje MS přístupy použité při řešení několika konkrétních proteomických a lipidomických projektů. Dílčími cíly této části bylo (1) určit polohu dvojné vazby v molekulách peptidů nebo lipidů, (2) identifikovat nové alergeny v pšeničné mouce, (3) sledovat změny v proteomu lidských leukemických buněk (mimo jiné izoforem 14-3-3 proteinu) po podání léčiva indukujícího apoptózu.

Abstract

Mass spectrometry (MS) is a rapid, specific and very sensitive analytical method with a broad spectrum of proteomic applications such as protein identification and sequencing, 3D protein structure characterization or study of protein-protein interaction. The introduction of two ionization techniques in late 1980's that are able to ionize the large biomolecules such as proteins, oligosaccharides or nucleic acids with no or low fragmentation has started the rapidly expanding field of MS-based proteomics.

The presented thesis was aimed at the application of mass spectrometric approaches to answer several proteomic questions. Firstly we have employed the chemical cross-linking in combination with MS analysis to solve the 3D structure and protein-protein interactions of three model systems: (1) homodimeric human regulatory protein 14-3-3ζ, (2) model of 14-3-3ζ and regulatory domain of tyrosine hydroxylase, and (3) system of two membrane proteins, cytochrome P450 2B4 and cytochrome b_5, involved in xenobiotics biotransformation. This approach works in aqueous solutions under physiological conditions and thus preserves native structure of the investigated proteins.

The second part of the thesis was focused on MS identification of proteins/peptides in fungal spores of *Aspergillus* and *Pseudallescheria* strains, namely on discovery and characterization of new biomarkers for early stage detection of serious invasive mycoses caused by these molds.

The last part was devoted to the elucidation of particular problems in proteomic and lipidomic projects such as (1) localization of double bond in peptides or lipids by MS, (2) identification of new wheat flour allergens, and (3) determination of proteome changes in leukemic cells during apoptosis induced by medical treatment (including changes in the expression of 14-3-3 proteins).

Obsah:

Použité zkratky **7**

1. Úvod a metody **9**

1.1. Hmotnostní spektrometrie 10
1.1.1. Ionizace MALDI 12
1.1.2. Ionizace ESI 13
1.1.3. Analyzátor iontů TOF 14
1.1.4. Analyzátor iontů FT-ICR 15
1.2. Metody pro určování proteinové struktury pomocí hmotnostní spektrometrie .. 17
1.2.1. Peptidové mapování a tandemová hmotnostní spektrometrie 17
1.2.2. Síťovací reakce 19
1.3. Modelové systémy 22
1.3.1. Dimer proteinu 14-3-3 22
1.3.2. Cytochrom P450 2B4 a cytochrom b_5 24
1.3.3. Vláknité houby rodu *Aspergillus* 27
1.3.4. Patogenní houby druhu *Pseudallescheria boydii* 28

2. Cíle práce **30**

3. Výsledky **31**

3.1. Protein-proteinové interakce studované pomocí síťovacích reakcí s následnou MS identifikací 31
3.1.1. Mapování interakcí v homodimeru lidského proteinu 14-3-3ζ 31
3.1.2. Mapování interakcí mezi membránovými proteiny cytochromem b_5 a cytochromem P450 2B4 49
3.2. Charakterizace a identifikace fungálních proteinů a peptidů pomocí hmotnostní spektrometrie 74
3.2.1. Proteinové profily zástupců rodu *Aspergillus* 74
3.2.2. Pseudacykliny jako potenciální „markery“ onemocnění způsobených *Pseudallescheria boydii* 82
3.3. Ostatní proteomické a lipidomické projekty a klinické aplikace 89
3.3.1. Oxidace během NALDI-TOF MS jako nástroj pro určování polohy dvojných vazeb 89
3.3.2. Identifikace alergenů v proteomu pšenice 95
3.3.3. Proteinový profil leukemických buněk JURL-MK1 v apoptóze 109

4. Diskuze **123**

4.1. Protein-proteinové interakce 123
4.2. Charakterizace a identifikace fungálních proteinů a peptidů 133
4.3. Ostatní proteomické a lipidomické projekty a klinické aplikace 135

5. Závěry **139**

6. Seznam publikací **140**

7. Použitá literatura **141**

Použité zkratky

ACN	acetonitril
API	ionizace za atmosférického tlaku (z angl. *Atmospheric Pressure Ionization)*
CCA	α-kyano-4-hydroxy-*trans*-skořicová kyselina
CCF	sbírka kultur hub (z angl. *Culture Collection of Fungi*)
CD spektroskopie	spektroskopie měřící cirkulární dichroismus molekul
CID	fragmentace molekul v hmotnostním analyzátoru v přítomnosti kolizního plynu (z angl. *Collision Induced Dissociation*)
CPR	NADPH:cytochrom P450 oxidoreduktasa (EC 1.6.2.4)
CYP	cytochrom P450 (EC 1.14.14.1)
Da	Dalton, jednotka hmotnosti
DLPC	1,2-dilauroylfosfatidylcholin
EDC	1-ethyl-3-[3-dimethyl(aminopropyl)] karbodiimid hydrochlorid
ESI MS	hmotnostní spektrometrie s ionizací za pomoci elektrospreje (z angl. *Electrospray Ionization Mass Spectrometry*)
FT-ICR	iontová cyklotronová rezonance s Fourierovou transformací (z angl. *Fourier Transform - Ion Cyclotron Resonance)*
GC	plynová chromatografie (z angl. *Gas chromatography*)
H/D výměna	izotopová vodík - deuteriová výměna
IEF	isoelektrická fokusace
IPTG	isopropyl-1-thio-β-D-galaktopyranosid
LC	kapalinová chromatografie (z angl. *Liquid Chromatography*)
MALDI MS	hmotnostní spektrometrie s desorpcí/ionizací laserem za účasti matrice (z angl. *Matrix-Assisted Laser Desorption/ Ionization Mass Spectrometry*)
MFO	systém oxygenas se smíšenou funkcí (z angl. *Mixed Function Oxidases*)
MS	hmotnostní spektrometrie (z angl. *Mass Spectrometry*)
MS/MS	tandemová hmotnostní spektrometrie
MW	molekulová hmotnost (z angl. *Molecular Weight*)
NADPH	nikotinamidadenindinukleotid fosfát, redukovaná forma
NALDI MS	hmotnostní spektrometrie s desorpcí/ionizací laserem za účasti nanostruktur (z angl. *Nanostructure Assisted Laser Desorption/Ionization Mass Spectrometry*)
NHis14-3-3ζ	rekombinantní protein 14-3-3ζ s purifikační 6× histidinovou značkou na N-konci
NiNTA	afinitní kolona nikl-nitrilotrioctová kyselina
NMR	nukleární magnetická rezonance

Orn	aminokyselina ornithin
PCR	polymerázová řetězová reakce
PKA	cAMP-dependentní protein kinasa (Promega)
PMF	peptidové mapování pomocí MS (z angl. *Peptide Mass Fingerprinting*)
pSer, pS	fosforylovaný serin
pThr, pT	fosforylovaný threonin
QQQ	trojitý kvadrupólový hmotnostní analyzátor
RP-HPLC	vysokoúčinná kapalinová chromatografie na koloně s obrácenou fází
SDS	dodecylsulfát sodný
SDS-PAGE	diskontinuální elektroforéza na polyakrylamidovém gelu v přítomnosti SDS
TH1R	regulační doména lidské tyrosinhydroxylasy (EC 1.14.16.2)
dPTH1R	difosforylovaná regulační doména tyrosinhydroxylasy (pSer19), pSer40)
TOF	hmotnostní analyzátor měřící dobu letu (z angl. *Time of Flight*)
WT	přirozená forma proteinu (z angl. *Wild Type*)
14-3-3ζS58D	mutovaný protein 14-3-3ζ se záměnou Ser58 za Asp58
14-3-3ζΔHis	rekombinantní protein 14-3-3ζ po odštěpení purifikační 6× histidinové značky na N-konci
2DE	dvoudimenzionální elektroforéza

1. Úvod a metody

Proteomika se zabývá studiem celého buněčného proteomu (souboru všech proteinů v buňce v konkrétním čase a za daných podmínek) ve smyslu řešení struktury a funkce jednotlivých proteinů. **Buněčný proteom** je velmi dynamický systém, který odráží fyziologický stav buňky ovlivněné okolním prostředím. Ten se může projevit např. změněnou expresí konkrétních proteinů, posttranslačními modifikacemi nebo změnou v subcelulární lokalizaci proteinů. Sledování změn v proteomu buněk zdravé a nemocné populace může vést např. k identifikaci diagnostického znaku nádorového onemocnění a vývoj biochemických technik pro včasnou detekci nemoci i nalezení účinného léčebného postupu. **Hmotnostní spektrometrie** jako rychlá, citlivá a specifická metoda je v současné době využívána prakticky ve všech takových projektech [Aebersold 2003].

Všechny biochemické procesy, které probíhají v živé buňce jsou zcela závislé na strukturních vlastnostech proteinů a jejich komplexů (ať už se jedná o enzymově katalyzované či imunitní reakce, odpověď buňky na stres nebo zdánlivě méně důležité funkce bílkovin jako přenašečů a stavebních kamenů). **Strukturní proteomika** se snaží identifikovat všechny proteiny v proteinových komplexech nebo organelách, určit jejich lokalizaci a charakterizovat všechny protein-proteinové interakce [Graves 2002]. Studiem prostorové struktury všech biomolekul se zabývá strukturní **bioinformatika**. Tento obor zahrnuje jednak metody umožňující zkoumat strukturu proteinů, tak i přístup pro zpracování získaných dat a jejich převedení do přehledné a všeobecně použitelné formy. Poznatky získané vyřešením primární, sekundární, terciární i kvartérní struktury proteinů se známými funkcemi mohou být úspěšně využity k predikci funkce neznámých proteinů za předpokladu, že jejich primární sekvence jsou vzájemně homologické [Altman 2003].

Mezi běžné metody používané pro určování struktury proteinů patří:

- pro určování primární struktury: Edmanovo odbourávání, cDNA sekvenace, enzymatické štěpení ve spojení s **peptidovým mapováním pomocí hmotnostní spektrometrie nebo s tandemovou hmotnostní spektrometrií**
- pro určování sekundární struktury: spektroskopické metody (CD spektroskopie, Ramanova spektroskopie aj.)

- pro určování terciární struktury: rentgenová krystalografie, NMR, elektronová mikroskopie; **hmotnostní spektrometrie v kombinaci s chemickými modifikacemi nebo s izotopovou vodík-deuteriovou (H/D) výměnou**
- pro určování kvartérní struktury: **chemické modifikace a hmotnostní spektrometrie**, počítačové modelování na základě znalosti terciárních struktur všech komponent v komplexu.

1.1. Hmotnostní spektrometrie

Hmotnostní spektrometrie (z angl. *Mass Spectrometry*, MS) je analytická metoda, která umožňuje charakterizovat (nejen) biologické molekuly na základě chování jejich molekulových iontů a fragmentů v elektrickém nebo magnetickém poli. Jedná se o metodu rychlou, efektivní a citlivou, která nalezla v dnešní době mnoho aplikací v klinické biochemii a molekulární biologii. Zejména díky své citlivosti a rychlosti analýzy se hmotnostní spektrometrie řadí mezi hlavní analytické metody používané v metabolomice, lipidomice i proteomice. Velkou experimentální variabilitu lze ilustrovat příklady, kdy je hmotnostní spektrometrie např. schopna vyhodnotit změny v proteinovém profilu buněk v důsledku působení různých léčiv [Kuželová 2010], charakterizovat potenciální diagnostické znaky houbových infekcí (aspergilóz) [Šulc 2009] nebo popsat polohu dvojných vazeb v řetězcích mastných kyselin [Pavlásková 2011]. Navíc, vhodnými experimenty, např. izotopovou H/D výměnou nebo chemickou síťovací reakcí prováděnou na proteinových komplexech s následnou MS analýzou, lze získat také informace o terciární struktuře proteinů a protein-proteinových interakcích [publikace č. 7].

Součástí každého **hmotnostního spektrometru** je: **iontový zdroj, analyzátor iontů a detektor**, kdy minimálně poslední dvě jmenované části jsou umístěny ve vysokém vakuu zajišťujícím vysokou přesnost měření (Obrázek 1A, str. 11). Výstupem měření je hmotnostní spektrum, které znázorňuje poměr hmotnosti každého jednotlivého analyzovaného iontového druhu na jeho náboji (m/z) vynesený proti relativní intenzitě příslušných iontů (I). Podle způsobu ionizace vzorku rozlišujeme dva základní typy iontových zdrojů používané v proteomice – MALDI a ESI (viz kap. 1.1.1 a kap. 1.1.2; Obrázek 1B, str. 11), jejichž zavedení v 80. letech minulého století umožnilo aplikovat hmotnostní spektrometrii také na biomolekuly (peptidy, proteiny, nukleové kyseliny, oligosacharidy) bez jejich nežádoucí fragmentace. Mezi základní typy analyzátorů iontů,

které jsou schopny dělit ionty studovaného analytu (nikoliv neutrální molekuly) před dopadem na detektor, patří průletový analyzátor (TOF; viz kap.1.1.3; Obrázek 1C), iontová past, kvadrupólový analyzátor (a jejich kombinace), orbitrap a FT-ICR (viz kap. 1.1.4; Obrázek 1C).

V dalším textu budou detailněji představeny pouze ty analyzátory a techniky, které byly použity pro experimenty související s touto disertační prací. Konkrétně se jednalo o techniky MALDI-TOF/TOF MS, NALDI-TOF MS a LC ESI-FT-ICR MS.

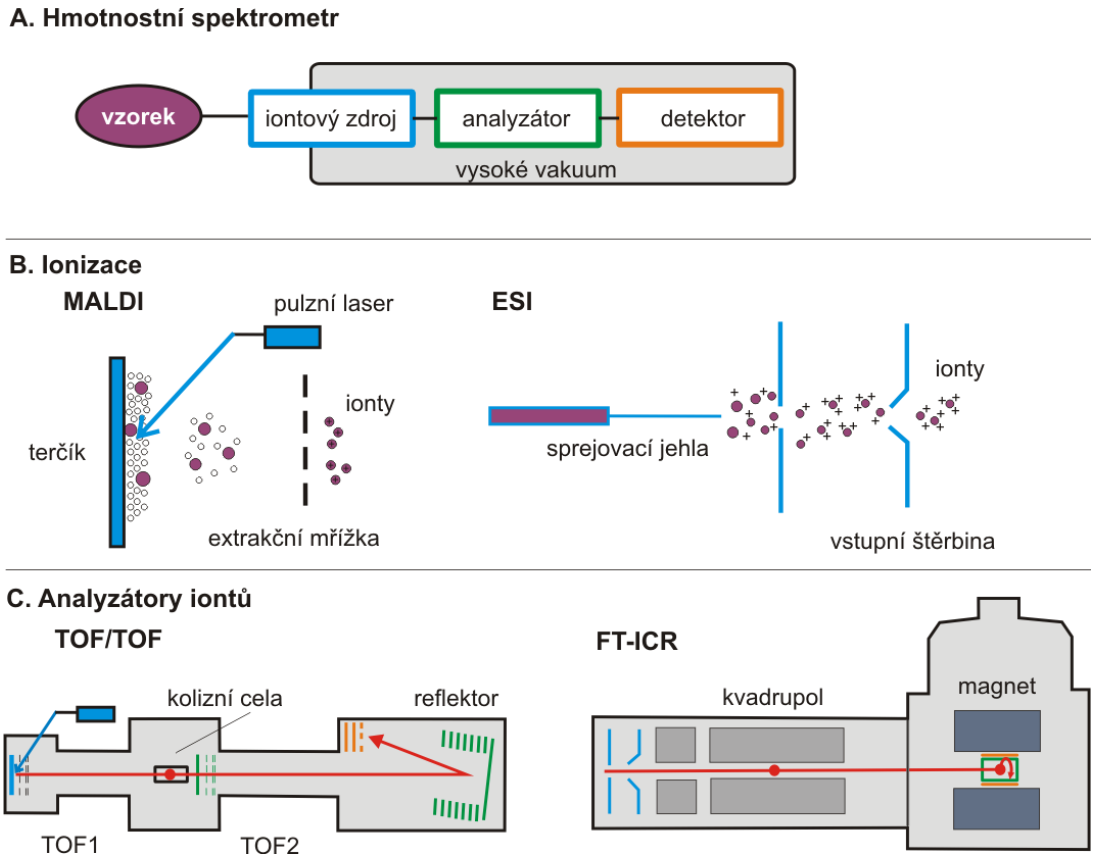

Obrázek 1. Hmotnosní spektrometry používané v proteomických aplikacích. A. Schéma hmotnostního spektrometru. B. Schéma ionizačních technik MALDI (z angl. *Matrix-Assisted Laser Desorption/Ionization*) a ESI (z angl. *ElectroSpray Ionization*). C. Schéma analyzátoru TOF/TOF (z angl. *Time of Flight*) a FT-ICR (z angl. *Fourier Transform - Ion Cyclotron Resonance*). Upraveno podle [Aebersold 2003].

1.1.1. Ionizace MALDI

Ionizační technika MALDI (z angl. *Matrix-Assisted Laser Desorption/Ionization*) patří (stejně jako ionizace elektrosprejem, ESI) mezi tzv. **měkké ionizační techniky**, které jsou schopny šetrně převádět polární vzorek do plynné fáze, aniž by docházelo k jeho nežádoucí fragmentaci. MALDI ionizace byla vyvinuta a představena v 80. letech minulého století hned dvěma skupinami vědců (Karas a Hillenkamp v Německu a Tanaka a spol. v Japonsku, který za ni získal v roce 2002 Nobelovu cenu) [Karas 1988; Tanaka 1988] a znamenala rozšíření použití hmotnostní spektrometrie např. při studiu a charakterizaci biomolekul.

Technika MALDI využívá pro šetrné převedení analytu do plynné fáze **přítomnost nízkomolekulární aromatické kyseliny, tzv. matrice**, která v nadbytku asi 10 000:1 působí jako rozpouštědlo efektivně od sebe oddělující molekuly analytu (viz Obrázek 1B, str. 11). Matrice zároveň absorbuje většinu energie pulzu laseru po ozáření směsi vzorku a matrice, takže nedochází k nežádoucí fragmentaci vzorku. Získanou energii následně předává na molekuly analytu za jeho současné protonace či deprotonace, čímž vznikají převážně jedenkrát nabité kladné a záporné ionty molekul vzorku. Matrice používané pro MALDI ionizaci musí splňovat následující kritéria: musí mít absorpční maxima co nejblíže vlnové délce použitého laseru, snadno se mísit se vzorky a krystalizovat s nimi, a být schopny analyzovaný vzorek s vysokou účinností protonovat nebo deprotonovat za vzniku měřitelných molekulových iontů [Dass 2007a]. Volbou vhodné matrice a intenzity laseru nedochází k nechtěné fragmentaci vzorku a získaná MALDI hmotnostní spektra si zachovávají působivou jednoduchost interpretace, když u iontů nesoucích pouze jeden náboj odpovídá jejich *m/z* přímo hmotnosti iontu [Aebersold 2003]. Tabulka 1 na str. 13 shrnuje nejčastěji používané matrice pro biologické aplikace [Dass 2007a].

Významnou výhodou MALDI ionizace (oproti ESI) je kromě jednoduché interpretace hmotnostních spekter iontů nesoucích jeden náboj také možnost analyzovat vzorky obsahující příměsi solí nebo jiných součástí pufrů (v milimolárních koncentracích). Proto je v nejrůznějších proteomických projektech MALDI MS primární volbou pro identifikaci proteinů na základě mapování jejich peptidových profilů (PMF, z angl. *Peptide-Mass Fingerprinting*; kap. 1.2.1, str. 17) [Kuželová 2010].

Tabulka 1. Nejčastěji používané matrice pro MALDI MS.

MALDI Matrice	Rozpouštědlo	Použití pro
DHB 2,5-dihydroxybenzoová kys.	ACN, methanol, voda, chloroform, aceton	oligosacharidy, peptidy, proteiny
5-hydroxy-2-methoxybenzoová kys.	ACN, voda	lipidy
HABA 2[4-hydroxyfenylazo] benzoová kys.	ACN, methanol, voda	proteiny, lipidy
CCA α-kyano-4-hydroxyskořicová kys.	ACN, voda, ethanol, aceton	peptidy, lipidy, nukleotidy
SA 3,5-dimethoxy-4-hydroxyskořicová kys.	ACN, voda, aceton, chloroform	lipidy, peptidy, proteiny
FA 4-hydroxy-3-methoxyskořicová kys.	ACN, propanol, voda	proteiny, glykoproteiny
DHAP 2,6-dihydroxyacetofenon	ACN, voda	proteiny, oligonukleotidy
PA pyridin-2-karboxylová kys.	ethanol	nukleotidy, oligonukleotidy

Pro analýzu nízkomolekulárních látek byla nedávno představena modifikovaná technika laserové ionizace bez přítomnosti matrice, tzv. **technika NALDI** (z angl. *Nanostructure-Assisted Laser Desorption/Ionization*). Zatímco v MALDI experimentu je velmi obtížné detekovat látky menší než 700 Da v důsledku interference iontů samotné matrice, NALDI povrchy dosahují v této oblasti až 10-krát nižších detekčních limitů [Daniels 2008]. Komerčně dostupné nosiče (Bruker Daltonics) jsou pokryty vrstvenou strukturou nanovláken a hydrofobní organickou vrstvou na povrchu, která umožňuje nanášení vzorků v běžných pufrech a vodných roztocích. Kromě vzorků ve formě roztoku lze pomocí NALDI úspěšně analyzovat i celé tkáňové řezy nebo jejich otisky a porovnávat např. lipidové profily různých tkání [Vidová 2010].

1.1.2. Ionizace ESI

Techniky ionizace za atmosférického tlaku (API, z angl. *Atmospheric Pressure Ionization*), mezi které se řadí také **ionizace elektrosprejem** (ESI, z angl. *ElectroSpray Ionization*) patří v současné době mezi vůbec nejčastější způsoby ionizace vzorku před vstupem do hmotnostního analyzátoru. Také vývoj této techniky, která pomohla rozšíření hmotnostní spektrometrie pro biologické aplikace, byl oceněn v roce 2002 Nobelovou

cenou [Fenn 1989]. Na rozdíl od MALDI techniky, která ionizuje vzorky v pevném stavu, ESI ionizace vychází z roztoku analytu, který je rozstřikován z vyhřívané kapiláry do oblasti s vysokým napětím, kde kapičky vzorku získají elektrický náboj. Odpařováním a zmenšováním kapek např. pomocí sušícího inertního plynu dojde nakonec k překonání sil držících kapku s ionty pohromadě a vzniklé ionty jsou emitovány do oblasti hmotnostního analyzátoru (Obrázek 1B, str. 11).

Kvalitu ESI ionizace ovlivňuje chemický charakter analyzované látky, použitá rozpouštědla, průtok vzorku a pomocných plynů (např. sušící plyn v okolí sprejovací kapiláry), typ kapiláry i napětí na jejím hrotu. ESI ionizace je ve srovnání s MALDI citlivější na čistotu analyzovaných vzorků a přítomnost solí, nečistot, detergentů či organických pufrů. Všechny případné kontaminace snižují citlivost analýzy a mohou se vzorkem tvořit nežádoucí adukty a zvyšovat tak složitost hmotnostního spektra, jehož interpretace je pak velmi obtížná. I v případě analýzy čistých vzorků je interpretace ESI hmotnostních spekter obtížnější než v případě MALDI spekter, protože ESI ionizací velkých biomolekul vždy vznikají vícenásobně nabité ionty a jediná látka je tak distribuována v rozsahu různých hmotností *m/z*, když *z* odpovídá nábojovému stavu např. 2+, 3+ a 4+ [Dass 2007a]. I přes všechna uvedená úskalí, je ESI technika ionizace vysoce účinná a v MS experimentech často používaná. Objevuje se v nejrůznějších uspořádáních hmotnostně spektrometrických experimentů a může být spojena prakticky se všemi analyzátory (s TOF, s kvadrupólovým analyzátorem, trojitým kvadrupólem, iontovou pastí i FT-ICR celou).

Velkou výhodou ESI ionizace ve strukturní analýze proteinů a biologických makromolekul je možnost jejího přímého spojení s kapalinovou chromatografií. Při použití vodných rozpouštědel s hodnotami pH blízkými fyziologickým podmínkám nedochází v proteinových komplexech k porušení kovalentních vazeb ani většiny nekovalentních interakcí [Hernandez 2001]. **Spojením LC-MS** vzniká velmi citlivý a efektivní nástroj pro analýzu proteinů a peptidů i ve složitých biologických směsích.

1.1.3. Analyzátor iontů TOF

Průletový analyzátor TOF (z angl. *Time of Flight*) měří dobu letu iontů z iontového zdroje k detektoru a bývá nejčastěji spojován s MALDI iontovým zdrojem. Detektor zaznamenává intenzitu signálu v čase *I(t)* a převádí ji do hmotnostní *m/z* domény.

Doba letu *t* je úměrná hmotnosti iontu *m/z* podle vztahu

$$m/z = 2eU(t^2/L^2) \quad (1)$$

kde *m* je hmotnost iontu, *z* je jeho náboj, *e* je elementární náboj, *U* je urychlovací napětí a *L* je délka trubice analyzátoru. Protože všem iontům je při výstupu z iontového zdroje udělen stejný urychlovací impuls a elementární náboj i délka trubice jsou pro všechny ionty konstatní, vyplývá z rovnice (1), že doba letu je přímo úměrná hmotnosti iontu *m/z*. Tedy ionty s nižší hmotností dopadnou na detektor dříve než ionty s větší hmotností [Dass 2007b].

Hlavní výhody pro používání TOF analyzátoru jsou jeho teoreticky neomezený hmotnostní rozsah (měří se doba letu iontů), jednoduchost, citlivost a krátká doba záznamu spektra (~10^{-4} s). V této souvislosti je často využíváno spojení TOF analyzátoru s pulsní ionizací MALDI, protože během každého z např. 500 pulsů laseru je TOF schopen zaznamenat celé hmotnostní spektrum [Dass 2007b].

Vyššího rozlišení a přesnosti měření u TOF analyzátorů lze dosáhnout zvýšením urychlovacího napětí, zpožděnou extrakcí nebo přidáním iontového zrcadla, tzv. reflektoru, do letové trubice (Obrázek 1C, str. 11). Reflektor je schopen fokusovat ionty o stejné *m/z* ale rozdílné kinetické energii (která vzniká při vstupu do hmotnostního analyzátoru distribucí urychlovacího napětí) tak, aby na detektor dopadly v užším časovém intervalu. Odezvou v hmotnostním spektru jsou pak užší píky pro každý signál *m/z* a tedy celkově vyšší rozlišení a lepší přesnost.

1.1.4. Analyzátor iontů FT-ICR

Iontová cyklotronová resonance s využitím Fourierovy transformace (FT-ICR, z angl. *Fourier Transform - Ion Cyclotron Resonance*) patří v současné době mezi analyzátory iontů s nejvyšším možným rozlišením a přesností. FT-ICR dosahuje přesnosti měření nižší než 1 ppm, která umožňuje snadnější identifikaci velkých biologických makromolekul, jakými jsou proteiny a jejich komplexy. Mezi současnými hmotnostními analyzátory iontů dosahuje FT-ICR nejvyšší přesnosti, citlivosti a rozlišení.

Ačkoliv byl princip FT-ICR znám již v polovině minulého století, teprve práce A. Marshalla a M. Comisarowa v 70. letech 20. století vedly k jeho většímu rozšíření [Comisarow 1974]. FT-ICR analyzátor primárně a s vysokou přesností zaznamenává

frekvenci proudu generovaného ionty oscilujícími v ICR cele. Frekvenční záznam je poté ve dvou dílčích krocích převeden pomocí Fourierovy transformace a hmotnostní kalibrace na klasické hmotnostní spektrum (Obrázek 2). Pro více detailů o principu FT-ICR doporučuji český souhrnný článek [Boháč 2005].

Z uvedeného principu zároveň vyplývá, že FT-ICR hmotnostní analyzátor je stejně jako iontová past typ nedestruktivního analyzátoru a po prvním měření mohou být ionty v ICR cele využity pro další experimenty (např. tandemovou hmotnostní spektrometrii MS/MS) [Dass 2007b].

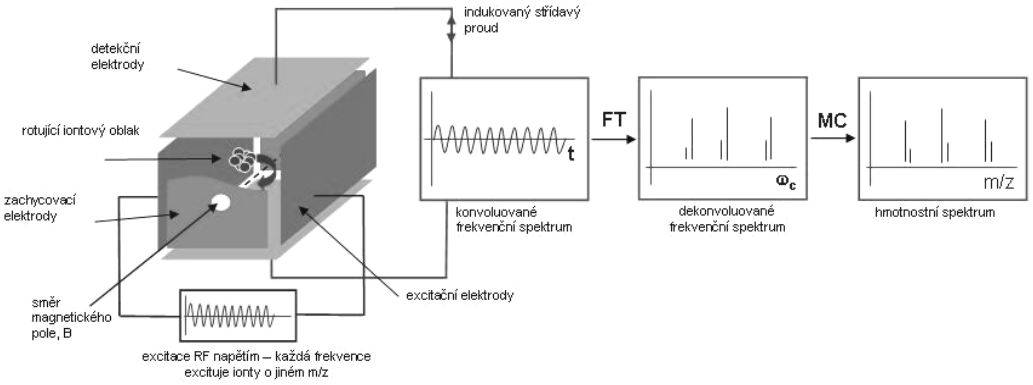

Obrázek 2. Schématické znázornění FT-ICR hmotnostního analyzátoru a vznik signálu v MS experimentu. Různé ionty v ICR cele jsou excitované různými frekvencemi radiofrekvenčního (RF) napětí a detekční elektrody po obvodu cely zaznamenávají hodnotu frekvence ionty indukovaného proudu. Ta je následně převedena Fourierovou transformací (FT) na dekonvoluované frekvenční spektrum a to je pomocí hmotnostní kalibrace (MC) převedeno na klasické hmotnostní spektrum závislosti *m/z* na intenzitě *I*. Obrázek byl převzat ze souhrnného článku [Boháč 2005].

1.2. Metody pro určování proteinové struktury pomocí hmotnostní spektrometrie

Hmotnostní spektrometrie (MS) je v proteomice využívána především k identifikaci a určování primární struktury proteinových molekul (určování sekvence, mutací, posttranslačních modifikací) pomocí přístupů **peptidového mapování** a **tandemové hmotnostní spektrometrie**. Využijeme-li kombinaci MS s technikami **chemického zesítění** a **izotopovou H/D výměnou**, můžeme z MS experimentu získat cenné informace také o terciární struktuře proteinů a o interakcích v proteinových komplexech.

1.2.1. Peptidové mapování a tandemová hmotnostní spektrometrie

Technika peptidového mapování (z angl. *Peptide Mass Fingerprinting*, PMF) identifikuje proteiny na základě unikátních hmotnostních profilů jejich peptidů, které jsou pro každý protein jakýmsi univerzálním „otiskem prstu“. MS analýze předchází purifikační krok, nejčastěji elektroforetické dělení na 1D nebo 2D gelové elektroforéze, a enzymatické štěpení vybraných proteinových proužků nebo skvrn z 2D gelu specifickými proteasami [Kocher 2007]. Změřená peptidová mapa je porovnána s teoretickými mapami peptidů všech proteinů v databázi a výsledek je přiřazen na základě nejlepší shody (Obrázek 3) [Dass 2007c].

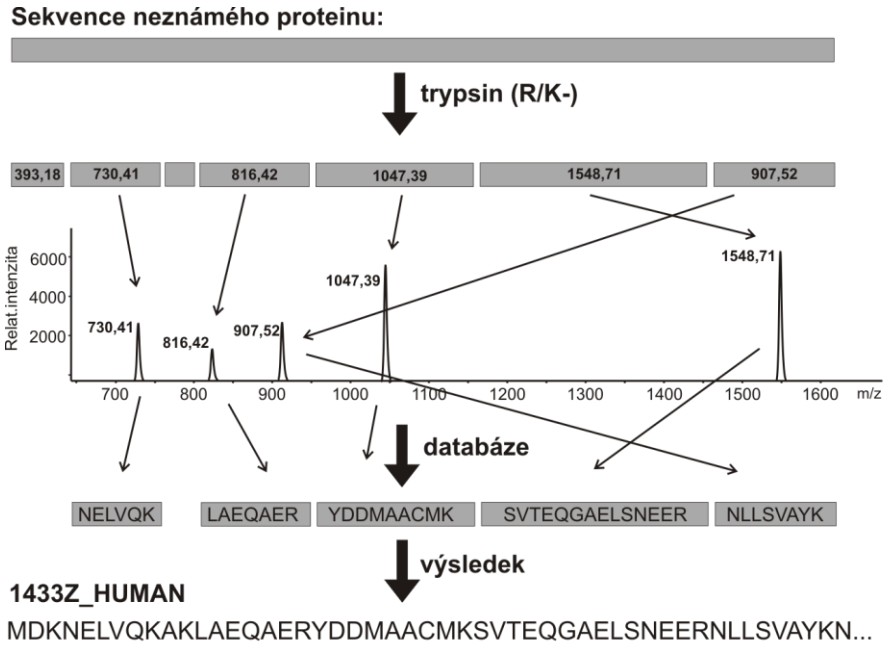

Obrázek 3. Schéma peptidového mapování (PMF) pomocí hmotnostní spektrometrie. Analyzovaný protein je nejprve rozštěpen specifickou proteasou (trypsin) na peptidy, které jsou dále analyzovány pomocí hmotnostní spektrometrie. Hmotnosti *m/z* ze získané peptidové mapy jsou porovnány s teoretickými mapami všech proteinů v databázi (např. SwissProt) a výsledek je přiřazen na základě nejlepší shody.

Peptidové mapování v kombinaci s tandemovou hmotnostní spektrometrií je účinná metoda pro určování primární struktury proteinů. Na rozdíl od ostatních technik (např. Edmanova odbourávání) je schopna charakterizovat také posttranslační modifikace. Často se používá pro potvrzení sekvence rekombinantních proteinů, pro charakterizaci proteinů v nekovalentních komplexech nebo pro určení změn proteinových profilů různými léčivy ovlivněných buněčných liniích [Kuželová 2010].

Tandemová hmotnostní spektrometrie (MS/MS) je úspěšně používána pro identifikace proteinů i pro *de novo* určování proteinových sekvencí neznámých vzorků, rozlišení více proteinů v jediné skvrně na 2D gelu a v případě, že hledaný protein není zahrnut v prohledávané databázi (Tabulka 2, str. 19) [Šotkovský 2011]. Při MS/MS analýze je v prvním MS experimentu vybrán studovaný prekurzor (např. neznámý signál *m/z* v hmotnostním spektru) a všechny ostatní ionty jsou odstíněny. Zvýšením aktivační energie dochází k excitaci iontů prekurzoru a k jejich rozpadu na charakteristické fragmenty, které jsou změřeny ve druhém MS experimentu. MS/MS spektra mohou být měřena na každém hmotnostním spektrometru, který obsahuje alespoň dva iontové analyzátory (např. TOF/TOF, Q-TOF, QQQ) nebo nedestruktivní typ analyzátoru, který je schopen uchovávat ionty (ICR, iontová past).

V případě peptidů a použití fragmentace v přítomnosti molekul inertního plynu (tzv. CID z angl. *Collision Induced Dissociation*) dochází po zvýšení aktivační energie přednostně k fragmentaci na peptidové vazbě, čemuž odpovídá vznik komplementárních y- a b- iontů (nomenklatura viz Obrázek 4). Každý signál y- či b- iontu ve spektru nese informaci o charakteristické ztrátě jedné, dvou, tří atd. aminokyselin od C- nebo N- konce peptidu. Podle rozdílů mezi dvěma následujícími y- nebo b- fragmenty lze určit druh přítomné aminokyseliny a opakováním tohoto postupu lze odvodit celou primární sekvenci peptidu [Aebersold 2003]. V některých případech stačí k průkazné identifikaci proteinu

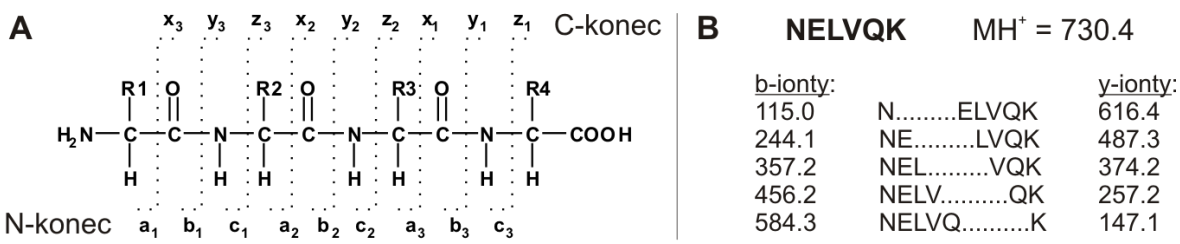

Obrázek 4. A. Schéma fragmentace peptidů a nomenklatura fragmentových iontů. B. Seznam y- a b-iontových sérií peptidu proteinu 1433Z_HUMAN o *m/z* 730.4.

odečíst z fragmentačního spektra pouze sérii několika aminokyselin, tzv. sekvenční značku (angl. *tag*), na základě které lze dohledat možné kandidáty.

Tabulka 2. Přehled dostupných databází pro PMF a MS/MS (upraveno podle Dass 2007c).

Databáze	Typ	Internetová adresa	Instituce [a]
EMBL	nukleotidová	www.embl-heidelberg.de/services/index.html	EMBL
NCBI	nukleotidová proteinová	www.ncbi.nlm.nih.gov	NCBI
Swiss-Prot	proteinová	www.ebi.ac.uk/swissprot/	EBI
TrEMBL	proteinová	www.expasy.org	
OWL	proteinová	www.leeds.ac.uk/bmb/owl/owl.html	
dbEST	sekvenční tag	www.ncbi.nlm.nih.gov/dbEST/index.html	NCBI

[a] EMBL, European Molecular Biotechnology Laboratory; NCBI, National Center for Biotechnology Information; EBI, European Bioinformatics Institute.

1.2.2. Síťovací reakce

Chemické síťovací reakce (angl. *cross-linking*) jsou v kombinaci s hmotnostně spektrometrickou analýzou (MS) používány pro **určování prostorové struktury** nativních proteinů a proteinových komplexů již od 90. let minulého století [Young 2000]. V současnosti je tato technika na vzestupu, zejména díky větší dostupnosti hmotnostních spektrometrů s vysokou přesností a existenci softwarových nástrojů pro snadnější vyhodnocování získaných MS dat. Výběr nejvhodnějšího experimentálního uspořádání síťovací reakce ulehčuje široká nabídka síťovacích činidel a pracovních protokolů. Obecný přehled poskytují souhrnné publikace [Back 2003; Sinz 2006].

Všechna používaná síťovací činidla obsahují ve své struktuře jednu až tři reaktivní funkční skupiny, které jsou schopné vytvářet kovalentní vazbu s různými nebo stejnými reakčními skupinami postranních řetězců aminokyselin v závislosti na chemické reaktivitě činidla. Nově vzniklé vazby úspěšně **fixují proteiny v původně nekovalentních komplexech** a umožňují tak jejich další studium. Předpokladem pro vznik nové vazby je dostatečné prostorové přiblížení spojovaných aminokyselin a zároveň rychlá reakce síťovacího činidla [Hermanson 2005].

V současnosti existují dva hlavní experimentální přístupy, jakými probíhají síťovací reakce a následná MS analýza kovalentně propojených produktů. První přístup je tzv. „top-down“, který měří přímo celé kovalentně spojené proteinové komplexy, bez nutnosti

předchozí separace zesíťovaných komplexů (oddělení dimerů od monomerů probíhá přímo v hmotnostním analyzátoru). Míra zesítění je určována na základě dílčích fragmentací ionizované molekuly komplexu různými disociačními technikami [Novák 2003]. Tento přístup lze použít pouze pro menší proteinové komplexy nebo po předchozí částečné proteolýze komplexu na delší peptidy a umožňují jej pouze analyzátory s vysokým rozlišením (FT-ICR) [Sinz 2006]. Častěji používaným experimentálním uspořádáním je tzv. „bottom-up“ přístup, který místa spojení mezi proteiny identifikuje pomocí MS z komplexní směsi peptidů po naštěpení zesíťovaného proteinového komplexu specifickou proteasou (Obrázek 5) [Dihazi 2003]. Nevýhodou tohoto přístupu je nutná separace zesíťovaných produktů od nezreagovaných látek (např. 1D elektroforéza). Vyhodnocení MS dat probíhá na základě porovnání hmotnostních spekter peptidů z kontrolního vzorku bez přítomnosti síťovacího činidla a ze vzorku po působení síťovacího činidla. Nalezené rozdíly odpovídají zesíťovaným peptidům, ve kterých jsou konkrétní aminokyseliny **identifikovány na základě specifity použitého síťovacího činidla, použité proteasy a znalosti proteinové sekvence**. Určení pozice aminokyselin výrazně zjednodušuje práce s MS daty změřenými s vysokou přesností (pod 3 ppm) a MS/MS analýza.

Při určování prostorových struktur proteinových komplexů poskytují techniky chemického zesítění velmi cenné výsledky, protože pracují s proteiny v roztoku a zaručují tak studium molekul za fyziologických podmínek, na rozdíl od běžně používaných technik rentgenové krystalografie nebo nukleární magnetické rezonance, které určují strukturu

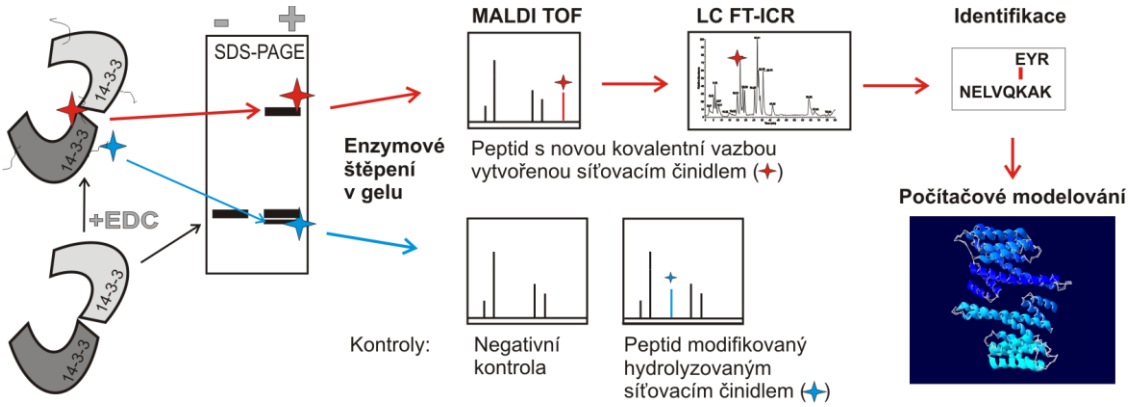

Obrázek 5. Schéma síťovací reakce v dimeru 14-3-3 s tzv. „bottom-up“ MS analýzou interagujících aminokyselin. Po přidání síťovacího činidla (+EDC) do roztoku monomerů proteinu 14-3-3 vznikají kovalentně vázané dimery (červená hvězda), které jsou od nezreagovaných nebo modifikovaných monomerů (modrá hvězda) odděleny na SDS-PAGE. Dimery jsou z gelu vyříznuty, naštěpeny proteasou a peptidové mapy jsou porovnány s kontrolními. Aminokyselinové sekvence jsou vytipovaným peptidům přiřazeny na základě parametrů specifity použitého síťovacího činidla a proteasy, popř. z MS/MS experimentu.

proteinů v arteficielních rozpouštědlech [Sinz 2007; Singh 2010]. Poznatky získané technikou chemického zesítění s úspěchem doplňují a upřesňují strukturní modely získané právě těmito technikami [publikace č. 6 a 7]. Chemické modifikace jsou např. schopné zachytit nekovalentní interakce v proteinových komplexech nebo popsat interakce flexibilních oblastí proteinů, které nemohou být ve struktuře krystalu zachyceny [Novák 2007; Leitner 2010].

1.3. Modelové systémy

Tato podkapitola seznamuje s hlavními modelovými systémy studovanými v rámci prezentované disertační práce.

Představená technika chemického zesítění s MS analýzou tvoří hlavní část práce a byla použita pro mapování interakcí a 3D struktury ve dvou vybraných modelových systémech:

1) v dimeru lidského regulačního proteinu 14-3-3ζ,

2) v dimerickém komplexu mezi membránovými proteiny cytochromem P450 2B4 a cytochromem b_5.

Pomocí hmotnostní spektrometrie byly dále studovány modelové systémy vláknitých hub rodu *Aspergillus* a *Pseudallescheria* s cílem identifikovat a charakterizovat jejich zástupce mj. z klinických izolátů. Konkrétně se jednalo o studium:

3) proteomu spór klinických izolátů a vzorků ze sbírky CCF hub rodu *Aspergillus*,

4) cyklických peptidů na povrchu spór pathogenního druhu *Pseudallescheria boydii*.

1.3.1. Dimer proteinu 14-3-3

Protein 14-3-3 patří mezi důležité regulační molekuly díky své schopnosti interagovat s proteiny, které se účastní důležitých signálních drah buněčné regulace, např. při regulaci buněčného cyklu, při transkripci, transportu molekul mezi organelami, ale i DNA replikaci a malignantní transformaci [Tzivion 2002; Obšilová 2008]. Do současné doby bylo popsáno několik stovek molekul interagujících se 14-3-3 proteiny. Různé koncentrace 14-3-3 byly nalezeny také u neurodegenerativních onemocnění jakými jsou Alzheimerova choroba, Creutzfeld-Jakobova choroba nebo Parkinsonova nemoc [Wilker 2004; Mackie 2005]. Role 14-3-3 proteinu v buňce je velmi významná a pro pochopení jeho funkce v organismu je klíčové znát detailně jeho prostorovou strukturu.

Lidský protein 14-3-3 je dimerická molekula, jejíž každý monomer (30 kDa) je složen z devíti antiparalelních helixů spojených krátkými smyčkami s centrálním vazebným kanálem. Při čelním pohledu připomíná tvar molekuly dimeru koňskou podkovu (Obrázek 6, str. 23). U člověka je 14-3-3 exprimován v sedmi různých isoformách (β, γ, ε, η, σ, τ a ζ), které se liší aminokyselinovou sekvencí, substrátovou specifitou i četností výskytu v různých tkáních [Woodcock 2003]. Všechny isoformy mohou vytvářet

in vivo homodimery i heterodimery mezi jednotlivými isoformami (s vyjímkou isoformy σ, která tvoří pouze homodimery), čímž se zvyšuje množství kombinací jednotlivých substrátů, které se mohou vázat na 14-3-3 dimer a být tak regulovány.

Nejvíce **konzervované aminokyselinové zbytky** mezi všemi lidskými isoformami obecně **se nacházejí ve vazebném kanálu** a z většiny se jedná o kladně nabité aminokyseliny. Právě kladný náboj vazebného místa předurčuje jako nejvhodnější substráty molekuly se záporným nábojem. Jako modelové vazebné motivy substrátů pro vazbu na 14-3-3 proteiny byly identifikovány dva fosforylované motivy: RSXpSXP a RXY/FXpSXP, kde pS značí fosforylaci serinu [Rittinger 1999]. Později byl publikován ještě další fosforylovaný vazebný motiv na C-konci proteinu 14-3-3 [Coblitz 2006] a objevily se také práce popisující vazbu nefosforylovaných substrátů [Henriksson 2002]. Bylo dokázáno, že C-koncová oblast hraje důležitou roli autoinhibitoru, který je v nepřítomnosti substrátu navázán do vazebného kanálu a chrání jej před vazbou nesprávných substrátů. Při interakci se substrátem autoinhibiční C-koncová část odstupuje a účastní se interakcí koordinujících substrát vůči celé molekule 14-3-3 [Šilhan 2004].
Funkce proteinu 14-3-3 úzce souvisí s jeho **spontánním seskupováním do dimerů**. Přestože je každý monomer schopen vázat substráty samostatně, jedna z jeho nejdůležitějších katalytických vlastností je usnadnění vzájemné interakce mezi dvěma různými molekulami navázanými na dimer 14-3-3. Další popsané funkce jsou ochrana vázaného substrátu před účinkem některých kinas či proteas, nebo vnitrobuněčný transport vybraných molekul (např. BAD, Cdc25) do cytosolu, kde je 14-3-3 primárně lokalizovaný [Muslin 2000].

Dimerický stav proteinu 14-3-3 je udržován **na základě elektrostatických a hydrofóbních interakcí v N-terminálních oblastech** obou podjednotek. První dva helixy

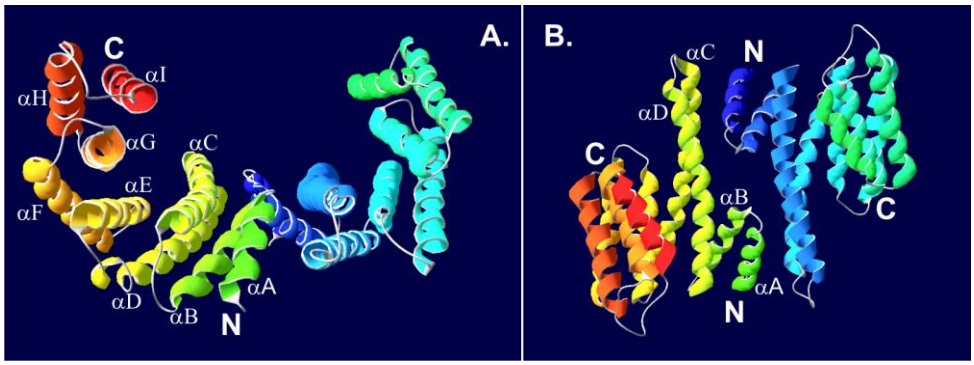

Obrázek 6. Dimer proteinu 14-3-3ζ při pohledu A. zpředu a B. zdola. Každá podjednotka se skládá z 9 helixů (A-I) spojených osmi krátkými smyčkami. N-koncové helixy A-D každé podjednotky se podílejí na nekovalentních interakcích dimeru (pdb 1A40).

(A1, B1) jednoho monomeru interagují s třetím a čtvrtým helixem druhého monomeru (C2, D2). Fosforylace *in vivo* na tomto rozhraní (na serinu 58) slouží buňce jako regulační krok k rozvolnění dimeru a přerušení zprostředkování interakcí mezi navázanými substráty. Nicméně, monomerizací není ovlivněna schopnost molekul samostatně vázat substráty [Woodcock 2003].

V naší práci jsme se zaměřili na **studium nativní struktury lidské isoformy 14-3-3ζ**. Její struktura byla objasněna na základě rengenostrukturní analýzy již v r. 1995 [Liu 1995] a brzy následovaly také modely s vazebnými substráty [Petosa 1998; Obšil 2001]. Publikované krystalografické modely zachycují téměř 99 % celkové sekvence proteinu 14-3-3ζ, včetně interakcí podjednotek na rozhraní dimeru. Výjimkou je ale N-koncová oblast začátku prvního helixu A, která je pro možnosti krystalizace příliš flexiblní a není proto zobrazena na rentgenové difrakci. Výsledky této disertační práce detailně popisují interakce právě této N-terminální oblasti, které byly získány použitím kombinace technik chemické síťovací reakce a H/D výměny a hmotnostní spektrometrie a ukazují na její důležitost v mechanismu dimerizace 14-3-3 proteinů.

1.3.2. Cytochrom P450 2B4 a cytochrom b_5

Cytochromy P450 patří mezi klíčové enzymy biotransformačních reakcí eukaryot i prokaryot. Jsou kódovány množstvím odlišných genů, které dávají vzniknout celé rodině hemoproteinů s odlišnou strukturou i substrátovou specifitou. Dosud bylo popsáno 57 lidských forem cytochromu P450 a převážná část z nich se účastní biosyntetických a degradačních drah sterolů, mastných kyselin a vitamínů [Wilderman 2010]. Menší část se ale přímo **podílí na biotransformačních reakcích cizorodých látek**, jako jsou např. léčiva či chemické karcinogeny. Pro volbu správného léčebného postupu je důležité znát mechanismy přeměny podaného léčiva a pravděpodobnost jeho aktivace nebo vyloučení z organismu v závislosti na působení různých forem tohoto enzymu s odlišným zastoupením u každého pacienta [Stiborová 1999].

Na rozdíl od rozpustných prokaryotických forem jsou eukaryotické cytochromy P450 inkorporovány do membrány endoplazmatického retikula a mitochondrií [Nelson 1987], kde jsou součástí vícesložkového systému tzv. oxygenas se smíšenou funkcí (z angl. *Mixed Function Oxidases*, MFO). Cytochrom P450 je monooxygenasa schopná **oxidovat hydrofóbní substrát** (Obrázek 7, str. 25) díky spolupůsobení NADPH:cytochrom P450

reduktasy (CPR), která poskytuje ve dvou krocích dva elektrony - nejdříve k rozštěpení biatomické molekuly kyslíku a poté k inkorporaci jednoho atomu kyslíku do molekuly substrátu [Porter 1991; Coon 1992]. Vzniklý produkt je polárnější než původní substrát a pomocí dalších konjugačních reakcí může být snadněji vyloučen z organismu [Stiborová 2004]. Kromě NADPH:cytochrom P450 reduktasy může druhý elektron potřebný k oxidaci substrátu cytochromu P450 poskytovat také cytochrom b_5. V závislosti na různých faktorech (substrát, isoforma P450) pak může oxidaci substrátu přítomnost cytochromu b_5 aktivovat [Zhang 2007], inhibovat nebo změnit kvalitu vznikajících produktů [Stiborová 2006].

Cytochromy P450 se podle různého stupně homologie dělí do genetických rodin a podrodin, které jsou označovány zkratkou CYP [Nelson 2006]. **Cytochrom P450 2B4 (CYP2B4) je původem králičí protein, ortholog lidské isoformy CYP2B6**, která se účastní metabolismu některých léčiv (např. cyklofosfamid, tamoxifen, diazepam) i aktivace některých karcinogenů (aflatoxin B1, 6-aminochrysen) [Stiborová 1999; Jinno 2003]. Rychlost a směr přeměny těchto látek působením CYP2B4 je ovlivňováno také interakcí s cytochromem b_5, který může inhibovat nebo aktivovat katalytickou aktivitu CYP2B4 v závislosti na koncentraci cytochromu b_5, přítomném substrátu i přítomnosti ostatních složek MFO [Zhang 2005; Stiborová 2006]. Největší vliv na směr katalýzy má poměr mezi CPR a cytochromem b_5 v interakci s CYP2B4 v MFO systému. Protože oba proteiny interagují s CYP2B4 ve vzájemně se překrývajících vazebných oblastech [Bridges 1998] a protože cytochrom b_5 není schopen předávat na CYP2B4 první potřebný elektron v důsledku vysokého rozdílu potenciálů mezi proteiny [Zhang 2003], vyšší počet molekul cytochromu b_5 bude pravděpodobně soutěžit o vazebné místo s CPR na povrchu CYP2B4

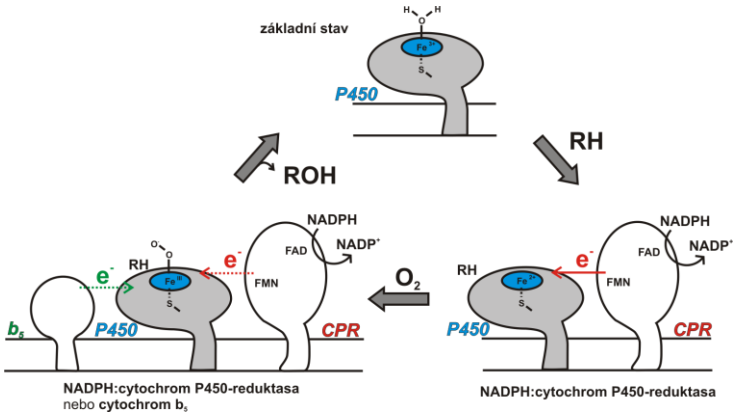

Obrázek 7. Schéma oxidace substrátu RH cytochromem P450 za spolupůsobení výhradně NADPH:cytochrom P450 reduktasy (CPR) v prvním kroku oxidace a poté CPR nebo cytochromu b_5 ve druhém kroku.

a tím způsobovat inhibici přenosu prvního elektronu z CPR na CYP2B4 a tedy i celého katalytického cyklu CYP2B4. V případě, že je molekul cytochromu b_5 méně než molekul CPR, může v závislosti na typu substrátu docházet i k urychlení katalytické přeměny až 100-krát [Im 2011].

Interakce mezi CYP2B4 a oběma redukčními partnery není řízena žádným specifickým vazebným motivem (jako je to např. u molekuly 14-3-3ζ), ale předpokládá se, že probíhá na základě nespecifického elektrostatického párování kladných nábojů na proximální straně (v blízkosti thiolátového ligandu hemu) CYP2B4 a záporných oblastí v molekule CPR nebo cytochromu b_5. Vazebná místa obou redoxních partnerů nejsou pravděpodobně identická, ale výrazně se vzájemně překrývají (Obrázek 8) [Zhang 2005].

V současné době existuje devět strukturně odlišných krystalografických modelů proteinu CYP2B4 s inkorporovanýn ligandem, substrátem či volným aktivním centrem. Bohužel všechny tyto struktury byly získány studiem rekombinantních proteinů s pozměněnou sekvencí v membránové části cytochromu P450. Studie využívající techniku izotopové H/D výměny s následnou identifikací pomocí hmotnostní spektrometrie prokázala, že všechny publikované konformace jsou energeticky přípustné a v roztoku vzájemně přecházejí [Wilderman 2010].

V naší práci jsme studovali nativní proteiny CYP2B4 a cytochrom b_5 izolované včetně membránové kotvy a rozšířili jsme doposud známé vazebné místo pro cytochrom b_5 na povrchu cytochromu P450 2B4. Dále jsme popsali vliv přítomnosti cytochromu b_5 na enzymatickou aktivitu CYP2B4 v důsledku přenosu elektronu nebo strukturní modulace. [publikace č.7].

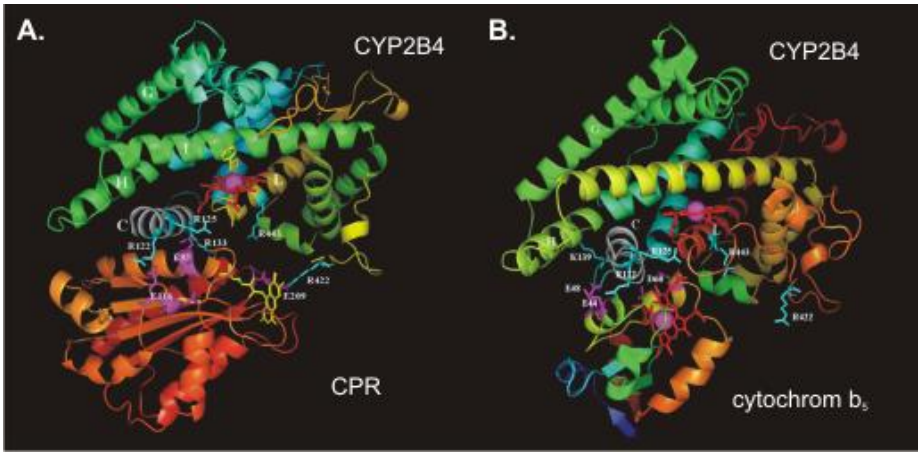

Obrázek 8. A. Model interakce mezi CYP2B4 a CPR, B. mezi CYP2B4 a cytochromem b_5. Převzato ze [Zhang 2005].

1.3.3. Vláknité houby rodu *Aspergillus*

Houby patří mezi nejrozšířenější eukaryotické heterotrofní organismy na světě. Rod *Aspergillus* se řadí mezi vřeckovýtrusné houby (*Ascomycetes*) (Tabulka 3, str. 28), jejichž zástupci jsou využíváni zejména v potravinářství a v biotechnologických odvětvích. Patří sem ovšem také rostlinní parazité nebo patogenní zástupci způsobující v lidském organismu velmi vážná onemocnění (otravy, aspergilóza, pneumónie).

Se zástupci rodu *Aspergillus* se setkáváme jako s plísní vyskytující se zejména na starém dřevě, listech, na vlhkých stěnách budov nebo špatně skladovaných potravinách. Plíseň v průběhu života uvolňuje do okolního vzduchu miliardy spór. Spóry (konidie) jsou velmi odolné útvary, které se samovolně uvolňují z konidioforů na vzdušném myceliu a primárně slouží houbám k asexuálnímu rozmnožování. Spory i mycelium obsahují různé toxiny, které mohou způsobovat alergie a otravy. Ačkoliv zdravým jedinců každodenní setkání se spórami ve vdechovaném vzduchu většinou nezpůsobuje závažné zdravotní problémy, jinak je tomu u jedinců s oslabenou imunitou, např. imunokompromitovaných pacientů po transplantacích či chemoterapiích. U nich mohou vyvolat závažná invazivní nebo alergická onemocnění souhrnně označovaná jako **aspergilózy**, které napadají zejména plíce a dýchací cesty. Nejčastějším původcem je druh *Aspergillus fumigatus*, méně často *A. niger*, *A. flavus* nebo *A. terreus* [Walsh 2001]. Při včasné detekci (hodiny až dny) je nemoc léčitelná antimykotiky, při pozdějším započetí léčby bohužel končí často smrtí nemocného [Lin 2001].

Ve struktuře houbových spór je přítomno několik typů látek, které mohou způsobovat hypersenzitivitu imunitního systému. Jsou to mykotoxiny (např. aflatoxiny druhu *A. flavus*), glykoproteiny (galaktomannan), povrchové proteiny a nízkomolekulární látky. Současná spolehlivá diagnostika aspergilózy je po zjištění základních symptomů (dýchací problémy, bolest na prsou, horečka) založena na imunologickém stanovení hladiny protilátek proti galaktomannanu, který je specifickým diagnostickým znakem pro aspergilózy, dále na ověření přítomnosti kolonií aspergillů na histopatologickém nálezu, a na mikrobiologické kultivaci [Alexander 2002]. Tyto metody jsou ale časově náročné a nejsou schopny zachytit aspergilózu v časném stádiu, kdy je ještě možné použít úspěšně antimykotika. Dále se používá rentgen hrudníku nebo počítačová tomografie (CT), ale ani tyto přístupy nepatří mezi metody včasné diagnostiky a navíc nejsou dostatečně specifické pro onemocnění způsobená houbami rodu *Aspergillus* [Walsh 2008].

Slibnou možnost včasné a specifické diagnostiky představuje metoda PCR uvedená v roce 2006, která je založená na amplifikaci specifických genů rodu *Aspergillus* [Donnelly 2006]. Bohužel dodnes není tato metoda standardizována a není ani komerčně dostupná. Nadále tedy **přetrvává potřeba nalézt metodu včasné a specifické detekce aspergilózy**, která by umožňovala rychlejší nasazení léčby a tudíž i lepší prognózu pro pacienty.

Tabulka 3. Taxonomické zařazení hub rodů *Aspergillus* a *Pseudallescheria.*

Říše	Fungi	Fungi
Kmen	Ascomycetes	Ascomycetes
Třída	Euascomycetes	Euascomycetes
Řád	Eurotiales	Microascales
Čeleď	Trichocomaceae	Microascaceae
Rod	**Aspergillus**	**Pseudallescheria**

1.3.4. Patogenní houby druhu *Pseudallescheria boydii*

Zástupci rodu *Pseudallescheria* patří stejně jako rod *Aspergillus* mezi vřeckovýtrusné houby (Ascomycetes) (viz Tabulka 3) a jsou také vážnými lidskými patogeny. Vyskytují se zejména v půdě, hnoji, znečištěných vodách a rozmnožují se sporami, které uvolňují do vzduchu (Obrázek 10, str. 29). Životní cyklus této vláknité houby má dvě různá stádia - pohlavně se rozmnožující *P. boydii* (tzv. teleomorf) a mitoticky se rozmnožující *Scedosporium apiospermum* nebo *Graphium eumorphum* (tzv. anamorf). Obě stádia jsou nezávislá, vznikají v různých časech a různých podmínkách.

S. apiospermum a *S. prolificans* způsobují závažné systémové mykózy (někdy souhrně označované jako **scedosporiózy**) respiračního traktu a centrální nervové soustavy u imunokompromitovaných pacientů (asi 1 % z celkového počtu invazivních fungálních mykóz) s úmrtností nad 75 % při rozsáhlejší infekci [Sedláček 2008]. Léčba je založena na podávání antifungálních léčiv, popř. odstranění postižené tkáně, s dobrou prognózou uzdravení, je-li nasazena brzy po propuknutí onemocnění [Cardoso 2009]. Bohužel, stejně jako u aspergilóz ani u mykóz způsobených *S. apiospermum* **neexistuje dodnes spolehlivá a především včasná diagnostika**. Současné metody spoléhají na biopsii zasažené tkáně a kultivaci houby, které jsou příliš zdlouhavé. Situaci navíc komplikuje známá rezistence *P. boydii* a *S. prolificans* na mnoho antifungálních preparátů (např. Amfotericin B), které jsou

nasazovány v léčbě aspergilóz, s nimiž má scedosporióza na první pohled stejné příznaky [O'Brian 2005].

V současnosti se zkoumají dostatečně citlivé, rychlé a specifické metody, které by byly schopné detekovat v reálném vzorku např. sacharidové antigeny v buněčných stěnách spór [Thornton 2009], hydrolytické enzymy nebo malé metabolity unikátní pro *P. boydii* [Pavlásková 2010]. Znalost těchto povrchových antigenů stejně jako sekretovaných molekul, které mohou být virulentními faktory, umožní lépe porozumět mechanismu, jakým *P. boydii* a *S. apiospermum* interagují s hostitelskou buňkou a následně mohou pomoci při včasné léčbě [Santos 2009].

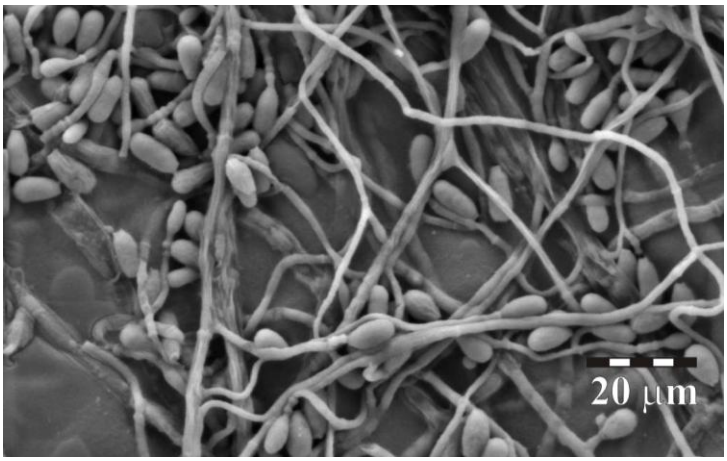

Obrázek 10. Vzdušné mycelium a konidie kmene *Pseudallescheria boydii* CCF 3082 (RNDr. O. Benada, CSc., MBÚ AV ČR v.v.i., 2006).

2. Cíle práce

Cílem této práce bylo použití současných přístupů hmotnostní spektrometrie při řešení několika proteomických otázek. První část byla zaměřena na **studium protein-proteinových interakcí** pomocí nestandardní metodiky založené na kovalentním zesítění proteinových komplexů s jejich následnou analýzou pomocí hmotnostní spektrometrie**.** Konkrétně jsme studovali protein-proteinové interakce v těchto modelových systémech:

1. V dimerickém komplexu lidského regulačního proteinu 14-3-3ζ, jehož publikovaná krystalová struktura neobsahuje informace o flexibilních C- a N- koncových doménách (kap. 3.1.1, str. 31).
2. V komplexu proteinu 14-3-3ζ s jeho přirozeným substrátem, tyrosinhydroxylasou (resp. její regulační doménou, jejíž interakce se 14-3-3 proteiny je regulována fosforylací) (kap. 4.1, str. 123).
3. V systému dvou membránových proteinů cytochromu P450 2B4 a cytochromu b_5, které se účastní biotransformace cizorodých látek v králičím MFO systému a jejichž interagující oblasti stále nebyly jednoznačně popsány (kap.3.1.2, str. 49).

Druhá část práce měla za cíl použití hmotnostní spektrometrii pro **identifikaci a charakterizaci fungálních proteinů a peptidů**, s důrazem na hledání specifických diagnostických znaků pro potřeby včasné detekce závažných houbových infekcí způsobovaných:

4. Zástupci vláknitých hub rodu *Aspergillus* (kap. 3.2.1, str. 74).
5. Zástupci vláknitých hub rodu *Pseudallescheria* (kap. 3.2.2, str. 82).

Cílem poslední části práce bylo použití hmotnostní spektrometrie pro **charakterizaci proteinů nebo lipidů a měnících se proteinových profilů** v dalších proteomických a lipidomických projektech. Konkrétně byly stanoveny tyto dílčí cíle:

6. Nalézt možnost rychlého určování polohy dvojných vazeb v molekulách peptidů nebo lipidů (kap. 3.3.1, str. 89).
7. Identifikovat nové alergeny v pšeničné mouce (kap. 3.3.2, str. 95).
8. Popsat změny v proteomu lidských leukemických buněk JURL-MK1 v apoptóze (kap. 3.3.3, str. 109).

3. Výsledky

3.1. Protein-proteinové interakce studované pomocí síťovacích reakcí s následnou MS identifikací

3.1.1. Mapování interakcí v homodimeru lidského proteinu 14-3-3ζ

v publikaci

The Combination of H/D Exchange and Chemical Cross-linking with Mass Spectrometry: Mapping of Human 14-3-3ζ Homodimer Interaction

Pavlásková K., Mrázek H., Ječmen T., Halada P., Man P., Novák P., Obšil T., Šulc M.

Biochem Biophys Res Commun. (připraveno k odeslání)

Prohlášení spoluautorů

„Prohlašuji, že Kateřina Pavlásková se patřičně podílela (80 %) na plánování experimentů, jejich měření, interpretaci výsledků a sepisování této publikace.“

V Praze dne:

Doc. RNDr. Miroslav Šulc, PhD.

The Combination of H/D Exchange and Chemical Cross-linking with Mass Spectrometry: Mapping of Human 14-3-3ζ Homodimer Interaction

Kateřina Pavlásková[1,3], Hynek Mrázek[1,3], Tomáš Ječmen[1,3], Petr Halada[1], Petr Man[1], Petr Novák[1], Tomáš Obšil[2,4], Miroslav Šulc[1,3]

[1]Institute of Microbiology v.v.i. and [2]Institute of Physiology v.v.i., Academy of Sciences of the Czech Republic, Vídeňská 1083, 14220 Prague 4, Czech Republic
[3]Department of Biochemistry and [4]Department of Physical Chemistry, Faculty of Science, Charles University, Hlavova 2030, 12843, Prague 2, Czech Republic

To whom correspondence should be addressed:
Assoc. Prof. Miroslav Šulc; Institute of Microbiology v.v.i., Academy of Sciences of the Czech Republic, Vídeňská 1083, 14220 Prague 4, Czech Republic; Email: msulc@biomed.cas.cz; Tel. +420241062644; Fax. +4202241062156

Abbreviations: EDC, 1-ethyl-3-[3-dimethyl(aminopropyl)]carbodiimide hydrochloride; DTT, dithiothreitol; EDTA, ethylenediaminetetraacetic acid; MALDI-TOF, matrix assisted laser desorption/ionization-time of flight; LC-FTICR MS, liquid chromatography coupled with Fourier transform ion cyclotron resonance mass spectrometry; LC-MS/MS, liquid chromatography coupled with tandem mass spectrometry; MeCN, acetonitrile; SDS-PAGE, one dimensional sodium dodecylsulfate polyacrylamide gel electrophoresis; TCEP, Tris(2-carboxymethyl) phospine hydrochloride; TFA, trifluoroacetic acid.

Abstract

The H/D exchange or chemical cross-linking by soluble carbodiimide (EDC) has been employed in combination with the high resolution mass spectrometry (MS) to characterize contact surface regions involved in the transient interaction between two molecules of human 14-3-3ζ regulatory protein.

The hydrogen/deuterium (H/D) exchange experiment disclosed low resolution mapping of interaction in homodimeric 14-3-3ζ complex. The protection of two sequential segments has been determined, the N-terminal sequence (the first 28

residues) from one subunit interacts with region αC′ and αD′-helices (residues 45-103) of the other molecule across the dimer interface. To identify interacting aminoacid residues within studied complex, the chemical cross-linking reaction was accomplished to produce the covalent homodimer detected on SDS-PAGE. The MS analysis (after in gel digestion with trypsin) using both high resolution and tandem mass spectrometry determined cross-linked aminoacid residues. The salt bridge between Lys9 and Glu81 has been found to participate in the 14-3-3ζ isotype homodimerization. Also the identified interactions of N-terminal amino group with Glu70 or Glu81 have never been reported mainly due to lack of this N-terminal part in any published 14-3-3 X-ray diffraction crystal structure.

Based on our findings, the combination of used experimental approaches is suitable to map interaction between two proteins in the environment preserving their native structures and also allows description of regions with uncharacterized structure in studied protein complexes.

Key words: protein-protein interaction, chemical cross-linking, H/D exchange, mass spectrometry, 14-3-3 homodimer

Introduction

The 14-3-3 proteins represent a broad class of highly conserved regulatory proteins found in all eukaryotic cells. Their main overall function depends on self-assembling into dimers *in vivo* and *in vitro* [1]. The dimerization is mediated by electrostatic interactions between the N-terminal regions of two 14-3-3 subunits and can be regulated by site-specific phosphorylation *in vivo* and *in vitro* [2]. It has previously been described that three salt bridges involving Arg18-Glu89, Glu5-Lys74, and Asp21-Lys85, as well as several buried polar and hydrophobic residues (Leu12, Ala16, Ser58, Val62, Ile65, and Tyr82) are involved in maintaining the homodimer interface in the 14-3-3ζ isoform [3]. Computer modeling studies along with experiments showed that both, Ser58 phosporylation or also mutation to Asp58 at this site, would compromise 14-3-3 ability to dimerize [4]. However, the monomerization does not affect the binding of the substrate alone [5], but is able to disrupt the 14-3-3 homodimer mediated interaction between two ligands of 14-3-3 protein involved in different cellular pathways

Hydrogen/deuterium (H/D) exchange experiments provide information on the local stability of proteins. Their coupling with nuclear magnetic resonance (NMR) or mass spectrometry analysis (MS) has been particularly valuable in characterization of the protein structure during folding process, or protein interaction with membranes, or protein-protein interactions, or elucidation of structurally disordered proteins [6]. Principally, this method detects the change in isotopic composition due to the exchange of main-chain amide hydrogens for deuterium atoms in samples exposed to D_2O in time. The level of deuterium incorporation reflects faithfully the degree of protein folding or connection of selected regions in protein-protein interactions. Compared to NMR, MS provides information of lower resolution, but has fewer constraints concerning the quality, size and the state of the protein. However, the low resolution of this approach can be improved significantly using several different proteases for protein digestion, or if the combination with other bio-conjugation techniques, e.g. chemical cross-linking is applied.

The chemical cross-linking in combination with MS analysis is becoming a valuable tool for the structure determination of protein complexes in their native states in a reasonable time-scale using small quantities of protein [for references see review 7]. One of these experimental approaches is to incubate a cross-linker with two purified proteins of known aminoacid sequence to produce a mixture of covalently cross-linked heterodimers. The abundance of diverse protein orientations in mixture statistically depends on presence of each species in reaction. The next steps are separation of monomers and heterodimers (e.g. SDS-PAGE), digestion of cross-linked species to peptides, and analysis of resulting peptide mixture employing MS technique. The high accuracy MS data allow to determine the unique combination of two cross-linked peptide sequences that also fit to protease specificity (e.g. trypsin generates peptides with C-terminal arginine or lysine). The deduction which two aminoacid residues participate in the covalent coupling of two cross-linked peptides is performed based on acquisition of the tandem mass spectrometry (MS/MS), providing a structural information of analyzed specie, and reaction specificity of used chemical cross-linker. In our experiments used zero-length cross-linking reagent 1-ethyl-3-[3-dimethyl(aminopropyl)]carbodiimide hydrochloride (EDC) reacts with a carboxyl group on the first protein, forming an amine-reactive O-acylisourea intermediate that may

condensate with an amine on the second protein yielding a conjugate of the two molecules joined by a stable amide bond corresponding to salt bridge interaction. This knowledge of cross-linking reaction mechanism provides usually enough information to deduce approximately constrained distance between two cross-linked aminoacid residues to map interacting interface in the studied protein complex (e.g. EDC is able to connect amine and carboxylic acid groups within distances of under 5 Å [8]).

We present a successful application of H/D exchange and chemical cross-linking experiments in combination with MS analysis for characterization of regulatory 14-3-3ζ protein homodimer assembling and determination of the aminoacid residues participating in this homodimer interface domain.

Material and methods

2.1. Chemicals

Bovine serum albumin, dithiothreitol (DTT), formic acid, pepsin and thrombin were purchased from Sigma Chemical Co. (St. Louis, USA). 1-ethyl-3-[3-dimethyl(aminopropyl)]carbodiimide hydrochloride (EDC), Coomassie Brilliant Blue R-250, ethylenediaminetetraacetic acid (EDTA), formic acid, iodoacetamide, trifluoroacetic acid (TFA), Tris(2-carboxymethyl) phospine hydrochloride (TCEP) and pyridine were from Fluka Chemical Co. (St. Louis, USA). Ni-NTA Sepharose and MonoQ Sepharose Fast Flow were purchased from GE Healthcare (Uppsala, Sweden), bicinchoninic acid from Pierce (Rockford, USA), trypsin from Promega (Madison, USA), acetonitrile (MeCN) and water of LiChrosolv quality from Merck (Darmstadt, Germany). The other chemicals were obtained from Lachema (Brno, Czech Republic).

2.2. Expression and purification of 14-3-3ζ proteins and their characterization

All human 14-3-3ζ proteins, wild type (WT), UniProtKB database sequence P63104, and its mutant version containing mutations Ser58Asp, denoted as S58D, were prepared as described previously [9]. Recombinant proteins with N-terminal His-tag (NHis-14-3-3ζWT and NHis-14-3-3ζS58D) were purified from *E.coli* BL-21 lysate using Ni-NTA Sepharose and MonoQ ion-exchange chromatography (GE Healthcare). From the His-tag region consisting 19 residues before the first methionine, marked (-19) to (-1), a 16 residues long peptide was cleaved using thrombin (Sigma) and separated

from protein on Ni-NTA Sepharose column yielding the 14-3-3ζWT and 14-3-3ζS58D proteins with three N-terminal aminoacid residues remaining from His-tag, (-3)GSH(-1). The electrophoresis (SDS-PAGE [10]) was used to prove protein homogeneity and purity. Each protein band was analyzed by mass spectrometry after trypsin digestion to confirm sequences of all pure proteins [11]. Protein concentrations were assessed using bicinchoninic acid and bovine serum albumin as a standard [12].

2.3. H/D exchange experiment

Experiments were initiated by 10-fold dilution of the protein in deuterated 20 mM TrisCl buffer (pD=7.5), 150 mM NaCl, 1 mM EDTA and 1 mM DTT. In selected time points (1 min, 10 min, 1 hr, 5 hrs and 24 hrs) were taken samples aliquots and H/D exchange was quenched by lowering both pH value and temperature (addition of cold HCl; vigorous mixing; flash-freezing with following storage in liquid nitrogene). The protein digestion was carried out using equimolar concentration of pepsin solution for 2 min on ice, formed peptide mixture was analyzed using LC-FTICR MS (LC Packings, Amsterdam, The Netherlands coupled with 9.4 T, Bruker Daltonics, Billerica, MA, USA) and deuteration levels were extracted from obtained positive ion mass spectra as described previously [6].

2.4. Preparation, separation and proteolysis of cross-linking products

The cross-linking reaction using different EDC concentrations (4, 10, or 40 μg/mL) was carried out with 2 μM 14-3-3ζ protein in system containing 50 mM pyridine:HCl buffer (pH 6.0) and 150mM NaCl at room temperature for 2 hours. The cross-linking reaction was quenched by 2-mercaptoethanol present in electrophoretic sample buffer prior separation on 12% SDS-PAGE. The protein bands were visualized using 0.25% (w/v) Coomassie Brilliant Blue R-250. The excised protein spots from SDS-PAGE gel were de-stained, all cysteine residues in proteins were modified using TCEP and iodoacetamide, and processed for MALDI-TOF mass spectrometry by in-gel digestion with trypsin as described previously [11]. The mixture of extracted peptides was applied on a peptide micro-trap microcolumn (Michrom Bioresources, Auburn, CA, USA) to remove any salt and buffer components prior to LC-MS analysis.

2.5. LC-FTICR MS analysis

The peptides eluted from the micro-trap were dried on rotation vacuum concentrator (SPEED-VAC, Savant, USA) and dissolved in 5% aqueous MeCN containing 0.1% formic acid under sonication. A portion (5 µL) was loaded onto a reverse-phase column (Magic C18, 0.3 mm diameter, 150 mm long, 5 µm particle size, 200 Å pore size, Michrom Bioresources, Auburn, CA, USA) and eluted using gradient mobile phase: solvent A, 0.1% formic acid in 5% aqueous MeCN; solvent B, 0.08% formic acid in 90% aqueous MeCN; gradient (in % B buffer), 0% for 1 min, 0–15% in 4 min, 15–60% in 30 min, 60–100% in 5 min; flow rate, 3 µL/min. All chromatographic separations were performed at 20 °C using an Ultimate 1000 capillary HPLC system (LC Packings, Amsterdam, The Netherlands). The column effluent was directly interfaced to an APEX Qe FTICR mass spectrometer equipped with a 9.4 T superconducting magnet (Bruker Daltonics, Billerica, MA, USA). Positive ion MS spectra were acquired in a broad *m/z* range (300–2000). Every received monoisotopic mass was automatically matched to a theoretical library of cross-linked, modified and/or unmodified proteolytic products using protein sequences from UniProtKB database (P63104) with additional three N-terminal residues (-3)GSH(-1).

2.6. Off-line LC-MS/MS analysis

The portion (5 µL) of peptides dissolved in 5% aqueous MeCN containing 0.1% formic acid was loaded also onto a reverse-phase column (Magic C18, 0.3 mm diameter, 150 mm long, 5 µm particle size, 200 Å pore size, Michrom Bioresources, Auburn, CA, USA) and separated using gradient system conditions as follows: solvent A, 0.1% trifluoroacetic acid in 1% aqueous MeCN; solvent B, 0.08% trifluoroacetic acid in 90% aqueous MeCN; gradient (in % B buffer), 0–40% in 24 min, flow rate, 2 µL/min. All chromatographic separations were performed at 20 °C using an Ultimate 1000 capillary HPLC system (LC Packings, Amsterdam, The Netherlands). The column effluent was directly spotted onto PAC96 target (Bruker Daltonics, Bremen, Germany) using a Proteineer FC spotting device (Bruker Daltonics). Automatic MALDI MS analyses were performed on a Ultraflex III TOF/TOF spectrometer (Bruker Daltonics) under the control of Compass 1.2 and WarpLC 1.2 software. MS/MS spectra of the cross-linked peptides were acquired and interpreted manually.

Results and Discussion

The H/D exchange and chemical cross-linking in combination with mass spectrometry were used for the mapping of protein interface between two subunits in 14-3-3ζ homodimer. To accomplish our goal, the highly purified and well characterized recombinant proteins (14-3-3ζWT and 14-3-3ζS58D) were prepared from *E.coli* lysate up to the electrophoretical homogeneity employing techniques preserved a native structure of these proteins. The MALDI-TOF mass spectrometry analysis of trypsinized proteins using mass fingerprinting approach confirmed the identity of all proteins (for individual values of protein concentration and sequence coverage see Table 1) and confirmed N-terminal sequence of every construct. High number of matched peptides from all searched *m/z* signals received in results of manual interpretation indicated high purity of all analyzed protein preparations.

<Table 1 here>

The chemical cross-linking reaction using zero-length cross-linker EDC successfully forms a covalent homodimeric product of both 14-3-3ζWT and N-His14-3-3ζWT proteins in all used EDC concentrations (labeled by arrow in the Figure 1A). In agreement with literature, the 14-3-3ζS58D mutant significantly reduced the homodimer production in all EDC concentrations. The mutation S58D introduced the negative charge on this site to mimic the Ser58 phosphorylation by PKA and PKB/AKT1 that regulate 14-3-3 homodimer assembling in organism [2,13]. Unfortunately, the EDC forms homodimeric product also for N-His14-3-3ζS58D protein, probably due to unspecific N-His region interactions. These results suggested that presence of full-length His-tag sequence can probably produce artificial protein-protein interaction. The introduction of three N-terminal residues (-3)GSH(-1) of 14-3-3ζS58D construct did not performed unspecific protein-protein interaction. Therefore, any following experiments, chemical cross-linking or H/D exchange, were performed only with 14-3-3ζ proteins with removed His-tag sequence (14-3-3ζWT and 14-3-3ζS58D).

<Figure 1 here>

The two sequence segments of homodimeric 14-3-3ζWT and monomeric 14-3-3ζS58D demonstrated different H/D exchange behavior. These H/D exchange results,

presented in Figure 2, revealed the H/D exchange protection of homodimeric 14-3-3ζWT N-terminal sequence, covered residues (-3)-25 corresponding to the first αA helix, and residues 45-103, formed region αC′ and αD′-helices, in comparison to monomeric 14-3-3ζS58D molecule. The presented data are in a good agreement with results previously described in literature. It was postulated, that two sequential segments are responsible for 14-3-3 dimerization, the first αA helix (residues 5-21) from one subunit interact with region αC′ and αD′-helices (residues 58-89) of the other molecule across the dimer interface [14]. Our H/D exchange experimental data revealed not only low resolution structural data of 14-3-3ζ homodimer assembling, but also indicate different kinetics of both identified regions through the dimerization process. Protection 14-3-3ζWT is detected in all times acquired for the region of αC′ and αD′-helices and probably this region is deeply buried and its assembling is very fast. On the other hand, the N-terminal region corresponding to the first αA helix, revealed no or very low protection in the beginning of H/D experiment (1 min) indicating the partial re-arrangement and relaxation of this region after dilution in D_2O. Because of the next time values of H/D back-exchange (10 min or higher) correspond to protection of this region indicating its comeback and participation on 14-3-3ζWT homodimer assembling.

<Figure 2 here>

To locate the cross-linked regions and the residues involved in 14-3-3ζWT homodimeric complex, the LC-MS with nano-electrospray ionization and high resolution FTICR detection was used. Obtained dataset of experimental *m/z* values was automatically reduced to produce output files of monoisotopic masses that were searched against a database of theoretical monoisotopic masses of cross-linked products: mass of any 14-3-3ζWT trypsinised peptide plus mass of any 14-3-3ζWT trypsinised peptide minus mass of water eliminated during EDC cross-linking reaction. Table 2 presents (in each row) the experimentally observed and corresponding calculated *m/z* values, mass error of calculated and experimental *m/z* values (maximally 3 ppm) and sequence of the covalently cross-linked peptides (in the first and the second molecule of 14-3-3ζWT homodimer). The theoretically deduced covalently cross-linked aminoacid residues are underlined.

Only one experimental monoisotopic $[M+H]^+$ mass value *m/z* 1377.7478 permitted to deduce the unique combination of covalent cross-link (14-3-3ζWT peptides NELVQKAK and EYR with an mass error value 0.8 ppm). These peptides, generated using trypsin in the step of proteolytic digestion, contain C-terminal lysine and arginine, respectively. Only gama carboxy group of glutamic acid (Glu81) within peptide EYR allows the EDC cross-linking reaction with any amino group of NELVQKAK peptide (EDC couples carboxyl groups of side chain residues as well as protein C-termini to primary amine of either lysine or protein N-termini). Epsilon amino group of C-terminal lysine in peptide NELVQKAK can not be used for EDC cross-linking reaction, because it was distinguished and cleaved by trypsin. There remains only one epsilon amino group (Lys9) within NELVQKAK peptide for EDC cross-link. Therefore, in this case we could deduce both unique aminoacid residues in covalently fixed interaction in 14-3-3ζWT homodimer. Unfortunately similar approach could not be applied to deduce all other aminoacid residues involved in protein-protein interface, because more than one possibility was present (Table 2). Therefore, only MS/MS experiment of all other species can provide structural information.

<Table 2 here>

The off-line LC-MS/MS analysis using MALDI-TOF/TOF was employed to acquire the MS/MS data from *m/z* signals presented in Table 2 identify aminoacid residues fixed within interaction after EDC cross-linking reaction. There are generally three groups of identified cross-links with overlapping sequences formed by protease miscleavage activity in Table 2. The first group containing the already identified member with value *m/z* 1377.7478 reported the contact of Lys9 residue with Glu81. The recorded MS/MS spectra and their manual interpretation confirmed deduced covalent bond formed by EDC and involving Lys9 and Glu81 residues (Figure 2A). Surprisingly, the signal *m/z* 2033.0209 and its oxidized variant *m/z* 2049.0186, belongs to the same group of aminoacids in contact, epsilon amino group of Lys9 and gamma carboxy group of Glu81 (Figure 2B with incorporated fragmentation schema). Almost the whole identified y-series from fragment with value *m/z* 795 and higher assigned the modification of Lys9 with peptide Glu81-Agr83. Similarly, whole b-fragment series, complementary to y-fragments, from N-termini of peptide (-3)-11 until the value m/z 1255 determined no modification of this peptide until residue Gln8. In parallel with this

b-series, the series with lost of the methanesulfenic acid (-64Da) from oxidized methionine Met1 [15] was identified. The second group of covalent cross-link found by MS was Glu81 with N-terminal amino group of 14-3-3ζWT protein, residue Gly(-3), was represent by MS/MS of signal *m/z* 1833.884 and its oxidized variant at *m/z* 1849.8816 shown in Figure 3C. There are possible two variants of Glu81 residue contact with Lys3 or N-terminal amino group of Gly(-3). The identified y-fragmentation series till value *m/z* 1344 excluded any modification of peptide (-3)-9 sequence from C-terminus till Ser(-2) (e.g. the fragment with value *m/z* 858 exclusively determined the unoccupied epsilon amino group of Lys3). The last identified group of cross-links, have belonged to suggested contact of 14-3-3 protein N-terminal amino group with residue Glu70 and is represented by MS/MS of signal *m/z* 2000.9668 and its oxidized form with signal *m/z* 2016.9625 displayed in Figure 3D.

<Figure 3 here>

We have identified three novel salt bridges (Lys9-Glu81, N-terminal amino group in contact with Glu70 or Glu81) situated within two regions of 14-3-3ζWT sequence that also demonstrated involvement in 14-3-3 homodimerization by H/D exchange. Our presented data are also in agreement with previously postulated results [1,14]. Although we did not identified any of three previously described salt bridges involving Arg18-Glu89, Glu5-Lys74, and Asp21-Lys85 [3], we present solid experimental evidence, that previously predicted salt bridge involving Lys9 and Glu83 of the 14-3-3σ isotype homodimerization [16], has alternatively been also mimicked by detected Lys9-Glu81 in 14-3-3ζWT homodimer interaction using EDC cross-linker. The structure based sequence alignment of human 14-3-3 isoforms revealed highly conserved positive charge in position of Lys9 (14-3-3ζWT numbering) in all analyzed 14-3-3 isoforms, and negatively charged aminoacid residues in position of Glu81 (14-3-3ζWT numbering) is presented in 14-3-3 isoform zeta, beta, sigma, tau/theta, and epsilon [3]. This finding supports an alternative existence such as salt bridge in these 14-3-3 human isoforms. The identified N-terminal amino group interaction with Glu70 and Glu81, experimentally covered for the first time by our data, has never been reported or discussed mainly because the structure of this N-terminal region has never been presented in any X-ray crystal structure. Therefore, our data extend the 14-3-

3ζWT homodimer assembling site and describe existence of three novel salt bridges within this contact site.

The role of identified N-terminal amino group in 14-3-3 homodimerization process has never been discussed in literature due to lack of this structure in published structures. The acetylation of this N-terminal amino group has been reported in most human brain isoforms using specific antibody [17]. In mammalian isoforms, acetylation is thought to increase isoforms half-life protecting the N-terminus from degradation and does not have a known effect on 14-3-3 protein function [18]. Except the regulation of protein stability by acetylation, the affecting of DNA binding and also regulation of protein-protein interaction are suggested for acetylation [19]. Based on our experimental evidence that unmodified N-terminal amino group is involved in 14-3-3ζ homodimer interface, we can proposed a potential regulatory and/or modulatory role of the N-terminal amino group acetylation for the 14-3-3 protein dimerization process in organism.

Conclusions

Our presented results demonstrate successful combination of H/D exchange and bio-conjugation techniques with mass spectrometry to map the protein-protein interaction of human 14-3-3ζ homodimer. Both, the chemical cross-linking and H/D exchange results were in good agreement with previously described 14-3-3ζ protein regions involved in homodimerization process (αA helix from one subunit interact with region αC′ and αD′-helices of the other molecule). Moreover, our data revealed the three novel salt bridges within 14-3-3ζ homodimer interface (Lys9-Glu81, N-terminal amino group interaction with Glu70 or Glu81) to extend area of 14-3-3ζ contact site.

Acknowledgements

The study was supported by grants of the Grant Agency of Charles University (258179), the Ministry of Education of the Czech Republic (LC545), and an institutional research concept of the Institute of Microbiology, Academy of Sciences of the Czech Republic (AV0Z50200510).

References

[1] D.H. Jones, S. Ley, A. Aitken, Isoforms of 14-3-3 protein can form homo- and heterodimers in vivo and in vitro: implications for function as adapter proteins, FEBS Lett. 368 (1995) 55-58.

[2] Y.M. Gu, Y.H. Jin, J.K. Choi, K.H. Baek, C.Y. Yeo, K.Y. Lee, Protein kinase A phosphorylates and regulates dimerization of 14-3-3 epsilon, FEBS Lett. 580 (2006) 305-310.

[3] A.K. Gardino, S.J. Smerdon, M.B. Yaffe, Structural determinants of 14-3-3 binding specificities and regulation of subcellular localization of 14-3-3-ligand complexes: a comparison of the X-ray crystal structures of all human 14-3-3 isoforms, Semin Cancer Biol. 16 (2006) 173-82.

[4] D.W. Powell, M.J. Rane, B.A. Joughin, R. Kalmukova, J.H. Hong, B. Tidor, W.L. Dean, W.M. Pierce, J.B. Klein, M.B. Yaffe, K.R. McLeish, Proteomic identification of 14-3-3zeta as a mitogen-activated protein kinase-activated protein kinase 2 substrate: role in dimer formation and ligand binding. Mol Cell Biol. 23 (2003) 5376-5387.

[5] J.M. Woodcock, J. Murphy, F.C. Stomski, M.C. Berndt, A.F. Lopez, The dimeric versus monomeric status of 14-3-3zeta is controlled by phosphorylation of Ser58 at the dimer interface, J Biol Chem. 178 (2003) 36323-36327.

[6] P. Man, C. Montagner, G. Vernier, B. Dublet, A. Chenal, E. Forest, V. Forge, Defining the interacting regions between apomyoglobin and lipid membrane by hydrogen/deuterium exchange coupled to mass spectrometry, J Mol Biol. 368 (2007) 464-72.

[7] A. Sinz, Chemical cross-linking and mass spectrometry to map three-dimensional protein structures and protein-protein interactions, Mass Spectrom Rev. 25 (2006) 663-682.

[8] S. Kalkhof, C. Ihling, K. Mechtler, A. Sinz, Chemical cross-linking and high-performance Fourier transform ion cyclotron resonance mass spectrometry for protein interaction analysis: application to a calmodulin/target peptide complex, Anal Chem. 77 (2005) 495-503.

[9] V. Obsilova, P. Herman, J. Vecer, M. Sulc, J. Teisinger, T. Obsil, 14-3-3zeta C-terminal stretch changes its conformation upon ligand binding and phosphorylation at Thr232, J Biol Chem. 279 (2004) 4531-4540.

[10] J.A. Smith, Analysis of Proteins, in F. Ansubel (Ed.), Short Protocols in Molecular Biology, John Wiley & Sons, Inc., 1995. pp. 10.5-10-11.

[11] M. Sulc, P. Hodek, M. Stiborova, The binding affinity of carcinogenic N-nitrosodimethylamine and N-nitrosomethylaniline to cytochromes P450 2B4, 2E1 and 3A6 does not dictate the rate of their enzymatic N-demethylation, Gen Physiol Biophys. 29 (2010) 175-185.

[12] K.J. Wiechelman, R.D. Braun, J.D. Fitzpatric, Investigation of the bicinchoninic acid protein assay identification of the groups resposible for color formation, Anal Biochem. 17 (1988) 231-237.

[13] Y. Ma, S. Pitson, T. Hercus, J. Murphy, A. Lopez, J. Woodcock, Sphingosine activates protein kinase A type II by a novel cAMP-independent mechanism, J Biol Chem. 280 (2005) 26011-26017.

[14] A. Aitken, H. Baxter, T. Dubois, S. Clokie, S. Mackie, K. Mitchell, A. Peden, E. Zemlickova, Specificity of 14-3-3 isoform dimer interactions and phosphorylation. Biochem Soc Trans. 30 (2002) 351-360.

[15] Z. Guan, N. A. Yates, R. Bakhtiar, Detection and characterization of methionine oxidation in peptides by collision-induced dissociation and electron capture dissociation, J. Am. Soc. Mass Spectrom. 14 (2003) 605–613.

[16] E. Wilker, M.B. Yaffe, 14-3-3 Proteins--a focus on cancer and human disease. J Mol Cell Cardiol. 37 (2004) 633-642.

[17] H. Martin, Y. Patel, D. Jones, S. Howell, K. Robinson, A. Aitken, Antibodies against the major brain isoforms of 14-3-3 protein. An antibody specific for the N-acetylated amino-terminus of a protein, FEBS Lett. 331 (1993) 296-303.

[18] B. Fuller, S.M. Jr Stevens, P.C. Sehnke, R.J. Ferl, Proteomic analysis of the 14-3-3 family in Arabidopsis. Proteomics, 6 (2006) 3050-3059.

[19] T. Kouzarides, Acetylation: a regulatory modification to rival phosphorylation? EMBO J. 19 (2000) 1176-1179.

Table 1 Characterization of purified recombinant human 14-3-3ζ proteins.

Quantity [Unit] Purified protein	Additional N-terminal aminoacid residues before starting methionine (1)M	Protein concentration [mg/mL]	Sequence coverage [%]	Matched/ Searched peptides
NHis-14-3-3ζWT	(-19)GSSHHHHHHSSGLVPRGSH-(1)M	6.52±0.32	81	23/24
NHis14-3-3ζS58D	(-19)GSSHHHHHHSSGLVPRGSH-(1)M	4.37±0.25	82	22/23
14-3-3ζWT	(-3)GSH-(1)M	8.15±0.37	77	38/40
14-3-3ζS58D	(-3)GSH-(1)M	2.45±0.2	73	38/39

Legend: Numbers in the table are averages±S.D. of three parallel experiments. Assay conditions are described in Section 2. MALDI-TOF peak lists were searched manually against a protein sequences with peptide mass tolerance ± 50 ppm.

Table 2 Identified EDC cross-linked products in 14-3-3ζ homodimer by LC-FTICR mass spectrometry.

	$[M+H]^+$ experimental	$[M+H]^+$ calculated	Error [ppm]	molecule (1)	molecule (2)
1				4-11	81-83
	1377.74780	1377.74890	0.8	NELVQKAK	EYR
				(-3)-11	81-83
	2033.02090	2033.02370	1.4	GSHMDKNELVQKAK	EYR
				(-3)-11+ox-M	81-83
	2049.01429	2049.01860	2.1	GSHMDKNELVQKAK	EYR
2				(-3)-9	81-83
	1833.88845	1833.88669	1.0	GSHMDKNELVQK	EYR
				(-3)-9+ox-M	81-83
	1849.88160	1849.88660	2.7	GSHMDKNELVQK	EYR
3				(-3)-9	69-74
	2000.96680	2000.97110	2.1	GSHMDKNELVQK	TEGAEK
				(-3)-9+ox-M	69-74
	2016.96250	2016.96590	1.7	GSHMDKNELVQK	TEGAEK

Legend: underlined aminoacids in peptide sequences label a deduced EDC reactive residues and ox-M marks an oxidized methionine.

Figures

Figure 1 Monitoring of 14-3-3ζ homodimer formation using increasing concentration of EDC

(A) 14-3-3ζWT and NHis-14-3-3ζWT, (B)14-3-3ζS58D and NHis-14-3-3ζS58D, on 12% SDS-PAGE (Coomassie Brilliant Blue R-250 staining, Sigma wide-range molecular weight standards). Arrow labels the homodimeric product and asterisk marks monomer.

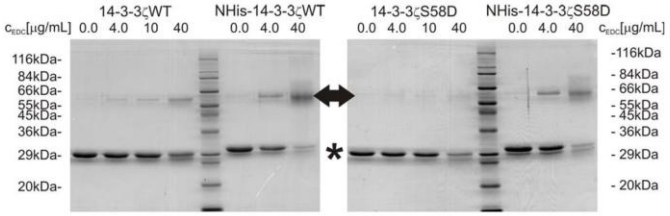

15

Figure 2 Kinetics for H/D back-exchange for selected peptides generated from dimeric 14-3-3ζWT and monomeric 14-3-3ζS58D by pepsin proteolysis.

Kinetics is shown for times between 1min and 24hr of back-exchange (x-axis correspond logarithmic scale of time in seconds). The y-axis represents percentage of H/D back-exchange (average value of two parallel experiments). The numbers for the first and last aminoacids of the peptide are shown on the top left corner of each graph. Symbols in the graphs: (blue square) 14-3-3ζS58D; (red circle) 14-3-3ζWT.

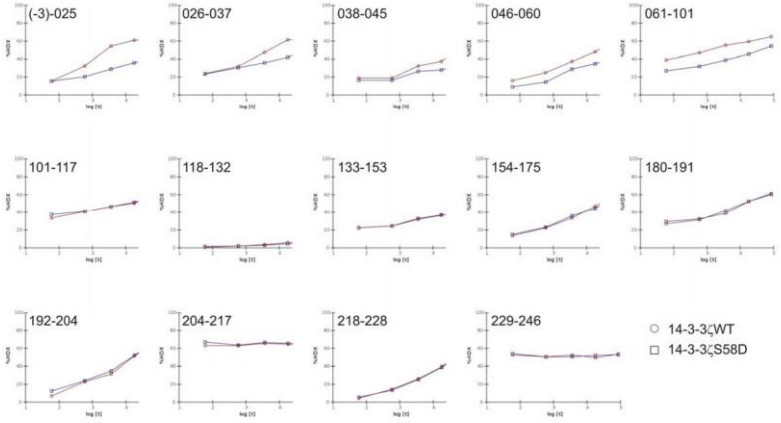

16

Figure 3 Acquired MS/MS spectra after trypsin digestion of 14-3-3 homodimer band and corresponding covalently cross-linked structures using EDC with detected fragments ions.

The structures of covalently cross-linked (A1) Lys9-Glu81, (B1) Lys9-Glu81, (C1) N-terminal amino group-Glu81, or (D1) N-terminal amino group-Glu70, determined from MS/MS daughter ion spectra of detected peak at *m/z* 1377.7 (A2), *m/z* 2048.85 (B2), *m/z* 1833.88 (C2) or *m/z* 2016.93 (D2). Masses of fragments that lost the methanesulfenic acid (-64 Da) from oxidized methionine are given in parentheses [15]. The residue numbering corresponds that of the full-length sequence of the 14-3-3 (UniProtKB database accession number P63104). Intens., intensity.

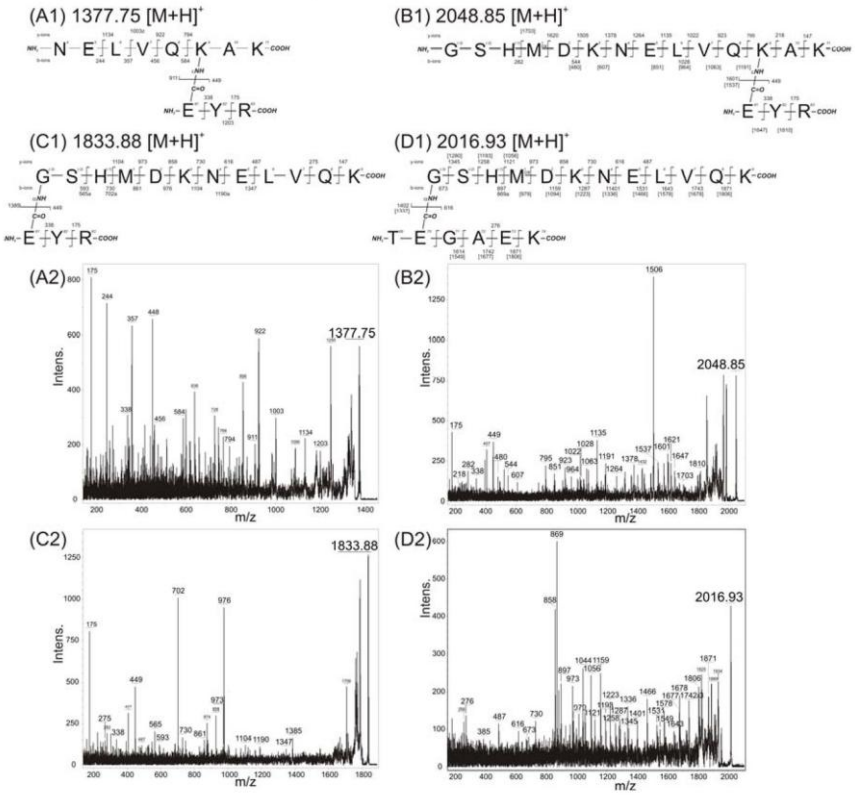

3.1.2. Mapování interakcí mezi membránovými proteiny cytochromem b_5 a cytochromem P450 2B4

v publikaci

Mapping of Interaction between Two Membrane Proteins, Cytochrome b_5 and P450 2B4 - Enlargement of P450 2B4 Binding Site for Cytochrome b_5

Šulc M., **Pavlásková K**., Ječmen T., Novák P., Martínek V., Stiborová M., Hudeček J., Hodek P.

Arch Biochem Biophys. (odesláno do redakce dne 16.7.2011)

Prohlášení spoluautorů

„Prohlašuji, že Kateřina Pavlásková se patřičně podílela (40 %) na plánování experimentů, jejich měření, interpretaci výsledků a sepisování této publikace.“

V Praze dne:

Doc. RNDr. Miroslav Šulc, PhD.

Mapping of Interaction between Two Membrane Proteins, Cytochrome b_5 and P450 2B4 – Enlargement of P450 2B4 Binding Site for Cytochrome b_5

Miroslav Šulc[1,2,*], Kateřina Pavlásková[1,2,*], Tomáš Ječmen[2], Petr Novák[1], Václav Martínek[2], Marie Stiborová[2], Jiří Hudeček[2], Petr Hodek[2]

[1]*Institute of Microbiology Academy of Sciences of the Czech Republic, v.v.i., Vídeňská 1083, 14220 Prague 4, Czech Republic*
[2]*Department of Biochemistry, Faculty of Science, Charles University, Hlavova 2030, 12843, Prague 2, Czech Republic*

[*]Equal authorship

To whom correspondence should be addressed:
Prof. Petr Hodek; Department of Biochemistry, Faculty of Science, Charles University, Hlavova 2030, 12843, Prague 2, Czech Republic; email: hodek@natur.cuni.cz; tel. +420-221951285; fax. +420221951283

Abbreviations: cytochrome P-450, P450; DLPC, dilauroylphosphatidylcholine; EDC, 1-ethyl-3-[3-dimethyl(aminopropyl)]carbodiimide hydrochloride; MALDI-TOF, matrix assisted laser desorption/ionization-time of flight; LC-FTICR MS, liquid chromatography coupled with Fourier transform ion cyclotron resonance mass spectrometry; MeCN, acetonitrile; SDS-PAGE, one dimensional sodium dodecylsulfate polyacrylamide gel electrophoresis; TCEP, Tris(2-carboxymethyl) phospine hydrochloride.

Abstract

The chemical cross-linking by soluble carbodiimide (EDC) in combination with the high resolution mass spectrometry has been employed to characterize contact surface regions involved in the transient interaction between two membrane proteins, cytochrome P-450 2B4 (P450 2B4) and cytochrome b_5. This reaction was accomplished in equimolar catalytic complex of P450 2B4:cytochrome b_5 that revealed stimulatory

effect on P450 2B4 *O*-depentylation activity of 7-pentoxy resorufine in reconstituted system with NADPH:P450 reductase. The covalent P450-cytochrome b_5 hetero-dimers detected on SDS-PAGE were analyzed (after in gel digestion with trypsin) using LC-FTICR mass spectrometry to identify crosslinked amino-acid residues.

Four P450 2B4 amino-acid residues, Asp134, Lys139, Glu424 and Glu439, located on P450 2B4 proximal surface have been found to participate in the interaction with cytochrome b_5. Moreover, our data extend the cytochrome b_5 site towards the region previously predicted exclusively for NADPH:P450 reductase and support the idea of overlapping P450 2B4 binding sites for both these proteins. The computed *in silico* models of P450 2B4:cytochrome b_5 complex using amino-acids detected in cross-links suggest two different types of cytochrome b_5 orientations: the first allowing potential cytochrome b_5 electron donation to P450, the second one only cytochrome b_5 induced modulation of P450 structural changes.

Based on our findings, the used experimental approach is a suitable to map interaction between two membrane proteins in the lipid environment preserving their native structures.

Key words: protein-protein interaction, chemical cross-linking, mass spectrometry, cytochrome b_5, cytochrome P-450 2B4

Introduction

In the history of the investigation of protein–protein interactions, the first mention of cytochrome b_5 was in case of interaction with cytochrome c. The first structural model of this complex was published in 1976 using crystalografic structures of both individual components [1]. From that time, the structural characterization of this complex has been vigorously attempted by many experimental techniques and all results clearly point out that the interaction is driven mainly by electrostatic interactions under a physiological pH. Cytochrome b_5 has two negative patches capable of interaction with a single positive surface area of cytochrome c [2].

On the other hand, the detailed mechanism and functional consequences of cytochrome b_5 and cytochrome P-450 (P450) interaction remain to be solved. Both these membrane hemoproteins compose together with flavoprotein NADPH:P450

reductase a mixed function oxidase (MFO) system localized in the endoplasmic reticulum [3]. The crucial function of this MFO system consist in the monooxygenation of mainly hydrophobic compounds resulting in detoxification of xenobiotics and/or metabolism of endogenous substrates. Unfortunately the detoxification of some xenobiotics is sometimes reversed to produce compounds more toxic/carcinogenic that are able to modify biomolecules such as DNA, RNA and proteins with negative consequences for organism [4]. Thus, P450s are known to be involved in the activation of some chemical carcinogens.

The knowledge of the interaction between P450 and its redox partners (NADPH:P450 reductase and cytochrome b_5) is fundamental to understand not only reaction mechanism of P450 and electron transport from its redox partner but also to increase the knowledge about metabolism of xenobiotic with all positive or negative aspects for organism. The cytochrome b_5 has been shown to stimulate, inhibit or have no effect on activity of P450s depending on the P450 isoform, the substrate, and experimental conditions [for references see review 5]. In general, cytochrome b_5 has been suggested to act either as a mediator of electron flow to oxyferrous P450 [6] or as an allosteric modifier of the P450 system [7] infleuncing the P450 reaction rate or even the pattern of P450 produced metabolites [8,9]. The potential roles of cytochrome b_5 in P450 2B4 mediated catalysis have been recently well reviewed in literature [10,11]. The studied rabbit P450 2B4 isoform, is an orthologue to human P450 2B6, involved in oxidation of a number of structurally different carcinogens (e.g. nicotine, aflatoxin B1, styrene, and aminochrysene) and the drugs (e.g. diazepam, cyclophosphamide, iphosphamide, tamoxifen, antipyrine, and lidocaine) [for references see 12].

The chemical cross-linking is becoming a valuable tool for the low resolution structure determination of protein complexes in their native states. In combination with mass spectrometry analysis of the cross-linked products it is possible to determine cross-linked residues in a binary complex of proteins in a reasonable time-scale using small quantities of protein. Literature data prove this approach to be useful in solving the protein–protein interactions [for references see review 13]. One of these experimental approaches is to incubate cross-linker with two purified proteins of known amino-acid sequence to produce a mixture of covalently cross-linked heterodimers with several different amino-acid residues participating in novel covalent junction between

both these proteins. The abundance of these orientations statistically depends on presence of each species in reaction mixture. The next step is to separate monomers and heterodimers based on molecular weight of every product employing SDS-PAGE electrophoresis, then to digest cross-linked species to peptides using protease, and to analyze resulting peptide mixture by mass spectrometry with high accuracy. The high accuracy and high resolution MS data allows to determine the unique combination of two cross-linked peptide sequences that also fit to protease specificity (e.g. trypsin generates a peptides with C-terminal arginine or lysine). The deduction which two amino-acid residues participate in the covalent coupling of two cross-linked peptides is performed based on peptide sequence and reaction specificity of used chemical reagent. For example, a "zero length cross-linking reagent" 1-ethyl-3-[3-dimethyl(aminopropyl)]carbodiimide hydrochloride (EDC) reacts with a carboxyl group on the first protein, forming an amine-reactive O-acylisourea intermediate that may condenses with an amine on the second protein yielding a conjugate of the two molecules joined by a stable amide bond. The amide bond formed by reaction provides a neutral linkage of amino and carboxy-group of two closely located or interacting amino-acid residues. This provides enough information to estimate the distance between the two cross-linked residues and to map interacting interface in the protein complex studied. The zero-length cross-linker EDC is able to connect amine and carboxylic acid groups within distances of under 5 Å [14]. Our approach applied to study protein-protein interaction is similar to "bottom-up" approach that has previously been proven especially to determine valuable low-resolution three-dimensional structures of protein [15,16].

Here we present an application of chemical cross-linking in reconstituted systems containing purified native proteins incorporated into membrane. The identification of amino-acid residues participating in the interface between cytochrome b_5 and P450 2B4 may help to improve in elucidation of the function of this protein-protein interaction in the P450 reaction mechanism.

Material and methods

2.1. Chemicals

7-pentoxyresorufine (7-pentyl-7-hydroxy-3-H-phenoxazin-3-one) and bovine serum albumin were purchased from Sigma Chemical Co. (St. Louis, USA). 1-ethyl-3-[3-dimethyl(aminopropyl)]carbodiimide hydrochloride (EDC), Coomassie Brilliant Blue R-250, dilauroylphosphatidylcholine (DLPC), formic acid, iodoacetamide, Tris(2-carboxymethyl) phospine hydrochloride (TCEP) and pyridine were from Fluka Chemical Co. (St. Louis, USA). Phenobarbital was from Kulich Co. (Hradec Králové, Czech Republic), bicinchoninic acid from Pierce (Rockford, USA), trypsin from Promega (Madison, USA), acetonitrile (MeCN) and water of LiChrosolv quality from Merck (Darmstadt, Germany). The other chemicals were obtained from Lachema (Brno, Czech Republic).

2.2. Purification of P450 2B4, cytochrome b_5 and NADPH:P450 reductase and their characterization

All proteins were purified from microsomes prepared from rabbit liver using previously described analogous procedures [17]. To induce protein expression of all purified enzymes, previously described animal pre-treatment with phenobarbital was used [18]. The electrophoresis (SDS-PAGE) was used to confirm protein homogeneity and purity [19]. Each protein band was analyzed by mass spectrometry after trypsin digestion to confirm sequences of all pure proteins. The total P450 content was measured based on complex of reduced P450 with carbon monoxide [20], the total NADPH:P450 reductase or cytochrome b_5 content were determined using absorbance of the purified protein at 455 nm or at 412 nm, respectively [21]. Protein concentrations were assessed using bicinchoninic acid and bovine serum albumin as a standard [22].

2.3. O-depentylation of 7-pentoxyresorufine by purified proteins in reconstituted system

The preparation of reconstituted system in DLPC vesicles as well as an optimal ratio of P450 2B4 and NADPH:P450 reductase was estimated as described previously [17]. Briefly, the optimal ratio of P450 2B4 and cytochrome b_5 was determined using P450 2B4 specific 7-pentoxy resorufine-*O*-depentylase activity with 30 μM substrate,

2 μM P450 2B4 and 2 μM NADPH:P450 reductase using a fluorescence spectrometer LS55 ($\lambda_{excitation}$ 530 nm, $\lambda_{emission}$ 588 nm, PerkinElmer, Waltham, USA) after 10 min incubation at 37 °C in 0.15 mM DLPC vesicles, 50 mM pyridine:HCl buffer (pH 6.5) and 150 mM sodium chloride. Three different P450 2B4:cytochrome b_5 ratios were tested (1:1, 1:2, and 1:4). Experiments with increasing concentration of sodium salt (0, 50, 150, and 500 mM) were performed in the same system with P450 2B4, NADPH:P450 reductase and cytochrome b_5 in 1:1:1 molar ratio.

2.4. Cross-linking, separation and proteolysis of cross-linked products

The cross-linking reaction with 0.05 mg/mL of EDC was carried out with 2 μM P450 2B4 and 2 μM cytochrome b_5 in reconstituted system containing 0.15 mM DLPC and 50 mM pyridine-HCl buffer (pH 6.5) for 10 hrs in final volume of 20 μL at 37 °C in a shaking incubator. The concentration of NaCl was adjusted in individual samples to 0, 50, 150 and 500 mM. The EDC cross-linking reaction was quenched by 2-mercaptoethanol present in electrophoresis sample buffer, and after boiling and centrifugation the sample was loaded on SDS-PAGE. The electrophoretically separated protein bands were visualized using 0.25% (w/v) Coomassie Brilliant Blue R-250. The excised protein spots from SDS-PAGE gel were de-stained, all cysteine residues in protein bands were modified using TCEP and iodoacetamide, and processed for MALDI-TOF mass spectrometry by in-gel digestion with trypsin as described previously [17]. The mixture of extracted peptides was applied on a peptide micro-trap microcolumn (Michrom Bioresources, Auburn, CA, USA) to remove any salt and buffer components prior to LC-MS analysis.

2.5. LC-FTICR MS analysis

The peptides eluted from the micro-trap were dried on rotation vacuum concentrator (SPEED-VAC, Savant, USA) and dissolved in 5% aqueous MeCN containing 0.1% formic acid under sonication. A portion (5 μL) was loaded onto a reverse-phase column (Magic C18, 0.3 mm diameter, 150 mm long, 5 μm particle size, 200 Å pore size, Michrom Bioresources, Auburn, CA, USA) and eluted using gradient mobile phase: solvent A, 0.1% formic acid in 5% aqueous MeCN; solvent B, 0.08% formic acid in 90% aqueous MeCN; gradient (in % B buffer), 0% for 1 min, 0–15% in

4 min, 15–60% in 30 min, 60–100% in 5 min; flow rate, 3 μL/min. All chromatographic separations were performed at 20 °C using an Ultimate 1000 capillary HPLC system (LC Packings, Amsterdam, The Netherlands). The column effluent was directly interfaced to an APEX Qe FTICR mass spectrometer equipped with a 9.4 T superconducting magnet and an ion Combi Source (Bruker Daltonics, Billerica, MA, USA). Mass spectra were obtained by accumulating ions in the collision hexapole and running the quadrupole mass filter in non mass-selective RF-only mode so that ions of a broad *m/z* range (300–2000) were allowed to enter the analyzer cell. All spectra were acquired in positive ion mode.

2.6. Data analysis

Data Analysis software package (Bruker Daltonics) and macro for LC-MS data reduction (Sandia National Laboratories Livermore, CA, USA and Institute of Microbiology, Prague, Czech Republic) were used to create output files of monoisotopic masses as described previously [23]. Every received monoisotopic mass was automatically matched to a theoretical library of cross-linked, modified and/or unmodified proteolytic products using protein sequences from UniProtKB database (CP2B4_RABIT, CYB5_RABIT). Sequence alignments of rabbit P450 2B4 and human P450s 1A1, 1A2, 2B6 and 2E1 were generated using Clustal X version 2.0.12 program [24].

2.7. Protein-protein docking

In silico protein-protein docking of rabbit P450 2B4 and soluble domain of rabbit cytochrome b_5 was performed using the flexible docking approach implemented in program HADDOCK. This software utilizes information on predicted protein interfaces for ambiguous interaction restraints to drive the docking process. The recommended docking procedure is in detail described elsewhere [25]. Three approaches how to utilize the experimental data have been applied. In the first one, one of the two pairs of identified covalent cross-links, that do not mutually exclude, (A) Glu424 (P450 2B4)-Lys24 (cytochrome b_5) and Glu439 (P450 2B4)-Lys19 (cytochrome b_5) or (B) Glu424 (P450 2B4)-Lys91 (cytochrome b_5) and Lys139 (P450 2B4)-Asp8 (cytochrome b_5), respectively, were given as constrain distances of protein-protein interaction. Secondly,

the docking calculation was performed using all P450 2B4 amino-acid residues (Asp134, Lys139, Glu424 and Glu439) determined in cross-links as active "anchors" of protein-protein interaction. In the last approach, the identified covalent cross-link Glu424 (P450 2B4)-Lys24 (cytochrome b_5) was used as a distance constrain of protein-protein interaction. For all three approaches all charged residues exposed on the both P450 2B4 and cytochrome b_5 surfaces were considered to be passively involved in this protein-protein interaction, no penalty was imposed if a passive residue was not directly involved in the mentioned interaction In order to extend the number of individual mutual orientations of both proteins the default values of (i) number of structures for rigid body docking, (ii) number of trials for rigid body minimisation and (iii) number of structures for the explicit solvent refinement were doubled and the optional solvated docking was performed.

We used our homologous model of truncated rabbit P450 2B4 [26] as a starting structure representing the P450 2B4. The soluble domain of the rabbit cytochrome b_5 protein with heme cofactor, obtained based on PDB coordinates 1DO9 from RCSB protein databank [27] was considered as the second starting structure.

Results and Discussion

The methods of chemical cross-linking and mass spectrometry were used for the mapping of protein interface between two membrane proteins, P450 2B4 isoform and cytochrome b_5. To accomplish our goal, the highly purified and well characterized proteins (P450 2B4 isoform, cytochrome b_5 and for metabolic activity measurements NADPH:P450 reductase) were obtained from liver homogenate up to the electrophoretical homogeneity employing techniques preserved a native structure of these proteins. The MALDI-TOF mass spectrometry analysis of trypsinized proteins using mass fingerprinting approach confirmed the identity of all three proteins (for individual values of MASCOT score and protein sequence coverage see Table 1). High number of matched peptides from all searched *m/z* signals received in MASCOT results indicated purity of all three proteins. Every protein sample was also characterized by determination of both protein and molar concentrations (for results see Table 1).

<Table 1 here>

All purified proteins were fully active in the reconstituted system (in the P450 2B4 selective *O*-depentylation of 7-pentoxy resorufine). This measurement characterized an optimal composition of studied *in vitro* system in respect of protein, lipid (DLPC) and/or substrate concentrations [17]. Also the conditions used in chemical cross-linking experiments and optimal for EDC chemistry (pyridine buffer, pH 6.5) were examined. The observed metabolic activity of P450 2B4 isoform without cytochrome b_5 in reconstituted system in pyridine buffer (pH 6.5) was 22.8±1.8 nmol resorufine/min.nmol P450 (100% of determined control activity). This type of buffer and its pH resulted in slight decrease of P450 activity compared to determined activity in phosphate buffer (pH 7.4) (33.9±1.9 nmol resorufine/min.nmol P450). Three molar ratios of P450 2B4:cytochrome b_5 (1:1, 1:2 or 1:4) revealed 162%, 82%, or 44% of P450 2B4 metabolic activity, respectively. The equimolar concentration of cytochrome b_5 stimulated the P450 2B4 activity as described earlier [5,28]. Two or four fold molar excess of cytochrome b_5 inhibited *O*-depentylase activity of P450 2B4, probably by competition of cytochrome b_5 with NADPH:P450 reductase for the binding site on the P450 2B4 surface, as already suggested [11,28,29].

The chemical cross-linking method using zero-length cross-linker EDC yields in a covalent heterodimeric product of cytochrome b_5:P450 2B4 complex reconstituted in membrane of dilauroyl phosphatidyl choline (labeled by arrow in the Figure 1). Similar experiment in presence of NADPH:P450 reductase in addition to cytochrome b_5 and P450 2B4 was also performed, but production of cytochrome b_5:P450 2B4 covalent heterodimeric product was not affected (data not shown). Increasing salt content (0–500 mM of NaCl) did not prevent formation of the cytochrome b_5:P450 2B4 cross-linked product and cytochrome b_5:P450 2B4 complex was still detectable even at the highest concentration (500 mM) of sodium chloride (albeit in somewhat lower amount). To compare these chemical cross-linking results with metabolic assay, the effect of increasing ion strength (50–500 mM of NaCl) was also tested using P450 2B4 dependent 7-pentoxy resorufine dealkylation in the presence of equimolar amount of cytochrome b_5. These metabolic activities were consistent with our chemical cross-linking experiments. The results of both experimental approaches suggest not only the electrostatic character of the interaction but also a significant contribution of

hydrophobic effect in the formation of cytochrome b_5:P450 2B4 binary complex. This data are in agreement with published data [30,31].

<Figure 1 here>

To identify individual components of the complex MALDI-TOF MS analysis of trypsin-digested protein band (cytochrome b_5:P450 2B4 indicated by arrow on SDS-PAGE in Figure 1) was employed and resulted in the 61% of cytochrome b_5 and 55% of P450 2B4 sequences coverage, respectively.

To locate the cross-linked regions and the residues involved in cytochrome b_5:P450 2B4 complex, the LC-MS with nano-electrospray ionization and high resolution FT-ICR detection was used and obtained dataset of experimental *m/z* values was automatically reduced to produce output files of monoisotopic masses. Every observed monoisotopic mass was searched against a database of theoretical monoisotopic masses of cross-linked products: mass of any P450 2B4 trypsinised peptide plus mass of any cytochrome b_5 trypsinised peptide minus mass of water eliminated during EDC cross-linking reaction. Table 2 presents (in each row) the experimentally observed and corresponding calculated *m/z* values, mass error of calculated and experimental *m/z* values (maximally 2 ppm) and sequence of the covalently cross-linked peptides. All identified peptide sequences permitted to deduce only one possible combination of the covalent cross-link (see Table 2). For example, the experimental monoisotopic $[M+H]^+$ mass *m/z* value 2479.2371 revealed the unique combination of P450 2B4 peptide DFGMGKRSVEERIQEEAR and cytochrome b_5 peptide DVK with an error 0.4 ppm. Both these peptides generated using trypsin in the step of proteolytic digestion contain C-terminal arginine or lysine. The ε-NH_2 group of C-terminal lysine in the peptide DVK derived from cytochrome b_5 can be excluded as an cross-link component, because it is distinguished and cleaved by trypsin, and only β-carboxylate of aspartic acid (Asp8) in cytochrome b_5 peptide DVK allows the cross-linking reaction with any amino group of P450 2B4 peptide (EDC couples carboxyl groups of side chain residues as well as protein C-termini to primary amine of either lysine or protein N-termini). There is only one epsilon amino group (Lys139) within P450 2B4 peptide DFGMGKRSVEERIQEEAR.

Using similar approach, all other amino-acid residues involved in protein-protein interface of cytochrome b_5:P450 2B4 binary complex were deduced (Asp134, Lys139,

Glu424 and Glu439). All these P450 2B4 amino-acid residues (underlined in sequences in Table 2) are located on the P450 2B4 proximal surface (Figure 2).

<Table 2 here>

<Figure 2 here>

Two identified P450 2B4 amino-acid residues, Asp134 and Lys139, are located within region of C/C* α-helices and their termini. It was postulated, that both P450 redox partners (cytochrome b_5 and NADPH:P450 reductase) bind P450 at the highly dynamic C-helix (region (A) see Figure 3), then P450 molecule undergoes a conformational change to facilitate proton delivery to the reduced oxyferrous intermediate and subsequent formation of the catalytically active oxyferryl intermediate [5]. Also amino-acid residue Lys433 was predicted to be in contact with cytochrome b_5 [11,29]. This P450 2B4 Lys433 is situated in the close vicinity of P450 2B4 amino-acid Glu434 and Glu439 (identified in our cross-linking experiment), which are located in region starting at the meander of β-bulge and ending at the beginning of L α-helix (region (B) in Figure 3).

High level of sequence homology even identity within these both P450 regions (A and B) has been demonstrated in sequence alignment analysis of several human P450 (P450 2B6, 2E1, 1A1 and 1A2) using Clustal X software (Figure 3). For example, our sequence alignment revealed identical amino-acid residues in human P450 2B6 and 2E1 in the position of P450 2B4 Lys139. Also high level of identity was found for both P450 2B4 amino-acid Glu434 and Glu439 in all presented sequences (P450 2B6, 2E1, 1A1 and 1A2).

<Figure 3 here>

Interestingly, mainly positively charged basic amino-acid residues were directly predicted on P450 proximal surface to bind cytochrome b_5 or NADPH:P450 reductase so far (literature data are summarized in Table 3). The negatively charged acidic amino-acids were assigned only to compensate basic charge of residues located in their vicinity by ion-pairing (e.g. Asp134-Arg133, Glu143-Lys139, Glu424-Arg422, Glu439-Arg443).

Our cross-linking experiment gives evidence that three P450 2B4 acidic residues (Asp134, Glu424 and Glu439) are exposed on the P450 2B4 proximal surface (Figure 2) and are also in contact with cytochrome b_5 molecule. The P450 2B4 Glu424 and Glu439

were previously predicted to form ion-pairs with Arg422 and Arg443. Both these arginine residues were exclusively described to be involved in binding of NADPH:P450 reductase [29]. Therefore we propose that two highly conserved Glu424 and Glu439 found within the region (B) of P450 2B4 (Figure 3), extend the size of previously described P450 2B4 binding site for cytochrome b_5**.** This conclusion is in agreement with data obtained for P450 2E1 [32].

<Table 3 here>

To support our findings, *in silico* simulation of P450 2B4:cytochrome b_5 interaction the protein-protein docking method was used. We have employed semi flexible half-blind docking approach using contemporary modeling procedures implemented in program HADDOCK [25]. Because some of identified covalent cross-links are mutually incompatible, we have performed flexible docking taking into account maximal number of covalent cross-links (Table 2). Simulation resulted in two possible orientations (A, B) fitting two unique cross-links (Figure 4). Orientation A corresponds to cross-linked Glu424 (P450 2B4)-Lys24 (cytochrome b_5) and Glu439 (P450 2B4)-Lys19 (cytochrome b_5). The second set of cross-links, Glu424 (P450 2B4)-Lys91 (cytochrome b_5) and Lys139 (P450 2B4)-Asp8 (cytochrome b_5), is adopted in orientation B. The proposed membrane orientation and distance between hydrophobic layer of membrane and C-terminus of cytochrome b_5 using OPM database [33] is acceptable in both calculated binary complexes (Figure 4). In these complexes cytochrome b_5 heme is oriented out of P450 2B4 proximal surface, thus only P450 2B4:cytochrome b_5 interactions may result in allosteric modulation of P450 metabolic activity.

<Figure 4 here>

Since the cytochrome b_5 has been suggested as an electron donor of P450 2B4 we searched for additional orientations of P450 2B4:cytochrome b_5 in their complex [34]. The protein docking was driven to find the most favorable interaction between P450 2B4 and cytochrome b_5, based on P450 2B4 residues Asp134, Lys139, Glu424 and Glu439 involved in cross-links (Figure 5). HADDOCK score of the top structure was -213.7 +/- 17.0 a.u. with high contribution of electrostatic interactions to the resulting score. These findings are in a good agreement with predominant stabilization of protein-protein complex by complementary charged residues suitably pre-organized

on the contact interface [11,29]. Our results of chemical cross-linking experiments supported by metabolic assay results studying the effect of increasing ion strength (50–500 mM of NaCl) suggested also significant contribution of hydrophobic effect in the cytochrome b_5:P450 2B4 binary complex formation. This argument is supported by the large calculated inter-molecular contact area (the buried surface area in the P450 2B4 and cytochrome b_5 binary complex was calculated as 2050 +/- 80 $Å^2$). Probably the extensive and tight van der Waals contacts in this interaction domain can protect the ionic pairs formed from the access of solvent and in this way stabilize the protein complex against the disruption by high salt concentration. Although we cannot perform the protein-protein docking in system associated with membrane directly, the relative orientation of the P450:cytochrome b_5 binary complex to the membrane can be deduced. We used the proposed membrane orientation available in OPM database [33] and obtained approximately 54 Å distance between hydrophobic layer of membrane and C-terminus of cytochrome b_5 in calculated binary complex (Figure 4A). This is consistent with the length of 22 amino acids segment between the C-terminal residue of used soluble domain of rabbit cytochrome b_5 (model 1DO9) and first hydrophobic residue of its proposed membrane anchor (Trp109). If all 22 amino acids of the linker were extended like a parallel β-sheet, the maximal distance is 75 Å (3.4 Å/residue) and is sufficient to facilitate proposed mutual orientation of P450 2B4:cytochrome b_5 also in membrane environment. Moreover, this docking model suggest a close interaction in place of the identified covalent cross-link Glu424 (P450 2B4)-Lys24 (cytochrome b_5). The subtracted distance between nitrogen atom of lysine amino-group (cytochrome b_5 Lys24) and carbon atom of glutamic acid carboxy-group (P450 2B4 Glu424) was 3.42 Å. This is in agreement with the proposed maximal distances of 5 Å for that the cross-linker EDC is be able to connect amine and carboxylic acid groups [14]. When the cross-link was used as constrain distance of the protein-protein interaction almost identical model was obtained (values of top structure: HADDOCK score was -159.1 +/- 11.0 a.u., the buried surface area was 1400 +/- 60 $Å^2$).

<Figure 5 here>

The P450:cytochrome b_5 binary complex, shown in Figure 5, revealed interesting data of cytochrome b_5 heme propionate interaction with P450 2B4 Arg133 exposed on the P450 proximal surface. This P450 2B4 Arg133 was previously

suggested to be buried in P450 cavity to interplay of electrostatic pairing of the P450 heme propionates [for references see 35]. In that previous work, the additional role of this P450 2B4 Arg133 has been discussed using the detailed analysis of distances between this P450 2B4 Arg133 and P450 heme propionates in available P450 2B4 crystal structures with or without substrate/inhibitor. We have found, that substrate/inhibitor binding into P450 cavity caused the P450 2B4 Arg133 movement away from the P450 heme propionate towards the proximal surface of P450 2B4. Then this P450 2B4 Arg133 exposed on P450 proximal surface is available to interact with cytochrome b_5 heme propionate. The highly conserved basic residue was obtained in this P450 2B4 Arg133 position in sequence alignment analysis of four human P450 isoforms (P450 2B6, 2E1, 1A1 and 1A2). Therefore, a possible involvement of this basic amino-acid residue (P450 2B4 Arg133) in modulation of P450 2B4 metabolic activity by substrate and/or cytochrome b_5 (P450 redox partner) binding may thus reflect the cytochrome b_5 allosteric modulation of P450 metabolic activity or cytochrome b_5 mediation of electron flow to oxyferrous P450 reported in literature [6,7].

Taking together, our data are consistent with two mutual orientations of cytochrome b_5 and P450 in their complexes. First, which is depicted in the Figure 5, represents a commonly accepted cytochrome b_5 binding, when its heme is close to the proximal surface of P450. This orientation allows both cytochrome b_5 roles, the electron donation to P450 as well as the induction of cytochrome P450 structural changes, resulting in the stimulation of its catalytic activity. The second orientation, which takes into account always two cross-links, suggests so far unpredicted position of cytochrome b_5 towards P450. In this orientation (shown in Figure 4) the heme of cytochrome b_5 is exposed to solvent and its distance to P450 does not make an electron transfer possible. Likely, these two cross-linked orientations found in P450:cytochrome b_5 hetero-dimers represent only a part of more complex arrangement of both proteins in the membrane environment. This assumption is supported by the presence of trimer (band of molecular weight close to 100 kDa) containing two molecules of P450 and one of cytochrome b_5 (see Figure 1). Mass spectrometry analysis identified both proteins in this band, however a low amount of this cross-link, did not allow detailed identification of covalently linked amino acids.

Conclusions

The presented combination of chemical cross-linking techniques with mass spectrometry allowed us to study the protein-protein interface of the P450:cytochrome b_5 complex in the membrane environment corresponding to its physiological localization and function in organism. Four amino acid residues in P450 2B4 (Asp134, Lys139, Glu424 and Glu439) have been found to be in contact with the cytochrome b_5. The chemical cross-linking experiments were complemented by *in silico* modeling. We suggest that not only the basic amino-acid residues previously described in the literature, but also acidic amino-acid residues are involved in P450 2B4 binding site for cytochrome b_5 and they enlarge its area. Additionally, the interaction of residue Arg133 from cytochrome P450 2B4 with heme propionate side-chain from cytochrome b_5 was predicted *in silico*.

Acknowledgements

This paper is dedicated to our friend Dr. Petr Sedmera in memoriam. The study was supported by grants of the Grant Agency of Charles University (258179), the Ministry of Education of the Czech Republic (LC545), the Grant Agency of Czech Republic (303/06/0928, 305/09/H008, 301/10/0356 and 303/09/0472), and an institutional research concept of the Institute of Microbiology, Academy of Sciences of the Czech Republic (AV0Z50200510).

References

[1] F.R. Salemme, J Mol Biol. 102 (1976) 563–568.

[2] L. Banci, I. Bertini, I.C. Felli, L. Krippahl, K. Kubicek, J.J. Moura, A. Rosato, J Biol Inorg Chem. 8 (2003) 777-786.

[3] M.J. Coon, Nutr Rev. 36 (1978) 319-328.

[4] F.P. Guengerich, Human cytochrome P450 enzymes, in: P.R. Ortiz de Montellano (Ed.), Cytochrome P450: Structure, Mechanism, and Biochemistry, Kluwer Press, New York, 2005, pp. 377–531.

[5] H. Zhang, E. Myshkin, L. Waskell, Biochem Biophys Res Commun. 338 (2005) 499-506.

[6] C. Bonfils, C. Balny, P. Maurel, J Biol Chem. 256 (1981) 9457-9465.

[7] P. Hlavica, Arch Biochem Biophys. 228 (1984) 600-608.

[8] M.K. Akhtar, S.L. Kelly, M.A. Kaderbhai, J Endocrinol. 187 (2005) 267-274.

[9] M. Stiborová, V. Martínek, H.H. Schmeiser, E. Frei, Neuro Endocrinol Lett. (Suppl. 2) (2006) 35-39.

[10] U.H. Dürr, L. Waskell, A. Ramamoorthy, Biochim Biophys Acta. 1768 (2007) 3235-3259.

[11] S.-Ch. Im, L. Waskell, Arch Biochem Biophys. 507 (2011) 144-153.

[12] M. Stiborová, L. Borek-Dohalská, P. Hodek, J. Mráz, E. Frei, Arch Biochem Biophys. 403 (2002) 41-49.

[13] A. Sinz, Mass Spectrom Rev. 25 (2006) 663-682.

[14] S. Kalkhof, C. Ihling, K. Mechtler, A. Sinz, Anal Chem. 77 (2005) 495-503.

[15] M.M. Young, N. Tang, J.C. Hempel, C.M. Oshiro, E.W. Taylor, I.D. Kuntz, B.W. Gibson, D. Dollinger, Proc Natl Acad Sci USA. 97 (2000) 5802–5806.

[16] A. Sinz, J Mass Spectrom. 38 (2003) 1225–1237.

[17] M. Sulc, P. Hodek, M. Stiborova, Gen Physiol Biophys 29 (2010) 175-185.

[18] M. Sulc, B. Kubickova, V. Maslova, P. Hodek, Gen Physiol Biophys. 23 (2004) 423-433.

[19] J.A. Smith, Analysis of Proteins, in: F. Ansubel (Ed.), Short Protocols in Molecular Biology. John Wiley & Sons, Inc., 1995 pp. 10.5-10.11.

[20] T. Omura, R. Sato, J. Biol. Chem. 239 (1964) 2370-2378.

[21] J.L. Vermilion, M.J. Coon, J .Biol. Chem. 253 (1978) 2694-2704.

[22] K.J. Wiechelman, R.D. Braun, J.D. Fitzpatric, Anal. Biochem. 17 (1988) 231-237.

[23] J.S. Schoeniger, G. Kruppa, P. Novak and M. Young, Biophys J. 84(Part 2 Suppl. S) (2003) 356A–356A.

[24] J.D. Thompson, T.J. Gibson, F. Plewniak, F. Jeanmougin, D. G. Higgins, Nucleic Acids Res. 25 (1997) 4876-4882.

[25] S.J. de Vries, M. van Dijk, A.M.J.J. Bonvin, The HADDOCK web server for data-driven biomolecular docking, Nat. Protocols 5 (2010) 883-897.

[26] P. Hodek, B. Sopko, L. Antonovic, M. Sulc, P. Novák, H.W. Strobel, Gen Physiol Biophys. 23 (2004) 467-488.

[27] L. Banci, I. Bertini, A Rosato, S. Scacchieri, Eur J Biochem. 267 (2000) 755-766.

[28] H. Zhang, S.C. Im, L. Waskell, J Biol Chem. 282 (2007) 29766-29776.

[29] A. Bridges, L. Gruenke, Y.T. Chang, I.A. Vakser, G. Loew, L. Waskell, J Biol Chem. 273 (1998) 17036-17049.

[30] S.G. Nadler, H.W. Strobel, Arch Biochem Biophys. 261(1988) 418-429.

[31] J.B. Schenkman, A.I. Voznesensky, I. Jansson, Arch Biochem Biophys. 314 (1994) 234-241.

[32] Q. Gao, C.E. Doneanu, S.A. Shaffer, E.T. Adman, D.R. Goodlett, S.D. Nelson, J Biol Chem. 281 (2006) 20404-20417.

[33] M.A. Lomize, A.L. Lomize, I.D. Pogozheva, H.I. Mosberg, Bioinformatics 22 (2006) 623-625.

[34] J.B. Schenkman, I. Jansson, Drug Metab Rev. 31 (1999) 351-364.

[35] M. Sulc, J. Hudecek, M. Stiborova, P. Hodek, Neuro Endocrinol Lett. 29 (2008) 722-727.

Table 1

Characterization of purified rabbit liver microsomal P450 2B4, cytochrome b_5 and NADPH:P450 reductase.

Quantity [Unit] Purified protein	Protein concentration [mg/mL]	Specific content [nmol/mg]	Identified sequence code	MASCOT score	Sequence coverage [%]	Matched/ Searched peptides
P450 2B4	3.8±0.3	11.0	CP2B4_RABIT	288	46	26/28
cytochrome b_5	1.8±0.2	11.1	CYB5_RABIT	216	61	10/12
NADPH:P450 reductase	1.4±0.2	9.6	NCPR_RABIT	337	45	33/34

Legend: Numbers in the table are averages±S.D. of three parallel experiments. Assay conditions are described in Section 2. Mowse Score (Probability Based Mowse score is -10*Log(P), where P is the probability that the observed match is a random event. Scores greater than 54 were significant ($p<0.05$). MALDI-TOF peak lists were searched against a SwissProt protein database subset of the Other mammalia taxonomy group using MASCOT™ software with the following settings: enzyme chemistry - trypsin, missed cleavages 1, carbamidomethyl modification of cysteine, variable single oxidation of methionine and peptide mass tolerance ± 50 ppm.

Table 2

Identified EDC cross-linked products between cytochrome b_5 and P450 2B4 by LC-FTICR mass spectrometry.

P450 Region	$[M+H]^+$ experimental	$[M+H]^+$ calculated	Error [ppm]	P450 2B4 peptide	Cytochrome b_5 peptide
(A)	2479.2371	2479.2361	0.4	134-151 DFGMGKRSVEERIQEEAR	8-10 DVK
	2504.2917	2504.2878	1.6	126-140 RFSLATMRDFGMGKR	19-24 KHNHSK
	2657.4001	2657.3999	0.1	134-140 DFGMGKR	19-33 KHNHSKSTWLILHHK
(B)	1719.9058	1719.9076	1.0	435-443+CAM ICLGEGIAR	19-24 KHNHSK
	1785.9193	1785.9208	0.8	423-433+ox-M NEGFMPFSLGK	90-94 SKLSK
	3117.5918	3117.5955	1.2	423-434+ox-M NEGFMPFSLGKR	20-33 HNHSKSTWLILHHK

Legend: underlined amino-acids in peptide sequences label a reactive residue, ox-M marks an oxidized methionine and CAM means a cysteine modified with carbamidomethyl. Experimental conditions were as described in Section 2.

Table 3

Summarization of literature data related to identified P-450 region (A), Asp134 and Lys139, and region (B), Glu424 and Glu439, interacting with redox partners (cytochrome b_5, NADPH:P450 reductase) [29,32].

P450 isoform		methodology approach	P450 2B4	
			Region (A) Asp134, Lys139	Region (B) Glu424, Glu439
P450 2B4: cytochrome b_5	[29]	homology modeling and site direct mutagenesis	Arg133, Phe135, Met 137, Lys139	Lys433
		predicted function	NADPH:P450 reductase and cytochrome b_5 binding	cytochrome b_5 binding
P450 2B4: NADPH:P450 reductase	[29]	*in silico* modeling	-	Arg422, Arg443
		predicted function		exclusive interaction with NADPH:P450 reductase
P450 2E1: cytochrome b_5	[32]	chemical cross-linking and site direct mutagenesis	-	Lys428, Lys434
		homology modeling and site direct mutagenesis	Arg126	Lys422, Arg444
		predicted function		cytochrome b_5 binding

Figure Legends

Figure 1

Monitoring of cytochrome b_5:P450 2B4 heterodimer formation using EDC cross-linker in buffer with increasing concentration of sodium salt (0, 50, 150 and 500 mM) on 8% SDS-PAGE electrophoresis (Coomassie Brilliant Blue R-250 staining, Sigma wide-range molecular weight standards). Arrow labels the heterodimeric products and asterisk marks both monomers.

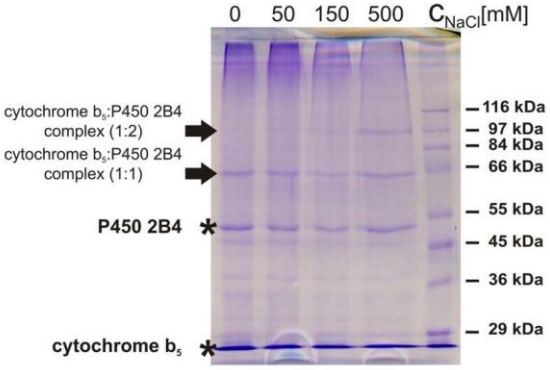

20

Figure 2. P450 2B4 solvent-accessible surface with colored electrostatic properties from front or side view. All found cross-linked amino-acid residues and heme are highlighted (heme – blue, Lys139 - green, Asp134, Glu424 and 439 – violet).The membrane associated part of the enzyme is positioned at bottom. (based on PDB coordinates published previously [26])

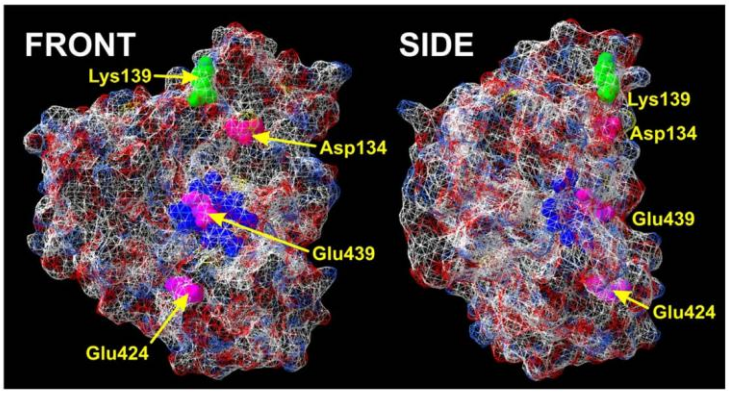

21

Figure 3

The multiple sequence alignment of two rabbit P450 2B4 sequence regions, amino-acid residues between 110-160 (A) and 396-452 (B), and corresponding regions of four human P450 isoforms (P450 2B6, 2E1, 1A1 and 1A2) using CLUSTAL X version 2.0.12 software.

```
REGION (A)                                   134  139
CYP2B4_RABIT.  110 GYGVIFA--NGERWRALRRFSLATMRDFGMGKRSV-------EERIQEEARCLVEELRKS 160
CYP2B6_HUMAN.  110 GYGVIFA--NGNRWKVLRRFSVTTMRDFGMGKRSV-------EERIQEEAQCLIEELRKS 160
CYP2E1_HUMAN.  111 DRGIIFN--NGPTWKDIRRFSLTTLRNYGMGKQGN-------ESRIQREAHFLLEALRKT 161
CYP1A1_HUMAN.  118 GQSMSFSPDSGPVWAARRRLAQNGLKSFSIASDPASSTSCYLEEHVSKEAEVLISTLQEL 177
CYP1A2_HUMAN.  120 GQSLTFSTDSGPVWAARRRLAQNALNTFSIASDPASSSSCYLEEHVSKEAKALISRLQEL 179
                    . .: *   .*  *   **::   :. :.:..          *.::..**. *:. *::

REGION (B)                                   424            439
CYP2B4_RABIT.  396 LHDPRYFETPNTFNPGHFLDANG---ALKRNEGFMPFSLGKRICLGEGIARTELFLFFTT 452
CYP2B6_HUMAN.  397 LHDPHYFEKPDAFNPDHFLDANG---ALKKTEAFIPFSLGKRICLGEGIARAELFLFFTT 452
CYP2E1_HUMAN.  397 LYDNQEFPDPEKFKPEHFLNENG---KFKYSDYFKPFSTGKRVCAGEGLARMELFLLLCA 453
CYP1A1_HUMAN.  415 NHDQKLWVNPSEFLPERFLTPDG-AIDKVLSEKVIIFGMGKRKCIGETIARWEVFLFLAI 473
CYP1A2_HUMAN.  415 NHDPELWEDPSEFRPERFLTADGTAINKPLSEKMMLFGMGKRRCIGEVLAKWEIFLFLAI 474
                    :* . :  *. * * :**  :*       .: .  *. *** * ** :*: *:**::
```

Legend: underlined bold amino-acids label a reactive residue in cross-linking experiments, italics means a predicted amino-acid residues involved in P450 2B4 [29] or P450 2E1 [32] interaction with cytochrome b_5. A line above the alignment is used to mark strongly conserved positions: an asterisk "*" indicates positions which have a single, fully conserved residue, a colon ":" indicates that one of the following 'strong' groups is fully conserved, and point "." indicates that one of the following 'weaker' groups is fully conserved. The strong and weak groups using Gonnet Pam250 matrix are defined as strong score > 0.5 and weak score =< 0.5 respectively. Experimental conditions were as described in Section 2.

Figure 4. The structure of the cytochrome b_5:P450 2B4 binary complex prepared using PyMOL protein-protein docking calculations with constrain distances (orientation A) Glu424 (P450 2B4)-Lys24 (cytochrome b_5) and Glu439 (P450 2B4)-Lys19 (cytochrome b_5) or (orientation B) Glu424 (P450 2B4)-Lys91 (cytochrome b_5) and Lys139 (P450 2B4)-Asp8 (cytochrome b_5), respectively. The membrane association of the P450 2B4 is positioned at the bottom.

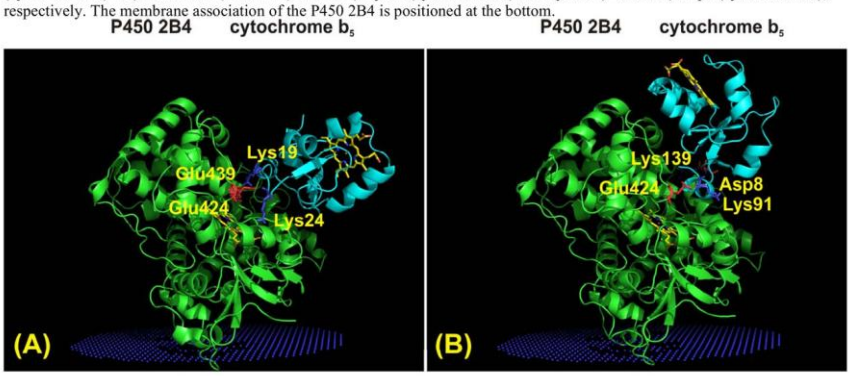

23

Figure 5. The structure of the cytochrome b_5:P450 2B4 binary complex predicted by protein-protein docking calculations (A) and its detailed view within the interface of this complex (B) prepared using PyMOL. The EDC covalently cross-linked P450 2B4 amino-acid residues (Asp134, Lys139, Glu424 and Glu439) are rendered as sticks (yellow). The interaction of cytochrome b_5 heme propionate (green) with P450 2B4 Arg133 (orange) is represented as dashed line. The membrane association of the P450 2B4 is positioned at the bottom.

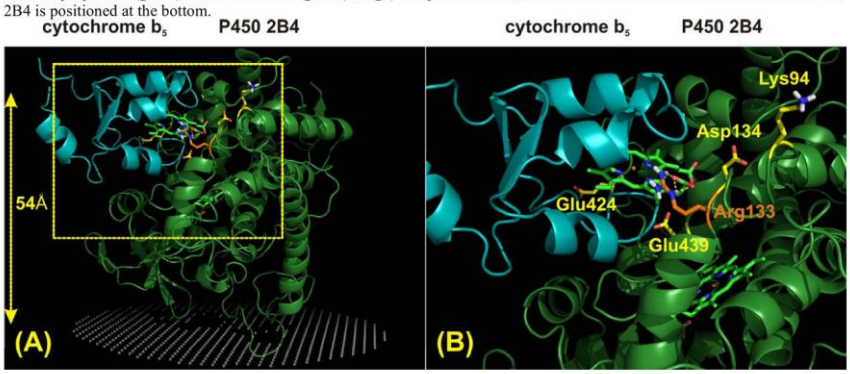

3.2. Charakterizace a identifikace fungálních proteinů a peptidů pomocí hmotnostní spektrometrie

3.2.1. Proteinové profily zástupců rodu *Aspergillus*

v publikaci

Biomarkers of Aspergillus Spores: Strain Typing and Protein Identification

Šulc M., **Pešlová K**., Žabka M., Hajdúch M., Havlíček V.

Int J Mass Spectrom. 280, 162-168 (2009)

Prohlášení spoluautorů

„Prohlašuji, že Kateřina Pavlásková (roz. Pešlová) se patřičně podílela (40 %) na plánování experimentů, jejich měření, interpretaci výsledků a sepisování této publikace.“

V Praze dne:

Doc. RNDr. Miroslav Šulc, PhD.

Author's personal copy

International Journal of Mass Spectrometry 280 (2009) 162–168

Contents lists available at ScienceDirect

International Journal of Mass Spectrometry

journal homepage: www.elsevier.com/locate/ijms

Biomarkers of *Aspergillus* spores: Strain typing and protein identification

Miroslav Sulc[a,b], Katerina Peslova[a,b], Martin Zabka[a], Marian Hajduch[c], Vladimir Havlicek[a,d,*]

[a] Institute of Microbiology, Academy of Sciences of the Czech Republic, Videnska 1083, CZ 142 20 Prague, Czech Republic
[b] Department of Biochemistry, Faculty of Science, Charles University, Hlavova 2030, CZ 128 43 Prague, Czech Republic
[c] Departments of Pediatrics and Oncology, Palacky University and University Hospital in Olomouc, Puskinova 6, CZ 775 20 Olomouc, Czech Republic
[d] Department of Analytical Chemistry, Palacky University, Tr. Svobody 8, CZ 771 46 Olomouc, Czech Republic

ARTICLE INFO

Article history:
Received 17 June 2008
Received in revised form 11 August 2008
Accepted 12 August 2008
Available online 28 August 2008

Keywords:
Aspergillus
Spore
MALDI-TOF
Protein
Profiling

ABSTRACT

We applied both matrix-assisted laser desorption/ionization time of flight (MALDI-TOF) mass spectrometric and 1D sodium dodecylsulfate polyacrylamide gel electrophoretic (1D-PAGE) approaches for direct analysis of intact fungal spores of twenty four *Aspergillus* species. In parallel, we optimized various protocols for protein extraction from *Aspergillus* spores using acidic conditions, step organic gradient and variable sonication treatment. The MALDI-TOF mass spectra obtained from optimally prepared samples provided a reproducible fingerprint demonstrating the capability of the MALDI-TOF approach to type and characterize different fungal strains within the *Aspergillus* genus. Mass spectra of intact fungal spores provided signals mostly below 20 kDa. The minimum material amount represented 0.3 μg (10,000 spores). Proteins with higher molecular weight were detected by 1D-PAGE. Eleven proteins were identified from three selected strains in the range 5–25 kDa by the proteomic approach. Hemolysin and hydrophobin have the highest relevance in host–pathogen interactions.

© 2008 Elsevier B.V. All rights reserved.

1. Introduction

Mass spectral characterization of bacteria is a well established experimental method and provides many interesting possibilities for the study of various environmental problems, e.g. food and beverages technologies, biodegradation and bacteria typing. In the latter case mass spectrometry uses primarily two approaches, MALDI and ESI (Electrospray Ionization) ionization of the sample, that allow us to study whole cells as well as bacterial proteins, DNA, lipids, exotoxins, lipooligosaccharides and peptidoglycans [1,2]. The typing of various intact microorganisms and the use of different mass spectral protocols have been extensively reviewed [3,4], mostly focused on the analysis of bacteria.

On the other hand, mass spectral characterization of intact fungal spores is not yet well described in the literature. Fungal spores are typically larger than bacterial cells and have rigid walls which structurally, but not chemically, resemble plant cells [5]. Different types of spores are formed following either asexual (the products of mitosis) or sexual (the products of meiosis) processes. Some fungal spores are able to survive at extreme conditions (elevated temperature and/or pressure) and can cause allergies with irritations of the eyes, nose, throat, and lungs [6]. Systemic mycotic infections or intoxications are also caused by molds and become a serious clinical problem for immunocompromised individuals [7]. Invasive infections caused by *Aspergillus*, mainly *Aspergillus fumigatus*, have one of the highest mortality rates, where 90–100% of immunocompromised patients die despite treatment [8]. *Aspergillus* is the second most common fungal pathogen after *Candida*. Aspergillosis and candidiasis together account for more than 80% of all fungal episodes in both bone marrow and solid organ transplantations [9].

This work was inspired by a high-sensitivity identification of *Bacillus* spores by matrix-assisted laser desorption/ionization time of flight (MALDI-TOF) mass spectrometry [10]. Also, preliminary results in *Penicillium* spore characterization by MALDI-TOF with different matrices demonstrated its ability for fungal spore classification [5]. Moreover, certain toxigenic strains of *A. flavus* and *A. parasiticus*, known to contaminate food and produce toxic secondary metabolites with mutagenic and carcinogenic effects (i.e. aflatoxins), have also been characterized by MALDI-TOF mass spectrometry [11].

* Corresponding author at: Institute of Microbiology, Academy of Sciences of the Czech Republic, Videnska 1083, CZ 142 20 Prague, Czech Republic.
Tel.: +420 241062786; fax: +420 241062156.
E-mail address: vlhavlic@biomed.cas.cz (V. Havlicek).

1387-3806/$ – see front matter © 2008 Elsevier B.V. All rights reserved.
doi:10.1016/j.ijms.2008.08.012

Author's personal copy

Table 1
Aspergillus strains involved in the study

Name of species	Number	Source	Year of isolation
A. fumigatus	CCF3227	Laboratory air	2000
A. fumigatus	CCF1187	Throat of a patient	1970
A. fumigatus	GR-1	Mouse aspergilloma	2000
A. fumigatus	CZ-2	Mouse aspergilloma	2001
A. fumigatus	CCF3623	Human maxillary cavity	2003
A. fumigatus	CCF1293	Throat of a miner	1968
A. fumigatus	CCF1292	Throat of a miner	1967
A. fumigatus	CCF1059	Root of sugar beet	1965
A. niger	MZ-3	Laboratory air	2002
A. niger	CCF3264	Mouldy twist from wheat flour	1999
A. niger	CCF2477	Patented strain	1967
A. niger	CCF1297	Throat of a miner	1967
Emericela nidulans	CCF3379	Human auditory meatus	2003
Emericela rugulosa	CCF3089	Human pericardium	1998
A. ochraceus	CCF1893	Cave air	1983
A. flavipes	CCF2026	From archives	1986
A. flavus	CCF3201	Black tea	2000
A. flavus	CCF2497	Seed of *Cicer arietinum*	1987
A. flavus	CCF1288	Throat of a miner	1967
A. flavus	CCF1058	Root of sugar beet	1965
A. parasiticus	CCF3137	Soil of tropical rain forest	2000
A. parasiticus	CCF1299	Throat of a miner	1967
A. oryzae	CCF1602	Food	1977
A. oryzae	CCF1066	ATCC10063	1996

Legend: CCF, Culture Collection of Fungi; ATCC, American Type Culture Collection; GR-1, CZ-2 and MZ-3 are fungal isolates from own collection (GR-1, CZ-2 were provided by M. Hajduch, MZ-3 by M. Zabka).

In this paper we report on the analysis of intact *Aspergillus* spores by MALDI-TOF mass spectrometry. We probed spore protein profiles by both the mass spectral and gel approaches. We tuned the experimental parameters and built a mass spectral database with twenty four *Aspergillus* strains. Eleven fungal proteins were identified by tandem mass spectrometry in three selected strains.

2. Experimental

2.1. Aspergillus cultivation and spore harvesting

Dry spores of *Aspergillus* strains (Table 1) were obtained at a Biosafety Level two laboratory. Cultivation was carried out in conical Erlenmeyer flasks at room temperature for 21 days with sterilized barleycorn. The inoculum was prepared from a culture performed on Sabouraud-dextrose agar in Petri-dishes (7 days). Spore collection from the fully sporulated culture in conical Erlenmeyer flasks was carried out by a vacuum collector covered with a 1.0 μm nitrocellulose membrane filter (Whatman, UK) and a stream of nitrogen.

2.2. Optimization of MALDI-TOF-compatible protein extraction protocol

Six variants of spore sample treatment were tested with *A. fumigatus* CCF3227 to increase both the quantitative and qualitative abundance of detected proteins (Table 2A). Two conditions were tested for MALDI-TOF analysis: variable amount of spores on the target mixed with a single MALDI matrix (Table 2A, protocol number 2, CHCA) and variable MALDI matrix with a fixed spore amount (protocol number 1, 0.1 mg of spores on the target). In both these experiments the aqueous spore suspension was dried in SPEED-VAC DNA-110 (ThermoSavant, USA) and the dry pellet was diluted in 2 μL of matrix solution [20 mg/mL of matrix in 50% aqueous acetonitrile/0.1% trifluoroacetic acid (TFA, v/v)]. 1 μL of the mixture was directly subjected on the MALDI target and the droplet was allowed to dry at ambient temperature.

Further, we optimized protein extraction conditions as shown in Table 2A (protocols no. 3–6). An aqueous suspension of intact spores (equivalent to 0.1 mg) was dried in SPEED-VAC, diluted

Table 2
Optimizing the protein extraction conditions (*Aspergillus fumigatus* CCF3227 exclusively used) for MALDI-TOF (A) and 1D-electrophoresis (B) profiling

A	Optimized parameter	Variable value/type of optimized parameter					
1	Type of MALDI-TOF matrix	CHCA	FA	DHB	SA		
2	Amount of spores [μg]	100	10	2.5	0.62		
3	TFA extraction [% (v/v)]	0.1	0.2	0.5	1	1.5	2
4	Aqueous MeCN extraction [% (v/v)]	0	10	20	40	60	80
5	Combination of 40% aqueous MeCN with TFA extraction [% (v/v)]	0.1	0.2	0.5	1	1.5	2
6	Sonication strength	3 × 2 s (50 W, amplitude 60) by a probe				15 min in a water bath	

B	Extraction solution	Sonication conditions
1	T50E1U8D100S1	Probe 3 × 2 s (50 W, amplitude 60), 1 min break on ice
2	T50E1U8D100S1	15 min in a water bath
3	40% MeCN (v/v)	15 min in bath
4	40% MeCN/0.1% TFA (v/v)	15 min in bath

Legend A: CHCA, α-cyano-4-hydroxy-cinnamic acid; DHB, dihydroxybenzoic acid; FA, ferulic acid; SA, sinapinic acid; TFA, trifluoroacetic acid; MeCN, acetonitrile.
Legend B: Composition of T50E1U8D100S1 buffer: 50 mM Tris-Cl, 1 mM ethylene diamine tetra-acetic acid, 8 M urea, 100 mM dithiothreitol, 1% sodium dodecylsulfate, pH 8.0; MeCN, acetonitrile; TFA, trifluoroacetic acid.

Author's personal copy

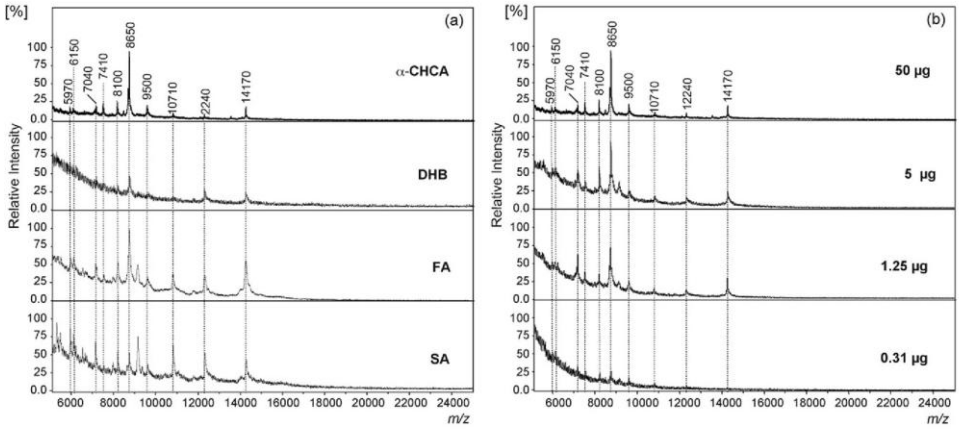

Fig. 1. MALDI-TOF mass spectra of *Aspergillus fumigatus* CCF3227: (a) 50 µg of spores in four matrices: α-cyano-4-hydroxy-cinnamic acid (CHCA), dihydroxybenzoic acid (DHB), ferulic acid (FA), or sinapinic acid (SA), respectively. (b) Four different amounts of spores in CHCA matrix: 50, 5, 1.25, or 0.31 µg, respectively.

in selected extraction solution, sonicated for 15 min in a water bath sonicator (Table 2A, protocols 3 and 4) and after centrifugation (MiniSpin Eppendorf, 13,000 RPM, 5 min) the supernatant was dried in SPEED-VAC. The dry residue was processed with the CHCA matrix as described previously and analyzed by MALDI-TOF mass spectrometry. In protocol 6 (Table 2A) we tested the influence of sonication power on the extent both of protein extraction as well as spore destruction. The suspension of intact spores (equivalent to 0.1 mg) was sonicated either for 15 min in a water bath sonicator or three times for 2 s by sonication probe (50 W, amplitude 60, Cole-Parmer, USA) interlaced with one minute of cooling on ice. Then the suspension was let to dry in SPEED-VAC and processed for MALDI-TOF analysis as described previously.

Mass spectra were measured in a linear mode on a MALDI-TOF mass spectrometer BIFLEX (Bruker-Franzen, Bremen, Germany) equipped with a SCOUT 26 sample inlet, a nitrogen laser (337 nm) (Laser Science, Cambridge, USA) and a gridless delayed extraction ion source. Spectra were accumulated from 100 to 150 laser shots. Positive-ion mass spectra were calibrated externally using the average masses of $[M+2H]^{2+}$, $[M+H]^{+}$, and $[2M+H]^{+}$ lysozyme ions. Mass accuracy better than 0.2% was usually achieved.

2.3. Protein extraction optimization for 1D-PAGE

To obtain a comparative protein profile to the mass spectral approach we also used 1D-electrophoresis (Table 2B). An aqueous solution of intact spores (*A. fumigatus* CCF3227, 0.5 mg) was

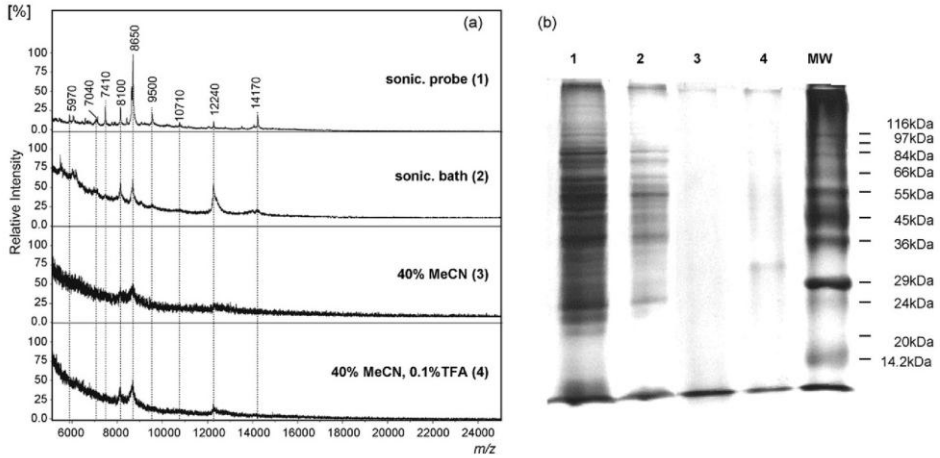

Fig. 2. MALDI-TOF mass spectra (a) or 1D-electrophoresis (12% gel, silver staining, MW—Sigma wide-range molecular weight standards) (b) of *Aspergillus fumigatus* CCF3227 spores under various protein extraction conditions (Table 2).

Author's personal copy

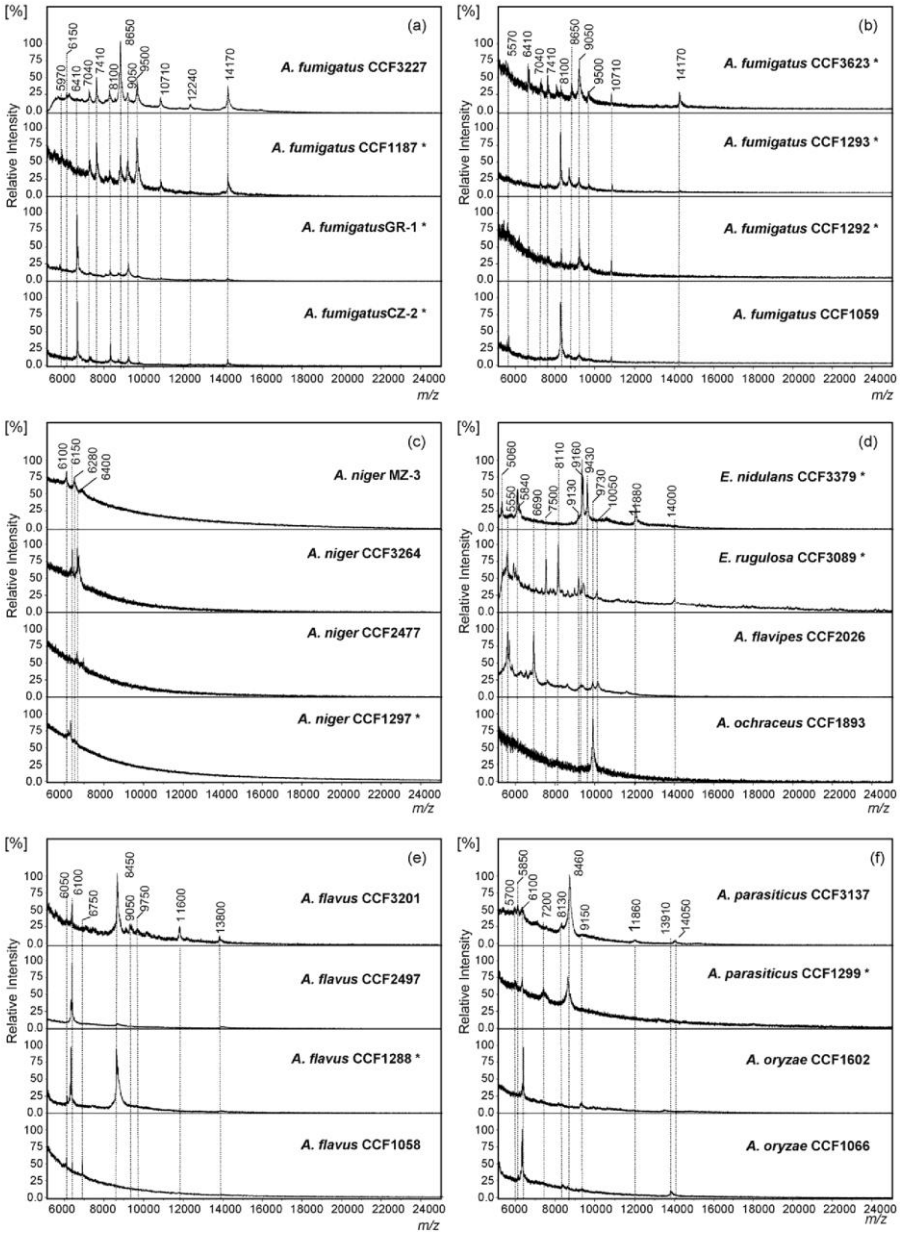

Fig. 3. MALDI-TOF mass spectra of *Aspergillus* spores under study.

Author's personal copy

Table 3
MALDI-TOF mass spectral characterization of *Aspergillus fumigatus* strains

Species	Accession number	*m/z* values									
		6410	7040	7410	**8100**	8650	**9050**	9500	**10710**	12240	14170
A. fumigatus	CCF3227	–	±	+	**+**	++	±	+	±	±	+
	CCF1187	–	±	++	±	+	**+**	++	**+**	–	+
	GR-1	++	–	–	±	–	**+**	±	±	–	±
	CZ-2	++	–	–	**+**	–	**+**	±	±	±	±
	CCF3623	+	±	+	±	±	**++**	±	**+**	–	+
	CCF1293	–	±	±	**++**	+	**+**	±	±	–	±
	CCF1292	–	–	±	**+**	–	**+**	±	**+**	–	–
	CCF1059	–	–	–	**++**	–	±	–	±	–	–

Legend: (–) not observed, (±) weak (5–20%), (+) medium (20–50%), (++) abundant (50–100%) relative intensity; signals in bold represent species common to all strains.

dried in SPEED-VAC. Dry residue was then diluted in selected extraction solution, sonicated either for 15 min in a water bath sonicator or three times for two seconds (50 W, amplitude 60; Cole-Parmer, USA) with a sonication probe, interlaced with one minute of cooling on ice. After centrifugation (MiniSpin Eppendorf, 13,000 RPM, 5 min) the supernatant was directly added to a sample buffer [50 mM Tris-Cl pH 6.8, 100 mM DTT, 2% SDS (w/v), 0.1% bromophenol blue (w/v), 10% glycerol (v/v)] and loaded on 12% or 15% polyacrylamide gel in the presence of sodium dodecylsulfate. After protein separation on 1D-gel the protein bands were detected by silver [12] or Coomassie Brilliant Blue R-250 [(CBB, 0.25% (w/v)] staining.

2.4. Protein identification by enzymatic in-gel digestion and μLC–MS/MS analysis

CBB-stained bands were excised from the gel, cut into small pieces and destained by 0.1 M 4-ethylmorpholine acetate (pH 8.1) in 50% acetonitrile (v/v, MeCN). The gel pieces were further washed with water, shrunk by dehydration in MeCN and reswelled again in water. After the supernatant removal the gel was partly dried in a SPEED-VAC concentrator and then reconstituted in a cleavage buffer containing 0.05 M 4-ethylmorpholine acetate, 10% MeCN (v/v), and sequencing grade trypsin (20 ng/mL; Promega). After overnight digestion at 37 °C, the resulting peptides were extracted twice to 40% MeCN/0.1% trifluoroacetic acid (v/v). The extracts were pooled, completely dried, dissolved in 5% ACN/0.5% acetic acid (v/v) and loaded onto a column (0.180 mm × 100 mm) packed with MAGIC C18 (5 μm, 200 Å) RP resin (Michrom BioResources) and separated using a gradient from 5% MeCN/0.5% acetic acid to 40% MeCN/0.5% acetic acid for 70 min. The column was connected directly to an LCQ^{DECA} ion trap mass spectrometer (ThermoFisher, San Jose, CA) equipped with a nanoelectrospray ion source. Full scan spectra were recorded over the mass range 380–1600 Da followed by MS/MS scans of the three most intense ions in the preceding full scan. Dynamic exclusion was set with two repeat counts, repeat duration of 30 s and 3 min exclusion duration window. Peak lists in DTA format were created by lcq_dta.exe program (ThermoFisher, San Jose, CA) with the following criteria: MW range 700–3300 Da; minimum number of ions 20; minimum TIC 5×10^4; precursor charge state +1, +2, +3; and grouped scans 1. Peak lists were searched against a UniProtKB protein database subset of the Fungi/*Metazoa* group using SEQUEST™ software (ThermoFisher, San Jose, CA) with the following settings: enzyme chemistry-trypsin, missed cleavages 2, no modification of cysteine, variable single oxidation of methionine, precursor-ion tolerance 2 Da, fragment-ion tolerance 0.8 Da. All MS/MS spectra assignments were validated manually.

3. Results and discussion

3.1. Tuning the extraction and MALDI acquisition conditions

In our study, four MALDI matrices were probed with *A. fumigatus* CCF3227 spores (Fig. 1). In this comparison the spores (50 μg) were extracted to 50% acetonitrile (v/v). Excluding the DHB, all used matrices provided rich ion profiles. The best signal/noise ratio and the narrowest peaks with little signal suppression were obtained in the CHCA matrix, which was then selected for all subsequent experiments. The same matrix was used for bacterial cells and their spores [13]. In the contrast, other authors also used the DHB, [2-(4-hydroxyphenylazo)]benzoic acid and 3,5-dimethoxy-4-hydroxycinnamic acid matrices for typing the *Penicillium* spp., *Scytalidium dimidiatum* and *Trychophyton rubrum* spores in the 2–13 kDa mass range [5].

To determine the limit of spore detection in MALDI-TOF analysis, variable quantities of *A. fumigatus* CCF3227 spores were used

Table 4
MALDI-TOF mass spectral characterization of *Aspergillus flavi* group strains (*A. flavus*, *A. oryzae* and *A. parasiticus*)

Species	Accession number	*m/z* values							
		5850	6050	**6100**	6750	8460	11600	13800	14050
A. flavus	CCF3201	–	±	+	–	++	±	±	–
	CCF2497	–	–	++	–	±	–	±	–
	CCF1288	–	±	++	–	++	–	±	–
	CCF1058	–	±	±	+	–	–	–	–
A. oryzae	CCF3137	±	–	±	–	++	±	–	±
	CCF1299	±	–	±	–	+	–	–	–
A. parasiticus	CCF1602	–	–	++	–	–	–	–	–
	CCF1066	–	–	++	–	±	±	+	–

Legend: (–) not observed, (±) weak (5–20%), (+) medium (20–50%), (++) abundant (50–100%) relative intensity; signals in bold represent species common to all strains.

Author's personal copy

(a)

Band	NCBI acc.n.	Protein name [species]
Af1-3	gi|19577409	hydrophobin [A. fumigatus]
Af4	gi|19743612	nucleoside diphosphate kinase [E. nidulans]
	gi|1220098	hemolysin [A. fumigatus]
Af5	gi|5326835	superoxide dismutase [Cu-Zn] [A. fumigatus]
An2	gi|2632155	histone H2A[A. niger]
An3	gi|19743612	nucleoside diphosphate kinase [E. nidulans]
Er2	gi|2632155	histone H2A[A. niger]
	gi|19743612	nucleoside diphosphate kinase [E. nidulans]
Er3	gi|19743612	nucleoside diphosphate kinase [E. nidulans]
Er4	gi|40743823	histone H2B[A. nidulans]
	gi|4322946	cyclophilin-like peptidyl prolyl cis-trans isomerase [A. niger]

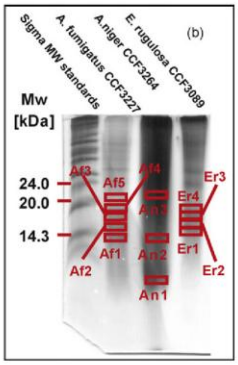

Fig. 4. The list of identified low MW proteins (a) of 1D-PAGE (15% gel, CBB R-250 staining, MW—Sigma wide-range molecular weight standards) separated protein bands of three selected *Aspergillus* strains (b).

(0.15–100 μg). Fig. 1b demonstrates decent ion signals even at spore amounts as low as 0.31 μg (dry material) corresponding to signal/noise ratio >2.5 for *m/z* 8650. This value corresponds to about 6500 fungal spores as determined in a Neubauer counting chamber and is consistent with the sensitivity reported for *Bacillus* species [10]. Interestingly, some authors claim even 1000 times higher sensitivity [11]. In our study some tested strains provided only poor signals. Hence, 50 μg of spore material was used in typing experiments (see below).

Further, we tested several protein extraction protocols such as the step gradient of aqueous acetonitrile with or without trifluoroacetic acid and sonication treatment (Fig. 2). *A. fumigatus* CCF3227 spores (0.1 mg) were used in this assay. Optimal "extraction" conditions include ultrasonic treatment with a probe running at high power (see Section 2). Cells had to be cooled down during the treatment to minimize biomolecular thermal degradation. The addition of 0.1% TFA (v/v) helps both MALDI-TOF and 1D-PAGE analyses. Mutual comparison of MALDI-TOF and 1D-PAGE protein typing results defines the following benefits and drawbacks of both approaches. MALDI-TOF analysis in concert with the reported extraction protocol discriminates species with molecular weight higher than 15,000 Da. However, MALDI is much more sensitive (about 1600 times in this particular case). On the other hand, the less sensitive 1D-PAGE analysis of *Aspergillus* strains enables one to use some proteomic approach for subsequent fungal protein identification (see below).

Finally, we also evaluated the influence of spore aging/storage on the protein profile. The study was carried out with *A. fumigatus* CCF3227. We evaluated MALDI-TOF profiles of spores stored as aqueous suspension at −20 °C for variable times (15 months, 30 months, or 5 years) of storage or we analyzed freshly harvested spores. Interestingly, we did not see any significant qualitative changes in mass spectral profiles (data not shown). This result indicates that fungal spore material can be used for typing purposes, as the biomolecular organic content remains almost constant.

3.2. Fungal strain typing

Optimal sample preparation conditions were used for the acquisition of reference spectra of 24 *Aspergillus* strains. In the optimized protocol the intact spores were processed as aqueous suspension (0.1 mg, dry material), destroyed by sonication probe, dried, mixed with the CHCA matrix solution and directly subjected on the MALDI target. Shared features in MALDI-TOF mass spectra (Fig. 3) indicate the phylogenetic and morphologic proximity of individual *Aspergillus* genera.

A. fumigatus set of strains is well characterized by common biomarker signals at *m/z* 8100, 9050 (Table 3) and 10,710, that are often accompanied by ions at *m/z* 9500 and 14,170 (Fig. 3a and b). On the contrary, *Aspergillus niger* strains exhibit a characteristic peak pattern in the range *m/z* 6100–6400 as illustrated in Fig. 3c. The poor signal of *A. niger* mass spectra might be rationalized by the presence of black pigments detected in low molecular weight MALDI-TOF mass spectra on the spores (data not shown), possibly interfering with the ionization process of biomolecules.

It is worth mentioning that MALDI-TOF spectra of other fungal strains could also be phylogenetically related as examined by *A. flavi* group strains shown in Table 4. The analysis of four *A. flavus* strains (Fig. 3e) reveals two shared markers at *m/z* 6100 and 8450. Whereas the species at *m/z* 6100 can also be observed both in *A. parasiticus* and *A. oryzae* strains (Fig. 3f), the latter ion *m/z* 8450 was present in the mass spectra just of *A. parasiticus* and represents the base peak there. The observation of a diagnostic marker at *m/z* 6100 was not a surprise: it has already been reported in the literature for multiple *Aspergilli* [11]. The *A. flavus* and *A. oryzae* spectra have clearly provided this peak, in contrast to suppression of this signal in other *Aspergillus* strains. On the other hand, *A. parasiticus* strains have revealed a signal at *m/z* 5850 which was not present in *A. flavus* and *A. oryzae* strains and could be used for distinguishing purposes. Interestingly, this relationship is in agreement with the origin of *A. oryzae* proposed from *A. flavus* [14] and *A. parasiticus* from *A. soyae* [11].

Although almost all described species are characterized by quite a high degree of morphological similarity, the fungal species differ in the production of carcinogenic aflatoxins [15]. While about 30–85% of *A. flavus* and *A. parasiticus* strains maintained in the American Type Culture Collection (ATCC) had produced detectable amounts of aflatoxins, no strain of *A. oryzae* is reported as an aflatoxin producer [16]. These data were supported also by DNA Southern blot analysis [17]. Coincidentally, MALDI-TOF mass spectra of *A. flavus* and *A. parasiticus* have shown the following interesting similarity. Two *A. flavus* (CCF1288, CCF3201) and both *A. parasiticus* (CCF1299, CCF3137) strains revealed an ion at *m/z* 8450. We cannot exclude that the generation of this ion is consistent with the production of aflatoxins reported by [18].

Author's personal copy

Other *A. flavus* (CCF1058, CCF2497) strains do not generate this biomarker.

All typing experiments were performed in triplicate and a constant pattern was usually recorded.

3.3. Fungal protein identification

There are several proteomic approaches to identify proteins that correspond to signals detected in MALDI-TOF spectra. In case of an organism with completely sequenced and reported genome, the molecular weights of a microorganism's proteins, obtained from its mass spectrum, are compared to those retrieved from the corresponding genome and/or protein databases [19]. Because our selected *Aspergilli* strains (*A. fumigatus*, *Emericella rugulosa* and *A. niger*) did not belong to organisms with a completely sequenced genome, a bottom-up proteomic approach was used as a platform for fungal protein identification in the range of molecular weight 5–25 kDa (Fig. 4). In-gel trypsin digestion was performed on selected 1D-PAGE strips prior to LC–MS/MS analysis. Proteins were identified by SEQUEST™ algorithm and the results are summarized in Fig. 4a. In *A. fumigatus* we detected four bands of hydrophobin, indicating multiple forms with different posttranslational modifications (Table S1, Supplementary Information Section). Like hemolysin, hydrophobin is an accepted fungal virulence factor. Another enzyme found in *A. fumigatus* was superoxide dismutase [Cu–Zn]. In *Emericella* as well as in *A. niger* we identified different forms of histones (H2A and H2B family). Nucleoside diphosphate kinase was ubiquitous in all three examined strains. Protein identification is demonstrated in the case of hydrophobin tryptic peptide as an example (Fig. S1, Supplementary Information Section), $[M+2H]^{2+}$ at m/z 566.3.

4. Conclusion

The MALDI-TOF protein profiling of intact fungal spores represents a fast approach for microorganism identification. Mass spectrometry can generate a unique fingerprint, which can be used for strain classification. This approach was successfully used for distinguishing *A. flavus*, *A. parasiticus*, *A. oryzae* and *A. fumigatus* strains. Selected protein biomarkers could speculatively correlate with the production of some secondary metabolites, e.g. aflatoxins [18]. Similarly, protein biomarkers, as well as some small secondary metabolites, might be correlated with phylogenetic evolution and used in metabonomic applications.

Although no general and specific marker in all *Aspergillus* isolates with a clinical origin (Fig. 4) was found in this work, the set of identified protein molecules present on fungal spores can potentially be used in human/veterinary medical mycology for early diagnosing purposes.

Acknowledgments

This paper is dedicated to our friend and colleague, Prof. Zdenek Herman. This work was supported by the Czech Science Foundation (203/05/P575), the Ministry of Education, Youth, and Sports of the Czech Republic (LC07017, MSM 6198959216) and an institutional research concept of the Institute of Microbiology, Academy of Sciences of the Czech Republic (AV0Z50200510). We also thank the Culture Collection of Fungi (CCF), Charles University, Prague, Czech Republic, for providing the *Aspergillus* strains. The authors would like to thank Douglas E. Markham for his helpful remarks and proofreading.

Appendix A. Supplementary data

Supplementary data associated with this article can be found, in the online version, at doi:10.1016/j.ijms.2008.08.012.

References

[1] B.L. van Baar, FEMS Microbiol. Rev. 24 (2000) 193.
[2] J. Nedved, M. Sulc, A. Jegorov, A. Giannakopulos, V. Havlicek, in: J. Van Eyk, M.J. Dunn (Eds.), From Diagnosis to Therapy, WILEY-VCH Verlag GmbH & Co., Weinheim, 2007, p. 481.
[3] P. Pribil, C. Fenselau, Anal. Chem. 77 (2005) 6092.
[4] C. Fenselau, P.A. Demirev, Mass Spectrom. Rev. 20 (2001) 157.
[5] K.J. Welham, M.A. Domin, K. Johnson, L. Jones, D.S. Ashton, Rapid Commun. Mass Spectrom. 14 (2000) 307.
[6] B. Kendrick, The Fifth Kingdom, third ed., Focus Publishing/R. Pullins Co., Newburyport, 2000.
[7] V.P. Kurup, H.D. Shen, B. Banerjee, Microbes Infect. 2 (2000) 1101.
[8] S.J. Lin, J. Schranz, S.M. Teutsch, Clin. Infect. Dis. 32 (2001) 358.
[9] C. Viscoli, E. Castagnola, Int. J. Infect. Dis. 3 (1999) 109.
[10] Y. Hathout, P.A. Demirev, Y.P. Ho, J.L. Bundy, V. Ryzhov, L. Sapp, J. Stutler, J. Jackman, C. Fenselau, Appl. Environ. Microbiol. 65 (1999) 4313.
[11] T.Y. Li, B.H. Liu, Y.Ch. Chen, Rapid Commun. Mass Spectrom. 14 (2000) 2393.
[12] J. Sambrook, E.F. Fritsch, T. Maniatis, Molecular Cloning: A laboratory Manual, second ed., Cold Spring Harbor Laboratory Press, New York, 1989.
[13] P. Lasch, H. Nattermann, M. Erhard, M. Stämmler, R. Grunow, N. Bannert, B. Appel, D. Naumann, Anal. Chem. 80 (2008) 2026.
[14] D.T. Wicklow, Appl. Environ. Microbiol. 47 (1984) 299.
[15] T.R. Jorgensen, J. Food Prot. 70 (2007) 2916.
[16] D.L. Wei, S.C. Jong, Mycopathologia 93 (1986) 19.
[17] M.A. Klich, J. Yu, P.K. Chang, E.J. Mullaney, D. Bhatnagar, T.E. Cleveland, Appl. Environ. Microbiol. 44 (1995) 439.
[18] V. Ostry, J. Ruprich, J. Skarková, I. Prochazkova, A. Kubatova, Mycotoxin Res. 17 (2001) 178.
[19] B. Amiri-Eliasi, C. Fenselau, Anal. Chem. 73 (2001) 5228.

3.2.2. Pseudacykliny jako potenciální „markery“ onemocnění způsobených *Pseudallescheria boydii*

v publikaci

Characterization of Pseudacyclins A-E, a Suite of Cyclic Peptides Produced by Pseudallescheria boydii

Pavlásková K., Nedvěd J., Kuzma M., Žabka M., Šulc M., Sklenář J., Novák P., Benada O., Kofroňová O., Hajdúch M., Derrick P.J., Lemr K., Jegorov A., Havlíček V.

J Nat Prod. 73(6), 1027-1032 (2010)

Prohlášení spoluautorů

„Prohlašuji, že Kateřina Pavlásková se patřičně podílela (30 %) na plánování experimentů, jejich měření, interpretaci výsledků a sepisování této publikace.“

V Praze dne:

Doc. RNDr. Miroslav Šulc, PhD.

J. Nat. Prod. **2010,** *73,* 1027–1032 **1027**

Characterization of Pseudacyclins A−E, a Suite of Cyclic Peptides Produced by *Pseudallescheria boydii*

Katerina Pavlaskova,[†] Jan Nedved,[†] Marek Kuzma,[†] Martin Zabka,[†,‡] Miroslav Sulc,[†] Jan Sklenar,[†] Petr Novak,[†] Oldrich Benada,[†] Olga Kofronova,[†] Marian Hajduch,[§] Peter J. Derrick,[⊥] Karel Lemr,[†,∥] Alexandr Jegorov,[▽] and Vladimir Havlicek*[,†,▽]

Institute of Microbiology, Videnska 1083, 142 20 Prague 4, Czech Republic, Laboratory of Experimental Medicine, Palacky University and University Hospital, Puskinova 6, 775 20 Olomouc, Czech Republic, Department of Fundamental Sciences, Massey University, Private Bag 11222, Palmerston North 4442, New Zealand, Department of Analytical Chemistry, Palacky University, Tr. 17. Listopadu 12, Olomouc, Czech Republic, and TEVA Pharmaceuticals, Branisovska 31, 370 05 Ceske Budejovice, Czech Republic

Received August 18, 2009

Pseudallescheria boydii sensu lato is an emerging fungal pathogen causing fatal infections in both immunocompromised and immunocompetent hosts. In this work, two *P. boydii* isolates (human and animal origin) have been identified as being producers of cyclic peptides. Five putative nonribosomal peptides with a unique structure, which have been named pseudacyclins, were characterized by nuclear magnetic resonance spectroscopy and mass spectrometry. The most abundant representative of the pseudacyclins was quantified also on fungal spores. The presence of these peptides on inhaled fungal spores creates the possibility for exploitation of pseudacyclins as early indicators of fungal infections caused by *Pseudallescheria* species.

Infections caused by the *Pseudallescheria boydii sensu lato* fungal complex have been classified as opportunistic systemic mycoses causing fatal invasive infections in immunocompromised and immunocompetent hosts.[1−3] The fungal strains involved in the complex exert very high levels of antifungal resistance,[4] with *Scedosporium aurantiacum* being the most resistant species.[5] *P. boydii* has now become the second most frequent filamentous mold recovered from cases involving particular patient groups, e.g., colonizing the respiratory tract of cystic fibrosis patients or causing delayed brain infection in the near drowning syndrome.[6,7]

P. boydii sensu lato is a complex of fungal species currently involving *P. angusta, P. boydii sensu stricto, P. desertorum, P. elipsoidea, P. fusoidea, P. minutispora, Scedosporium apiospermum, S. aurantiacum*, and *S. dehoogii.*[8] *P. boydii* and *S. apiospermum*, traditionally considered as the teleomorph and anamorph of the same species, in fact belong to two different species. The high mortality rate related to *S. prolificans* infection is alarming, exceeding 87% in patients with disseminated disease.[4] *S. prolificans* was reported to be more virulent than *S. apiospermum*. In the animal studies *S. aurantiacum* and *S. dehoogii* killed 70−80% of the immunocompetent mice, whereas *P. boydii sensu stricto*, *P. minutispora*, and *S. apiospermum* killed only 0−20% of the animals.[9]

Although *P. boydii* was first described in human disease in India as one of the agents of mycetoma more than 150 years ago and the first infection caused by *Scedosporium* was reported in 1889, a reliable commercially available tool for early diagnosis of infections caused by *P. boydii* complex is still missing. Current experimental tools are based on either *P. boydii* genotyping[10] or detection of saccharidic antigens representing the fungal cell-wall components.[11] Certain skepticism arising from quite low sensitivities of some of these techniques means that cultivation and microscopy of biopsies still represent the gold standard.[12]

Long-standing and/or unreliable diagnostics currently stimulate the analytical community to develop alternative tools that can be used in early stage diagnosing and characterization of infections caused by multiple species acting cooperatively. In genotyping methods nucleotide substitutions do not necessarily result in alteration in the amino acid composition, and subsequent changes in the electrophoretic profile may not be visualized.[10] On the contrary, going down from a gene to a protein/peptide level gives inherently more precise information.[13] For peptide/protein analysis, mass spectrometry is being used as the exclusive tool, which in selected cases makes possible not only the determination of the fungal genus but also distinctions among the different strains.[14] The emerging protocols are mostly based on proteomics or peptidomics approaches.[15] It has to be emphasized that all of the reported successful attempts to date have been made only under *in vitro* conditions. However, the sensitivity of modern molecular tools is enormous: just 10 fungal conidia are necessary for detection of a particular strain even in a fungal complex.[16]

Not many secreted organic substances have been reported specifically for the *P. boydii* complex.[17] A 33 kDa extracellular serine protease/peptidase from *S. apiospermum* was described as degrading human fibrinogen, suggesting a role as a mediator of tissue injury and inflammation.[18] Silva et al. have reported two extracellular metallopeptidases of 28 and 35 kDa that are released from mycelia of *P. boydii.*[19] These peptidases were found to break down portions of fibronectin and laminin.[20]

Oligosaccharidic structures can potentially be used in serologic diagnostics of *P. boydii.*[21,22] Fungal cerebrosides represent another interesting glyco-related subgroup of antigens.[23] A recent paper reports on the preparation of two monoclonal antibodies that selectively bind to a major antigen with a molecular mass of approximately 120 kDa secreted by *P. boydii.*[11] Promising specificities achieved *in vitro* to *Pseudallescheria*, *Graphium*, and *Petriella* species and *S. apiospermum* remain to be evaluated with clinical samples.

Fungal melanin structures, derived from the precursor molecule 1,8-dihydroxynapthalene through the polyketide biosynthetic pathway, may serve as scavengers for oxygen and nitrogen reactive species produced by phagocytic cells during the oxidative burst and thus contribute to fungal pathogenesis.[24]

Metabonomics represents another modern approach for low molecular mass fungal biomarkers. All of these small organic molecules reported as of July 2009 to be produced by the *P. boydii*

* Corresponding author. Tel: +420-241062786. Fax: +420-241062749. E-mail: vlhavlic@biomed.cas.cz.
[†] Institute of Microbiology, Prague.
[‡] Present address: Crop Research Institute, Prague 6, Czech Republic.
[§] Palacky University and University Hospital.
[⊥] Massey University.
[∥] Department of Analytical Chemistry, Palacky University.
[▽] TEVA Pharmaceuticals.

10.1021/np900472c © 2010 American Chemical Society and American Society of Pharmacognosy
Published on Web 05/28/2010

Table 1. Non-saccharidic Small-Molecule Metabolites Described in *Pseudallescheria/Scedosporium* Strains As of July 2009

trivial name	$[M + H]^+$	formula	species	ref
pseurotin A	127.0502	$C_5H_7N_2O_2$	*P. boydii* IFM 4642	27
AS-183	311.2581	$C_{19}H_{35}O_3$	*S.* sp. SPC-15549	28
gliotoxin	327.0468	$C_{13}H_{15}N_2O_4S_2$	*P.* sp. MFB165	26
tyroscherin	334.2741	$C_{21}H_{36}NO_2$	*P.* sp.	29
dehydroxybisdethiobis(methylthio)gliotoxin	341.0988	$C_{15}H_{21}N_2O_3S_2$	*P.* sp. MFB165	26
YM-193221	346.2741	$C_{22}H_{36}NO_2$	*P. ellipsoidea* CBS128.78	30
bisdethiobis(methylthio)gliotoxin	357.0937	$C_{15}H_{21}N_2O_4S_2$	*P.* sp. MFB165	26
dimerumic acid[a]	485.2606	$C_{22}H_{37}N_4O_8$	*S. apiospermum*,e.g., IHEM 14263	31
pseudacyclin E, [Val[5],Val[6]]PcA, **5**[b]	712.4392	$C_{37}H_{58}N_7O_7$	*P. boydii* CBS 119458	this work
pseudacyclin B, [Val[5]]PcA, **2**	726.4549	$C_{38}H_{60}N_7O_7$	*P. boydii* CBS 119458	this work
pseudacyclin D, [Val[6]]PcA, **4**	726.4549	$C_{38}H_{60}N_7O_7$	*P. boydii* CBS 119458	this work
pseudacyclin A, **1**	740.4705	$C_{39}H_{62}N_7O_7$	*P. boydii* CBS 119458, CBS 116779	this work
2-*N*-methylcoprogen B[a]	741.4029	$C_{34}H_{57}N_6O_{12}$	*S. aurantiacum* *S. apiospermum*	31
pseudacyclin C, [Me-acetyl-Ile[6]]PcA, **3**	754.4858	$C_{40}H_{64}N_7O_7$	*P. boydii* CBS 119458	this work

[a] In the literature the siderophores dimerumic acid and 2-*N*-methylcoprogen B were reported as $[M + Fe - 2H]^+$ species (*m/z* 538.1721 and 794.3144, respectively). [b] PcA stands for pseudacyclin A.

complex are summarized in Table 1. Some of these are thought to be important virulence factors, e.g., the gliotoxin family.[25,26] In this work we have focused on characterization of the five cyclic peptides with unique structures and produced by two *Pseudallescheria* strains. The structure of the most abundant cyclopeptide belonging to this family has been named pseudacyclin A (**1**).

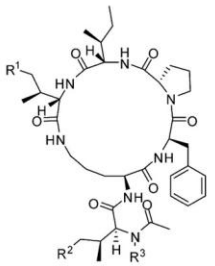

	R^1	R^2	R^3
Pseudacyclin A (**1**)	CH_3	CH_3	H
Pseudacyclin B (**2**)	H	CH_3	H
Pseudacyclin C (**3**)	CH_3	CH_3	CH_3
Pseudacyclin D (**4**)	CH_3	H	H
Pseudacyclin E (**5**)	H	H	H

Results and Discussion

Two *P. boydii* isolates, one of human and the other of animal origin, have been identified as cyclic peptide producers. Upon receipt from Centraalbureau voor Schimmelcultures (CBS), both *P. boydii* strains were checked for their authenticity by rDNA sequencing. A high similarity in the ITS1-5.8S-ITS2 region between CBS 119458 and CBS 116779 was observed (data not shown). *P. boydii* CBS 119458 strain was also checked by surface culture and microscopic tools (see the Supporting Information).

Fungal strains CBS 119458 and CBS 116779 were shown to produce pseudacyclin A (**1**), a new cyclic hexapeptide containing three isoleucine residues (one of which is *N*-acetylated) and one residue each of phenylalanine, ornithine, and proline. The molecule presents a unique structure of a type previously not reported. The structure was determined by 2D NMR spectroscopy as 2-acetylamino-3-methylpentanoic acid (5-benzyl-14,17-di-*sec*-butyl-4,7,13,16,19-pentaoxo-eicosahydro-3a,6,12,15,18-pentaaza-cyclopentacyclooctadecen-8-yl)amide. NMR analyses based on a combination of 1D and 2D NMR experiments determined six subunits constituting compound **1**: ornithine (Orn^1), phenylalanine (Phe^2), proline (Pro^3), and three isoleucines (Ile^4, Ile^5, Ile^6). *N*-Acetylation of Ile^6 was confirmed by HMBC correlations of the

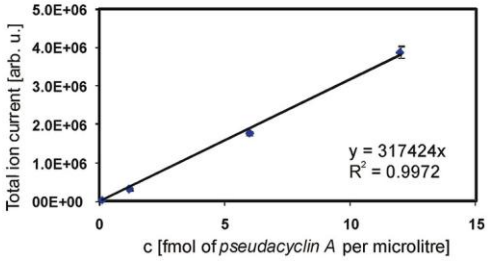

Figure 1. Standard calibration curve relating a total-ion-current mass-detector signal to the concentration of pseudacyclin A in femtomoles per microliter (LCQ-DECA ion trap, SRM mode, parent ion *m/z* 740.5 selected with a 5 Th window, product ion range scanned between 582 and 588 Th).

methyl signal at 1.97 ppm and an amide NH at 7.03 ppm to the carbonyl carbon at 172.2 ppm (Table 2). The sequence determination of **1** was accomplished by HMBC using correlations between the secondary amide proton and the corresponding carbonyl carbon resonances. It gained the contiguous sequence of residues $-Pro^3$-Ile^4-Ile^5-*Nδ*-Orn^1(N^1-*N*-Ac-Ile^6)-Phe^2-. The cyclic structure was also confirmed by negative carboxypeptidase Y treatment as well as resistance to the esterification by ethanol (data not shown). Enantioselective analysis of **1** has been performed according to protocol[32] and has shown the L configuration for all amino acids except for D-Phe-2.

A higher production of pseudacyclin A was observed with the second strain CBS 119458. In this particular case, the cyclopeptide was also detected on the fungal spores (for spore treatment protocol see ref 15). Semiquantitative measurements by mass spectrometry indicated that there was 5×10^{-20} mol of pseudacyclin A on one CBS 119458 spore, which corresponds roughly to 30 000 molecules per spore (Figure 1). Mass spectrometry works routinely in the detection range of interest. It should be noted, however, that the reported selected reaction monitoring (SRM) measurement was carried out with peptide standards. The detection limit during a whole blood or a tissue measurement could be hampered by chemical noise and by marker losses caused by extraction procedures. Its actual presence on both fungal spores and growing mycelium could create the possibility for exploiting these unique molecules as early indicators of fungal infections caused by *Pseudallescheria* sp. Pseudacyclins can in principle be detected as either circulating free peptides or protein-bound molecules. In terms of specificity, cyclic peptides might represent a viable alternative to current experimental diagnostic tools based on less specific polysaccharidic antigens. The actual role of cyclic peptides in *P.*

Table 2. NMR Data of Pseudacyclin A (**1**) (399.87 MHz for ^{1}H and 100.55 MHz for ^{13}C, CD_3CN, 303 K).

residue	atom	δ_C[a]	δ_H (*J* in Hz)	HMBC (H to C correlations)
Orn-1	CO	172.4, C		
	NH		7.62, d (8.7)	6-CO
	α	53.7, CH	4.23, ddd (3.3, 8.7, 12.1)	1-CO, 1*β*
	β	27.5, CH_2	1.89[a], m	
			1.46[a], m	1α, 1*γ*, 1*δ*
	γ	25.2, CH_2	1.57[a], m	
			1.26[a], m	
	δ	38.6, CH_2	3.47, m	
			2.77, m	
	δ-NH		7.23[b], m	5-CO
Phe-2	CO	171.8, C		
	NH		7.35, d (7.8)	1-CO
	α	53.6, CH	4.74, ddd (6.6, 7.8, 8.7)	1-CO, 2-CO, 2-*ipso*, 2*β*
	β	38.4, CH_2	2.97, dd (8.7, 13.1)	2-CO, 2-*ipso*, 2-*ortho*, 2α
			2.88, dd (6.6, 13.1)	2-CO, 2-*ipso*, 2-*ortho*, 2α
	ipso	137.9, C		
	ortho	130.2[c], CH	7.22[a], m	2*β*
	meta	129.2[c], CH	7.26[a], m	2-*ipso*, 2-*meta*
	para	127.6, CH	7.23[a], m	
Pro-3	CO	171.7, C		
	α	61.5, CH	4.30, dd (2.8, 8.4)	3-CO, 3*β*, 3*γ*, 3*δ*
	β	30.1, CH_2	1.95[a], m	3-CO
			1.85[a], m	3-CO
	γ	24.8, CH_2	1.69[a], m	
	δ	47.4, CH_2	3.62, ddd (3.7, 7.7, 9.8)	
			2.86, ddd (7.3, 9.0, 9.8)	3*β*, 3*γ*
Ile-4	CO	172.9, C		
	NH		6.55, d (8.9)	3-CO, 4-CO
	α	56.7, CH	4.46, dd (3.5, 8.9)	3-CO, 4-CO, 4*β*, 4*γ*
	β	40.1, CH	1.90, m	
	γ	24.1, CH_2	1.26, m	
			0.94[a], m	
	δ	11.9, CH_3	0.81, t (7.3)	4*β*, 4*γ*
	β-CH_3	16.2, CH_3	0.83, d (6.7)	4α, 4*β*, 4*γ*
Ile-5	CO	171.9, C		
	NH		6.75, d (6.2)	4-CO
	α	61.0, CH	3.86, dd (6.2, 9.0)	5-CO, 5*β*, 5*γ*, 5*β*-CH_3
	β	35.9, CH	1.73[a], m	
	γ	26.0, CH_2	1.60[a], m	
			1.18[a], m	5*β*, 5*δ*, 5*β*-CH_3
	δ	10.8, CH_3	0.87, t (7.3)	5*β*, 5*γ*
	β-CH_3	15.5, CH_3	0.89, d (6.7)	5α, 5*β*, 5*γ*
N-Ac-Ile-6	CO	172.7, C		
	NH		7.03, d (7.6)	6-N-CO
	α	60.1, CH	4.00, dd (7.6, 7.6)	6-N-CO, 6-CO, 6*β*, 6*γ*, 6*β*-CH_3
	β	37.0, CH	1.85, m	
	γ	25.9, CH_2	1.57, m	
			1.21, m	6*β*, 6*δ*, 6*β*-CH_3
	δ	11.4, CH_3	0.90, t (7.4)	6*β*, 6*γ*
	β-CH_3	16.3, CH_3	1.00, d (6.8)	6α, 6*β*, 6*γ*
	N-CO	172.2, C		
	NAc	22.9, CH_3	1.97, s	6-N-CO

[a] ^{13}C NMR data have been obtained from HSQC and HMBC spectra. gHSQC and HMBC readouts. [b] gCOSY readouts. [c] 2C.

boydii metabolism remains unknown, but immunosuppressive activity cannot be ruled out.

Pseudacyclin A (**1**) can be described as cyclo-[*N*δ-L-Orn^1(*N*^{1}-*N*-acetyl-L-Ile^6)-D-Phe^2-L-Pro^3-L-Ile^4-L-Ile^5]. Noncoded amino acid constituents might indicate the nonribosomal origin of the peptide. The structure contains one *N*-acetylisoleucine and one ornithine, residues that are also conserved in most of the pseudacyclin analogues detected in fermentation broths of a high-producing strain, CBS 119458 (Table 1). Their sequences were deduced from tandem mass spectra. It was found that there was amino acid variability at the fifth and sixth position of the peptide cycloskeleton. Infrared multiphoton dissociation (IRMPD) mass spectra have revealed the side-chain release (Ac-Ile-6 in the case of **1**) as the major dominating fragmentation process (Figure 2). The product ion *m/z* 585 originated this way still maintains its cyclic structure (core), resulting in less specific ring-opening mechanisms. Luckily, the sequence-scrambling process[33] is not extensive in pseudacyclins, and two major ring-opening mechanisms dominate in the spectra. They start with primary splitting between amino acid residues 2-1 and 3-2, producing the corresponding $^{x\text{-}y}b_i$ and $^{x\text{-}y}a_i$ ion series. For the fragment ion nomenclature of cyclic peptides see ref 13.

In pseudacyclin B (**2**) the Ile^5 is replaced by an amino acid residue with C_5H_9NO increment, which does not contradict the presence of valine at this position. Formally, pseudacyclin B can be described as [Val^5]PcA (amino acid constituent in square brackets defines the residue change with respect to pseudacyclin A). In pseudacyclin C (**3**) the Ile^6 is methylated. This [Me-acetyl-Ile^6]PcA is the representative with the highest mass of the pseudacyclin family (**3**) and also has the longest retention time on a reversed-phase HPLC column (Figure 3). Pseudacyclin D (**4**) is a co-eluting isobar of pseudacyclin B, having the structure [Val^6]PcA. The co-elution is also observed with pseudacyclins with their protonated molecules at *m/z* 712.4401. Only one of them, pseudacyclin E (**5**), [Val^5,Val^6]PcA, is listed in the Experimental Section, but at least two other isobaric analogues were also detected in low amounts. The sequences of the minor pseudacyclins were inferred mostly

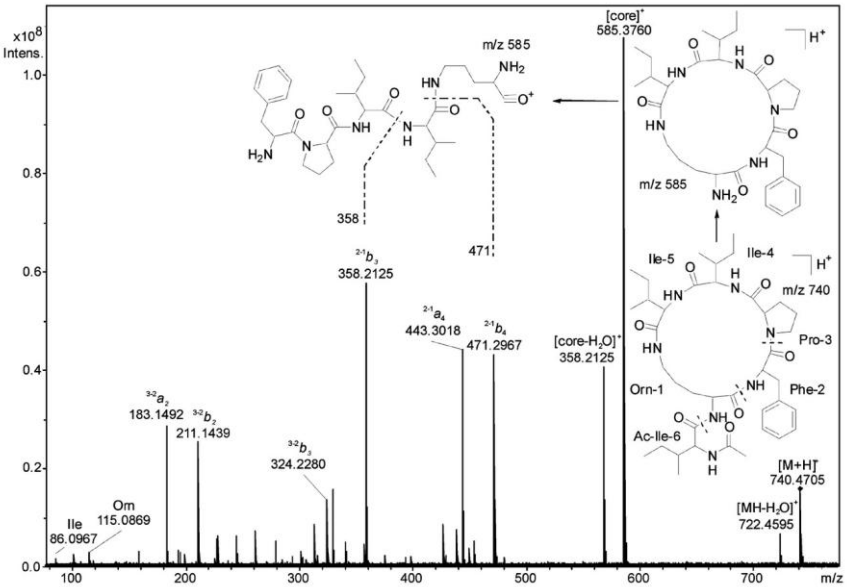

Figure 2. IRMPD mass spectrum of the protonated molecule of pseudacyclin A (**1**). See the text for the description of the fragmentation mechanisms and ion nomenclature. Major ring-opening sites marked.

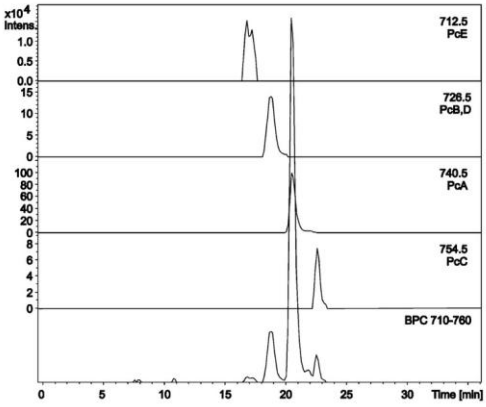

Figure 3. HPLC/MS separation of cyclic peptides. Absolute abundance (*Y* scale) semiquantitatively reflects the peptide ratio. BPC stands for base peak chromatogram reconstructed from the *m/z* 710−760 interval (Th).

from high-resolution product ion mass spectra recorded on an FT-ICR mass spectrometer.

Pseudacyclin A has revealed a potential immunosuppressive activity (Experimental Section). On the contrary, only weak NO-synthase inhibition activity and no bactericidal or bacteriostatic effects have been observed.

In addition to the pseudacyclin family, cyclic Phe-Pro was found to be a major constituent in solid-phase extracts of *P. boydii* CBS 119458 culture filtrates assessed by NMR (data not shown). In terms of microorganism specificity and potential diagnostic application, this diketopiperazine is not significant.

Our future work will be focused on the description of novel cyclic peptides that are ubiquitous to most of the strains forming the *P. boydii* complex. Antibodies to these peptides as well as pseudacyclins will represent the basis of a diagnostic ELISA set, which is currently in development. In summary, the current advances in mass spectrometry will lay the experimental foundation for modern sensitive diagnostic tools. We predict that mass imaging of tissues infected by molds will lead to discovery of specific fungal biomarkers. The analysis of intact tissues and bodily fluids will be enabled by ambient mass spectrometric techniques.[34] Single ion detection techniques may beat other instrumental competitors in terms of sensitivity.[35] Innovative molecular approaches together with new modern antifungal drugs then could translate these mass spectrometric advances from bench to bedside.

Experimental Section

General Experimental Procedures. Optical rotations were recorded on a Jasco DIP-370 polarimeter. UV spectra were measured on a Waters Acquity diode array detector. The IR spectrum was recorded on a Nicolet 205 FT-IR spectrometer. NMR spectra were recorded on a Varian^{UNITY} Inova-400 spectrometer[36] (399.87 MHz for ^{1}H and 100.55 MHz for ^{13}C). The residual solvent signal was used as an internal standard (δ_H 1.93 ppm, δ_C 1.30 ppm). ^{1}H NMR, ^{13}C NMR, COSY, TOCSY, HSQC, HMBC, and ROESY spectra were measured using standard manufacturers' software. The ^{1}H NMR spectrum was zero filled to 4-fold data points and multiplied by a window function (two-parameter double-exponential Lorentz−Gauss function) before Fourier transformation to improve the resolution. The ^{13}C NMR spectrum was zero filled to 2-fold data points. Then line broadening (1 Hz) was used to improve the signal-to-noise ratio. Protons were assigned by COSY and TOCSY, and the assignment was transferred to carbons by HSQC. Chemical shifts are given in δ-scale [ppm]; coupling constants are given in Hz. High-resolution mass spectra were measured by FT-ICR on an Apollo II ESI/MALDI ion source in positive-ion mode.[34] IRMPD mass spectra were generated by 0.35 s infrared laser shots (50% attenuation) applied to $[M + H]^+$ precursor ions isolated by a quadrupolar mass filter preceding the ICR cell. Dissociations were also performed in the collisional quadrupole of the instrument. Low-resolution mass spectra

and pseudacyclin A semiquantitation (in SRM mode) were obtained by an ESI-LCQ-DECA ion trap.[36] The parent ion *m/z* 740.5 was selected with a 5 Th window (product ion range scanned between 582 and 588 Th).

Culture Conditions. Fungal strains CBS 119458 (CCF 3082) and CBS 116779 (IHEM 21163, IP 1946.90) were received from Centraalbureau voor Schimmelcultures (CBS, Utrecht, The Netherlands, http://www.cbs.knaw.nl/databases/). *P. boydii* CBS 119458 was an isolate from a nasal cavity of a Husky with a chronic rhinitis (Czech Republic). CBS 116779 strain was isolated from a human sinus (China). Genetic and morphological authenticity and purity of the samples were controlled by culturing, rDNA sequencing, and electron and optical microscopy.

Submerged cultivation of both fungal strains has been carried out in 500 mL Erlenmeyer flasks (21 days, 28 °C). Czapek-Dox medium (200 mL) with reduced saccharose content was adjusted to the following optimum composition: $NaNO_3$ (2 g), K_2HPO_4 (1 g), KCl (0.5 g), $MgSO_4 \cdot 7H_2O$ (0.5 g), $FeSO_4$ (0.01 g), saccharose (10 g), H_2O (pH adjusted to 7.3). The inoculum was prepared by submersed 72 h precultivation. *P. boydii* spores (3×10^7) were added to 150 mL of inoculation media: saccharose (30 g), corn steep (20 g), KH_2PO_4 (2 g), H_2O. The preinoculum was mixed with inoculum in 1:10 ratio (v/v).

Extraction and Isolation. The culture filtrates (200 mL) in 30 Erlenmeyer flasks (500 mL) were extracted twice with CH_2Cl_2 (200 mL). Organic layers were pooled and dried. The dry residue (ca. 20 mg per single Erlenmeyer flask) was reconstituted in MeOH (0.2 mL) and diluted in HPLC solvent A (10× dilution; for composition see below). The resulting solution was injected on a Strata C18E column (1 g, Phenomenex) and desalted by 5% aqueous MeOH. The cartridge was then stepwise eluted with 20% MeOH/H_2O (step 1), 50% MeOH/H_2O (step 2), and 100% (step 3) MeOH. In each step ten 7 mL fractions were collected and evaporated in a speedvac. The fractions were subsequently examined for their metabolite contents. Step 1 (fraction 1) removed the UV-absorbing yellow-to-brownish interfering substances (possibly melanin structures). Diketopiperazines were found in the same step 1 (in fraction 2) by NMR spectroscopy (data not reported). Steps 2 and 3 yielded pseudacyclins. Promising fractions were purified on a reversed-phase Watrex WRP-18 (7 μm) preparative column with gradient elution (A, 5% CH_3CN/H_2O with 0.05% trifluoroacetic acid (TFA); B, 95% CH_3CN/H_2O with 0.05% (TFA), all Merck, gradient grade) at 8 mL/min flow rate and 40 °C. The gradient profile started with a 50 min hold at 0% B and continued with 0−12% B in 5 min; 12−70% B in 150 min, 70−100% B in 25 min, and 20 min hold at 100% B. Separated peptides were detected by UV (214 nm) and subjected to spectroscopic analyses. The total amount of the pure pseudacyclin A obtained from the CBS 119458 strain was 5 mg.

Pseudacyclin A (1): white, amorphous powder; UV (CH_3CN) λ_{max} (log ε) 201 (4.14) nm; IR (Nujol) ν_{max} 1379, 1449, 1525, 1647 cm^{-1}; positive ion HRMS/MS $[M + H]^+$ 740.4705 (calcd for $C_{39}H_{62}N_7O_7$, 740.4705); $[MH - CO]^+$ 712.4761 (calcd for $C_{38}H_{62}N_7O_6$, 712.4745); core 585.3760 (calcd for $C_{31}H_{49}N_6O_5$, 585.3759); ${}^{2-1}b_4$ 471.2967 (calcd for $C_{26}H_{39}N_4O_4$, 471.2966); ${}^{2-1}a_4$ 443.3018 (calcd for $C_{25}H_{39}N_4O_3$, 443.3017);${}^{2-1}b_3$ 358.2125 (calcd for $C_{20}H_{28}N_3O_3$, 358.2125); ${}^{3-2}b_3$ 324.2280 (calcd for $C_{17}H_{30}N_3O_3$, 324.2282); 270.1810 (calcd for $C_{13}H_{24}N_3O_3$, 270.1812).

Pseudacyclin B (2): positive-ion HRMS/MS $[M + H]^+$ 726.4549 (calcd for $C_{38}H_{60}N_7O_7$, 726.4549); $[MH - CO]^+$ 698.4594 (calcd for $C_{37}H_{60}N_7O_6$, 698.4600); core 571.3601 (calcd for $C_{30}H_{47}N_6O_5$, 571.3603); ${}^{2-1}b_4$ 457.2808 (calcd for $C_{25}H_{37}N_4O_4$, 457.2809); ${}^{2-1}a_4$ 429.2858 (calcd for $C_{24}H_{37}N_4O_3$, 429.2860); ${}^{2-1}b_3$ 358.2123 (calcd for $C_{20}H_{28}N_3O_3$, 358.2125); ${}^{3-2}b_3$ 310.2125 (calcd for $C_{16}H_{28}N_3O_3$, 310.2125); 270.1812 (calcd for $C_{13}H_{24}N_3O_3$, 270.1812).

Pseudacyclin C (3): positive-ion HRMS/MS $[M + H]^+$ 754.4858 (calcd for $C_{40}H_{64}N_7O_7$, 754.4862), $[MH - CO]^+$ 726.4903 (calcd for $C_{38}H_{60}N_7O_7$, 726.4549); core 599.3907 (calcd for $C_{32}H_{51}N_6O_5$, 599.3916); ${}^{2-1}b_4$ 471.2961 (calcd for $C_{26}H_{39}N_4O_4$, 471.2966); ${}^{2-1}a_4$ 443.3012 (calcd for $C_{25}H_{39}N_4O_3$, 443.3017); ${}^{2-1}b_3$ 358.2122 (calcd for $C_{20}H_{28}N_3O_3$, 358.2125); ${}^{3-2}b_3$ 324.2279 (calcd for $C_{17}H_{30}N_3O_3$, 324.2282); 284.1966 (calcd for $C_{14}H_{26}N_3O_3$, 284.1969).

Pseudacyclin D (4): positive-ion HRMS and low-resolution MS/MS $[M + H]^+$ 726.4549 (calcd for $C_{38}H_{60}N_7O_7$, 726.4549); $[MH - CO]^+$ 698.2; core 585.2; ${}^{2-1}b_4$ 471.1; ${}^{2-1}a_4$ 443.1; ${}^{2-1}b_3$ 358.0; ${}^{3-2}b_3$ 324.2.

Pseudacyclin E (5): positive-ion MS/MS and low-resolution MS/MS $[M + H]^+$ 712.4401 (calcd for $C_{37}H_{58}N_7O_7$, 712.4392); $[MH - CO]^+$ 684.4; core 571.2; ${}^{2-1}b_4$ 457.1; ${}^{2-1}a_4$ 429.1; ${}^{2-1}b_3$ 358.2; ${}^{3-2}b_3$ 310.0.

Evaluation of Biological Activities of Pseudacyclin A. Cytotoxic and antiproliferative activities of pseudacyclin A were analyzed on resting and mitogen-activated (5 μg/mL of concanavalin A, con A) human lymphocytes.[37] IC_{50} cytotoxicity values 32.0 ± 6.8 and 12.9 ± 4.2 μM were determined for resting and con A-activated lymphocytes, respectively. Preferential toxicity of pseudacyclin A to activated, but not resting, lymphocytes indicates a potential immunosuppressive activity of this metabolite. By contrast, pseudacyclin A induced only a weak inhibition of NO-synthase activity[38] measured as 24 h production of NO_2^- by polysaccharide (0.5 μg/mL)-activated B10R macrophages with an IC_{50} of 41.4 ± 10.4 μM. Antimicrobial activity of pseudacyclin A has been evaluated against the following set of standard reference strains: *S. aureus, E. faecalis, E. coli, P. aerugonosa, S. hemolyticus, C. albicans, C. crusei, C. tropicalis, C. parapsilosis*. No bactericidal or bacteriostatic effect has been observed.

Acknowledgment. This work was supported by the Ministry of Education, Youth and Sports of the Czech Republic (LC07017, ME10140, and MSM6198959216), European Commission (MTKD-CT-2004-014407), and Institutional Research Concept (AV0Z50200510). We acknowledge with thanks the expert assistance of J. Olsovska, P. Man, M. Kolarik (all IMIC, Prague), H. Zahradnickova (Ceske Budejovice), and L. Lepsa (Vidia, Prague). The authors also thank Prof. S. de Hoog, the Centraalbureau voor Schimmelcultures (CBS, Utrecht, The Netherlands), for providing us the fungal reference strains. The authors claim they do not have any association that might pose a conflict of interest.

Supporting Information Available: ^{1}H, HMBC, and HSQC NMR spectra for compound **1** and SEM images of a surface cultivation of *P. boydii* are provided free of charge via the Internet at http://pubs.acs.org.

References and Notes

(1) Tintelnot, K.; Just-Nubling, G.; Horre, R.; Graf, B.; Sobottka, I.; Seibold, M.; Haas, A.; Kaben, U.; De Hoog, G. S. *Med. Mycol.* **2009**, *47*, 351–358.
(2) Cortez, K. J.; Roilides, E.; Quiroz-Telles, F.; Meletiadis, J.; Antachopoulos, C.; Knudsen, T.; Buchanan, W.; Milanovich, J.; Sutton, D. A.; Fothergill, A.; Rinaldi, M. G.; Shea, Y. R.; Zaoutis, T.; Kottilil, S.; Walsh, T. J. *Clin. Microbiol. Rev.* **2008**, *21*, 157–197.
(3) Grenouillet, F.; Botterel, F.; Crouzet, J.; Larosa, F.; Hicheri, Y.; Forel, J. M.; Helias, P.; Ranque, S.; Delhaes, L. *Med. Mycol.* **2009**, *47*, 343–350.
(4) Rodriguez-Tudela, J. L.; Berenguer, J.; Guarro, J.; Kantarcioglu, A. S.; Horre, R.; De Hoog, G. S.; Cuenca-Estrella, M. *Med. Mycol.* **2009**, *47*, 359–370.
(5) Gilgado, F.; Serena, C.; Cano, J.; Gene, J.; Guarro, J. *Antimicrob. Agents Chemother.* **2006**, *50*, 4211–4213.
(6) Bouchara, J. P.; Horre, R.; de Hoog, S. *Med. Mycol.* **2009**, *47*, 341–342.
(7) Tintelnot, K.; Wagner, N.; Seibold, M.; de Hoog, G. S.; Horre, R. *Mycoses* **2008**, *51*, 11–16.
(8) Gilgado, F.; Cano, J.; Gene, J.; Sutton, D. A.; Guarro, J. *J. Clin. Microbiol.* **2008**, *46*, 766–771.
(9) Gilgado, F.; Cano, J.; Gene, J.; Serena, C.; Guarro, J. *Med. Mycol.* **2009**, *47*, 371–374.
(10) Harun, A.; Perdomo, H.; Gilgado, F.; Chen, S. C. A.; Cano, J.; Guarro, J.; Meyer, W. *Med. Mycol.* **2009**, *47*, 406–414.
(11) Thornton, C. R. *Clin. Vac. Immunol.* **2009**, *16*, 756–764.
(12) Hachem, R. Y.; Kontoyiannis, D. P.; Chemaly, R. F.; Jiang, Y.; Reitzel, R.; Raad, I. *J. Clin. Microbiol.* **2009**, *47*, 129–133.
(13) Jegorov, A.; Haiduch, M.; Sulc, M.; Havlicek, V. *J. Mass Spectrom.* **2006**, *41*, 563–576.
(14) Jegorov, A.; Paizs, B.; Kuzma, M.; Zabka, M.; Landa, Z.; Sulc, M.; Barrow, M. P.; Havlicek, V. *J. Mass Spectrom.* **2004**, *39*, 949–960.
(15) Sulc, M.; Peslova, K.; Zabka, M.; Hajduch, M.; Havlicek, V. *Int. J. Mass Spectrom.* **2009**, *280*, 162–168.
(16) Horka, M.; Ruzicka, F.; Kubesova, A.; Hola, V.; Slais, K. *Anal. Chem.* **2009**, *81*, 3997–4004.
(17) Pereira, M.; Silva, B.; Pinto, M.; Barreto-Bergter, E.; Santos, A. *Mycopathologia* **2009**, *167*, 25–30.
(18) Larcher, G.; Cimon, B.; Symoens, F.; Tronchin, G.; Chabasse, D.; Bouchara, J. P. *Biochem. J.* **1996**, *315*, 119–126.

(19) da Silva, B. A.; dos Santos, A. L. S.; Barreto-Bergter, E.; Pinto, M. R. *Curr. Microbiol.* **2006**, *53*, 18–22.
(20) Silva, B. A.; Pinto, M. R.; Soares, R. M. A.; Barreto-Bergter, E.; Santos, A. L. S. *Res. Microbiol.* **2006**, *157*, 425–432.
(21) Pinto, M. R.; Gorin, P. A. J.; Wait, R.; Mulloy, B.; Barreto-Bergter, E. *Glycobiology* **2005**, *15*, 895–904.
(22) Pinto, M. R.; Mulloy, B.; Haido, R. M. T.; Travassos, L. R.; Bergter, E. B. *Microbiology-Sgm* **2001**, *147*, 1499–1506.
(23) Pinto, M. R.; Rodrigues, M. L.; Travassos, L. R.; Haido, R. M. T.; Wait, R.; Barreto-Bergter, E. *Glycobiology* **2002**, *12*, 251–260.
(24) Nosanchuk, J. D.; Casadevall, A. *Cell. Microbiol.* **2003**, *5*, 203–223.
(25) Sugui, J. A.; Pardo, J.; Chang, Y. C.; Zarember, K. A.; Nardone, G.; Galvez, E. M.; Muellbacher, A.; Gallin, J. I.; Simon, M. M.; Kwon-Chung, K. J. *Eukaryot. Cell* **2007**, *6*, 1562–1569.
(26) Li, X. F.; Kim, S. K.; Nam, K. W.; Kang, J. S.; Choi, H. D.; Son, B. W. *J. Antibiot.* **2006**, *59*, 248–250.
(27) Maebayashi, Y.; Horie, Y.; Satoh, Y.; Yamazaki, M. *Mycotoxins* **1985**, *22*, 33–34.
(28) Kuroda, K.; Yoshida, M.; Uosaki, Y.; Ando, K.; Kawamoto, I.; Oishi, E.; Onuma, H.; Yamada, K.; Matsuda, Y. *J. Antibiot.* **1993**, *46*, 1196–1202.
(29) Katsuta, R.; Shibata, C.; Ishigami, K.; Watanabe, H.; Kitahara, T. *Tetrahedron Lett.* **2008**, *49*, 7042–7045.
(30) Kamigiri, K.; Tanaka, K.; Matsumoto, H.; Nagai, K.; Watanabe, M.; Suzuki, K. *J. Antibiot.* **2004**, *57*, 569–572.
(31) Bertrand, S.; Larcher, G.; Landreau, A.; Richomme, P.; Duval, O.; Bouchara, J. P. *BioMetals* **2009**, *22*, 1019–1029.
(32) Zahradnickova, H.; Husek, P.; Simek, P. *J. Sep. Sci.* **2009**, *32*, 3919–3924.
(33) Liu, W. T.; Ng, J.; Meluzzi, D.; Bandeira, N.; Gutierrez, M.; Simmons, T. L.; Schultz, A. W.; Linington, R. G.; Moore, B. S.; Gerwick, W. H.; Pevzner, P. A.; Dorrestein, P. C. *Anal. Chem.* **2009**, *81*, 4200–4209.
(34) Takats, Z.; Kobliha, V.; Sevcik, K.; Novak, P.; Kruppa, G.; Lemr, K.; Havlicek, V. *J. Mass Spectrom.* **2008**, *43*, 196–203.
(35) Naik, A. K.; Hanay, M. S.; Hiebert, W. K.; Feng, X. L.; Roukes, M. L. *Nat. Nanotechnol.* **2009**, *4*, 445–450.
(36) Kuzma, M.; Sedmera, P.; Jegorov, A.; Havlicek, V. *J. Nat. Prod.* **2009**, *72*, 159–163.
(37) Hajduch, M.; Mihal, V.; Minarik, J.; Faber, E.; Safarova, M.; Weigl, E.; Antalek, P. *Cytotechnology* **1996**, *19*, 243–245.
(38) Hajduch, M.; Nemcek, R.; Vitek, P.; Macela, A.; Kovarova, H. *Folia Biol.* **1998**, *44*, 193–200.

NP900472C

3.3. Ostatní proteomické a lipidomické projekty a klinické aplikace

3.3.1. Oxidace během NALDI-TOF MS jako nástroj pro určování polohy dvojných vazeb

v publikaci

Time-dependent Oxidation during Nano-assisted Laser Desorption Ionization Mass Spectrometry: A useful Tool for Structure Determination or a Source of Possible Confusion?

Pavlásková K., Strnadová M., Strohalm M., Havlíček V., Šulc M., Volný M.

Anal Chem. 83(14), 5661-5665 (2011)

Prohlášení spoluautorů

„Prohlašuji, že Kateřina Pavlásková se patřičně podílela (50 %) na plánování experimentů, jejich měření, interpretaci výsledků a sepisování této publikace.“

V Praze dne:

Doc. RNDr. Miroslav Šulc, PhD.

analytical chemistry

ARTICLE

pubs.acs.org/ac

Time-Dependent Oxidation during Nano-Assisted Laser Desorption Ionization Mass Spectrometry: A Useful Tool for Structure Determination or a Source of Possible Confusion?

Kateřina Pavlásková,[†] Marcela Strnadová,[†] Martin Strohalm,[†] Vladimír Havlíček,[†,‡] Miroslav Šulc,[†,*] and Michael Volný[†,*]

[†]Laboratory of Molecular Structure Characterization, Institute of Microbiology of the ASCR, v.v.i., Vídeňská 1083, Prague 4, CZ-142 20 Czech Republic

[‡]Department of Analytical Chemistry, Faculty of Science, Palacky University, 17. listopadu 12, CZ-771 46 Olomouc, Czech Republic

S *Supporting Information*

ABSTRACT: This work reports on a new and extremely simple approach for determination of a double bond position by a laser desorption ionization mass spectrometry. It is solely based on the catalytic properties of nanostructured surfaces used in nanoassisted laser desorption ionization experiments. These surfaces can induce oxidation of analytes, which results in a mass shift that can be detected by mass spectrometry. If a site of unsaturation is oxidized and cleaved, the m/z difference is diagnostic of the position of a double bond. By demonstrating that the oxidation depends on the analyte surface dwell time, it was proven that it is caused by the surface activity and not by the laser desorption ionization process itself. Control matrix-assisted laser desorption/ionization (MALDI) experiment showed only a limited partial oxidation and no time dependency of the process. The ability to determine a position of a double bond was demonstrated on polyunsaturated phospholipids and cyclosporine A. In some other cases, however, the unexpected oxidation could cause confusion, as demonstrated for a glycosphingolipid from a porcine brain extract.

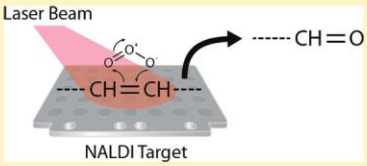

Determination of a double bond position has long been a traditional task in structural characterization of organic compounds and biologically important molecules by mass spectrometry.[1−5] For example, phospholipids, which are well-known to be a crucial structural component of cell membranes in almost all living organisms, form many isomeric species that may often differentiate only by the position of the unsaturation sites.[6] Modern soft-ionization mass spectrometry techniques provide fast and efficient analysis of phospholipids in biological extracts[6] as well as from different tissues directly.[7,8] Exact mass measurement reveals the possible phospholipid candidates based on the molecular formula and tandem mass spectrometry can further identify the headgroup and ideally also the acyl side chain lengths and the degree of unsaturation of each acyl connected by an ester bond.[6] Unfortunately, tandem mass spectrometry (MS^2) is unable to identify the position of double bonds within the acyl chains because there are usually no identifying fragments that would allow directly distinguishing between two different positions of unsaturation. Thus, the conventional collision-induced dissociation spectra (obtained under standard low-energy conditions) of the phospholipids that differ only in the position of a double bond are normally indistinguishable.[9,10]

Different approaches that have been introduced to overcome this limitation of mass spectrometry in lipid analyses were recently reviewed.[11] The first is based on measuring MS^3 spectra.[12,13] This can be rather complicated, especially at low ion intensities. In addition, MS^3 experiment can be performed only with ion trap mass analyzers (not counting expensive ion cyclotron resonance spectrometers (ICR),[14] the very rare pentaquadrupole instruments[15] and other experimental designs). The second approach employs a selective derivatization prior to the analysis,[9,16,17] although in some cases, the oxidation agent can simply be used directly on a matrix-assisted laser desorption/ionization (MALDI) plate.[18] The third solution is based on an online ozonolysis of the double bond during electrospray ionization.[10,11,19,20] Lipid oxidation can also be induced in desorption electrospray[21] or in low-temperature plasma.[22]

This work reports on a new and simple approach for determination of a double bond position. It is solely based on the catalytic properties of the nanostructured NALDI (nanoassisted or nanowire-assisted laser desorption ionization) surfaces, and unlike in the previous MALDI reports,[18] no extra chemical agent is necessary. Each sample can be spotted twice on the NALDI surface. The first spot is then measured immediately, and the mass spectrum of the intact analyte is obtained. The second spot is measured after a dwell time of approximately 100 min (or more). If the acyl side

Received: March 30, 2011
Accepted: June 2, 2011

ACS Publications © XXXX American Chemical Society

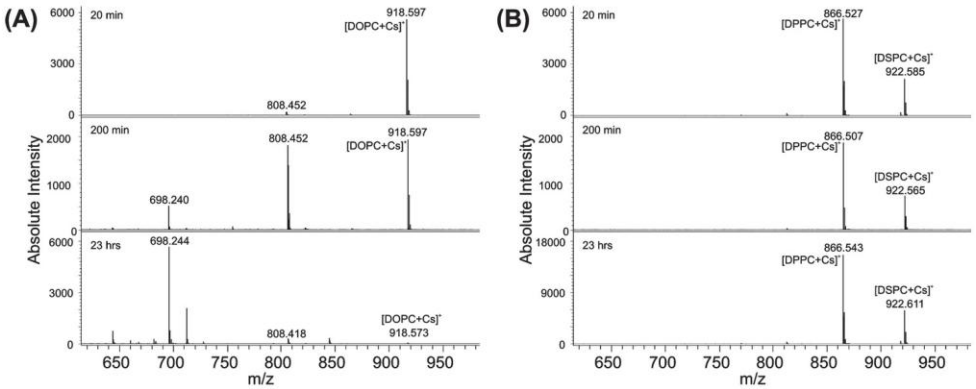

Figure 1. (panel A) Oxidation of DOPC measured by NALDI-TOF-MS. The peak at $m/z = 918$ corresponds to the cesiated molecule of DOPC; the peak at $m/z = 808$, to the first cleavage and oxidation of one double bond; and the peak at $m/z = 698$, to the oxidation and cleavage of both double bonds. (panel B) NALDI-TOF-MS spectrum of cesiated DPPC ($m/z = 866$) molecule and cesiated DSPC ($m/z = 922$) molecule. No chemical changes were detected in DPPC and DSPC, even after 23 h on the NALDI surface.

chain contains a double bond, it is oxidized and cleaved. A new peak that corresponds to surface-induced cleavage of this double bond appears in the mass spectrum at lower m/z. The m/z difference is diagnostic of the position of each double bond.

The silicon-based NALDI surfaces, which are commercially available, are one of the several existing substrates for matrix free LDI,[23] sometimes referred to as surface-assisted laser desorption ionization,[24] as originally proposed by Sunner.[25] The field of matrix-free LDI was significantly strengthened after introduction of desorption ionization on silicon by Siuzdak,[26] and silicon-based surfaces are still the most promising LDI surfaces.[27,28] There are many different concepts that use nanostructured semiconductors for LDI.[23,24] Commercial NALDI plates have developed from the original nanowire assisted LDI and have been previously reported as a useful tool for the analysis of small molecules by desorption ionization as well as for lipid imaging.[29−34] The NALDI target plate is layered with nanowires, which serve as an active, matrix-free surface for desorption-ionization of spotted samples. Once samples are dissolved in the desired solvent, no further sample preparation is required, and they can be spotted directly on the NALDI surface. We believe that our new technique, which facilitates the determination of the double bond position in an unsaturated acyl side chain, will further expand the usability of matrix-free LDI techniques from nanostructured surfaces in the analysis of lipids.

■ EXPERIMENTAL SECTION

Material. NALDI plates, which are produced by Nanosys, Inc. for Bruker Daltonics Inc., were purchased from the local Bruker representative. Cesium and potassium chlorides were purchased from Sigma-Aldrich. Cyclosporine A (CsA) and dihydrocyclosporine A (DhCsA) were research samples from TEVA Pharmaceuticals CR. All solvents used were from Merck. Lipid standards were purchased from AvantiLipids, and the following abbreviations are used throughout the text: GlcCer = *N*-(tetracosanoyl)-1-β-glucosyl-sphing-4-enine (d18:1/24:0), DLNPC = 1,2-dilinolenoyl-*sn*-glycero-3-phosphocholine, DSPC = 1,2-distearoyl-*sn*-glycero-3-phosphocholine (18:0/18:0), DOPC = 1,2-dioleoyl-*sn*-glycero-3-phosphocholine (18:1/18:1), and DPPC = 1,2-dipalmitoyl-*sn*-glycero-3-phosphocholine (16:0/16:0).

Sample Preparation for NALDI-MS and MALDI-MS. All lipidic solutions were prepared in chloroform first and diluted in methanol to 200 μM stock solutions. Lipids were then mixed with 50 mM solution of cesium chloride in water (1:1,v/v), the concentration was adjusted to 20 μM, and the solutions were then spotted on NALDI plates (3 μL). The plates were allowed to dry at room temperature. GlcCer (d18:1/24:0) was dissolved in chloroform and diluted in methanol (approximately on target amount was 0.1 mg). CsA and DhCsA were prepared as 2 nM methanolic solutions and mixed with 50 mM cesium chloride (1:1, v/v) prior spotting on the NALDI plate (3 μL). Control samples for MALDI were treated exactly the same way as NALDI samples, and they were deposited on a standard stainless steel plate and mixed with α-cyano-4-hydroxycinnamic acid matrix.

NALDI-TOF-MS. Time-of-flight (TOF) mass spectra were acquired in positive reflector mode using a Bruker Daltonics Ultraflex III MALDI time-of-flight mass spectrometer. MS data were acquired in the m/z range between 500 and 2000 by averaging signals from 1500 consecutive laser shots using target random-walk movement. Prior to each data acquisition, external calibration was conducted using a peptide calibration standard (Bruker Daltonics). The FlexAnalysis 3.0 program (Bruker Daltonics) was used to analyze the data.

NALDI-FTICR MS. High-resolution mass spectra were acquired using an APEX Ultra 9.4 T mass spectrometer equipped with Apollo II ESI/MALDI ion source (Bruker Daltonics). Mass spectra were acquired in a positive ion mode with 512k data points using a SmartBeam 200 Hz laser. Results were analyzed using Data Analysis 4.0 (Bruker Daltonics) and open source program mMass 3.10.[35]

■ RESULTS AND DISCUSSION

The lipid standards were deposited on the NALDI surface by a pipet and analyzed by laser desorption ionization. In addition to

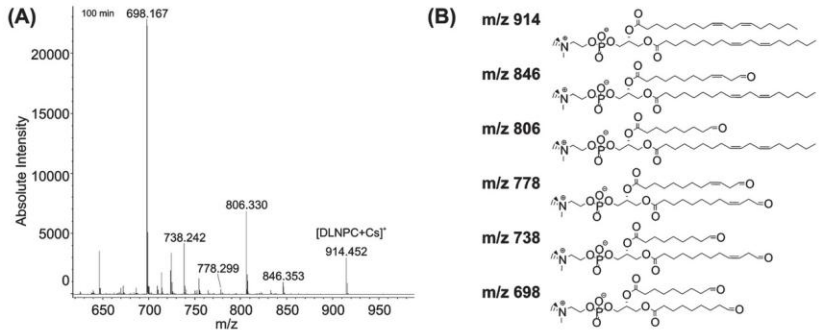

Figure 2. (panel A) NALDI-TOF-MS spectrum of DLNPC after 2 h on the NALDI surface and (panel B) the structures of the corresponding oxidation products.

protonated molecules, phospholipids readily ionize in a form of sodiated molecules. Addition of potassium or cesium chloride was used to force the equilibrium toward cationization and to obtain a single ion (potassiated or cesiated molecule, for each species).

Figure 1A shows oxidation of DOPC, which has two unsaturated sites, one on each acyl side chain. The peak at $m/z = 918$ corresponds to the cesium adduct; the peak at $m/z = 808$, to the oxidation and consecutive cleavage of the first double bond; and the peak at $m/z = 698$, to the oxidation and consecutive cleavage of both double bonds. The specific loss of 110 nominal mass units, which corresponds to the loss of eight methylene groups and one terminal methyl group (nine carbons total) and the oxidation of the new terminal carbon to an aldehyde group, allowed for assigning the site of unsaturation as shown in schema in Figure S1 (Supporting Information). The general procedure for calculating the number of carbons cleaved from the acyl chain (x) and thus the position of the double bond from the NALDI mass spectrum is rather trivial,

$$x = (\Delta m + 16)/14 \quad (1)$$

where Δm is the mass difference between the intact molecule and the product after oxidation and cleavage.

When phospholipids with fully saturated chains were analyzed, no other peaks were detected, except for the expected main alkali metal adduct. This can be seen in Figure 1B, which shows the NALDI-MS spectrum of a mixture of DPPC (16:0/16:0) and DSPC (18:0/18:0). The spectrum only shows peaks at m/z = 866 ($[\mathrm{DPPC} + \mathrm{Cs}]^+$) and 922 ($[\mathrm{DSPC} + \mathrm{Cs}]^+$) and no possible oxidation products. This result confirmed that oxidation of DOPC (18:1/18:1) happens only on the carbon double bonds and not on the phosphocholine headgroup and can thus be used for determination of a double bond position.

While the oxidation of symmetrically unsaturated DOPC (18:1/18:1) produced only two possible oxidation products, NALDI of multiply unsaturated DLNPC revealed five possible combinations of oxidation products, as shown in the spectrum in Figure 2A. The peak assignment is outlined in schema in Figure 2B, where the corresponding structures are listed. Although the mass spectrum has become more complex due to the presence of multiple oxidation products, it is still easy to assign the double bond positions. The peak at $m/z = 914$ corresponds to the intact cesiated molecule ($[\mathrm{DLNPC} + \mathrm{Cs}]^+$); the peak at m/z = 846, to the cleavage of the first double bond on one of the acyl chains; the peak at m/z = 806, to the cleavage of the second double bond on the same acyl chain; the peak at the m/z = 778, to the cleavage of the first double bonds on both acyl chains; and the peak at m/z = 698, to the cleavages of the second double bonds on both acyl chains. The remaining peak at m/z = 738 corresponds to the asymmetric cleavage of the first double bond on one acyl and the second double bond on the other one. The number of cleaved carbons is given by the equation:

$$x = (\Delta m + 18)/14 \quad (2)$$

for the direct oxidation and cleavage of the second double bond and

$$x = (\Delta m + 2)/14 \quad (3)$$

for the consecutive oxidation and cleavage of the already oxidized and cleaved acyl chain.

To gain more insight into the NALDI oxidation processes, we investigated the time dependence of the double bond oxidation on NALDI surfaces. The NALDI surface with an analyte deposited on several spots was stored at laboratory ambient conditions, and mass spectra were periodically measured. The results in Figure 3 show development of the DOPC oxidation in time. The first evidence of double bond cleavage appeared after roughly 2 h, and it wass completed in less than 24 h. The fact that the abundance of the oxidation products strongly depended on the storage time shows that the oxidation happened on the surface and not during the laser desorption ionization process.

In a control experiment, DOPC was measured by standard MALDI-MS. Although a small oxidation product at m/z = 808 appeared in the spectrum, no further oxidation was detected. The MALDI spectrum measured immediately after the sample was prepared was practically identical to the spectrum that was remeasured after the sample was left at ambient conditions for 24 h. The catalytic activity of the NALDI surface is not surprising, considering the high surface site density that likely allows for the existence of reactive oxygen species on the NALDI surface due to the adsorption and conversion of the atmospheric oxygen molecules.

Another fact is that the surface is prepared using colloidal gold nanoclusters deposited on a silicon wafer as catalysts. Nanowires are grown using SiH_4 vapor as a reactant for cold vapor deposition process. The silicon nanowire surface is further oxidized and derivatized with (pentafluorophenyl)-propyldimethylchlorosilane.[24,28,30]

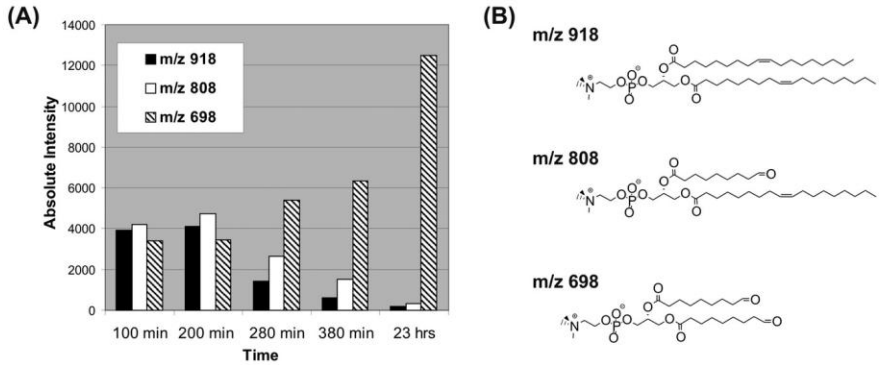

Figure 3. (panel A) Time dependency of the DOPC oxidation (100 min, 200 min, 280 min, 380 min, 23 h; intact DPPC used as internal standard) and (panel B) the structures of the corresponding oxidation products.

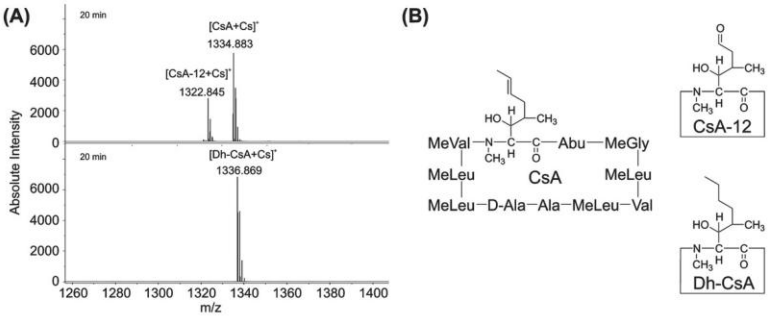

Figure 4. (panel A) NALDI-TOF-MS spectrum of cesiated cyclosporine A (top) and cesiated dihydrocyclosporine A (bottom) and (panel B) the corresponding structures.

It is not impossible that the final surface still maintains some catalytic activity, even after the production process is over. The reaction of reactive oxygen species with double bonds is expected to be energetically favorable. For instance, the addition of ozone to an alkene is exothermic by roughly 210 kJ/mol[36] and the known Criegee mechanism[37] describes how the alkene double bond is further cleaved by ozonolysis. We suggest that a similar phenomenon takes place on the NALDI surface, as well, and we believe that the time-dependent oxidation of double bonds in lipids on NALDI plates represents a useful tool for structure elucidation.

However, care must be taken in cases that analyte oxidizes unexpectedly and extremely rapidly. For instance, cyclosporine A (CsA), a cyclic nonribosomal peptide of 11 amino acids, which is used as a common immunosuppressant drug, underwent fast oxidation on NALDI surface that could be recognized in the NALDI mass spectrum as a mass shift of 12 mass units (Figure 4A, top). Contrary to CsA, its structural analog dihydrocyclosporine (DhCsA) (structure difference in Figure 4 B) did not show any indications of oxidation in the NALDI mass spectrum (Figure 4A, bottom). It is thus reasonable to conclude that the oxidation happened on the double bond that is present on the side chain of MeBmt ((4*R*)-4-[(*E*)-2-butenyl]-4,*N*-dimethyl-L-threonine) of CsA but not in the DhCsA. As in the case of phospholipids, the oxidation of CsA resulted in the subsequent bond cleavage and formation of an aldehyde group on the side chain, and it could be utilized to probe the presence of an unsaturated bond. However, in some other cases, the swift oxidation can affect a different functional group.

We analyzed commercially available cerebroside extract of porcine brain with predominant species GlcCer (d18:1/24:0) with molecular formula $C_{48}H_{93}NO_8$ (monoisotopic mass M = 811.6901). Potassium chloride was added to improve ionization by cationization, and NALDI mass spectrum was acquired immediately using a high-resolution FTICR mass spectrometer. Although the peak of potassiated molecule MK^+ was expected at m/z = 850.6532, the base peak in the spectrum (Figure S2 in Supporting Information) was at m/z = 864.6327, which corresponds to molecular formula $C_{48}H_{91}NO_9K^+$ (with 0.2 ppm mass accuracy). The gain of one oxygen accompanied by the loss of two hydrogens compared with the expected composition can be explained by the fast oxidation of the central secondary amine in the GlcCer (d18:1/24:0) molecule to a nitrone (Figure S2). We

must emphasize that unlike the double bond oxidation, the oxidation of the secondary amine on NALDI surfaces likely brings no useful structural information about the analyte and could actually cause a significant confusion in a routine analysis.

CONCLUSION

The NALDI surfaces have been shown to induce oxidation of analytes. The oxidation results in a different mass of the analytes, and the mass shift can thus be detected by mass spectrometry. By demonstrating the time dependency of the oxidation, we showed that it is caused by the surface activity and not by the ionization process itself. It can be speculated that catalytic properties of the NALDI surface are residuum of the manufacturing process. Alternatively, its high surface site density likely allows for storing a sufficient amount of adsorbed oxygen reactive species that can facilitate the reported oxidation processes.

Although there is a risk of confusion due to unexpected oxidation in some cases, we propose that the phenomenon of NALDI oxidation has a potential to be applied as a tool for determination of sites of unsaturation in different acyl chains, especially in lipid structural elucidation.

ASSOCIATED CONTENT

Supporting Information. Figures S1 and S2, as noted in text. This material is available free of charge via the Internet at http://pubs.acs.org.

AUTHOR INFORMATION

Corresponding Author
*E-mail: (Michael Volny, mass spectrometry) mvolny@gmail.com; (Miroslav Sulc, biochemistry) msulc@biomed.cas.cz.

ACKNOWLEDGMENT

The work was supported by the Czech Science Foundation (Project P206/10/P018) and Grant Agency of Charles University (Project 258179). M.V.'s research was supported by a Marie Curie International Reintegration Grant within the seventh European Community Framework Program. Other support was provided by the Ministry of Education, Youth, and Sports of the Czech Republic (LC545, ME10013) and by an Institutional research concept of the Institute of Microbiology (AV0Z50200510).

REFERENCES

(1) Andersson, B. A.; Christie, W. W.; Holman, R. T. *Lipids* **1975**, *10*, 215–219.
(2) Janssen, G.; Parmentier, G. *Biomed. Mass Spectrom.* **1978**, *5*, 439–443.
(3) Jensen, N. J.; Gross, M. L. *Mass Spectrom. Rev.* **1987**, *6*, 497–536.
(4) Kawaguchi, A.; Kobayashi, Y.; Ogawa, Y.; Okuda, S. *Chem. Pharm. Bull.* **1983**, *31*, 3228–3232.
(5) Schmitz, B.; Egge, H. *Chem. Phys. Lipids* **1979**, *25*, 287–298.
(6) Khalil, M. B.; Hou, W. M.; Zhou, H.; Elisma, F.; Swayne, L. A.; Blanchard, A. P.; Yao, Z. M.; Bennett, S. A. L.; Figeys, D. *Mass Spectrom. Rev.* **2010**, *29*, 877–929.
(7) Dill, A. L.; Ifa, D. R.; Manicke, N. E.; Zheng, O. Y.; Cooks, R. G. *J. Chromatogr., B: Anal. Technol. Biomed. Sci. Appl.* **2009**, *877*, 2883–2889.
(8) Pol, J.; Vidova, V.; Kruppa, G.; Kobliha, V.; Novak, P.; Lemr, K.; Kotiaho, T.; Kostiainen, R.; Havlicek, V.; Volny, M. *Anal. Chem.* **2009**, *81*, 8479–8487.
(9) Moe, M. K.; Anderssen, T.; Strom, M. B.; Jensen, E. *J. Am. Soc. Mass Spectrom.* **2005**, *16*, 46–59.
(10) Thomas, M. C.; Mitchell, T. W.; Harman, D. G.; Deeley, J. M.; Murphy, R. C.; Blanksby, S. J. *Anal. Chem.* **2007**, *79*, 5013–5022.
(11) Mitchell, T. W.; Pham, H.; Thomas, M. C.; Blanksby, S. J. *J. Chromat. B: Anal. Technol. Biomed. Sci. Appl.* **2009**, *877*, 2722–2735.
(12) Ekroos, K.; Ejsing, C. S.; Bahr, U.; Karas, M.; Simons, K.; Shevchenko, A. *J. Lipid Res.* **2003**, *44*, 2181–2192.
(13) Hsu, F. F.; Turk, J. *J. Am. Soc. Mass Spectrom.* **2008**, *19*, 1673–1680.
(14) Kruppa, G.; Schnier, P. D.; Tabei, K.; Van Orden, S.; Siegel, M. M. *Anal. Chem.* **2002**, *74*, 3877–3886.
(15) Schwartz, J. C.; Schey, K. L.; Cooks, R. G. *Int. J. Mass Spectrom. Ion Processes* **1990**, *101*, 1–20.
(16) Halket, J. M.; Zaikin, V. G. *Eur. J. Mass Spectrom.* **2005**, *11*, 127–160.
(17) Nilsson, R.; Liljenberg, C. *Phytochem. Anal.* **1991**, *2*, 253–259.
(18) Stubiger, G.; Belgacem, O.; Rehulka, P.; Bicker, W.; Binder, B. R.; Bochkov, V. *Anal. Chem.* **2010**, *82*, 5502–5510.
(19) Thomas, M. C.; Mitchell, T. W.; Blanksby, S. J. *J. Am. Chem. Soc.* **2006**, *128*, 58–59.
(20) Thomas, M. C.; Mitchell, T. W.; Harman, D. G.; Deeley, J. M.; Nealon, J. R.; Blanksby, S. J. *Anal. Chem.* **2008**, *80*, 303–311.
(21) Benassi, M.; Wu, C. P.; Nefliu, M.; Ifa, D. R.; Volny, M.; Cooks, R. G. *Int. J. Mass Spectrom.* **2009**, *280*, 235–240.
(22) Zhang, J. I.; Tao, W. A.; Cooks R. G. *Anal. Chem.* **2011**, *83*, 4738−4744
(23) Peterson, D. S. *Mass Spectrom. Rev.* **2007**, *26*, 19–34.
(24) Law, K. P.; Larkin, J. R. *Bioanal. Chem.* **2011**, *399*, 2597−2622.
(25) Sunner, J.; Dratz, E.; Chen, Y. C. *Anal. Chem.* **1995**, *67*, 4335–4342.
(26) Wei, J.; Buriak, J. M.; Siuzdak, G. *Nature* **1999**, *399*, 243–246.
(27) Law, K. P. *Int. J. Mass Spectrom.* **2010**, *290*, 72–84.
(28) Go, E. P.; Apon, J. V.; Luo, G. H.; Saghatelian, A.; Daniels, R. H.; Sahi, V.; Dubrow, R.; Cravatt, B. F.; Vertes, A.; Siuzdak, G. *Anal. Chem.* **2005**, *77*, 1641–1646.
(29) Kang, M. J.; Pyun, J. C.; Lee, J. C.; Choi, Y. J.; Park, J. H.; Park, J. G.; Lee, J. G.; Choi, H. J. *Rapid Commun. Mass Spectrom.* **2005**, *19*, 3166–3170.
(30) Luo, G. H.; Chen, Y.; Daniels, H.; Dubrow, R.; Vertes, A. *J. Phys. Chem. B* **2006**, *110*, 13381–13386.
(31) Guenin, E.; Lecouvey, M.; Hardouin, J. *Rapid Commun. Mass Spectrom.* **2009**, *23*, 1395–1400.
(32) Shenar, N.; Cantel, S.; Martinez, J.; Enjalbal, C. *Rapid Commun. Mass Spectrom.* **2009**, *23*, 2371–2379.
(33) Vidova, V.; Novak, P.; Strohalm, M.; Pol, J.; Havlicek, V.; Volny, M. *Anal. Chem.* **2010**, *82*, 4994–4997.
(34) Pol, J.; Novak, P.; Volny, M.; Kruppa, G. H.; Kostiainen, R.; Lemr, K.; Havlicek, V. *Eur. J. Mass Spectrom.* **2008**, *14*, 391–399.
(35) Strohalm, M.; Kavan, D.; Novak, P.; Volny, M.; Havlicek, V. *Anal. Chem.* **2010**, *82*, 4648–4651.
(36) Anglada, J. M.; Crehuet, R.; Bofill, J. M. *Chem.−Eur. J.* **1999**, *5*, 1809–1822.
(37) Criegee, R. *Angew. Chem.* **1975**, *14*, 745–752.

3.3.2. Identifikace alergenů v proteomu pšenice

v publikaci:

A New Approach to the Isolation and Characterization of Wheat Flour Allergens

Šotkovský P., Sklenář J., Halada P., Cinová J., Šetinová I., Kainarová A., Goliáš J., **Pavlásková K**., Honzová S., Tučková L.

Clin Exp Allergy. 41, 1031-1043 (2011)

Prohlášení spoluautorů

„Prohlašuji, že Kateřina Pavlásková se patřičně podílela (20 %) na plánování hmotnostně spektrometrických experimentů, jejich měření, interpretaci výsledků a sepisování této publikace.“

V Praze dne:

Doc. RNDr. Ludmila Tučková, DrSc.

doi: 10.1111/j.1365-2222.2011.03766.x
Clinical & Experimental Allergy, **41**, 1031–1043
© 2011 Blackwell Publishing Ltd

ORIGINAL ARTICLE **Allergens**

A new approach to the isolation and characterization of wheat flour allergens

P. Šotkovský[1], J. Sklenář[1], P. Halada[1], J. Cinová[1], I. Šetinová[2], A. Kainarová[1], J. Goliáš[1], K. Pavlásková[1], S. Honzová[2] and L. Tučková[1]
[1]*Institute of Microbiology, Academy of Sciences of the Czech Republic, Prague, Czech Republic and* [2]*SYNLAB (IMUMED), Prague, Czech Republic*

Clinical & Experimental Allergy

Summary

Background The incidence of food allergy to wheat is increasing. Its diagnosis depends on the purity of major allergens and their inclusion in tests. Isolation and characterization of wheat allergens are therefore of utmost importance.

Objective To purify and identify wheat flour allergens most frequently recognized by patients' IgE antibodies and to study their allergenicity.

Methods Water/salt-soluble extracts from wheat flour were prepared and separated using a combination of ultrafiltration, isoelectric focusing and liquid chromatography. Purified proteins were analysed by immunoblotting using pooled sera from patients with atopic dermatitis who possessed IgE specific to wheat. Wheat proteins found to bind IgE were subsequently identified by matrix-assisted laser desorption/ionisation-time of flight mass spectrometry. The frequency and intensity of IgE binding of isolated proteins were tested using individual sera from patients and controls.

Results We developed a procedure that allows isolation of wheat allergens from natural sources. Twenty-seven potential wheat allergens have been successfully identified; of these, the following seven are newly reported in food allergy: endogenous α-amylase/subtilisin inhibitor, trypsin/α-amylase inhibitor (AAI) CMX1/CMX3, thaumatin-like protein (TLP), xylanase inhibitor protein-1, β-glucosidase, class II chitinase and 26 kDa endochitinase. TLP and wheatwin were shown to activate patients' basophils to a similar extent as two well-known allergens, lipid transfer protein (Tri a 14) and AAI 0.19 (Tri a 28.0101).

Conclusion and Clinical Relevance Our new approach enables the isolation of water/salt-soluble wheat allergens in their native form in amounts sufficient both for biological testing (*in vivo* and *in vitro*) and for physicochemical characterization. Such studies will lead to a more detailed knowledge of allergenicity of wheat proteins and to improved accuracy of diagnostic tests.

Keywords basophil activation, IgE antibodies, isolation, purification, wheat allergens
Submitted 28 July 2010; revised 5 February 2011; accepted 21 March 2011

Correspondence:
Petr Šotkovský, Institute of Microbiology, Academy of Sciences of the Czech Republic, v.v.i., Videnska 1083, 142 20 Prague, Czech Republic.
E-mail: psotkovsky@gmail.com
Cite this as: P. Šotkovský, J. Sklenář, P. Halada, J. Cinová, I. Šetinová, A. Kainarová, J. Goliáš, K. Pavlásková, S. Honzová and L. Tučková, *Clinical & Experimental Allergy*, 2011 (41) 1031–1043.

Introduction

Wheat is an important part of human diet, but its ingestion can trigger IgE-mediated food allergies. The incidence of food allergies is increasing and these allergies are thought to affect 6–8% of children and 1–3% of adults [1, 2]. Depending on the route of allergen exposure, hypersensitivity reactions to wheat may cause a variety of symptoms. For example, ingestion may cause atopic dermatitis, gastrointestinal symptoms or wheat-dependent exercise-induced anaphylaxis; inhalation may cause baker's asthma; and skin contact may occasionally trigger IgE-mediated contact urticaria [3–5].

Diagnosis of food allergy to wheat is not simple. Although oral food challenge tests are considered to be good standard for diagnosis, they are time consuming and can induce severe clinical symptoms. Detection of food-specific IgE antibodies (Abs) by radioimmunoassays or by enzymatic immunoassays, along with a history compatible with IgE-mediated symptoms, are highly sensitive but have low specificity. Moreover, a certain degree of cross-reactivity cannot be excluded [6, 7]. Skin prick tests (SPTs) are diagnostic for baker's asthma, but not for atopic dermatitis [8]. In contrast, basophil activation tests are considered to be a reliable *in vitro* diagnostic technique [9].

Poor predictability and specificity of all currently known diagnostic approaches may be associated with the insufficient purity of wheat extracts used in specific IgE assays or with the lack of inclusion of all major allergens in these extracts. Furthermore, expression of IgE-reactive proteins depends on wheat seed maturation and varies in different wheat sources [10].

On the basis of their differential solubility, wheat proteins can be classified into water/salt-soluble albumins and globulins and water/salt-insoluble gliadins and glutenins. Proteins from all these different groups are responsible for baker's asthma as well as food allergies in adults and children. Wheat food allergy in children and adult patients with multiplicity and diversity of skin symptoms, such as wheat-induced atopic dermatitis, has been investigated by several laboratories [11–13]. Proteomic analysis of wheat flour proteins revealed a number of IgE reactive components in both water/salt-soluble and insoluble fractions [shown by immunoblotting, high-performance liquid chromatography (HPLC) and mass spectrometric analysis] [14–16]. Among the major allergens identified in the water/salt-soluble fraction of wheat flour and shown to be capable of sensitization after both ingestion and inhalation are the cereal α-amylase inhibitors (AAI) and α-amylase/trypsin inhibitors (AATI). This AATI family of inhibitors consists of tetrameric proteins, often called chloroform methanol (CM) proteins on the basis of their selective extraction in chloroform/methanol mixtures (CM1, CM2, CM3, CM16 and CM17). On the other hand, the three AAIs are dimeric (0.19 and 0.53) or monomeric (0.28). Wheat amylase/subtilisin inhibitor is a bifunctional protein capable of simultaneously inhibiting endogenous wheat α-amylase and the proteinase subtilisin [17, 18]. Using IgE from allergic individuals to probe cDNA expression library, AAI 0.19 and CM7, as well as new molecules with high cross-reactive potential, including thioredoxins and β-expansins, have been identified [19].

Cross-reactivity among wheat flour allergens, other cereal allergens (barley, rye, rice and maize) and grass pollen allergens is thought to be because of common IgE-reactive epitopes. However, patients with baker's asthma and those with IgE-mediated food allergy to wheat may be sensitive to different molecules [20–22]. The most important plant panallergens are the non-specific lipid transfer proteins (LTPs), which also act as food allergens, sensitizing individuals by the oral route or by inhalation [6, 23, 24]. Although proteomic analysis has identified other wheat proteins as IgE binding (e.g. β-amylase, peroxidase, thioredoxin and serpins), a proper panel of purified wheat allergens has not yet been developed. The list of these allergens is not complete yet and new allergens are still being discovered. Moreover, the clinical relevance of these proteins remains to be determined [14, 16, 25].

Recombinant allergens may be useful in diagnosing and/or treating allergies [26, 27], but so far only a small number of wheat allergens have been cloned and produced in recombinant form [28, 29]. Many recombinant allergens do not have the same immunological characteristics as their natural counterparts. Alterations of the amino acid sequence of allergens may influence protein folding, resulting in the reduction or total prevention of IgE binding. Several recombinant allergens have been produced in bacterial expression systems as non-glycosylated proteins, although some natural AAIs are glycosylated [30]. Thus, highly purified natural allergens are still indispensable in determining the allergenicity of recombinant and natural forms of allergens. Purified allergens are needed not only for the analysis of their structure and function but also in experimental model studies [31–34].

The aim of our study was to isolate, characterize and identify the most important water/salt-soluble wheat allergens from natural sources. Therefore, we developed a three-step isolation protocol, consisting of ultrafiltration, native (liquid-phase) isoelectric focusing (IEF, Rotofor®, Bio-Rad, Hercules, CA, USA) and affinity chromatography (HPLC). Wheat proteins recognized by IgE of allergic patients were identified by matrix-assisted laser desorption/ionisation-time of flight (MALDI-TOF) mass spectrometry. The intensity and frequency of IgE binding of both previously and newly identified potential allergens were determined, as well as – in some cases – their potential to activate basophils.

Materials and methods

Patients and controls

Sera were obtained from 22 patients (13 females, nine males; mean age 23 years; range: 3–63 years) with atopic dermatitis (P1–22). All 22 patients had a suspect history of wheat allergy and elevated specific IgE Abs (mean, 10.24 U/mL; range, 0.4–72 U/mL). An open challenge test was performed with cooked wheat pasta in 14 out of 22 patients and all 14 were positive. In the remaining eight patients, a significant clinical improvement was observed after elimination diet (avoidance of wheat-containing food for 1 month). Total serum IgE and IgE specific for wheat flour, gluten, wheat pollen, timothy grass pollen and birch tree pollen were analysed using an Immulite 2000 (DPC, Siemens Medial Solution Diagnosis, Flanders, NJ, USA). Sera from 10 patients allergic to pollen allergens (D1–10) were used as 'disease controls'. Clinical, demographic and serological characteristics of the 22 patients (P1–22) and 10 disease controls (D1–10) are reported in Table 1. Sera from nine healthy individuals with normal total and wheat-specific IgE Abs were used as negative controls (C1–9).

Table 1. Demographic, clinical and serological characteristics of patients and disease controls

Patient	Sex	Age	sIgE wheat (U/mL)	Total IgE (U/mL)	Symptoms	Open challenge	Other allergies	Disease control	Sex	Age	sIgE wheat (U/mL)	Total IgE (U/mL)
P1	F	5	72.00	355	EA	Pos.	e, m	D1	M	32	<0.10	350
P2	F	6	56.10	1545	EA, RC	Pos.	e, m	D2	M	43	<0.10	345
P3	F	39	4.13	5568	A, EA	ND	bu, f, mo, nu, ri	D3	F	34	0.20	106
P4	F	43	2.60	563	A, EA	Pos.	c, m, po, sh	D4	F	22	<0.10	364
P5	F	10	12.60	1083	A, EA, RC	Pos.	hdm, mo, po	D5	F	32	<0.10	12
P6	M	28	13.30	3590	D, EA, RC	Pos.	ap, nu, po	D6	F	49	<0.10	33
P7	F	29	15.00	21452	A, EA, RC	ND	c, d, hdm	D7	M	36	0.20	634
P8	M	25	1.86	14953	A, EA, RC	ND	hdm	D8	M	24	<0.10	1021
P9	F	63	1.86	45	EA, RC	Pos.	po	D9	F	44	<0.10	54
P10	F	21	3.40	2686	AB, EA, OAS, RC	Pos.	ca, ce, po	D10	F	46	<0.10	49
P11	F	33	3.97	2501	A, EA, OAS, RC	ND	ap, ca, co, nu					
P12	M	8	2.93	2404	EA, RC	Pos.	po					
P13	M	3	1.29	854	EA	Pos.	e, m					
P14	F	20	0.40	272	EA, RC	ND	po					
P15	M	5	3.55	1524	EA	Pos.	e, m					
P16	F	44	1.35	222	EA, IU	ND	co, e, po, sp					
P17	M	6	13.10	482	EA	Pos.	c, e, fr, ho, hon, m, mo, nu, po, se, ve					
P18	F	32	10.80	4331	A, D, EA, OAS, RC	Pos.	fr, hdm, mo, nu, po, se, ve					
P19	M	24	1.14	1757	EA, RC	ND	co, hdm, nu, po					
P20	M	6	0.70	546	A, EA, RC	Pos.	c, hdm, po					
P21	F	4	0.78	147	EA, RC	Pos.	e, m, nu, po					
P22	M	43	2.47	423	OAS, RC	ND	ap, po					

F, female; M, male; ND, not done; pos., positive; sIgE, specific IgE; U/mL, unit antigen per millilitre; A, asthma bronchiale; D dyspepsia; EA, eczema atopicum; IU, idiopathic urticaria; OAS, oral allergic syndrome; RC, rhinoconjunctivitis; a, animals; ap, apple; bu, buckwheat; c, cat; ca, carrot; ce, celery; co, codfish; d, dog; e, egg white; f, fish; fr, fruit; hdm, house dust mite; hon, honey; ho, horse; m, milk; mo, mould; nu, nuts; po, pollen; se, seeds; sh, shrimp; sp, spices; ri, rice; ve, vegetables.

Measurements of total and specific serum immunoglobulin E

The concentrations of total and wheat-specific IgE were determined by fluorescence enzyme immunoassay (Immulite 2000, DPC, Siemens Medical Solution Diagnosis) according to the manufacturer's instructions. Allergen-specific IgE concentrations above 0.35 kU/L were considered positive.

Wheat sample preparation

Unless otherwise specified, all chemicals were from Sigma (Steinheim, Germany). Wheat flour from cultivar Akteur (*Tritium aestivum*) was kindly provided by Professor J. Petr of the Czech University of Agriculture, Prague. Proteins were extracted from wheat flour (4 g) with PBS (40 mL) overnight at 4 °C, ultrasonicated (U50, IKA Laboratortechnik, Staufen, Germany) for 15 min on ice and centrifuged at 20 000 g for 15 min at 4 °C. Extracted proteins were sequentially separated using Amicon Ultra 100k, 30k and 10k ultrafiltration devices (Millipore, Billerica, MA, USA) in this order providing gross separation according to the molecular weight of the proteins. A 10 mL sample containing 0.35% CHAPS was loaded onto the 100k filter device with a 100 kDa molecular-weight cut-off for 30 min at 2500 g and 20 °C. The concentrated higher molecular-weight fraction was discarded and the filtrate was ultrafiltered using a 30k filter device with a 30 kDa molecular-weight cut-off. The concentrate was stored (fraction I) and the filtrate was purified using a 10k filter device with a 10 kDa molecular-weight cut-off, yielding fraction II (60 min, 2500 g and 20 °C). Protein concentration was determined using a Bicinchoninic Acid Protein Assay Kit (BCA, Pierce, IL, USA). Samples were divided into aliquots and stored at −20 °C.

Liquid-phase isoelectric focusing

Proteins in fractions I and II were separated according to their pI using a Rotofor® preparative cell (Bio-Rad). Fraction I contained proteins of molecular mass above 30 kDa and below 100 kDa, whereas fraction II contained proteins of molecular mass above 10 kDa and below 30 kDa. Proteins from fraction I (15 mL, containing 45 mg protein) were mixed with 0.5% CHAPS and diluted in

55 mL of distilled water containing 5% glycerol, 5% premixed Bio-Lyte pH 5–8, pH 3–10 (Bio-Rad) and ampholyte pH 4–6 (Fluka, Buchs, Switzerland). Proteins in fraction II were diluted similarly, except that premixed ampholytes pH 4–6 and pH 6–9 were used. Both samples were fractionated using a Rotofor® device, equipped with a standard focusing chamber (60 mL total volume) with 20 fractionation compartments. A constant power of 15 W was applied to the system, which was cooled to 4 °C with a water circulator, with fractionation completed within 4 h. A total of 20 fractions were collected, and the pH of each was measured using a microelectrode.

High-performance liquid chromatography

All separations were carried out using an HPLC system Gold 125NM solvent Module (Beckman Coulter, Miami, FL, USA). The sample was centrifuged for 10 min at 12 000 g. The supernatant was applied (containing 2 mg protein) to a polymeric reversed-phase PLRP-S 1000A, 8 μm, 250× 406 mm column (Varian, Palo Alto, CA, USA) and separated at a flow rate of 1 mL/min using a linear gradient (solvent A, 0.1% TFA/H_2O; solvent B, 0.1% TFA/acetonitrile). The gradient program started with 95% of solvent A and 5% of solvent B, and changed 5–25% B/5 min, 25–45% B/50 min, 45–70% B/5 min and 70–95% B/0.5 min. The column was washed with 95% solvent B (10 min) and equilibrated at initial conditions for 10 min. Protein samples were evaporated using a vacuum centrifuge (SpeedVac, Jouan, Winchester, VA, USA) and dissolved in PBS.

Sodium dodecyl sulfate polyacrylamide gel electrophoresis and immunoblotting

Each of the Rotofor® and HPLC fractions was analysed by SDS-PAGE (in concentration 1 mg/mL) using 15% gradient gels under reducing conditions (with 0.5 M DTT). Separated proteins were stained with Coomassie® Brilliant Blue R-250 (CBB). Selected fractions were electrotransferred to nitrocellulose membranes (NC2, SERVA, Heidelberg, Germany) for 1 h at room temperature. The membranes were blocked with PBS containing 0.5% Tween 20 and incubated with serum samples diluted 1 : 10 in blocking buffer overnight at 4 °C. After washing with PBS–0.1% Tween 20, the strips were incubated with peroxidase-labelled sheep anti-human IgE Abs (1 : 1000; The Binding Site, Birmingham, UK) for 1 h at room temperature. Blots were developed using SuperSignal West Pico Trial kits (Pierce) and luminescence was detected on a Kodak Medical X-ray film (Kodak, Rochester, NY, USA). Data were digitized and subjected to image analysis (AIDA 3.28, Raytest, Straubenhardt, Germany). Relative signal intensities derived from the chemiluminescent signal of IgE reaction with purified proteins were compared and corrected for local background signal (set as value 1). The resultant intensity is expressed as nine intervals (0–8; corresponding to intensity 1 → 801). Data are expressed as median values and 25% and 75% percentile.

Tryptic digestion and matrix-assisted laser desorption/ionization mass spectrometry

CBB-stained proteins were excised from gels, cut into small pieces and washed several times with 50 mM 4-ethylmorpholine acetate (pH 8.1) in 50% acetonitrile (MeCN). After complete destaining, the proteins were reduced with 30 mM TCEP at 65 °C for 30 min and alkylated by 30 mM iodoacetamide for 60 min in the dark. The gel pieces were further washed with de-ionized water, shrunk by dehydration in MeCN and reswollen in water. The supernatants were removed and the gels were partly dried in a SpeedVac concentrator. The gel pieces were then reconstituted in a cleavage buffer containing 25 mM 4-ethylmorpholine acetate, 5% MeCN and sequencing-grade trypsin (100 ng; Promega, Madison, WI, USA). After overnight digestion, the resulting peptides were extracted with 40% MeCN/0.5% TFA. A solution of α-cyano-4-hydroxycinnamic acid in aqueous 50% MeCN/0.1% TFA (5 mg/mL) was used as an MALDI matrix. A 0.5 μL aliquot of a sample was deposited onto the MALDI target and allowed to air-dry at room temperature, followed by the addition of 0.5 μL of the matrix solution.

MALDI mass spectra were measured using an Ultraflex III instrument (Bruker Daltonics, Bremen, Germany) equipped with a Smartbeam™ solid-state laser and LIFT™ technology for MS/MS analysis. The spectra were acquired in the mass range of 700–4000 Da and calibrated internally using monoisotopic $[M+H]^+$ ions of trypsin autoproteolytic fragments (842.5 and 2211.1 Da).

Protein identification

Peak lists in XML data format were created using the flexAnalysis 3.0 program with the SNAP peak detection algorithm. No smoothing was used, and the maximum number of assigned peaks was set at 50. After peak labelling, all known contaminant signals were manually removed. The peak lists were searched using the MASCOT search engine against the SwissProt 57.13 or Trembl 40.13 database subset of green plant proteins with search settings including a peptide tolerance of 30 p.p.m., a missed cleavage site value of 2, and variable carbamidomethylation of cysteine and oxidation of methionine. There were no restrictions on protein molecular weight or pI. We identified proteins with a MOWSE score over a threshold of 57 (SwissProt) or 71 (Trembl). If the score was only slightly higher than the threshold value or the sequence coverage was too low, we confirmed the identity of the protein candidate by MS/MS analysis. In addition to the above MASCOT settings, a fragment mass tolerance of 0.6 Da and instrument-type MALDI-TOF-TOF was applied

to search MS/MS spectra. Amino acid sequences of identified proteins were analysed using the multiple sequence alignment software Clustal W (http://www.ebi.ac.uk/clustalw).

Basophil activation test

Flow cytometric basophil activation tests were performed after stimulation of blood cells with four isolated wheat allergens [AAI 0.19, LTP, thaumatin-like protein (TLP) and wheatwin] or control (PBS, anti-IgE), as described previously [14]. The same blood samples were obtained from the patients, disease controls and healthy donors (Table 1). Briefly, 100 μL of heparinized whole blood and 10 μL of stimulation buffer were incubated (30 min at 37 °C) containing commercially available wheat extract (1000 IC/mL Stallergens, Antony Cedex, France) or selected allergens (concentration 1 mg/mL) diluted 1 : 10.

After incubation, the samples were transferred on ice and stained with mAb anti-(cluster differentiation) CD203/PE (Beckman Coulter) and anti-CD63/FITC (Exbio, Prague, Czech Republic) for 15 min. Erythrocytes were lysed using ammonium chloride. After washing the cells, we measured the percentage of activated basophils expressing CD63 and CD203c by flow cytometry (FC500, Beckman Coulter). Before this study, the basophil activation test had been performed in a pilot study in patients (seven per allergen) with AAI 0.19, LTP, TLP and wheatwin for four increasing dilutions (1 : 2, 1 : 10, 1 : 50 and 1 : 100). On the basis of these data, allergen dilution 1 : 10 was selected as optimal. No basophil activation could be induced in the controls. The ROC analysis of basophil activation was performed for all four proteins to determine the optimal cut-off values. Values above the cut-off, 9% of activated basophils for AAI 0.19 and LTP, 11.9% for TLP and 16% for wheatwin, were considered as positive.

Results

Preparation of salt-soluble wheat proteins and fractionation in Rotofor® cells

Salt-soluble proteins of molecular mass ranging from 5 to 120 kDa were extracted from the flour of the wheat cultivar Akteur (*T. aestivum*) were separated using Amicon 100k, 30k and 10k filter devices and were characterized by SDS-PAGE (Fig. 1a; lane 0). Protein aggregates were efficiently removed in the step with Amicon 100k filter device. Fraction 1 consisted mainly of proteins with molecular mass between 100 and 30 kDa, whereas fraction II contained only low-molecular-mass components below 30 kDa.

Proteins in fraction I (Fig. 1a, lane I) were further purified in the Rotofor® cell. Liquid-phase IEF considerably purified wheat proteins and yielded 20 fractions

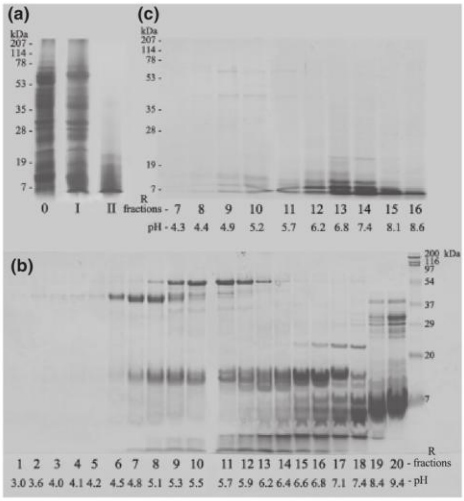

Fig. 1. SDS-PAGE analysis of wheat flour PBS extracts (a) and Rotofor® fractions (b and c). (a) Spectrum of wheat flour proteins extracted with PBS (0) and purified using Amicon 100k and 30k filter devices (fraction I). Fraction I was concentrated using a 10k filter device (fraction II). (b and c) Proteins from fractions (b) I and (c) II were separated by liquid-phase isoelectric focusing in Rotofor® cell into 20 fractions (R1–R20). All gels were stained with Coomassie brilliant blue.

(R1–R20) with pH ranging from 3.0 to 9.4, as documented by SDS-PAGE (Fig. 1b). Fractions R6–R13 contained predominantly protein bands of 50 kDa, fractions R19 and R20 contained proteins of 20–40 kDa, fractions R7–R18 contained proteins of molecular mass below 20 kDa and fractions R11–R20 were enriched in low-molecular-mass components below 10 kDa. Because of their high protein content and their reactivity with IgE Abs from patients' sera (data not shown), eight Rotofor® fractions (R7, R11, R14–R18 and R20) were selected for further purification by HPLC.

Similarly, proteins from fraction II were separated in the Rotofor® cell into 20 fractions with pH ranging from 3.7 to 9.5. Proteins were detected in nine fractions (R8–R16) and were enriched in fractions R13 and R14 (Fig. 1c). Four Rotofor® fractions (R9, R10, R13 and R14) were selected for purification by HPLC.

Purification and identification of major wheat allergens by high-performance liquid chromatography and mass spectrometry

Selected Rotofor® fractions were further purified by HPLC (PLRP-S column) and the resulting fractions were

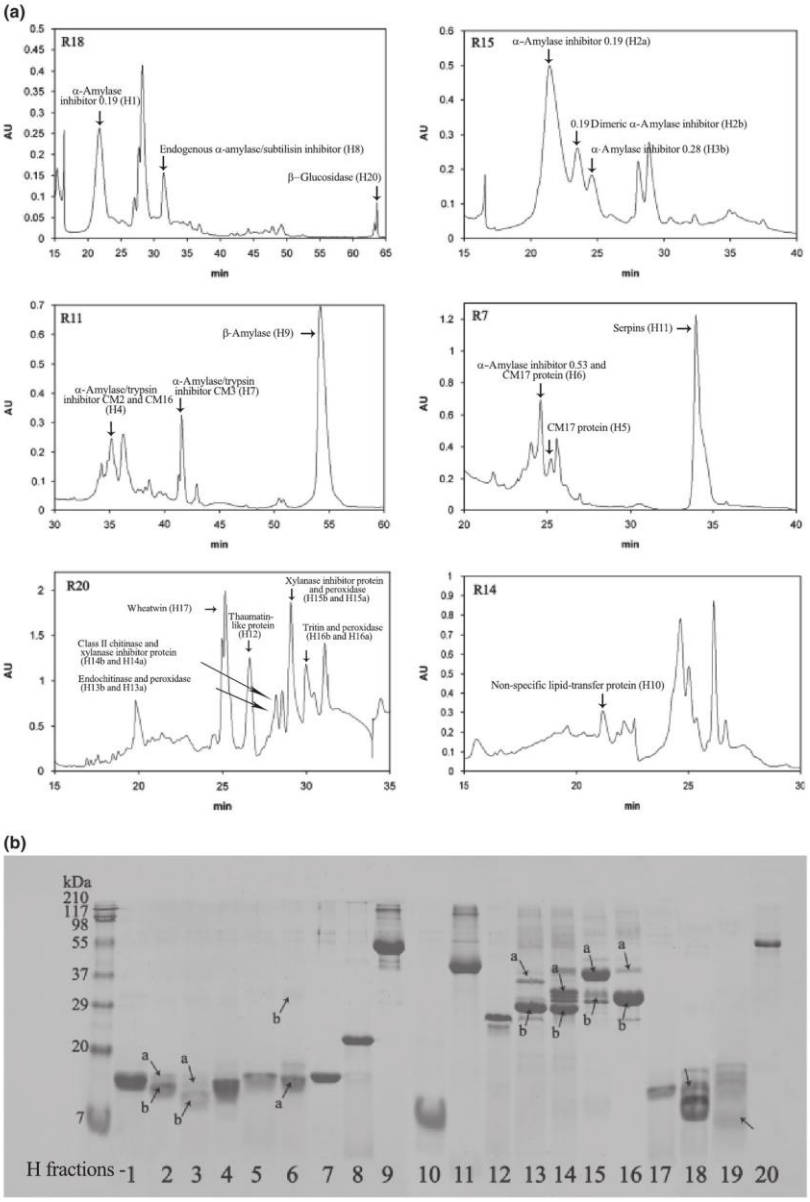

Fig. 2. (a) Examples of the chromatographic profiles of Rotofor® fractions R18, R15, R11, R7 and R20 (shown in Fig. 1b) and fraction R14 (shown in Fig. 1c) obtained from reversed-phase HPLC. The HPLC fraction numbers (H1–H20) and the peaks with arrows indicate purified and identified wheat proteins corresponding to those listed in Table 2. (b) Coomassie blue staining of selected wheat proteins purified by HPLC and separated by SDS-PAGE. The HPLC fraction numbers indicate the bands corresponding to the allergens identified in Table 2.

Table 2. Isolated wheat proteins identified by MS analysis (MALDI-TOF)

H fractions	Protein (allergen) name	Accession no.	MW (kDa)	pI	Protein yield (mg)	Peptides matched	Sequence coverage (%)	MS/MS confirmation	R fraction
1	α-Amylase inhibitor 0.19 (Tri a 28.0101)	IAA1_WHEAT	13.30	6.60	1.73	8	74	LAHISEWCR HGAQEGQAGTGAFPR	18
2a	α-Amylase inhibitor 0.19 (Tri a 28.0101)	IAA1_WHEAT	13.30	6.60	0.61	4	44	No	15
2b, 3a	0.19 dimeric α-amylase inhibitor	Q5UHH6_WHEAT	13.20	6.50		8	59	No	15
3b	α-Amylase inhibitor 0.28 (Tri a aAI)	IAA2_WHEAT	16.80	7.40		8	54	No	15
6a	α-Amylase inhibitor 0.53 (Tri a 28)	IAA5_WHEAT	13.20	5.20	0.16	8	54	No	7
6b	α-Amylase inhibitor 0.53 (Tri a 28)	IAA5_WHEAT	13.20	5.20		4	47	LQCNGSQVPEAVLR EHGVSEGQAGTGAFPSCR	7
6a	CM 17 protein	Q41540_WHEAT	16.00	5.00		5	35	No	7
6b	CM 17 protein	Q41540_WHEAT	16.00	5.00		4	23	SRPDQSGLMELPGCPR	7
5	CM 17 protein	Q41540_WHEAT	16.00	5.00	<0.10	8	39	No	7
18	α-Amylase/trypsin inhibitor CM1	IAAC1_WHEAT	15.50	7.50	<0.10	2	24	No	11
4	α-Amylase/trypsin inhibitor CM2 (Tri a 29)	IAAC2_WHEAT	15.50	6.80	0.10	5	29	No	11
4	α-Amylase/trypsin inhibitor CM16 (Tri a CM16)	IAC16_WHEAT	15.80	5.30		10	45	No	11
7	α-Amylase/trypsin inhibitor CM3 (Tri a 30)	IAAC3_WHEAT	18.20	7.40	0.20	10	69	No	11
19	Trypsin/α-amylase inhibitor CMX1/CMX3	IACX1_WHEAT	13.80	9.20	<0.10	2		EFIAGIVGR EITYESLNACAEYAVR	17
8	Endogenous α-amylase/subtilisin inhibitor	IAAS_WHEAT	19.60	6.70	0.34			WHIDSELVSGR STEWHIDSELVSGR	18
13b	26 kDa endochitinase 1	CHI1_HORVU	33.40	8.50	<0.10	10	44	No	20
14b	Class II chitinase	Q4Z8L8_WHEAT	28.20	8.60	<0.10	13	73	No	20
10	Non-specific lipid-transfer protein (Tri a 14)	NLTP1_WHEAT	11.90	8.50	0.33	3	30	No	14 (Fig. 1c)
17	Wheatwin-1	WHW1_WHEAT	15.60	7.60	0.51	5	45	No	20
17	Wheatwin-2	WHW2_WHEAT	15.90	8.20		6	56	No	20
12	Thaumatin-like protein	Q8S4P7_WHEAT	23.60	7.80	0.71	12	55	No	20
9	β-Amylase	AMYB_HORVU	60.00	5.60	0.23	7	17	No	11
11	Serpin-Z1A	SPZ1A_WHEAT	43.10	5.60	<0.10	7	27	No	7
	Serpin-Z1B	SPZ1B_WHEAT	43.00	5.40		6	24	No	
	Serpin-Z1C	SPZ1C_WHEAT	42.80	5.60		5	20	No	
	Serpin-Z2A	SPZ2A_WHEAT	43.30	5.40		11	41	No	
	Serpin-Z2B	SPZ2B_WHEAT	43.00	5.20		5	15	No	
13a, 15a, 16a	Peroxidase 1	Q8LK23_WHEAT	38.80	8.10	0.16	23	57	No	20
16b	Tritin (rRNA N-glycosidase)	Q07810_WHEAT	29.60	9.70		15	66	No	20
14a, 15b	Xylanase inhibitor protein 1	XIP1_WHEAT	33.20	8.60		21	61	No	20
20	β-Glucosidase	Q40025_HORVU	57.40	7.20	<0.10			LDFVWYEPHSDSNADQAAAQR	18

Protein yield corresponds to the amount of proteins isolated from 15 mL ultrafiltrated sample (containing 45 mg protein), separated by one Rotofor run and purified by HPLC.
The allergenic molecules are named by the International Union of the Immunological Societies (IUIS) Allergen Nomenclature Sub-Committee.
The H fraction numbers refer to Fig. 2 and the R fraction numbers refer to Fig. 1b.
Tri a, *Triticum aestivum*.

© 2011 Blackwell Publishing Ltd, *Clinical & Experimental Allergy*, **41**: 1031–1043

analysed by SDS-PAGE. Figure 2a shows the chromatograms of six Rotofor® fractions (five obtained from Amicon fraction I – R7, R11, R15, R18 and R20, and one from fraction II – R14). All HPLC fractions were analysed by immunoblotting using patients' pooled sera (data not shown) and fractions containing separated IgE-binding proteins were selected for identification by MALDI-TOF mass spectrometry. Using these methodological approaches and protein database searches, we succeeded in identifying 27 wheat proteins (Table 2). These IgE-binding proteins were detected in 20 HPLC fractions, H1–H20. SDS-PAGE analysis and Coomassie blue staining of these fractions (Fig. 2b) revealed six well-resolved peaks (fractions H1, H7, H8, H10, H12 and H17), each corresponding to a single protein band of sufficient yield (Table 2). The first peak (H1) corresponded to AAI, AAI 0.19, which had been eluted uncontaminated after HPLC separation of Rotofor® fraction R18 (Figs 2a and b). Rotofor® fractions R14–R17 contained AAI 0.19 with decreasing amounts of 0.19 dimeric AAI (H2b) and AAI 0.28 (H3b) proteins (see R15 Fig. 2a). Other identified proteins, such as wheatwin (H17) and TLP (H12), were observed only in Rotofor® fraction R20. Protein AATI CM3 (H7) was identified in all Rotofor® fractions, except for R20, separated by HPLC, whereas endogenous protein AATI (H8) was found in Rotofor® fractions R14–R18. LTP (H10) was isolated primarily from Rotofor® fraction R14, which had been obtained especially from fraction II. The other HPLC fractions (H13, H14, H15 and H16) contained mixtures of proteins, including peroxidase, tritin, xylanase inhibitor protein (XIP), endochitinase and class II chitinase. HPLC fraction H4 contained proteins AATI CM2 and CM16 and fraction H6 contained AAI 0.53 and CM17 protein. HPLC fraction H11 contained a mixture of five members of the serpin family. Fractions H5, H9, H18 and H19 contained one major IgE-binding protein together with small amounts of other proteins. Fraction H20 contained a low amount of β-glucosidase. Out of the 27 identified proteins, the following seven are new potential wheat allergens: endogenous α-amylase/subtilisin inhibitor, trypsin/AAI CMX1/CMX3, TLP, XIP-1, β-glucosidase, class II chitinase and 26 kDa endochitinase.

Reactivity of patients' immunoglobulin E antibodies with isolated proteins

To characterize the intensity and frequency with which IgE Abs bind the individual wheat components, 17 purified HPLC fractions (H1–H17) were immunoblotted with sera from all 22 patients, 10 disease controls and nine healthy controls. An example of the reactivity of IgE from one patient (P1), one disease control (D1) and one healthy control (C8) with isolated wheat proteins is shown in Fig. 3. The data summarized in Table 3 document the individual diversity of IgE response. However, all patients

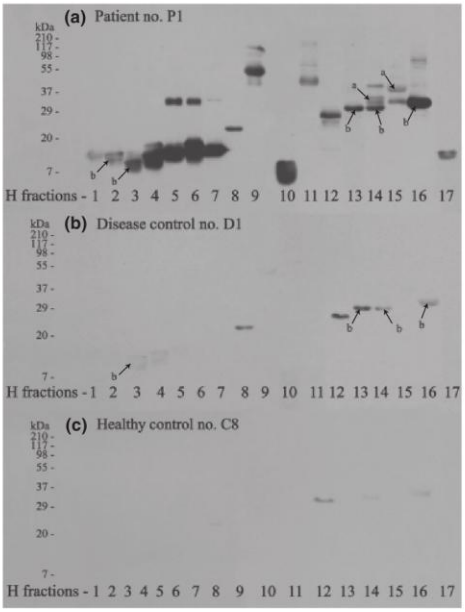

Fig. 3. An example of IgE immunoblotting of purified wheat proteins with the sera of (a) one patient, (b) a disease control and (c) a healthy control. The HPLC fraction numbers indicate the bands corresponding to the allergens identified in Table 2.

sera tested (100%) showed positive IgE reactions with α-amylase inhibitors AAI 0.28 (H3b), AATI CM16 and CM2 (H4), TLP (H12) and tritin (H16b). Of the 22 sera, 20 or 21 (91% or 95%) reacted with CM17 (H5), CM17 and AAI 0.53 (H6), 26 kDa endochitinase (H13b), XIP (H14a) and class II chitinase (H14b). The frequency of recognition of other wheat proteins was also high ranging from 54% to 86%. The densitometric evaluation of intensity of IgE binding on immunoblots documents the differences of binding of individual wheat proteins (Table 3). The IgE of patients reacted with the highest intensity (median 6.0–8.0) with the following already known allergens: AATI CM16 and CM2 (H4), CM17 and AAI 0.53 (H6), CM17 (H5) and tritin (H16b), as well as with the newly identified IgE-binding wheat components TLP (H12), 26 kDa endochitinase (H13b) and class II chitinase (H14b). In contrast, the lowest binding intensity was determined for AATI CM3 (H7) and wheatwin (H17) (median 1 and 2, respectively).

We also performed IgE immunoblotting of purified proteins with sera from 10 disease controls. Endogenous AAI (H8) and tritin (H16b) were recognized by seven sera (70%); other proteins were recognized by $<50\%$ sera or did not react. Nevertheless, the intensity of IgE binding

Table 3. Reactivity of IgE antibodies of patients and disease controls on immunoblot analysis with selected proteins

Protein name	AAI 0.19	0.19 dimeric AAI	AAI 0.28	AATI CM16 & CM2	CM17	CM17 & AAI 0.53	AATI CM3	Endo-genous AAI	β-Amylase	LTP	Serpins	TLP	26 kDa endochitinase	XIP	Class II chitinase	Peroxidase	Tritin	Wheatwin
H fraction	1	2b	3b	4	5	6	7	8	9	10	11	12	13b	14a	14b	15a	16b	17
Patients																		
P1	1	3	7	8	8	8	8	4	8	8	3	5	5	3	5	3	8	4
P2	5	4	6	8	6	4	4	6	4	6	0	8	6	1	6	3	6	7
P3	2	2	3	8	6	8	0	2	5	0	1	6	5	3	5	0	1	1
P4	1	1	2	8	8	8	0	1	0	0	0	7	6	8	7	4	5	0
P5	7	5	4	8	6	5	1	4	7	1	5	8	8	8	8	8	8	4
P6	8	7	5	8	5	8	3	6	8	3	8	8	8	8	8	8	8	7
P7	8	5	4	8	4	8	0	4	7	4	3	8	8	8	8	8	7	3
P8	8	7	8	8	8	8	4	6	4	8	ND	8	8	8	8	8	8	3
P9	3	4	7	8	2	2	2	4	1	4	0	8	7	3	7	3	8	4
P10	5	5	6	8	3	8	1	3	7	6	5	8	7	8	7	8	8	6
P11	3	2	3	8	5	7	0	0	0	0	ND	2	3	8	3	8	5	0
P12	4	3	5	6	6	5	0	1	0	2	ND	3	2	5	2	1	3	0
P13	1	1	3	7	7	8	0	2	3	0	ND	7	6	8	6	5	6	0
P14	6	7	8	8	2	2	1	4	3	2	ND	8	7	3	7	0	8	0
P15	4	3	8	8	5	5	1	6	5	6	ND	8	8	2	8	3	8	0
P16	5	4	7	8	0	0	0	3	1	0	ND	5	4	6	4	3	8	1
P17	0	0	2	ND	8	8	0	0	0	0	ND	4	2	6	2	6	5	0
P18	0	0	4	ND	0	0	0	1	0	0	ND	1	0	0	0	0	7	0
P19	0	0	3	4	2	1	0	0	0	0	ND	3	3	0	3	0	4	0
P20	8	8	8	8	8	8	7	6	8	8	ND	8	8	5	8	8	8	8
P21	8	7	5	5	8	8	2	5	8	7	ND	8	7	3	7	5	8	3
P22	8	8	8	8	8	8	7	7	8	8	ND	8	7	7	7	7	8	8
Median	4.5	4	5	8	6	8	1	4	4	2.5	3	8	6.5	5.5	7	4.5	8	2
IQR	1–8	1.75–7	3–7.25	8–8	2.75–8	3.5–8	0–3.25	1–6	0–7.25	0–6.25	0–5	4.75–8	3.75–8	3–8	3.75–8	2.5–8	5–8	0–4.5
Disease controls																		
D1	0	0	0	0	0	0	0	1	0	0	0	2	2	0	1	0	1	0
D2	0	0	0	0	0	0	0	1	0	0	0	0	ND	0	ND	0	1	0
D3	0	0	3	3	0	0	0	1	0	0	ND	3	3	0	3	1	3	2
D4	0	1	3	3	0	0	0	1	0	0	ND	2	1	1	1	1	3	1
D5	1	1	4	ND	0	0	0	2	1	0	ND	3	3	3	3	0	5	0
D6	1	1	2	ND	ND	ND	0	2	1	0	ND	3	2	0	2	2	3	0
D7	1	2	4	ND	ND	ND	0	1	0	0	ND	0	ND	0	ND	0	5	0
D8	0	0	0	ND	0	0	0	0	0	0	ND	0	0	0	0	1	0	0
D9	0	0	0	ND	0	0	0	0	0	0	ND	0	0	0	0	1	0	0
D10	0	0	0	ND	0	0	0	0	0	0	ND	0	0	0	0	0	0	0
Median	0	0	1	1.5	0	0	0	1	0	0	0	1	1.5	0	1	0.5	2	0
IQR	0–1	0–1	0–3.25	0–3	0–0	0–0	0–0	0–1.25	0–0.25	0–0	0–0	0–3	0–2.75	0–0.25	0–2.75	0–1	0–3.5	0–0.25

Range of chemiluminescence intensity: 0, 1–100; 1, 101–200; 2, 201–300; 3, 301–400; 4, 401–500; 5, 501–600; 6, 601–700; 7, 701–800; 8, 801 <.

The resultant chemiluminescence intensity is corrected for local background signal (set as value 1) and expressed as an interval of measured values.

The H fraction numbers refer to Table 1.

AAI, α-amylase inhibitor; AATI, α-amylase/trypsin inhibitor; LTP, non-specific lipid-transfer protein; TLP, thaumatin-like protein; XIP, xylanase inhibitor protein; ND, not done; IQR: interquartile range, 25–75 percentile.

© 2011 Blackwell Publishing Ltd,

calculated for disease controls was low (median 0–2). None of the sera from the nine healthy donors reacted with any of the isolated proteins, except for low non-specific reactions of secondary anti-human IgE Ab with TLP (H12) and tritin (H16b) (Fig. 3c).

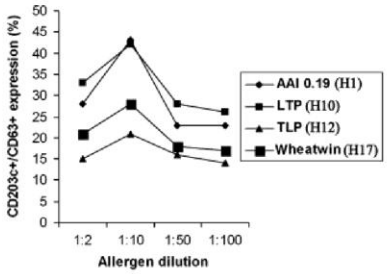

Fig. 4. CD203c/CD63 expression of basophils from seven patients in a dose–response curve after incubation with allergens: AAI 0.19 (H1), LTP (H10), TLP (H12) and wheatwin (H17) (dilution: 1 : 2, 1 : 10, 1 : 50 and 1 : 100).

Comparison of the identified α-amylase inhibitors

Of the 27 identified wheat allergens, 11 belonged to the AAI family. These inhibitors could be divided into three groups based on sequence homology obtained from the NCBI database (compared by Clustal W program). The first group consisted of four inhibitors, AAI 0.19, 0.53, 0.28 and 0.19 dimeric; the second consisted of five proteins, AATI CM1, CM2, CM3, CM16 and CM17; and the third one consisted of two inhibitors, endogenous AAI and AATI CMX1/CMX3. Homology among the proteins in the first group ranged from 55% to 94%. Inhibitors from the third group showed very low sequence homologies with other proteins. Independently on the degree of structural homology, each of these inhibitors was found to bind

Table 4. Basophil activaton test (%)

Protein name	AAI 0.19	LTP	TLP	Wheatwin	Wash buffer (negative control)	Stimulation with anti-IgE (positive control)
H fraction	1	10	12	17		
Patients						
P1	80	89	ND	ND	6	91
P2	89	57	84	70	10	92
P3	ND	ND	14	45	5	51
P4	32	27	22	22	13	53
P5	17	19	ND	ND	2	85
P6	7.7	30	34	30	5	88
P7	ND	ND	19	31	12	77
P8	ND	ND	11	22	10	87
P9	ND	ND	15	19	11	49
P10	9.1	9.2	3.3	7.2	3	71
P11	ND	ND	15	24	5	96
P12	3.3	6.5	ND	ND	2	93
P13	ND	ND	12	19	10	79
P14	12	9.5	ND	ND	7	76
P15	26	25	16	21	8	62
P16	ND	ND	22	11	10	60
P17	ND	ND	12	27	6	19
P18	ND	ND	2.3	7.9	2	42
P19	ND	ND	1.7	2.1	1.5	95
P20	5.2	4.6	ND	ND	4	62
P21	ND	ND	20	21	3	45
P22	ND	ND	9.4	8.2	4	66
Healthy controls						
C1	6.5	5.9	ND	14	4.5	61
C2	7.3	7.5	10	12	4.4	75
C3	14	6.5	6.7	10	4.1	49
C4	8.7	8.1	10	13	8	41
C5	1.7	12	7.1	9.5	1.5	45
C6	2.4	2.7	1.5	1.7	1	55
C7	ND	ND	11	6.1	6	45
C8	ND	ND	8.2	4.3	3	57
C9	ND	ND	11	14	9	58
cut-off	9	9	11.9	16		

AAI, α-amylase inhibitor; LTP, non-specific lipid-transfer protein; TLP, thaumatin-like protein; ND, not done.

patients' IgE Abs, but the intensities of their binding varied (Table 3).

Activation of basophils from allergic patients with purified allergens

The biological activity of purified allergens was tested using the basophil activation test. Blood samples were obtained from 22 patients with clinical symptoms of wheat allergy and with positive basophil activation tests to a commercial wheat extract, from 10 disease controls and from nine healthy donors. These blood samples were exposed to four isolated wheat proteins, AAI 0.19 (H1), LTP (H10), TLP (H12) and wheatwin (H17). A bell-shaped dose–response curve for all four allergens was obtained (Fig. 4) and the optimal dilution was selected (1 : 10). Positive cell activation was detected in response to LTP in eight out of 10 patients (80%), to AAI 0.19 in seven out of 10 patients (70%) and to TLP and wheatwin in 12 out of 17 patients (71%) (Table 4).

We compared the number of patients positive for allergens AAI 0.19, LTP, TLP and wheatwin in either IgE immunoblot or in the basophil activation test (analysing both IgE binding and cell activation). We have shown that for all allergens tested in IgE immunoblot, the proportion of positive cases ranged from 60% to 100%. This proportion was somewhat lower in the basophil activation test and the range was more narrow (70–80%).

Discussion

Extensive analysis of allergenic molecules is necessary for allergy diagnosis and treatment. We developed a new, rapid procedure for isolation of wheat flour allergens in amounts allowing subsequent structural and functional analysis. We succeeded in purifying relevant IgE binding proteins from a water/salt-soluble extract of wheat flour using Amicon devices, Rotofor® and HPLC techniques.

The advantage of Rotofor® (protein separation based on pI value – preparative IEF) is its capacity to optimally fractionate milligrams to grams of total protein. However, the apparent pI of Rotofor® fractions may not exactly match the predicted pI of separated proteins; these proteins may be rather spread over two or more fractions [35]. With isolation of natural non-denatured allergen epitopes in mind, we used native (liquid-phase) preparative IEF that resulted in substantial protein enrichment and provided the basis for a successful isolation of native allergens. The purification of individual water/salt-soluble wheat proteins from their mixtures included the preparative reversed-phase HPLC. The purified proteins were subsequently analysed by SDS-PAGE, and IgE-binding proteins (selected by immunoblot) were identified by MALDI-TOF mass spectrometry. This isolation scheme yielded 27 IgE-binding wheat proteins, including the following previously described proteins: AAIs (Tri a 28; Tri a 28.0101; Tri a 29; Tri a 30; Tri a CM16 and Tri a aAI), non-specific LTP (Tri a 14), peroxidase, serpins and β-amylase (identified on 1D or 2D electrophoresis – 14, 16, 30). Some of them were purified here for the first time. In addition, we newly identified the following potential allergens: endogenous α-amylase/subtilisin inhibitor, trypsin/AAI CMX1/CMX3, TLP, XIP-1, β-glucosidase, class II chitinase and 26 kDa endochitinase as associated with food allergy. The fact that some of these proteins do not match wheat components identified so far (such as 26 kDa endochitinase, β-glucosidase) could be explained by the lack of knowledge of the complete genome. The corresponding protein/peptide sequences of wheat may be missing in the current databases.

The findings of the reactivity of patients' IgE with AAIs are not unambiguous. For instance, although the endogenous α-amylase/subtilisin inhibitor has not been reported as an allergen [25], we observed a reactivity of this purified protein with IgE Abs from 19 out of the 22 patients, albeit with only medium intensity (median 4). In previous studies, purified AATI CM3 but not CM2 or CM16 reacted with IgE from patients [17], and SPTs were positive with CM3 and CM16 but not CM2 in a patient with anaphylactic reaction to wheat flour [36]. We found that the most frequently recognized AAIs were 0.28 AAI and a mixture of CM16 and CM2, all of them reacting with IgE Abs of our patients. However, the frequency of IgE biding with other inhibitors, such as 0.19 AAI, 0.19 dimeric and CM17 was also high.

We succeeded in identifying and purifying wheat LTP, a food panallergen that is also a major allergen associated with baker's asthma [23]. We found that IgE Abs of 64% patients in our cohort reacted with our purified wheat LTP, which is a higher percentage then previously reported (41% and 28%) [16, 37]. We also purified tritin (a 29.6 kDa ribosome-inactivating protein from *T. aestivum)* previously identified from the water/salt-insoluble fraction of raw wheat [16]; its clinical relevance has not yet been clarified. This wheat component was recognized by all our patients (22/22) with high binding intensity (median 8), and also by some of our disease controls (7/10, median 2).

TLP is one of the successfully isolated new IgE-binding wheat proteins associated with food allergy. In our cohort, TLP was recognized by IgE Abs of all 22 patients and the intensity of IgE binding (median 8) was significantly higher when compared with disease controls (median 1). TLP, as well as wheatwin, are members of the family of pathogenesis-related proteins, which play a role in plant defence. TLP is an important allergen in several fruits, such as apples, cherries, kiwis and grapes [38–40], and wheat TLP has recently been reported as the allergen in baker's respiratory allergy [41]. We showed previously that wheatwin-2 is an IgE immunoreactive protein [14], and the results presented here showed that wheatwin-1

and wheatwin-2 have sequence homology of 97%. Using MALDI-TOF mass spectrometry, we observed at least two unique peptides for each wheatwin sequence (data not shown). Furthermore, we have shown for the first time that newly identified wheat components, such as TLP and wheatwin bind to IgE from patients and can activate patients' basophils to an extent comparable with that of the well-characterized allergens, AAI 0.19 (Tri a 28.0101) and LTP (Tri a 14).

In addition, we purified other new IgE-binding wheat components, such as XIP, class II chitinase and 26 kDa endochitinase, which were not previously identified as allergens in individuals with food allergy (XIP was identified in patients with baker's asthma [41]) These components reacted strongly (median 5.5–7.0) with the vast majority of patients' IgE Abs (20/22, 21/22 and 21/22, respectively) and with a lower intensity (median 0–1.5) and frequency (2/10, 5/8 and 5/9) with IgE of disease controls.

In conclusion, using preparative liquid-phase IEF and HPLC, we have developed a new procedure enabling us to purify native forms of wheat allergens in amounts sufficient for further structural and functional studies. The advantage of this approach is that it can be easily modified for isolation of various allergens (by changing pI range in Rotofor® or HPLC elution profile). We purified 27 IgE-binding wheat components, including seven new ones. We have shown for the first time that purified allergens, such as AAI 0.19, LTP, TLP and wheatwin, can activate patients' basophils, confirming that our purified proteins maintain their biological activity.

Interestingly, wheat proteins, CM17 (H5), CM17 and AAI 0.53 (H6) as well as newly identified TLP (H12), 26 kDa endochitinase (H13b), XIP (H14a) and class II chitinase (H14b), were shown to belong to those reacting with the highest frequency and intensity with IgE of patients (median 5.5–8) and with low intensity with IgE of disease controls (median 0–1). These proteins may be candidates for clinically relevant wheat allergens.

Our isolation procedure will allow preparation of native allergens for studies of their structural features (linear and conformational epitopes), including the impact of post-translational modifications (e.g. glycosylation) on allergenicity. Better knowledge of the allergenicity of native proteins could lead to a selection of an appropriate vector for recombinant allergen preparation, improving both diagnostic tests and therapy.

Acknowledgements

This work was supported by grant GA310/07/0414 and 310/08/H077 from the Czech Science Foundation; SYNLAB.CZ (IMUMED); grant IAA500200801 from the Grant Agency of AS CR; Institutional Research Concept Grant AV0Z50200510; and grant 2B06155 and LC07017 from the Czech Ministry of Education, Youth and Sports.

References

1 Poole JA, Barriga K, Leung DYM *et al.* Timing of initial exposure to cereal grains and the risk of wheat allergy. *Pediatrics* 2006; **117**:2175–82.
2 Ostblom E, Lilja G, Pershagen G, van Hage M, Wickman M. Phenotypes of food hypersensitivity and development of allergic diseases during the first 8 years of life. *Clin Exp Allergy* 2008; **38**:1325–32.
3 Pourpak Z, Mansouri M, Mesdaghi M, Kazemnejad A, Farhoudi A. Wheat allergy: clinical and laboratory findings. *Int Arch Allergy Immunol* 2004; **133**:168–73.
4 Varjonen E, Petman L, Mäkinen-Kiljunen S. Immediate contact allergy from hydrolyzed wheat in a cosmetic cream. *Allergy* 2000; **55**:294–6.
5 Palosuo K. Update on wheat hypersensitivity. *Curr Opin Allergy Clin Immunol* 2003; **3**:205–9.
6 Tordesillas L, Pacios LF, Palacin A *et al.* Molecular basis of allergen cross-reactivity: non-specific lipid transfer proteins from wheat flour and peach fruit as models. *Mol Immunol* 2009; **47**:534–40.
7 Sampson HA. Utility of food-specific IgE concentrations in predicting symptomatic food allergy. *J Allergy Clin Immunol* 2001; **107**:891–6.
8 van Kampen V, Merget R, Rabstein S *et al.* Comparison of wheat and rye flour solutions for skin prick testing: a multicentre study (Stad 1). *Clin Exp Allergy* 2009; **39**:1896–902.
9 Tokuda R, Nagao M, Hiraguchi Y *et al.* Antigen-induced expression of CD203c on basophils predicts IgE-mediated wheat allergy. *Allergol Int* 2009; **58**:193–9.
10 Constantin C, Touraev A, Heberle-Bors E, Quirce S, Huber WD, Valenta R. Detection of antigens reactive to IgE and IgA during wheat seed maturation and in different wheat cultivars. *Int Arch Allergy Immunol* 2009; **149**:181–7.
11 Werfel T, Breuer C. Role of food allergy in atopic dermatitis. *Curr Opin Allergy Clin Immunol* 2004; **4**:379–85.
12 Brandtzaeg P. Food allergy: separating the science from the mythology. *Nat Rev Gastroenterol Hepatol* 2010; **7**: 380–400.
13 Scibilia J, Pastorello EA, Zisa G *et al.* Wheat allergy: a double-blind, placebo-controlled study in adults. *J Allergy Clin Immunol* 2006; **117**:433–9.
14 Sotkovsky P, Hubalek M, Hernychova L *et al.* Proteomic analysis of wheat proteins recognized by IgE antibodies of allergic patients. *Proteomics* 2008; **8**: 1677–91.
15 Akagawa M, Handoyo T, Ishii T, Kumazawa S, Morita N, Suyama K. Proteomic analysis of wheat flour allergens. *J Agric Food Chem* 2007; **55**:6863–70.
16 Pastorello EA, Farioli L, Conti A *et al.* Wheat IgE-mediated food allergy in European patients: α-amylase inhibitors, lipid transfer proteins and low molecular weight glutenins. Allergenic molecules recognized by double-blind, placebo-controlled food challenge. *Int Arch Allergy Immunol* 2007; **144**:10–22.
17 Kusaba-Nakayama M, Ki M, Iwamoto M, Shibata R, Sato M, Imaizumi K. CM3, one of the wheat α-amylase inhibitor

subunits, and binding of IgE in sera from Japanese with atopic dermatitis related to wheat. *Food Chem Toxicol* 2000; **38**:179–85.

18 Kusaba-Nakayama M, Ki M, Kawada E *et al.* Intestinal absorbability of wheat allergens, subunits of wheat α-amylase inhibitor, expressed by bacteria. *Biosci Biotechnol Biochem* 2001; **65**:2448–55.

19 Weichel M, Vergoossen NJ, Bonomi S *et al.* Screening the allergenic repertoires of wheat and maize with sera from double-blind, placebo-controlled food challenge positive patients. *Allergy* 2006; **61**:128–35.

20 Jones SM, Magnolfi CF, Cooke SK, Sampson HA. Immunologic cross-reactivity among cereal grains and grasses in children with food hypersensitivity. *J Allergy Clin Immunol* 1995; **96**:341–51.

21 Sander I, Raulf-Heimsoth M, Duser M, Flagge A, Czuppon AB, Baur X. Differentiation between cosensitization and cross-reactivity in wheat flour and grass pollen-sensitized subjects. *Int Arch Allergy Immunol* 1997; **112**:378–85.

22 Pourpak Z, Mesdaghi M, Mansouri M, Kazemnejad A, Toosi SB, Farhoudi A. Which cereal is a suitable substitute for wheat in children with wheat allergy? *Pediatr Allergy Immunol* 2005; **16**: 262–6.

23 Palacin A, Quirce S, Armentia A *et al.* Wheat lipid transfer protein is a major allergen associated with baker's asthma. *J Allergy Clin Immunol* 2007; **120**:1132–8.

24 Lauer I, Miguel-Moncin MS, Abel T *et al.* Identification of a plane pollen lipid transfer protein (Pla a 3) and its immunological relation to the peach lipid transfer protein, Pru p 3. *Clin Exp Allergy* 2007; **37**:261–9.

25 Tatham AS, Shewry PR. Allergens in wheat and related cereals. *Clin Exp Allergy* 2008; **38**:1712–26.

26 Bohle B, Vieths S. Improving diagnostic tests for food allergy with recombinant allergens. *Methods* 2004; **32**:292–9.

27 Jutel M, Jaeger L, Suck R, Meyer H, Fiebig H, Cromwell O. Allergen-specific immunotherapy with recombinant grass pollen allergens. *J Allergy Clin Immunol* 2005; **116**:608–13.

28 Palacin A, Varela J, Quirce S *et al.* Recombinant lipid transfer protein Tri a 14: a novel heat and proteolytic resistant tool for the diagnosis of baker's asthma. *Clin Exp Allergy* 2009; **39**:1267–76.

29 Constantin C, Quirce S, Grote M *et al.* Molecular and immunological characterization of a wheat serine proteinase inhibitor as a novel allergen in baker's asthma. *J Immunol* 2008; **180**:7451–60.

30 Amano M, Ogawa H, Kojima K *et al.* Identification of the major allergens in wheat flour responsible for baker's asthma. *Biochem J* 1998; **330**:1229–34.

31 Bodinier M, Leroy M, Ah-Leung S *et al.* Sensitization and elicitation of an allergic reaction to wheat gliadins in mice. *J Agric Food Chem* 2009; **57**: 1219–25.

32 Mine Y, Yang M. Epitope characterization of ovalbumin in BALB/c mice using different entry routes. *Biochim Biophys Acta* 2007; **1774**:200–12.

33 Adel-Patient K, Nahori MA, Proust B *et al.* Elicitation of the allergic reaction in β-lactoglobulin-sensitized Balb/c mice: biochemical and clinical manifestations differ according to the structure of the allergen used for challenge. *Clin Exp Allergy* 2003; **33**:376–85.

34 Dearman RJ, Kimber I. Determination of protein allergenicity: studies in mice. *Toxicol Lett* 2001; **120**:181–6.

35 Gagné JP, Hunter JM, Labrecque B, Chabot B, Poirier GG. A proteomic approach to the identification of heterogeneous nuclear ribonucleoproteins as a new family of poly (ADP-ribose)-binding proteins. *Biochem J* 2003; **371**:331–40.

36 Zapatero L, Martínez MI, Alonso E *et al.* Oral wheat flour anaphylaxis related to wheat α-amylase inhibitor subunits CM3 and CM16. *Allergy* 2003; **58**:956.

37 Battais F, Courcoux P, Popineau Y *et al.* Food allergy to wheat: differences in immunoglobulin E-binding proteins as a function of age or symptoms. *J Cereal Sci* 2005; **42**:109–17.

38 Gavrovic-Jankulovic M, Cirkovic T, Vuckovic O *et al.* Isolation and biochemical characterization of a thaumatin-like kiwi allergen. *J Allergy Clin Immunol* 2002; **110**: 805–10.

39 Breiteneder H. Thaumatin-like proteins: a new family of pollen and fruit allergens. *Allergy* 2004; **59**:479–81.

40 Pastorello EA, Farioli L, Pravettoni V *et al.* Identification of grape and wine allergens as an endochitinase 4, a lipid-transfer protein, and a thaumatin. *J Allergy Clin Immunol* 2003; **111**: 350–9.

41 Lehto M, Airaksinen L, Puustinen A *et al.* Thaumatin-like protein and baker's respiratory allergy. *Ann Allergy Asthma Immunol* 2010; **104**:139–46.

© 2011 Blackwell Publishing Ltd, *Clinical & Experimental Allergy*, **41** : 1031–1043

3.3.3. Proteinový profil leukemických buněk JURL-MK1 v apoptóze

v publikaci:

Changes in Cell Adhesivity and Cytoskeleton-Related Proteins During Imatinib-Induced Apoptosis of Leukemic JURL-MK1 Cells

Kuželová K., Pluskalová M., Grebeňová D., **Pavlásková K.**, Halada P., Hrkal Z.

J Cell Biochem. 111(6), 1413-1425 (2010)

Prohlášení spoluautorů

„Prohlašuji, že Kateřina Pavlásková se patřičně podílela (25 %) na plánování hmotnostně spektrometrických experimentů, jejich měření, interpretaci výsledků a sepisování této publikace.“

V Praze dne:

RNDr. Kateřina Kuželová, PhD.

ARTICLE
Journal of Cellular Biochemistry 111:1413–1425 (2010)

Journal of Cellular Biochemistry

Changes in Cell Adhesivity and Cytoskeleton-Related Proteins During Imatinib-Induced Apoptosis of Leukemic JURL-MK1 Cells

K. Kuželová,[1*] M. Pluskalová,[1] D. Grebeňová,[1] K. Pavlásková,[2] P. Halada,[2] and Z. Hrkal[1]

[1] *Department of Cellular Biochemistry, Institute of Hematology and Blood Transfusion, Prague, Czech Republic*
[2] *Laboratory of Mass Spectrometry, Institute of Microbiology of the ASCR, v.v.i., Prague, Czech Republic*

ABSTRACT

The fusion protein Bcr–Abl, which is the molecular cause of chronic myelogenous leukemia (CML) interacts in multiple points with signaling pathways regulating the cellular adhesivity and cytoskeleton architecture and dynamics. We explored the effects of imatinib mesylate, an inhibitor of Bcr–Abl protein used in front-line CML therapy, on the adhesivity of JURL-MK1 cells to fibronectin and searched for underlying changes in the cell proteome. As imatinib induces apoptosis of JURL-MK1 cells, we used three different caspase inhibitors to discriminate between direct consequences of Bcr–Abl inhibition and secondary changes related to the apoptosis. Imatinib treatment caused a transient increase in JURL-MK1 cell adhesivity to fibronectin, possibly due to the switch off of Bcr–Abl activity. Subsequently, we observed a number of changes including a decrease in cell adhesivity, F-actin decomposition, reduction of integrin β1, CD44, and paxillin expression levels and a marked increase in cofilin phophorylation at Ser3. These events were generally related to the proceeding apoptosis but they differed in their sensitivity to the individual caspase inhibitors. J. Cell. Biochem. 111: 1413–1425, 2010. © 2010 Wiley-Liss, Inc.

KEY WORDS: IMATINIB; ADHESION; CYTOSKELETON; APOPTOSIS; Q-VD-OPH; COFILIN; JURL-MK1

Hematopoietic cell adhesion to the bone marrow is mainly mediated by interaction of integrins and other cell surface receptors with protein components of the extracellular matrix (ECM), such as fibronectin. These interactions not only retain the unmature cell in the bone marrow microenvironment where it is exposed to appropriate regulatory substances but also regulate the activity of different intracellular signal cascades that consequently modulate diverse cellular functions including the cell proliferation, migration, or apoptosis. Alterations of these signaling pathways are commonly found in neoplastic cells. Chronic myelogenous leukemia (CML) is a myeloproliferative disorder, which is initiated by chromosomal translocation resulting in the formation of the fusion Bcr–Abl gene [Goldman and Melo, 2003]. Bcr–Abl protein expression affects in multiple points the pathways mediating the signaling from integrins (focal adhesion pathways), both through its constitutive tyrosine-kinase activity and through domains regulating the activity of small Rho GTPases, the key molecules in the control of the architecture and dynamics of the cell cytoskeleton [Zandy et al., 2007; Vega and Ridley, 2008]. As the interaction of Bcr–Abl with focal adhesion signaling is complex, the resulting effect of Bcr–Abl expression on the cell adhesion is unpredictable and depends on the cellular context [Kuželová and Hrkal, 2008]. To date, the experimental analysis of Bcr–Abl effects on the cell adhesion to the bone marrow components (usually to fibronectin) have revealed both elevated and attenuated adhesion in different Bcr–Abl expressing cell types [Bazzoni et al., 1996; Salgia et al., 1997; Bhatia and Verfaillie, 1998; Kramer et al., 1999; Gaston et al., 2000; Zhao et al., 2001; Cheng et al., 2002; Salesse and Verfaillie, 2002; Wertheim et al., 2002, 2003; Ramaraj et al., 2004]. Barnes et al. (2005) have found that the final effect of Bcr–Abl expression on the adhesion of Bcr–Abl-transfected 32D cells depends on the amount of the fusion protein. Nevertheless, from our experience, Bcr–Abl expression level does not correlate with the cell adhesivity to fibronectin for different CML cell lines (our unpublished observation). Another possible source of variability in the experimental results is the fact that Bcr–Abl inhibition triggers

Additional supporting information may be found in the online version of this article.
Grant sponsor: Ministry of Health of the Czech Republic; Grant numbers: NR 9243-3, VZ 00023736; Grant sponsor: Ministry of Education, Youth and Sports of the Czech Republic; Grant numbers: LC 07017, AV0Z50200510.
*Correspondence to: K. Kuželová, Institute of Hematology and Blood Transfusion, U Nemocnice 1, 128 20 Prague 2, Czech Republic. E-mail: kuzel@uhkt.cz
Received 31 March 2010; Accepted 25 August 2010 • DOI 10.1002/jcb.22868 • © 2010 Wiley-Liss, Inc.
Published online 9 September 2010 in Wiley Online Library (wileyonlinelibrary.com).

apoptosis in the majority of CML cells. It is known that the apoptosis includes an early cell detachment from the environment and complex rearrangements of the actin cytoskeleton leading to the initial cell contraction and rounding, formation of membrane blebs, and eventual cell breakdown into apoptotic bodies [Coleman and Olson, 2002].

In the present work, we analyzed the changes in the cell adhesivity to fibronectin and in actin polymerization upon treatment of the CML cell line JURL-MK1 with the inhibitor of Bcr–Abl tyrosine kinase activity, imatinib mesylate. We compared the proteomes of control and treated cells and focused on the behavior of the proteins, which are known to be involved in the regulation of cytoskeleton dynamics and cell adhesivity. To characterize potential contribution of apoptotic processes, we used three caspase inhibitors, which differ in their ability to prevent various stages of the apoptosis.

MATERIALS AND METHODS

CHEMICALS

Imatinib mesylate was kindly provided by Novartis (Basel, Switzerland). The stock solution (10 mM) was prepared by dissolving imatinib mesylate in sterile distilled water and stored at minus 20°C. Human fibronectin (alpha-chymotryptic fragment, 120 K) and the labeled antibody against integrin β1 (CD29) were purchased from Chemicon International (CA). Caspase inhibitors zDEVDfmk, zVADfmk, and Q-VD-OPh were from Sigma (Prague, Czech Republic), Alexis Biochemicals (Lausen, Switzerland), and R&D Systems (Minneapolis), respectively. The inhibitor Y-27632, which inhibits ROCK1 and ROCK2 was from Calbiochem. Anti-β-actin antibody (cat. no A 5441), anti-Rho-GDI (cat. no R 3025), FITC-labeled phalloidin, and the fluorogenic substrate Ac-DEVD-AFC were obtained from Sigma, anti-paxillin (clone 5H11) and anti-ROCK1 (cat. no 07–903) antibodies from Millipore (Upstate). Anti-phospho-cofilin (pSer3, cat. no C8992), anti-tropomyosin3 (Sigma Prestige Antibodies™), and anti-tropomyosin4 antibodies were obtained from Sigma, anti-cofilin antibody from Chemicon International (cat. no AB3842), anti-tropomyosin1 (alpha) antibody from Abcam (Cambridge), anti-Bcr (cat. no sc-103) antibody, and FITC-conjugated anti-rabbit IgG (cat. no sc-2012) from Santa Cruz Biotechnology, Alexa Fluor 546-conjugated anti-rabbit IgG from Invitrogen (Mol. Probes, cat. no A11010), PE-conjugated anti-CD44 (cat. no MHCD4404) and anti-CD62P (cat. no MHCD6204) also from Invitrogen (Camarillo, CA). PE-conjugated anti-CD62L (cat. no 12–0629–73) was from eBiosciences. Rabbit polyclonal antibodies against LIMK1 (cat. no 3842) and against PAK1 (cat. no 2601) were from Cell Signaling Technology®.

CELL CULTURE

JURL-MK1 cells derived from a patient with CML were purchased from DSMZ (German Collection of Microorganisms and Cell Cultures, Braunschweig, Germany). The cells were cultured in RPMI 1640 medium supplemented with 10% fetal calf serum, 100 U/ml penicillin, and 100 μg/ml streptomycin at 37°C in 5% CO_2 humidified atmosphere.

CASPASE ACTIVITY

The activity of caspase-3 was determined by fluorometric measurement of the kinetics of 7-amino-4-trifluoromethyl coumarin (AFC) release from the fluorogenic substrate Ac-DEVD-AFC in the presence of cell lysates. The method was described in detail in Kuželová *et al.*, 2007. After the incubation with effectors the cells were washed and lysed and aliquots of cytosolic fractions were incubated for 30 min at 37°C with the fluorogenic substrate. The linear increase of fluorescence intensity at 520 nm was monitored during this incubation time using Fluostar Galaxy microplate reader (BMG Labtechnologies, Germany).

FLOW CYTOMETRY ANALYSIS

Flow cytometry measurements were performed on Coulter Epics XL flow cytometer.

The fraction of cells containing apoptotic DNA breaks was measured by TUNEL assay using the in situ Cell Death Detection Kit, Fluorescein (Roche Diagnostics GmbH, Mannheim, Germany) following the standard manufacturers protocol.

To analyze the expression level of integrin β1 or CD44 on the cell surface, the cells (5×10^5) were washed in PBS and stained with 5 μl PE-conjugated anti-integrin β1 or anti-CD44. After 40 min incubation at room temperature, the cells were washed twice in PBS and the fluorescence histograms of PE fluorescence were recorded using the flow cytometer.

To stain the actin polymers, the cells were washed in PBS and fixed and permeabilized using FIX&PERM cell permeabilization kit from An Der Grub (Kaumberg, Austria). Washing steps were performed in PBS supplemented with 1% BSA using short centrifugation times (2 min at 350 g). FITC-labeled phalloidin (3 μl) was added to cells suspended in 50 μl PERM solution. The samples were incubated for 40 min at room temperature, washed in PBS + 1% BSA and the green fluorescence was measured using the flow cytometer.

ADHESION ASSAY

The extent of JURL-MK1 cell adhesion to fibronectin was measured using the previously described protocol [Kuželová *et al.*, 2010]. Briefly, the cells were applied to fibronectin-coated wells of a microtitration plate and incubated for 1 h at 37°C. Then, the wells were washed with PBS/Ca^{2+}/Mg^{2+} using a multichannel adaptor to the succion pump and the remaining cells were quantified by means of fluorescent labeling (Cy-Quant Cell Proliferation Assay Kit; Molecular Probes). The adherent cell fraction (ACF) was calculated using the fluorescence signal from fibronectin-coated plate and that from reference plate, which contained the total cell number.

1-D ELECTROPHORESIS AND WESTERN-BLOTTING

Control and treated cells (3×10^6) were washed twice in PBS, suspended in 150 μl lysis buffer (300 mM NaCl, 50 mM Tris–HCl pH 8.0, 5 mM EDTA, 1 mM DTT, 1 mM PMSF, 1% NP-40, phosphatase inhibitor coctail 5 μl per 2×10^7 cells, protease inhibitor coctail 4 μl per 2×10^7 cells) and kept for 30 min on ice. The protein concentration was measured using a BioRad protein assay (BioRad Hercules, CA). Protein samples were heated to 100°C for 4 min in the presence of 5% 2-mercaptoethanol, chilled and subjected to one-dimensional electrophoresis (PAGE) in 6, 12, or 15% gel with SDS. As a rule, 15 μg total protein was applied to each well. Proteins were transferred to Hybond-ECL membrane at 90 V for 1–2 h (wet transfer).

Nitrocellulose membranes were blocked with 5% non-fat milk or 3% BSA in TBS-T (Tris-buffered saline, 0.1% Tween-20) for 1 h at room temperature, incubated with the appropriate antibody in TBS-T solution (1 h at room temperature or overnight at 4°C), washed in TBS-T and incubated with the horseradish peroxidase-conjugated anti-mouse or anti-rabbit secondary antibody. The antigens were detected using SuperSignal® West Pico Chemiluminiscent Substrate (Pierce Biotechnology, IL) according to the manufacturers instructions and visualized by autoradiography on X-ray film. Immunoblots were reacted in parallel with anti-β-actin as a control of the equal protein loading. The protein bands were evaluated by densitometry using AIDA version 4.08 (Raytest, Germany).

2-D ELECTROPHORESIS

The linear immobilized pH gradient gels ($180 \times 3.3 \times 0.5\,mm^3$), ReadyStrip™ IPG strips pH 3–10 (BioRad), were rehydrated overnight in 315 μl of the cell lysate containing 1 mg proteins, 7 M urea, 2 M thiourea, 1.2% CHAPS, 0.5% ASB-14, 30 mM Tris, 43 mM DTT, 0.2% Bio-Lyte 3–10. Isoelectric focusing (IEF) was performed using Protean IEF Cell instrument (BioRad) at 6,000 V for a total 40–60 kVh at 20°C. After the first dimension run, the strips were equilibrated with a solution containing Tris–HCl pH 8.8 (0.375 mM), urea (6 M), glycerol (20% v/v), DTT (2% w/v), SDS (2% w/v), and 0.01% bromphenol blue. Resulting free SH groups were blocked in the second equilibration step in which DTT was replaced with iodoacetamide (2.5% w/v).

The second dimension run was performed using a Protean II xi vertical electrophoresis system (BioRad), gel size $200 \times 200 \times 1\,mm^3$, in a Laemmli–SDS discontinuous buffer system and polyacrylamide gel gradient (9–16% T, 2.6% C). The equilibrated first dimension gel was placed directly onto the second dimension gel and overlaid with a solution containing 0.4% agarose in Tris–glycine–SDS pH 8.3 buffer (25 mM Tris, 192 mM glycine, 0.1% w/v SDS) heated to 70°C. Electrophoresis was performed at a constant current 35 mA/gel for 5 h at 10°C. The gels were fixed in a solution containing ethanol (40% v/v) and acetic acid (10% v/v) before staining. The gels were stained with Coomassie blue (CBB), scanned and analyzed employing Phoretix® 2D Expression Software (Nonlinear Dynamics, UK, version 2005). The selected protein spots were excised from the gel and subjected to MALDI-TOF MS analysis.

ENZYMATIC IN-GEL DIGESTION

CBB-stained protein spots were excised from the gel, cut into small pieces and destained with 50 mM 4-ethylmorpholine acetate (pH 8.1) in 50% acetonitrile (MeCN). After complete destaining, the gel was washed with water, shrunk by dehydration in MeCN and reswelled again in water. The supernatant was removed and the gel was partly dried in a SpeedVac concentrator. The gel pieces were then rehydrated in a cleavage buffer containing 25 mM 4-ethylmorpholine acetate, 5% MeCN and trypsin (100 ng; Promega), and incubated overnight at 37°C. The resulting peptides were extracted to 40% MeCN/0.1% TFA. An aqueous 50% MeCN/0.1% TFA solution of α-cyano-4-hydroxycinnamic acid (5 mg/ml; Sigma) was used as a MALDI matrix. The sample (0.5 μl) was deposited on the MALDI target and allowed to air-dry at room temperature. After complete evaporation, 0.5 μl of the matrix solution was added. If necessary, the peptides were desalted and concentrated using a GELoader microcolumn (Eppendorf, Hamburg, Germany) packed with a Poros Oligo R3 material [Larsen *et al.*, 2005]. The purified peptides were eluted from the microcolumn in

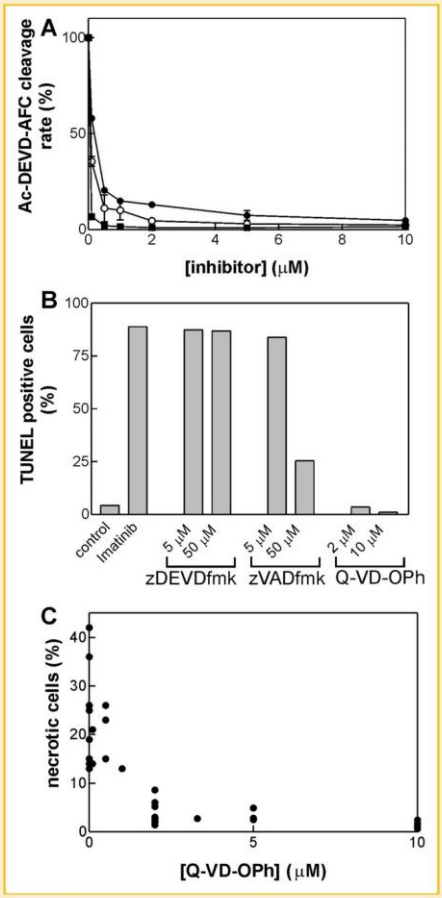

Fig. 1. The effect of caspase inhibitors on caspase-3 activity, apoptotic DNA fragmentation and cell death in imatinib-treated JURL-MK1 cells. The cells were treated with 1 μM imatinib alone or in combination with different concentration of zDEVDfmk, zVADfmk, or Q-VD-OPh as indicated. A: After 42 h incubation, the cells were harvested and the activity of caspase-3 in the cell lysate was measured using the fluorogenic caspase-3 substrate Ac-DEVD-AFC. Imatinib mesylate alone induced about 7–15 fold increase in caspase-3 activity over the controls. The given values of caspase-3 activity are relative to those from samples treated with imatinib only. Symbols: zDEVDfmk—open circles, zVADfmk—closed circles, Q-VD-OPh—squares. B: After 48 h incubation, the cells were harvested and the apoptotic DNA breaks were stained using TUNEL method. C: Fraction of Trypan blue-positive cells after 42–48 h incubation with imatinib alone or in combination with Q-VD-OPh at different concentrations. The points correspond to individual experiments.

several droplets directly onto MALDI plate using 1 μl of the matrix solution. The phosphopeptide enrichment was performed as described previously [Larsen *et al.*, 2005].

MALDI-TOF MASS SPECTROMETRY (MS) AND PROTEIN IDENTIFICATION

Mass spectra were measured on an Ultraflex III MALDI-TOF/TOF instrument (Bruker Daltonics, Bremen, Germany) equipped with a Smartbeam™ solid state laser and LIFT™ technology for MS/MS analysis. The spectra were acquired in the mass range of 700–4,000 Da and calibrated externally using peptide calibration mix II (Bruker Daltonics).

For PMF database searching, peak lists in XML data format were created using flexAnalysis 3.0 program with SNAP peak detection algorithm. No smoothing was applied and maximal number of assigned peaks was set to 50. After peak labeling all known contaminant signals were removed. The peak lists were searched using in-house MASCOT search engine against SwissProt 57.13 database subset of human proteins with the following search settings: peptide tolerance of 30 ppm, missed cleavage site value set to two, variable carbamidomethylation of cysteine, oxidation of methionine, and protein N-term acetylation. No restriction on protein molecular weight and pI value were applied. Proteins with MOWSE score over the threshold 56 calculated for the used settings were considered as identified. If the score was lower or only slightly higher than the threshold value, the identity of protein candidate was confirmed by MS/MS analysis. In addition to the above mentioned MASCOT settings fragment mass tolerance of 0.6 Da and instrument type MALDI-TOF-TOF was applied for MS/MS spectra searching.

IMMUNOFLUORESCENCE MICROSCOPY

JURL-MK1 cells were incubated with 1 μM imatinib mesylate for 40 h. Control and imatinib-treated cells were collected by

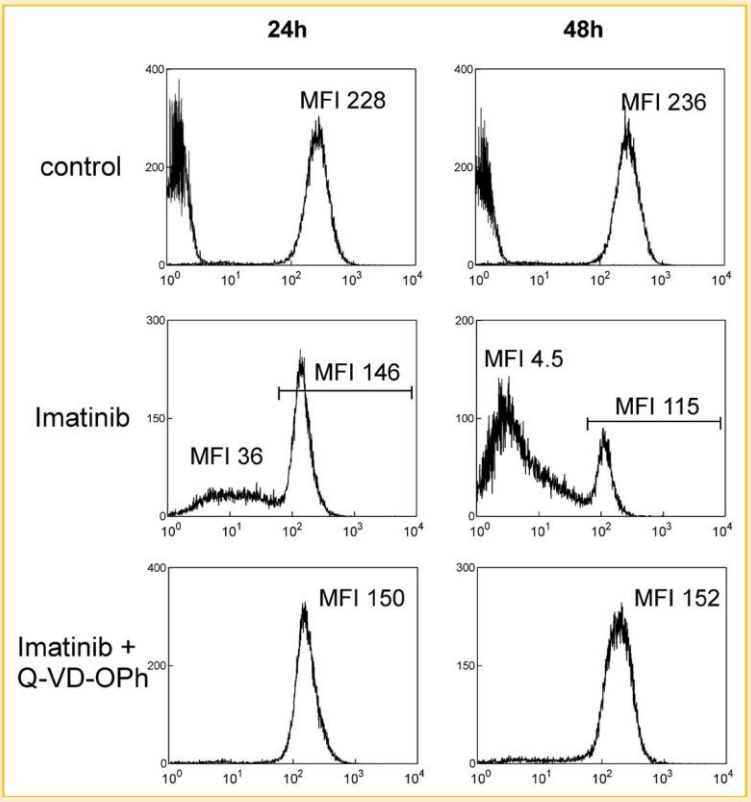

Fig. 2. F-actin depolymerization due to imatinib treatment of JURL-MK1 cells. The cells were treated with 1 μM imatinib mesylate alone or in combination with 2 μM Q-VD-OPh for 24 or 48 h as indicated. F-actin was labeled using FITC-phalloidin and quantified using flow-cytometry. MFI stands for mean fluorescence intensity. Negative controls (no staining) are shown on the left side of the upper panels. Three additional experiments yielded closely similar results.

centrifugation, washed in PBS, and plated on glass coverslips. Cells were fixed with 3% paraformaldehyde in PBS for 15 min and permeabilized with 0.3% Triton X-100 in PBS for 10 min. After blocking with 3% bovine serum albumin in PBS supplemented with 0.03% Tween-20 for 10 min, cells were stained with primary antibody at 37°C for 1 h. Antibodies were diluted in blocking buffer and dilutions were as follows; anti-pSer3-cofilin antibody 1:100, anti-cofilin 1:200. Subsequently, cells were washed three times with 0.1% Tween 20 in PBS for 10 min and stained with secondary antibody for 1 h (FITC-conjugated anti-rabbit IgG for pSer3-cofilin or Alexa Fluor 546-conjugated anti-rabbit IgG for cofilin, both diluted 1:200 in blocking buffer). After washing with PBS–Tween, the coverslips were mounted using Vectashield (for cofilin staining) or Vectashield containing propidium iodide (for pSer3-cofilin). Images were obtained using inverted fluorescence microscope Olympus IX 81 with Cell-R system with magnification 60×. The green fluorescence intensity from individual cells was evaluated using Phoretics™ 2D Expression (Nonlinear Dynamics).

RESULTS

In agreement with previous studies involving other Bcr–Abl positive cells [Dai *et al.*, 2004], imatinib treatment of JURL-MK1 cells resulted not only in the inhibition of Bcr–Abl tyrosine kinase activity but also in a subsequent decrease of Bcr–Abl expression level: we observed a reduction by (56 ± 17)% after 24 h and by (88 ± 18)% after 48 h treatment with imatinib (mean and standard deviation from five experiments, Supplementary Material: Fig. 1S). We have previously shown that imatinib mesylate induces apoptosis including a marked caspase-3 activation and DNA fragmentation in JURL-MK1 cells [Kuželová *et al.*, 2005].

CHARACTERIZATION OF CASPASE INHIBITORS

In the present work, we used three different caspase inhibitors which differ in their specificity towards the individual caspases: zDEVDfmk is considered to be relatively specific for caspase-3, zVADfmk is a broad range caspase inhibitor and Q-VD-OPh is a new generation broad caspase inhibitor, which is claimed to be more specific for the caspase family, more potent and less toxic to the cells. Fig. 1 shows the effect of these inhibitors on caspase-3 activity (panel A) and DNA-fragmentation (panel B) in Imatinib mesylate-treated JURL-MK1 cells. As only Q-VD-OPh was able to completely inhibit apoptotic DNA fragmentation (no increase in TUNEL-positive cell fraction compared to the control samples occurred for up to 70 h when imatinib was added simultaneously with 10 μM Q-VD-OPh, data not shown), we used prevalently this inhibitor for subsequent studies. Q-VD-OPh also markedly reduced the fraction of dead (Trypan blue-positive) cells in imatinib-treated samples (Fig. 1C). In control JURL-MK1 cell samples, the fraction of Trypan blue-positive cells was usually about 2%.

F-ACTIN DISASSEMBLY

To assess changes in the amount of polymeric actin (F-actin), JURL-MK1 cells were stained with FITC-labeled phalloidin and measured using a flow-cytometry apparatus. As shown in Fig. 2, imatinib mesylate treatment first induced a homogeneous moderate decrease of actin polymerization, which was followed by massive decomposition of F-actin structures. The initial decrease of F-actin amount occured progressively between 2 and 20 h of the treatment (data not shown) and was completely insensitive to apoptosis inhibition (see the loss of MFI in imatinib + Q-VD-OPh samples compared to the controls in Fig. 2). On the other hand, the subsequent F-actin disassembly was fully prevented by 2 μM Q-VD-OPh (Fig. 2, bottom). Similar effect was achieved using zVADfmk at 50 μM, but not at 5 μM concentration, while zDEVDfmk had no effect on imatinib-induced actin depolymerization (data not shown, Table I).

CHANGES IN CELL ADHESIVITY TO FIBRONECTIN

The cell adhesivity to fibronectin was studied using the previously described protocol [Kuželová *et al.*, 2010]. The fraction of adhered cells was usually of 20–30% in the case of untreated JURL-MK1 cells under our experimental conditions. Imatinib mesylate treatment induced a moderate increase in the cell adhesivity during the first 6 h of the treatment (Fig. 3, the values for ACF are expressed as the

TABLE I. The Ability of Different Caspase Inhibitors to Inhibit the Observed Imatinib Mesylate-Induced Changes in JURL-MK1 Cells.

	5–50 μM zDEVDfmk, or 5 μM zVADfmk	50 μM zVADfmk	Q-VD-OPh (2 μM/10 μM)
Caspase-3 activation	++	++	++
DNA fragmentation	–	+	++
Necrosis	–	+	++
Actin depolymerization 1	–	–	–
Actin depolymerization 2	–	++	++
Decreased adhesivity to FN	–	–	+/++
Cofilin phosphorylation	–	n.d.	+
tropomyosin 1 decrease	n.d.	n.d.	+/++
Tropomyosin 4 decrease	n.d.	n.d.	–
ROCK cleavage	n.d.	–	–
LIMK decrease	n.d.	–	+
RhoGDI decrease	n.d.	n.d.	++
PAK-1 decrease	n.d.	n.d.	+
Paxillin decrease	n.d.	n.d.	+/++
Integrin β1 decrease	n.d.	n.d.	++
CD44 decrease	n.d.	n.d.	–

–, No effect; +, partial inhibition; ++, complete inhibition; n.d., not determined.
Actin depolymerization 1 and 2: moderate decrease of F-actin level within the first 20 h of Imatinib treatment and subsequent massive F-actin decomposition, respectively.

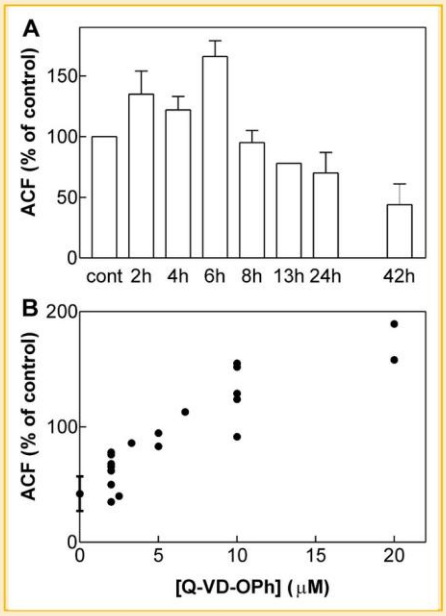

Fig. 3. JURL-MK1 adhesivity to fibronectin. Panel A: The cells were treated for up to 42 h (as indicated) with 1 μM imatinib mesylate, applied to fibronectin-coated microtitration plate and incubated for 1 h at 37°C. The ACF was then determined as described in Materials and Methods section and expressed as percentage of the untreated control. The plotted results represent means and standard deviation from 2 to 12 independent experiments. Panel B: Effect of simultaneous addition of Imatinib 1 μM and Q-VD-OPh at different concentrations on ACF. The point with error bars represents mean and standard deviation of ACF for cells treated with 1 μM imatinib only for 42–48 h (8 experiments). The other points correspond to samples treated with imatinib and Q-VD-OPh (2, 2.5, 3.3, 5, 6.7, 10, or 20 μM) for the same time intervals, the results are merged from several independent experiments.

percentage of the corresponding controls). Thereafter, the ACF progressively decreased to about a half of the control value after 42 h incubation. The loss of cell adhesivity was not affected by caspase inhibitors except for Q-VD-OPh, which displayed dose-dependent effects in the range of 2–20 μM concentrations (Fig. 3B).

2D-GEL ELECTROPHORESIS

The proteomic analysis of imatinib effects on JURL-MK1 cells was performed by means of 2D polyacrylamide gel electrophoresis (2D PAGE) in combination with mass spectrometry (MALDI-TOF). Fig. 4 shows the master map of JURL-MK1 cells and the identified proteins are listed in Table IS (Supplementary Material). An example of protein map obtained from cells treated with imatinib for 42 h is shown in Fig. 2S (Supplementary Material). By comparison of the protein maps obtained from control and imatinib-treated JURL-MK1 cells we found a reproducible increase in the intensity of the spots No 20 (cofilin), No 130 (stress-70 protein–GRP75) and No 147 (tropomyosin alpha-4, TPM4). Using a phosphopeptide-enriching GELoader microcolumn, we found that the spot No 20 contained the form of cofilin phosphorylated at Ser3. The intensity of several spots was systematically reduced by imatinib treatment: No 141 (deoxyuridine 5′-triphosphate nucleotidohydrolase), No 142 (nucleoside diphosphate kinase A), No 145 (proliferating cell nuclear antigen–PCNA), No 146 (elongation factor 1-beta), No 148 (tropomyosin alpha-3 chain), and Nos 149, 152, and 153 (14–3–3 proteins, isoforms epsilon, zeta/delta, and beta/alpha, respectively). The C-terminal cleavage of 14–3–3 proteins during imatinib-induced apoptosis has already been analyzed in our previous work [Kuželová *et al.*, 2009]. Among the other altered proteins, cofilin and tropomyosins are clearly related to the cytoskeleton architecture or cellular adhesion. We thus studied in detail their behavior after imatinib mesylate addition using specific antibodies: anti-cofilin, anti-phosphoSer3-cofilin, and anti-tropomyosins 1, 3, and 4.

COFILIN PHOSPHORYLATION DURING IMATINIB-INDUCED APOPTOSIS

While the expression level of cofilin displayed a mild decrease as a result of imatinib treatment (decrease to 82 ± 24%, mean and SD from four independent experiments), we observed a marked increase in the level of cofilin phosphorylation at Ser3 upon this treatment (Fig. 5A), which started as early as 2 h after imatinib addition (not shown). The average increase in cofilin phosphorylation after 42 h treatment was (7 ± 4) fold (mean and standard deviation from 13 independent experiments). Cofilin phosphorylation at Ser3 due to imatinib mesylate was at least partly inhibited by simultaneous addition of Q-VD-OPh: the increase in cofilin phosphorylation was reduced by (64 ± 27)% (mean and standard deviation from eight independent experiments) using 2 μM inhibitor (cf. lanes 4 and 5 in Fig. 5A). Increasing Q-VD-OPh concentration to 10 μM did not enhance the extent of the inhibition. The moderate imatinib-induced decrease in total cofilin level, if present, was also inhibited by Q-VD-OPh (Fig. 5A). We also tested the effect of Y-27632, a specific inhibitor of ROCK (Rho-associated kinase), which is a known upstream effector of cofilin phophorylation. The use of Y-27632 usually resulted in a decrease of cofilin phosphorylation in control JURL-MK1 cells (lane 3 in Fig. 5A) but this inhibitor had only minor effect on the pSer3-cofilin level in the cells treated with imatinib (lane 6 in Fig. 5A). Staining of 2D western blots by anti-pSer3-cofilin and anti-cofilin antibodies revealed a single spot corresponding to cofilin phosphorylated at Ser3 (probably the spot No 20 in Fig. 4) and two to three additional cofilin spots which are not recognized by the phospho-specific antibody (Fig. 5B). Thus, in spite of the increase in cofilin phosphorylation, a large pool of unphosphorylated cofilin is still present in imatinib-treated JURL-MK1 cells.

The intracellular localization of pSer3-cofilin and cofilin was studied by means of immunofluorescence microscopy. Both in the control and in imatinib-treated JURL-MK1 cells, p-cofilin was concentrated in small distinct areas, which were distributed throughout the cytoplasm (Fig. 6, upper panels). While the staining pattern did not essentially change after the treatment, the average cell fluorescence intensity corresponding to the labeled p-cofilin was higher in the treated cells. The histograms in Fig. 6 show the distribution of integrated fluorescence intensity from individual

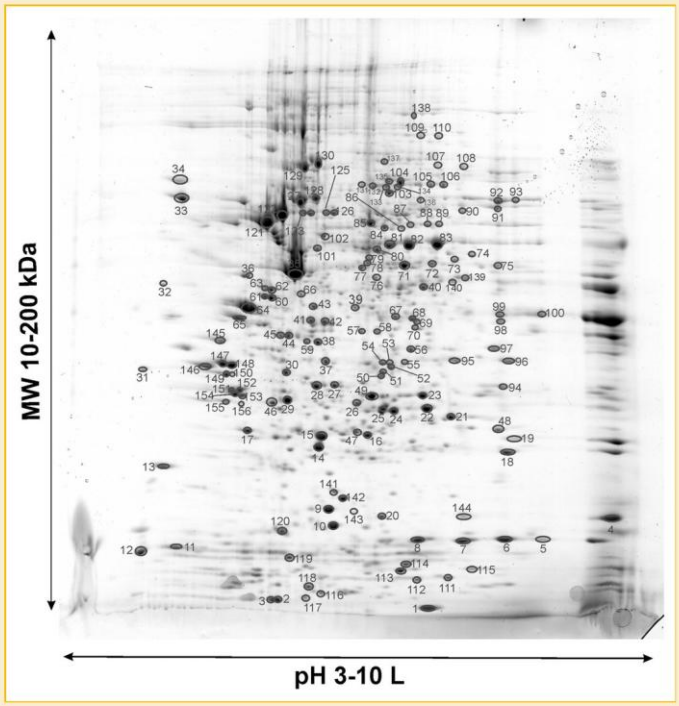

Fig. 4. Master map of JURL-MK1 cells. The protein mixture obtained from the whole cell lysates was resolved by isoelectric focusing followed by SDS electrophoresis. The gel was stained with Coomassie blue, the selected spots were excised from the gel and the proteins were identified using MALDI-TOF. The characterization of the numbered spots is given in Table IS (Supplementary Material).

cells for control (open symbols) and imatinib-treated (closed symbols) JURL-MK1 cells. When the cells where stained for total cofilin (independently of the phosphorylation status), we observed a rather diffuse signal which was localized mainly at the cell periphery in addition to the spotted pattern observed for phospho-cofilin (Fig. 6, lower right part).

CHANGES IN TROPOMYOSIN EXPRESSION LEVEL

Tropomyosins form part of actin filamentous structures and different tropomyosin isoforms are thought to be specifically involved in different types of actin filaments. Especially, high molecular weight (HMW) tropomyosins are associated with actin stress fiber formation while lower molecular weight (LMW) tropomyosins prevail in invasive cells. In 2D protein maps, we identified two spots containing LMW tropomyosin isoforms of TPM3 and TPM4, which were altered by imatinib mesylate treatment. Western blot analysis using specific antibodies did not confirm any consistent change in the expression levels of TPM3 while the amount of TPM4 was reduced by imatinib treatment (Fig. 5C). This decrease was insensitive to Q-VD-OPh addition. We also tested the level of HMW isoforms of TPM1, which are known to be implicated in stabilizing actin cytoskeleton filaments in non-muscle cells. We observed a decrease in the expression level of these isoforms following 24–48 h imatinib treatment which could be inhibited by Q-VD-OPh (Fig. 5C).

CHANGES IN KNOWN COFILIN REGULATORS

One of the most important regulation mechanisms of cofilin phosphorylation involves the kinases ROCK and their downstream effectors, LIM kinases (Fig. 3S, Supplementary Material). We thus explored their expression using specific antibodies. Imatinib mesylate induced cleavage of the protein ROCK1, which was insensitive to zVADfmk (up to 50 μM, not shown) and rather insensitive to Q-VD-OPh (up to 10 μM; Fig. 7). The results obtained with anti-LIMK1 and anti-phospho-LIMK1 antibodies were less conclusive: in different experiments, they ranged from no change to a large decrease both of the total protein level and of the phosphorylated form due to the imatinib treatment. The decrease, if present, was at least partly inhibited by 2 μM Q-VD-OPh (Fig. 7). Another protein, which is known to affect cofilin phosphorylation is PAK1 (p21-associated kinase 1, Fig. 3S). The level of PAK1 in JURL-MK1 cells markedly decreased as a result of imatinib mesylate

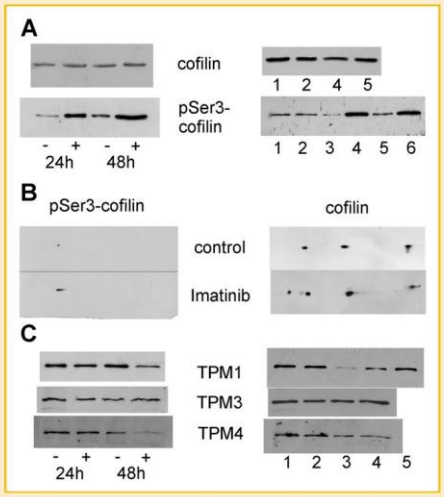

Fig. 5. Changes in cofilin and tropomyosin expression due to Imatinib treatment of JURL-MK1 cells. Panel A: Cofilin and pSer3-cofilin expression in JURL-MK1 cells cultivated for 24 or 48 h in the presence (+) or in the absence (−) of imatinib mesylate (left column) or incubated for 42 h with following agents: (1) control, (2) Q-VD-OPh 2 μM, (3) Y-27632 10 μM, (4) imatinib mesylate 1 μM, (5) imatinib with Q-VD-OPh, (6) imatinib with Y-27632. Panel B: 2D blots from control and imatinib-treated (1 μM, 42 h) cells using cofilin and pSer3-cofilin antibodies. Panel C: left: Expression of tropomyosin isoforms TPM1, TPM3, and TPM4 in cells cultivated for 24 or 48 h in the presence (+) or in the absence (−) of imatinib (left column) or incubated for 42 h with following agents: (1) control, (2) Q-VD-OPh 2 μM, (3) imatinib mesylate 1 μM, (4) imatinib with 2 μM Q-VD-OPh, (5) imatinib with 10 μM Q-VD-OPh.

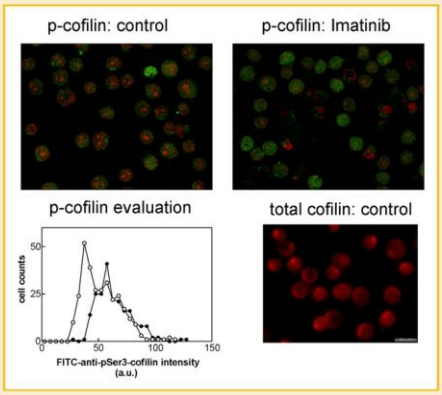

Fig. 6. Intracellular distribution of pSer3-cofilin and cofilin in JURL-MK1 cells. The control cells and the cells treated with 1 μM imatinib mesylate for 40 h were fixed, permeabilized and stained with anti-pSer3-cofilin (upper panels) or anti-cofilin (lower right panel) antibody and subsequently with FITC-labeled (green) or PE-labeled (red) secondary antibody, respectively. In the upper panels, the cell nuclei were stained with propidium iodide (red). The pictures were enregistred using Olympus IX81 microscope with Cell-R system, magnification 60×. Lower left part: Histograms of FITC-fluorescence intensity from anti-pSer3-cofilin-labeled control (open symbols) and imatinib-treated (closed symbols) cells. The green fluorescence intensity from individual cells was evaluated using Phoretix™ 2D Expression software. The experiment was repeated with similar results.

treatment and the decrease was partly reversible by Q-VD-OPh. The expression level of RhoGDI, a negative regulator of Rho GTPase activity, was also largely reduced by imatinib treatment and this effect was reversed by 2 μM Q-VD-OPh.

CHANGES IN SURFACIAL PROTEIN EXPRESSION

The cell adhesion to the proteins of the ECM is mainly mediated by integrins. In a previous work, we identified integrin β1 as the most important interaction partner for fibronectin in the case of JURL-MK1 cells [Kuželová *et al.*, 2010]. We used a PE-labeled anti-integrin β1 antibody to study the amount of this integrin at the surface of JURL-MK1 cells by means of flow-cytometry. The scattergrams presented in Fig. 8 reveal the presence of a cell subpopulation with altered scattering properties (especially with lower FSC indicating smaller cell size) in the imatinib-treated sample. Q-VD-OPh inhibits these imatinib-induced changes in the cell size and shape (Fig. 8, left panels C and D; we also made the same conclusion from the microscopic observation of cell preparations: Fig. 4S in Supplementary Material). Presumably, the observed morphological changes correspond to cell shrinking and membrane blebbing which are known to occur as a part of the apoptosis. Indeed, imatinib treatment leads to a large increase in Annexin-positive cell fraction and the majority of Annexin-positive cells are found in the region denoted as Alt (Fig. 5S, Supplementary Material). As it is shown in Fig. 8, the cells with altered morphology (i.e., apoptotic) display lowered surfacial expression of integrin β1 and the decrease in anti-integrin staining can be reversed by simultaneous addition of Q-VD-OPh.

Changes in the expression level of some other adhesion molecules have been previously reported to occur in CML cells and we thus analyzed the surfacial expression level of hyaluronic acid receptor (HCAM, CD44) and those of P and L-selectin (CD62P and CD62L). We observed about 50% reduction in PE-anti-CD44 staining due to 42 h imatinib treatment. This decrease occurred both in "normal" and "altered" subpopulations and was almost insensitive to Q-VD-OPh addition (Fig. 6S, Supplementary Material). On the other hand, neither control nor imatinib-treated JURL-MK1 cells were significantly labeled with anti-CD62 antibodies indicating that JURL-MK1 cells do not express selectins on their surface.

CHANGES IN PAXILLIN EXPRESSION LEVEL

During the cell adhesion, the integrins cluster and large protein complexes (so-called focal adhesions) are formed at their cytoplasmic tails. An important component of these complexes is the protein paxillin and labeled anti-paxillin antibodies are often used to stain focal adhesions for microscopic observations. We examine paxillin expression level using Western blotting and found

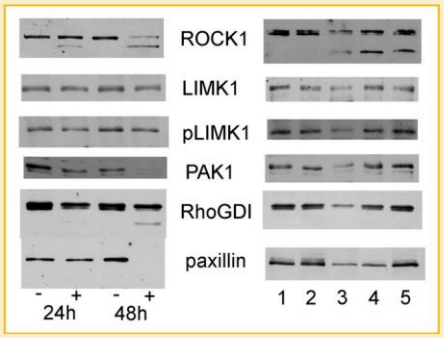

Fig. 7. Changes in protein expression levels induced by imatinib treatment in JURL-MK1 cells. Left column: Cells were incubated in the absence (−) or in the presence (+) of 1 μM imatinib mesylate for 24–48 h as indicated. Right column: Cells were incubated with 1 μM imatinib, Q-VD-OPh or with their combination for 42 h. The expression level of the specified proteins was assessed by Western blotting. Lane 1: control, lane 2: Q-VD-OPh, lane 3: imatinib mesylate, lanes 4 and 5: imatinib mesylate in combination with Q-VD-OPh 2 μM (4) or 10 μM (5).

that it was lowered due to imatinib treatment of JURL-MK1 cells. The inhibitor Q-VD-OPh was able to prevent this decrease in a dose-dependent manner similar to that observed for the decrease of the cell adhesivity to fibronectin: the effect was only modest at 2 μM Q-VD-OPh but complete inhibition was achieved using 10 μM Q-VD-OPh (Fig. 7, Table I).

The summary of the effect of caspase inhibitors on the individual changes occuring as a result of imatinib mesylate treatment of JURL-MK1 cells is given in Table I.

DISCUSSION

Altered adhesivity to the ECM is one of the characteristic features of CML, which is manifested by an expansion of myeloid cells and their premature release into the peripheral blood. The fusion protein Bcr–Abl which is the molecular cause of the disease, affects at multiple points the pathways leading from focal adhesions to the cytoskeleton [Kuželová and Hrkal, 2008]. The inhibition of Bcr–Abl tyrosine-kinase activity by imatinib mesylate eventually results in Bcr–Abl degradation (Fig. 1S, Supplementary Material) and presumably changes the activation state of the focal adhesion pathways. In parallel, imatinib mesylate induces apoptosis and the focal adhesion pathways can thus also be modulated as a part of apoptosis execution. Many structural and regulatory proteins which are involved in the cell adhesivity and cytoskeleton dynamics are substrates for caspases and caspase-mediated proteolysis is believed to contribute to focal adhesion disassembly, cell detachment from the ECM and the eventual cell collapse. We have previously shown that the treatment of JURL-MK1 cells with 1 μM imatinib mesylate triggers caspase-3 activation (reaching the maximum after about 40 h of treatment), apoptotic DNA fragmentation and cell death in the whole cell population [Kuželová *et al.*, 2005]. In the attempt to discriminate between primary and secondary effects of imatinib on JURL-MK1 cell adhesion signaling, we employed three different caspase inhibitors in combination with imatinib. All these inhibitors were able to suppress imatinib-induced activation of caspase-3 measured in an in vitro assay, even at concentrations lower than 2 μM (Fig. 1A). We also verified by anti-caspase-3 Western blotting that the inhibitors irreversibly bound to virtually all caspase-3 molecules under these conditions (see Kuželová *et al.*, 2007 for zDEVDfmk and zVADfmk, we performed similar experiments for Q-VD-OPh, data not shown). Anti-caspase-3 Western blots also showed that the inhibitors interfere with pro-caspase-3 processing and prevent the formation of the active caspase-3 at concentrations up from 0.5 μM. On the other hand, the individual inhibitors largely differ in their ability to prevent other apoptotic processes, such as DNA fragmentation (Fig. 1B). These results show that other proteins than caspase-3 must be involved in the execution of JURL-MK1 cell apoptosis induced by imatinib mesylate and these pathways are blocked by Q-VD-OPh.

Our experimental results show that the actin cytoskeleton of JURL-MK1 cells undergoes massive and complex rearrangements as a result of imatinib treatment. It is likely that the majority of F-actin fibres are progressively decomposed in relation with the proceeding apoptosis. The massive disruption can be prevented by caspase inhibitors zVADfmk (at 50 μM, data not shown) and Q-VD-OPh (Fig. 2), but not by zDEVDfmk at up to 50 μM concentration (data not shown, Table I). Caspase-3 is thus not the key player in this event. In addition, the early mild but homogeneous decrease in F-actin amount indicated by the decrease in MFI in Fig. 2 cannot be inhibited by any of the inhibitor used. This change may thus either be part of very early apoptotic processes (upstream of the activation of caspases or other proteases which are targeted by the inhibitors) or may result directly from the inhibition of Bcr–Abl signaling through cytoskeleton-regulating pathways.

JURL-MK1 cell adhesivity to fibronectin-coated surface was measured using the previously described sensitive assay with fluorescence detection (Fig. 3A). The initial moderate increase in the ACF during the first 6 h of imatinib treatment is probably directly due to the switch-off of Bcr–Abl action on the adhesion signaling pathways. We propose that this change is later overbalanced by apoptosis-related decrease in the cell adhesivity as the net decrease of ACF after 42 h Imatinib treatment was fully reversed using 10 μM Q-VD-OPh (Fig. 3B). While both the F-actin decomposition and the decrease in cellular adhesivity probably occur as integral parts of the apoptosis, the underlying mechanisms are not the same as they differ in their sensitivity to zVADfmk and Q-VD-OPh (Table I, Figs. 2 and 3). On the other hand, we observed a nice correlation as to the effects of Q-VD-OPh on the loss of JURL-MK1 cell adhesivity and on the decrease of the expression level of paxillin (cf. Figs. 3 and 7). This finding is consistent with the important role of the protein paxillin in the function of focal adhesion complexes and indicates that imatinib-induced decrease in paxillin level might be at least partly responsible for the loss of focal adhesion function. However, paxillin decrease is not due to caspase-3 activity (and probably not due to any other caspase) as 10 μM Q-VD-OPh is required to block this consequence of imatinib treatment while all the tested caspase

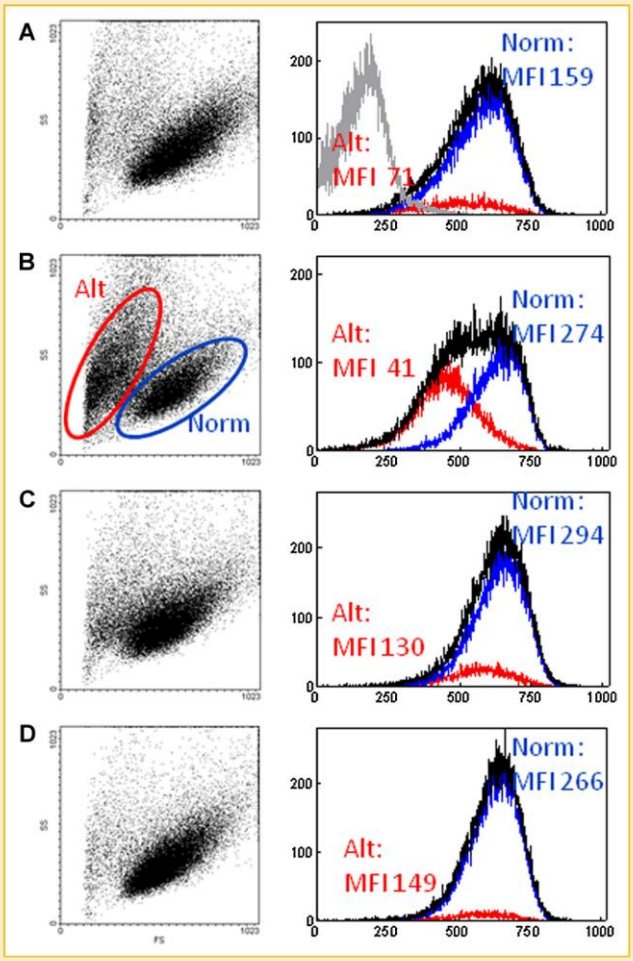

Fig. 8. Changes in surfacial integrin β1 expression due to imatinib mesylate treatment of JURL-MK1 cells. The cells were treated for 48 h with 1 μM imatinib alone or in combination with 2 μM Q-VD-OPh, labeled with PE-conjugated anti-β1 integrin and analyzed by means of flow cytometry. Left part: scattergrams (FSC—forward scatter, SSC—side scatter) with indicated gating regions for cells with normal (Norm) and altered (Alt) scattering properties. Right part: histograms of PE fluorescence intensity for all cells and for cells gated in regions Norm (blue) and Alt (red). MFI indicates the corresponding mean fluorescence intensity. A: untreated control (negative control without staining is shown on the left side of the histogram), B: imatinib mesylate, C: imatinib + 2 μM Q-VD-OPh, D: imatinib + 10 μM Q-VD-OPh. The negative control (i.e., no staining) is shown on the left side (gray line) of the upper histogram.

inhibitors at 0.5 μM concentration were able to prevent the caspase-3 activity.

We also found that imatinib mesylate treatment reduced the amount of integrin β1 on the surface of JURL-MK1 cells. The decrease was observed in cells with altered scattering properties (Fig. 8, lower FSC and slightly higher SSC indicate decreased cell size and increased granularity in the cell subpopulation denoted as Alt). As confirmed by Annexin staining, these morphological changes probably occur in relation with the apoptosis (Fig. 5S). As integrin β1 is the most important interaction partner for fibronectin, its lowered expression can contribute to the observed decrease in the cell adhesivity. However, the decrease in integrin β1 expression was largely prevented by 2 μM Q-VD-OPh (Fig. 8) whereas higher concentration of Q-VD-OPh (10 μM, Fig. 3) was required to restore the cell adhesivity. The partial loss of integrin β1 staining is thus not the major cause for the loss of the cell adhesivity and rather

represents a consequence of cell surface modification due to the apoptotic cell shrinking.

It was reported that the adhesion molecule CD44, a glycoprotein which is involved in the primary adhesion of lymphocytes to endothelial cells as well as in cell interaction with ECM, is required in homing of Bcr–Abl-expressing mouse leukemic stem cells [Krause *et al.*, 2006] and that an increase in CD44 expression was associated with acquired resistance to imatinib in K562 cell line [Grosso *et al.*, 2009]. We searched for potential changes in CD44 expression on JURL-MK1 cell surface upon imatinib treatment and confirmed that CD44 expression was reduced by imatinib independently of Q-VD-OPh addition (Fig. 6S, Supplementary Material). Thus, imatinib mesylate is likely to affect the primary adhesion of CML cells to the endothelial cells and the migration of hematopoietic stem cells to the bone marrow during the transplantation.

Imatinib was also reported to restore impared CD62L expression in CML cells [Fruehauf *et al.*, 2003] but we did not detect any change in very weak anti-selectin (both CD62L and CD62P) staining of JURL-MK1 cells upon imatinib treatment.

The proteomic analysis of imatinib effects revealed an increased phophorylation of cofilin at Ser3 (Fig. 5A). Cofilin is the pivotal mediator of actin dynamics, which promotes actin filament severing and depolymerization, facilitating the breakdown of existing filaments, and the enhancement of filament growth from newly created barbed ends [DesMarais et al., 2005; Burkhardt et al., 2008; Van Troys et al., 2008; van Rheenen et al., 2009]. It is involved in many processes, which include cytoskeletal rearrangements, such as mitosis, cytokinesis, cell migration, or cell adhesion and it was also reported to be required for cytochrome c release during mitochondrial apoptosis [Chua *et al.*, 2003; Zhu *et al.*, 2006]. Phosphorylation of cofilin at Ser3 is known to prevent its actin-depolymerization activity. For example, cofilin is present in its inactive/phosphorylated form in human peripheral blood T-lymphocytes and is activated upon their stimulation, which involves dynamic rearrangements of the actin cytoskeleton [Samstag and Nebl, 2005]. Cofilin is also activated during HIV infection of T-cells and helps the virus to overcome the static cortical actin restriction [Yoder *et al.*, 2008].

The increased phosphorylation of cofilin due to imatinib mesylate treatment of JURL-MK1 cells was indicated by the analysis of 2D protein maps (increased intensity of the spot No 20 in Fig. 4 which was identified as phosphorylated cofilin) and subsequently confirmed by means of Western blotting using phosphoSer3-specific antibody (Fig. 5A). An increase in phospho-cofilin staining intensity was detected also when the staining was performed on fixed and permeabilized whole cells and analyzed using a microscope (Fig. 6). The difference in the intensity of staining between control and treated cells was less marked in microscopic analysis (about twofold increase in phosphorylation) in comparison with Western blot analysis (about sevenfold increase), but this discrepancy can be due to lower accessibility of the epitope in the whole cell environment. Indeed, the microscopic analysis shows that phosphorylated cofilin is mainly located in cytoplasmic foci where it is likely to form complexes with other proteins such as 14–3–3s [Liang *et al.*, 2009]. Redistribution of cofilin into similar punctuated pattern has been previously observed by others, for example, after siRNA-mediated knock-down of cyclase-associated protein 1 (CAP1) that colocalizes with cofilin-1 to dynamic regions of the cortical actin cytoskeleton and promotes actin filament depolymerization [Bertling *et al.*, 2004]. Although the authors did not look at cofilin phosphorylation status, we presume that the translocated cofilin fraction may have been phosphorylated (inactivated) as CAP1 depletion led to similar cytoskeletal defects as cofilin knock-down.

The extensive F-actin decomposion occuring after JURL-MK1 cell treatment with imatinib mesylate could be due to an increased cofilin activity, which should be accompanied by a decrease in cofilin phosphorylation. The actual observation (a marked increase in cofilin phosphorylation) thus seems to be controversial. It is tempting to speculate, however, that some prominent F-actin structures have to be protected to assure the controlled cell disintegration into apoptotic bodies. Cofilin phosphorylation/inactivation in the vicinity of these structures could thus be an integral part of the programmed cell death. Indeed, the increase in cofilin phosphorylation at Ser3 occurring after imatinib treatment of JURL-MK1 cells can be at least partly suppressed by Q-VD-OPh (Fig. 5A). Our results are in line with those of Song et al. (2002) who reported that the expression of constitutively activated form of cofilin (unphosphorylatable at Ser3) suppressed both membrane blebbing and chromatin condensation in ROCK-expressing cells. On the other hand, cofilin dephosphorylation/activation was observed during H_2O_2-induced apoptosis of vascular smooth muscle cells [Lee *et al.*, 2006].

One of the major mechanisms of cofilin regulation involves the proteins ROCK, downstream effectors of RhoA GTPase (Fig. 3S). ROCK1 was reported to be constitutively activated through the cleavage of its autoinhibitory tail by caspase-3 [Coleman *et al.*, 2001] and is believed to play an essential role in morphological changes associated with the apoptosis [Coleman and Olson, 2002; Song *et al.*, 2002]. ROCK inhibition also impedes multiple myeloma cell homing to the bone marrow [Azab *et al.*, 2009]. We indeed observed ROCK1 cleavage (though not attributable to caspase-3 as any of caspase inhibitors used did not prevent the cleavage) during imatinib-induced apoptosis of JURL-MK1 cells (Fig. 7). We thus searched for possible effects of Y-27632, a specific inhibitor of ROCK1 and ROCK2. In control JURL-MK1 cells, Y-27632 (10 μM) decreased the level of cofilin phosphorylation (Fig. 5A, lane 3) and slighty reduced the intensity of F-actin staining with phalloidin (decrease in MFI was 10–15% after 24 h and the effect was not enhanced at higher Y-27632 concentration, data not shown). The inhibitor Y-27632 at this usually used concentration was thus probably efficient in ROCK inhibition, but despite this it did not significantly reduce imatinib-induced phosphorylation of cofilin (Fig. 5A, lane 6). ROCK is thus probably not the protein mediating cofilin phosphorylation during imatinib-induced apoptosis of JURL-MK1 cells. In line with this conclusion, we observed no increase in phosphorylation (i.e., no activation) of LIM kinase (Fig. 7), which is known to mediate the effect of ROCK on cofilin [Tomiyoshi et al., 2004; Scott and Olson, 2007]. Besides the pathway RhoA/ROCK/LIMK, multiple other mechanisms can contribute to the regulation of cofilin phosphorylation. These involve several p21-activated kinases (PAKs) [Coniglio *et al.*, 2008; Pandey *et al.*, 2009], integrin-linked kinase (ILK, [Kim *et al.*, 2008]), cofilin-specific

phosphatases [Huang et al., 2006; Eiseler et al., 2009; Kim et al., 2009], or actin-interactin protein 1 (Aip1), which works in cooperation with caspase-11 to promote cofilin-mediated actin depolymerization [Li *et al.*, 2007]. In our experimental system, the observed reduction in PAK1 level induced by imatinib mesylate (Fig. 7) could contribute to the increased cofilin phosphorylation as the activation of this kinase was reported to result in cofilin dephosphorylation [Coniglio *et al.*, 2008].

Spatially, the activity of cofilin is restricted by other actin-binding proteins, such as tropomyosins, which competes for accessibility of actin filament populations in different regions of the cell [DesMarais *et al.*, 2005; Fan *et al.*, 2008]. Tropomyosins are coiled-coil dimers that form continuous polymers along the major groove of most actin filaments. Different tropomyosin isoforms interact with different actin-binding proteins such as cofilin, Arp 2/3, or myosin and thereby confer different properties to the actin filaments [Gunning *et al.*, 2008; Kuhn and Bamburg, 2008]. Although the function of the individual tropomyosin isoforms is not well understood, the HMW isoforms of TPM1 are thought to increase the stability of actin stress fibers [Gunning *et al.*, 2008]. The reduced level of TPM1, which we found in imatinib-treated JURL-MK1 cells (Fig. 5C) thus could contribute to imatinib induced F-actin disassembly (Fig. 2).

ACKNOWLEDGMENTS

We wish to thank H. Pilcová, J. Sedlmaierová, and M. Voráčová for the expert technical assistance and O. Šebesta from the Faculty of Science of Charles University in Prague for taking the pictures from the fluorescence microscope. The authors apologize to all colleagues whose work could not be cited due to space limitation. This work was suppported by Ministry of Health of the Czech Republic NR 9243-3 and VZ 00023736 (to K.K., M.P., D.G., and Z.H.), Ministry of Education, Youth and Sports of the Czech Republic LC 07017 and AV0Z50200510 (to P.H. and K.P.).

REFERENCES

Azab AK, Azab F, Blotta S, Pitsillides CM, Thompson B, Runnels JM, Roccaro AM, Ngo HT, Melhem MR, Sacco A, Jia X, Anderson KC, Lin CP, Rollins BJ, Ghobrial IM. 2009. RhoA and Rac1 GTPases play major and differential roles in stromal cell-derived factor-1-induced cell adhesion and chemotaxis in multiple myeloma. Blood 114:619–629.

Barnes DJ, Schultheis B, Adedeji S, Melo JV. 2005. Dose-dependent effects of bcr-abl in cell line models of different stages of chronic myeloid leukemia. Oncogene 24:6432–6440.

Bazzoni G, Carlesso N, Griffin JD, Hemler ME. 1996. Bcr/Abl expression stimulates integrin function in hematopoietic cell lines. J Clin Invest 98:521–528.

Bertling E, Hotulainen P, Mattila PK, Matilainen T, Salminen M, Lappalainen P. 2004. Cyclase-associated protein 1 (CAP1) promotes cofilin-induced actin dynamics in mammalian nonmuscle cells. Mol Biol Cell 15:2324–2334.

Bhatia R, Verfaillie CM. 1998. Inhibition of BCR-ABL expression with antisense oligodeoxynucleotides restores beta1 integrin-mediated adhesion and proliferation inhibition in chronic myelogenous leukemia hematopoietic progenitors. Blood 91:3414–3422.

Burkhardt JK, Carrizosa E, Shaffer MH. 2008. The actin cytoskeleton in T cell activation. Annu Rev Immunol 26:233–259.

Cheng K, Kurzrock R, Qiu X, Estrov Z, Ku S, Dulski KM, Wang JY, Talpaz M. 2002. Reduced focal adhesion kinase and paxillin phosphorylation in BCR-ABL-transfected cells. Cancer 95:440–450.

Chua BT, Volbracht C, Tan KO, Li R, Yu VC, Li P. 2003. Mitochondrial translocation of cofilin is an early step in apoptosis induction. Nat Cell Biol 5:1083–1089.

Coleman ML, Olson MF. 2002. Rho GTPase signalling pathways in the morphological changes associated with apoptosis. Cell Death Differ 9:493–504.

Coleman ML, Sahai EA, Yeo M, Bosch M, Dewar A, Olson MF. 2001. Membrane blebbing during apoptosis results from caspase-mediated activation of ROCK I. Nat Cell Biol 3:339–345.

Coniglio SJ, Zavarella S, Symons MH. 2008. Pak1 and Pak2 mediate tumor cell invasion through distinct signaling mechanisms. Mol Cell Biol 28:4162–4172.

Dai Y, Rahmani M, Corey SJ, Dent P, Grant S. 2004. A Bcr/Abl-independent, lyn-dependent form of imatinib mesylate (STI-571) resistance is associated with altered expression of bcl-2. J Biol Chem 279:34227–34239.

DesMarais V, Ghosh M, Eddy R, Condeelis J. 2005. Cofilin takes the lead. J Cell Sci 118:19–26.

Eiseler T, Doppler H, Yan IK, Kitatani K, Mizuno K, Storz P. 2009. Protein kinase D1 regulates cofilin-mediated F-actin reorganization and cell motility through slingshot. Nat Cell Biol 11:545–556.

Fan X, Martin-Brown S, Florens L, Li R. 2008. Intrinsic capability of budding yeast cofilin to promote turnover of tropomyosin-bound actin filaments. PLoS One 3:e3641. DOI: 10.1371/journal.pone.0003641.

Fruehauf S, Topaly J, Schad M, Paschka P, Gschaidmeier H, Zeller WJ, Hochhaus A, Ho AD. 2003. Imatinib restores expression of CD62L in BCR-ABL-positive cells. J Leukoc Biol 73:600–603.

Gaston I, Stenberg PE, Bhat A, Druker BJ. 2000. Abl kinase but not PI3-kinase links to the cytoskeletal defects in bcr-abl transformed cells. Exp Hematol 28:351.

Goldman JM, Melo JV. 2003. Chronic myeloid leukemia—Advances in biology and new approaches to treatment. N Engl J Med 349:1451–1464.

Grosso S, Puissant A, Dufies M, Colosetti P, Jacquel A, Lebrigand K, Barbry P, Deckert M, Cassuto JP, Mari B, Auberger P. 2009. Gene expression profiling of imatinib and PD166326-resistant CML cell lines identifies fyn as a gene associated with resistance to BCR-ABL inhibitors. Mol Cancer Ther 8:1924–1933.

Gunning P, O'Neill G, Hardeman E. 2008. Tropomyosin-based regulation of the actin cytoskeleton in time and space. Physiol Rev 88:1–35.

Huang TY, DerMardirossian C, Bokoch GM. 2006. Cofilin phosphatases and regulation of actin dynamics. Curr Opin Cell Biol 18:26–31.

Kim YB, Choi S, Choi MC, Oh MA, Lee SA, Cho M, Mizuno K, Kim SH, Lee JW. 2008. Cell adhesion-dependent cofilin serine 3 phosphorylation by the integrin-linked kinase.c-src complex. J Biol Chem 283:10089–10096.

Kim JS, Huang TY, Bokoch GM. 2009. Reactive oxygen species regulate a slingshot-cofilin activation pathway. Mol Biol Cell 20:2650–2660.

Kramer A, Horner S, Willer A, Fruehauf S, Hochhaus A, Hallek M, Hehlmann R. 1999. Adhesion to fibronectin stimulates proliferation of wild-type and bcr/abl-transfected murine hematopoietic cells. Proc Natl Acad Sci USA 96:2087–2092.

Krause DS, Lazarides K, von Andrian UH, Van Etten RA. 2006. Requirement for CD44 in homing and engraftment of BCR-ABL-expressing leukemic stem cells. Nat Med 12:1175–1180.

Kuhn TB, Bamburg JR. 2008. Tropomyosin and ADF/cofilin as collaborators and competitors. Adv Exp Med Biol 644:232–249.

Kuželová K, Hrkal Z. 2008. Rho-signaling pathways in chronic myelogenous leukemia. Cardiovasc Hematol Disord Drug Targets 8:261–267.

Kuželová K, Grebeňová D, Marinov I, Hrkal Z. 2005. Fast apoptosis and erythroid differentiation induced by imatinib mesylate in JURL-MK1 cells. J Cell Biochem 95:268–280.

Kuželová K, Grebeňová D, Hrkal Z. 2007. Labeling of apoptotic JURL-MK1 cells by fluorescent caspase-3 inhibitor FAM-DEVD-fmk occurs mainly at site(s) different from caspase-3 active site. Cytometry A 71:605–611.

Kuželová K, Grebeňová D, Pluskalová M, Kavan D, Halada P, Hrkal Z. 2009. Isoform-specific cleavage of 14–3–3 proteins in apoptotic JURL-MK1 cells. J Cell Biochem 106:673–681.

Kuželová K, Pluskalová M, Brodská B, Otevřelová P, Elknerová K, Grebeňová D, Hrkal Z. 2010. Suberoylanilide hydroxamic acid (SAHA) at subtoxic concentrations increases the adhesivity of human leukemic cells to fibronectin. J Cell Biochem 109:184–195.

Larsen MR, Thingholm TE, Jensen ON, Roepstorff P, Jorgensen TJ. 2005. Highly selective enrichment of phosphorylated peptides from peptide mixtures using titanium dioxide microcolumns. Mol Cell Proteomics 4:873–886.

Lee CK, Park HJ, So HH, Kim HJ, Lee KS, Choi WS, Lee HM, Won KJ, Yoon TJ, Park TK, Kim B. 2006. Proteomic profiling and identification of cofilin responding to oxidative stress in vascular smooth muscle. Proteomics 6:6455–6475.

Li J, Brieher WM, Scimone ML, Kang SJ, Zhu H, Yin H, von Andrian UH, Mitchison T, Yuan J. 2007. Caspase-11 regulates cell migration by promoting Aip1-cofilin-mediated actin depolymerization. Nat Cell Biol 9:276–286.

Liang S, Yu Y, Yang P, Gu S, Xue Y, Chen X. 2009. Analysis of the protein complex associated with 14–3–3 epsilon by a deuterated-leucine labeling quantitative proteomics strategy. J Chromatogr B Analyt Technol Biomed Life Sci 877:627–634.

Pandey D, Goyal P, Dwivedi S, Siess W. 2009. Unraveling a novel Rac1-mediated signaling pathway that regulates cofilin dephosphorylation and secretion in thrombin-stimulated platelets. Blood 114:415–424.

Ramaraj P, Singh H, Niu N, Chu S, Holtz M, Yee JK, Bhatia R. 2004. Effect of mutational inactivation of tyrosine kinase activity on BCR/ABL-induced abnormalities in cell growth and adhesion in human hematopoietic progenitors. Cancer Res 64:5322–5331.

Salesse S, Verfaillie CM. 2002. Mechanisms underlying abnormal trafficking and expansion of malignant progenitors in CML: BCR/ABL-induced defects in integrin function in CML. Oncogene 21:8605–8611.

Salgia R, Li JL, Ewaniuk DS, Pear W, Pisick E, Burky SA, Ernst T, Sattler M, Chen LB, Griffin JD. 1997. BCR/ABL induces multiple abnormalities of cytoskeletal function. J Clin Invest 100:46–57.

Samstag Y, Nebl G. 2005. Ras initiates phosphatidyl-inositol-3-kinase (PI3K)/PKB mediated signalling pathways in untransformed human peripheral blood T lymphocytes. Adv Enzyme Regul 45:52–62.

Scott RW, Olson MF. 2007. LIM kinases: Function, regulation and association with human disease. J Mol Med 85:555–568.

Song Y, Hoang BQ, Chang DD. 2002. ROCK-II-induced membrane blebbing and chromatin condensation require actin cytoskeleton. Exp Cell Res 278:45–52.

Tomiyoshi G, Horita Y, Nishita M, Ohashi K, Mizuno K. 2004. Caspase-mediated cleavage and activation of LIM-kinase 1 and its role in apoptotic membrane blebbing. Genes Cells 9:591–600.

van Rheenen J, Condeelis J, Glogauer M. 2009. A common cofilin activity cycle in invasive tumor cells and inflammatory cells. J Cell Sci 122:305–311.

Van Troys M, Huyck L, Leyman S, Dhaese S, Vandekerkhove J, Ampe C. 2008. Ins and outs of ADF/cofilin activity and regulation. Eur J Cell Biol 87:649–667.

Vega FM, Ridley AJ. 2008. Rho GTPases in cancer cell biology. FEBS Lett 582:2093–2101.

Wertheim JA, Forsythe K, Druker BJ, Hammer D, Boettiger D, Pear WS. 2002. BCR-ABL-induced adhesion defects are tyrosine kinase-independent. Blood 99:4122–4130.

Wertheim JA, Perera SA, Hammer DA, Ren R, Boettiger D, Pear WS. 2003. Localization of BCR-ABL to F-actin regulates cell adhesion but does not attenuate CML development. Blood 102:2220–2228.

Yoder A, Yu D, Dong L, Iyer SR, Xu X, Kelly J, Liu J, Wang W, Vorster PJ, Agulto L, Stephany DA, Cooper JN, Marsh JW, Wu Y. 2008. HIV envelope-CXCR4 signaling activates cofilin to overcome cortical actin restriction in resting CD4 T cells. Cell 134:782–792.

Zandy NL, Playford M, Pendergast AM. 2007. Abl tyrosine kinases regulate cell-cell adhesion through rho GTPases. Proc Natl Acad Sci USA 104:17686–17691.

Zhao RC, Jiang Y, Verfaillie CM. 2001. A model of human p210(bcr/ABL)-mediated chronic myelogenous leukemia by transduction of primary normal human CD34(+) cells with a BCR/ABL-containing retroviral vector. Blood 97:2406–2412.

Zhu B, Fukada K, Zhu H, Kyprianou N. 2006. Prohibitin and cofilin are intracellular effectors of transforming growth factor beta signaling in human prostate cancer cells. Cancer Res 66:8640–8647.

4. Diskuze

4.1. Protein-proteinové interakce

Tato část disertační práce byla zaměřena na studium protein-proteinových interakcí za použití chemické síťovací reakce proteinů v komplexech s následnou MS identifikací kovalentních dimerů. Studovány byly systémy: (1) dimeru lidského regulačního proteinu 14-3-3ζ, (2) komplexu 14-3-3ζ a regulační domény tyrosinhydroxylasy, a (3) králičích membránových proteinů cytochromu P450 2B4 a cytochromu b_5. Metoda chemického síťování je schopna zachytit původně nekovalentní interakce v proteinových komplexech za dodržení fyziologických podmínek reakcí ve vodných roztocích pro potřeby následné identifikace konkrétních interagujících aminokyselin pomocí hmotnostní spektrometrie s vysokým rozlišením. Jedná se o alternativní metodu určování prostorové struktury proteinů k zavedeným metodám nukleární magnetické resonance a rentgenové krystalografie, které ale experimentálně nezaručují dodržení fyziologických podmínek.

Interakce v dimeru proteinu 14-3-3ζ

Regulační úloha proteinu 14-3-3ζ je úzce spojena s jeho samovolnou *in vivo* dimerizací. Dimerický stav proteinu 14-3-3ζ je založen na elektrostatických interakcích N-terminálních oblastí (5-21, 58-89) obou zúčastněných podjednotek a je porušen *in vivo* fosforylací serinového zbytku (Ser58) v této oblasti [Aitken 2002].

Naše experimenty byly prováděny **s lidským rekombinantním proteinem 14-3-3ζWT** a jeho mutantem s jednobodovou záměnou Ser58 za Asp58 (označeným 14-3-3ζS58D) jako monomerní formou. Záměna na pozici 58 napodobuje přítomnost fosfátové skupiny na Ser58, která slouží *in vivo* k rozpojení dimeru proteinu 14-3-3ζ [Powell 2003]. Postup izolace rekombinantních proteinů včetně primární struktury finálních preparátů shrnuje Obrázek 11A a C na str. 124 [Obšil 2001].

Nejprve byly provedeny síťovací reakce s proteinem 14-3-3ζ s neodštěpenou purifikační 6×His značkou na N-konci (označení NHis14-3-3ζWT a NHis14-3-3ζS58D, sekvence viz Obrázek 11C na str. 124). Reakce probíhaly v přítomnosti síťovacího činidla 1-ethyl-3-[3-dimethyl(aminopropyl)]karbodiimid hydrochloridu (EDC), které spojuje karboxylové a aminové skupiny postranních řetězců aminokyselin za vzniku nové amidové

vazby. Taková vazba vzniká mezi aminokyselinami přiblíženými v proteinových komplexech na vzdálenost elektrostatických interakcí. V případě přirozené formy proteinu NHis14-3-3ζWT byl produktem síťovací reakce s EDC podle očekávání kovalentní dimer dvou podjednotek 14-3-3ζ, který mohl být oddělen na SDS-PAGE (Obrázek 12A, dráha 3, strana 125). Nicméně kontrolní monomerní forma tohoto proteinu (NHis14-3-3ζS58D) reagovala za stejných podmínek síťovací reakce také za vzniku kovalentního dimeru (Obrázek 12A, dráha 4, str. 125). Protože však bylo v literatuře popsáno, že mutant proteinu 14-3-3 se záměnou Ser58 za Asp58 není schopen přirozeně vytvářet dimery [Powell 2003], může být důvodem vzniku dimerických produktů přítomná purifikační 6×His značka na jeho N-konci. Mezi dvěma molekulami NHis14-3-3ζS58D pravděpodobně dochází k nespecifickým interakcím způsobeným silným kladným nábojem na histidinové značce. Proto byla pro další síťovací experimenty purifikační značka odštěpena thrombinem.

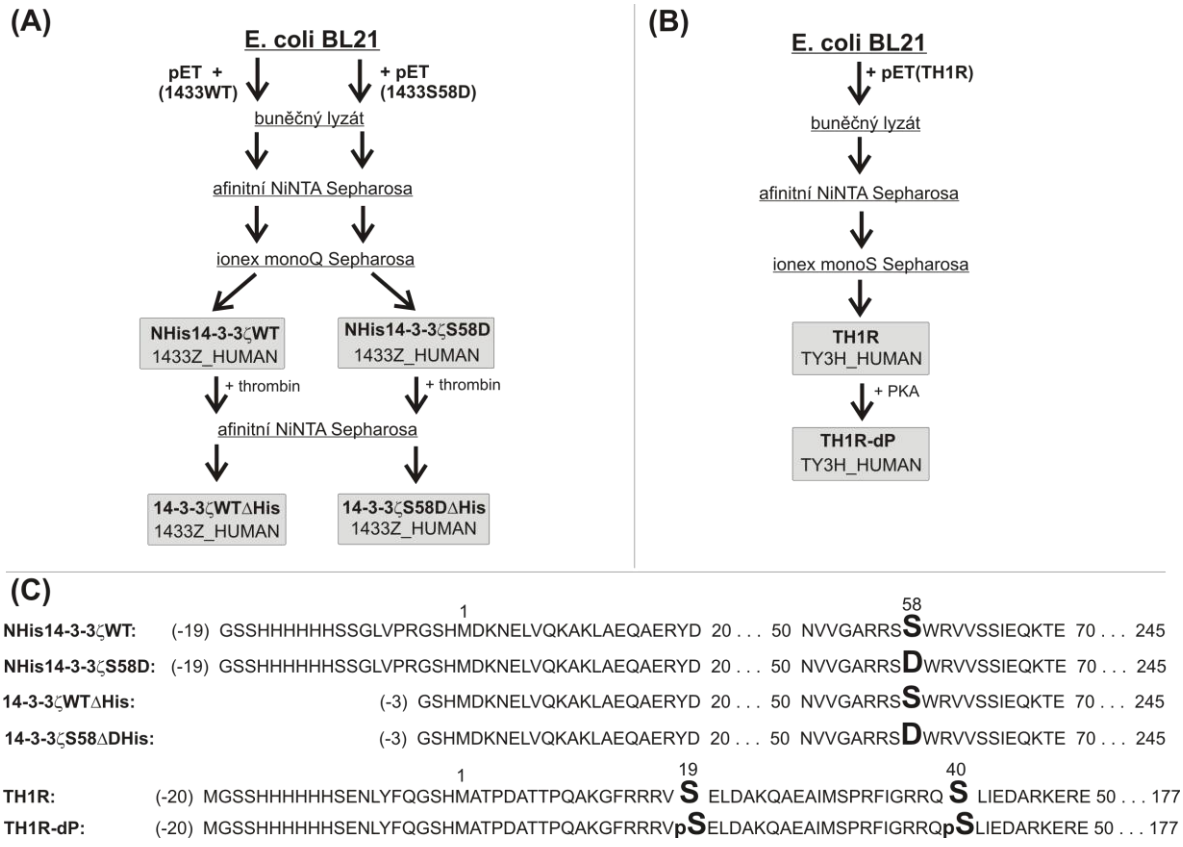

Obrázek 11. A. Schéma izolace rekombinantních proteinů 14-3-3ζWT a jednobodového mutantu 14-3-3ζS58D, B. Schéma izolace regulační domény tyrosinhydroxylasy (TH1R), C. Sekvence všech izolovaných proteinů. Čistota preparátů byla ověřena pomocí SDS-PAGE a PMF MALDI MS, označení proteinů 1433Z_HUMAN a TY3H_HUMAN bylo převzato ze Swiss-Prot databáze.

Nové síťovací reakce, které byly prováděny s oběma formami proteinu **14-3-3ζ bez histidinové purifikační značky** (14-3-3ζWTΔHis a 14-3-3ζS58DΔHis, schéma izolace a sekvence obou proteinů viz Obrázek 11A a C, str. 124) prokázaly vznik dimerických produktů především u přirozené formy 14-3-3ζWTΔHis a pouze minoritně u monomerního mutantu 14-3- 3ζS58DΔHis (Obrázek 12B, dráha 3 a 4). Podle nezostřené zóny dimeru mutantu po rozdělení na SDS-PAGE (dráha 4) lze soudit, že se jedná o nespecifickou interakci podjednotek v koncentrovaném roztoku proteinů (2 μM). Nicméně, obě tyto formy proteinu 14-3-3ζ obsahují na N-konci stále ještě tři aminokyseliny navíc v důsledku specifického štěpení původní sekvence thrombinem. Tato arteficielní sekvence (Gly(-3), Ser(-2), His(-1)) tvoří pouhé 1 % sekvence 14-3-3ζ na rozdíl od původní purifikační značky, která se svými 19 aminokyselinami tvoří 7 % sekvence 14-3-3ζ a podle výsledků předchozích síťovacích reakcí svým výrazným kladným nábojem ovlivňuje interakce na rozhraní dimeru. Zanedbatelný vliv tří dodatečných zbytků na N-konci 14-3-3ζ podporují data z literatury, kdy Aitken a spol. popsali, že threoninový zbytek na N-konci před prvním methioninem isoformy 14-3-3β nijak negativně neovlivňuje schopnost této isoformy dimerizovat [Aitken 2002].

Schopnost dimerizovat u obou forem proteinu 14-3-3ζΔHis po odštěpení histidinové purifikační značky byla **studována také pomocí H/D výměny** (schéma viz

Obrázek 13, str. 126) [Weiss 2007]. Porovnáním chování přirozeného 14-3-3ζWTΔHis a mutovaného 14-3-3ζS58DΔHis v prostředí deuterovaného pufru bylo zjištěno, že mutace na pozici Ser58 výrazně zvyšuje stupeň deuterace N-terminální oblasti Gly(-3) – Leu90. Stupeň deuterace ostatních částí byl u obou proteinů srovnatelný. Jsou-li některé oblasti proteinu těsně sbalené, nebo pokud se účastní vzájemných interakcí, nebudou vystaveny působení D_2O z roztoku a stupeň deuterace bude nízký. Vysoký stupeň

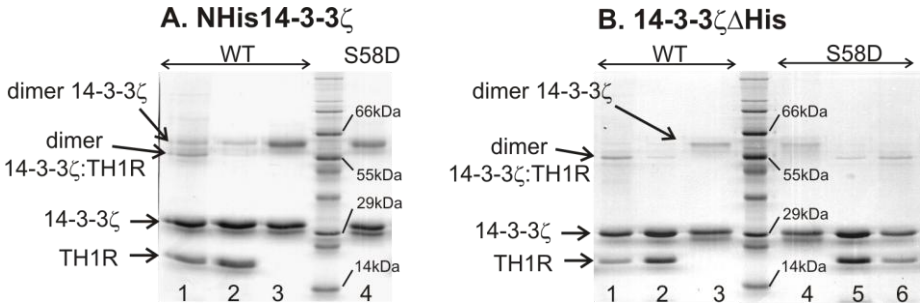

Obrázek 12. SDS-PAGE produktů síťovací reakce TH1R a 14-3-3ζ s EDC (10 μg/mL) A. NHis14-3-3ζ, B. 14-3-3ζΔHis. Dráha 1: dPTH1R a 14-3-3ζWT dráha 2: TH1R a 14-3-3ζWT, dráha 3: 14-3-3ζWT, dráha 4: 14-3-3ζS58D, dráha 5: TH1R a 14-3-3ζS58D, dráha 6: dPTH1R a 14-3-3ζS58D.

deuterace N-terminální oblasti u 14-3-3ζS58DΔHis naopak znamená její vyšší přístupnost deuterovanému pufru, protože se **neúčastní interakcí na rozhraní dimeru**, které by ji před působením H/D výměny chránily jako v případě 14-3-3ζWTΔHis. **Experimenty H/D výměny** tedy spolehlivě **prokázaly monomerní stav proteinu 14-3-3ζS58DΔHis v roztoku.**

Pomocí techniky síťovacích reakcí s následnou identifikací kovalentních dimerů pomocí LC-FT-ICR MS jsme v souladu s literaturou popsali **interakce dvou predikovaných oblastí na rozhraní dimeru 14-3-3ζWTΔHis** mezi helixem A jedné podjednotky a helixy C a D druhé podjednotky [Aitken 2002]. Konkrétní aminokyseliny účastnící se interakce byly určeny na základě LC-MALDI MS/MS experimentů s manuálním vyhodnocením fragmentačních spekter (viz Obrázek 3 v publikaci č. 6, str. 48).

Zajímavé je, že se nám podařilo kovalentně **zachytit interakci aminoskupiny N-koncového Gly(-3)** první podjednotky s místem predikovaným pro vazbu strukturovaného A-helixu (Asn4-Glu14) na druhé podjednotce. Taková interakce dosud nebyla popsána především proto, že v žádném publikovaném krystalografickém modelu nebyla z důvodu vysoké flexibility popsána struktura těchto několika N-koncových aminokyselin. Literatura uvádí interakce A-helixu [Aitken 2002; Yang 2006], nikoliv samotného N-konce proteinu. Bylo také publikováno, že většina nativních isoforem proteinu 14-3-3 má *in vivo* N-koncovou skupinu modifikovanou acetylací, která pravděpodobně slouží k ochraně proteinu před působením proteolytických enzymů a může být jedním z regulačních

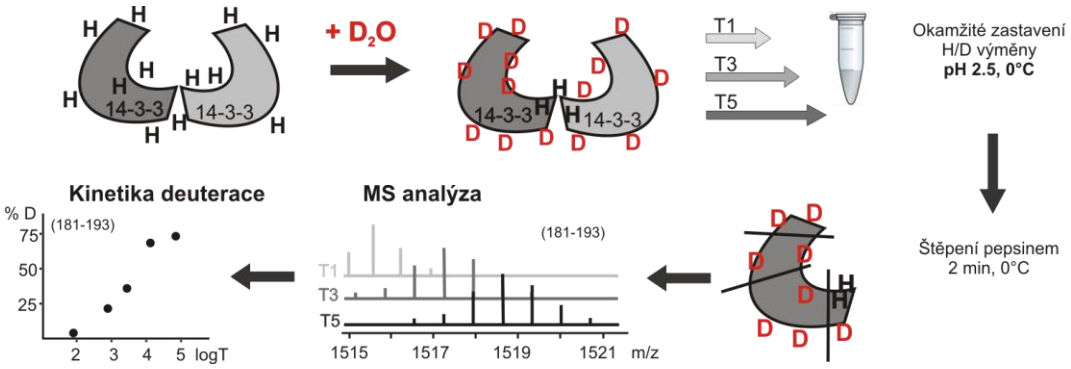

Obrázek 13. Schéma experimentu H/D výměny s MS analýzou na dimeru proteinu 14-3-3. Po expozici proteinů deuterovanému pufru jsou v různých časových intervalech odebírány alikvoty vzorku, u kterých je nejprve zastavena H/D výměna snížením pH a teploty, poté jsou proteolyticky naštěpeny a peptidové směsi z různých časů jsou následně analyzovány pomocí hmotnostní spektrometrie. Vynesením stupně deuterace každého peptidu v závislosti na délce expozice deuterovanému pufru jsou získány informace o kinetice sbalování celého proteinu nebo proteinového komplexu.

mechanismů funkce 14-3-3 v buňce [Fuller 2006]. V našem případě, kdy jsme pracovali s rekombinantním proteinem s odštěpenými 16 aminokyselinami z původních 19 tvořících purifikační 6×His značku, nebyla N-koncová skupina bráněna žádnou modifikací, jak bylo dokázáno MS experimenty. Chemická síťovací reakce prokázala její vysokou reaktivitu v dimeru 14-3-3ζWTΔHis a výsledky MS analýzy naznačily možnou orientaci koncových N-terminálních aminokyselin a poprvé popsaly existenci tří dalších iontových interakcí v dimeru 14-3-3ζ (Lys9-Glu81, Gly(-3)-Glu70, Gly(-3)-Glu81).

Interakce mezi proteinem 14-3-3ζ a regulační doménou tyrosinhydroxylasy

Negativní vliv purifikační 6×His značky u rekombinantních proteinů NHis14-3-3ζWT a NHis14-3-3ζS58D jsme pozorovali také u experimentů se substrátem 14-3-3ζ, s proteinem tyrosinhydroxylasou [Ichimura, 1988], resp. její N-terminální regulační doménou (aminokyseliny 1-157 ze sekvence lidské tyrosinhydroxylasy). Na této regulační doméně (TH1R) byla popsána čtyři fosforylační místa (na pozicích 8, 19, 31 a 40) pro různé kinasy. **Stupeň fosforylace TH1R ovlivňuje aktivitu celé tyrosinhydroxylasy, a také její vazbu na proteiny 14-3-3** [Dunkley 2004].

Také TH1R byla získána jako rekombinantní protein a postup její izolace, včetně přípravy dvakrát fosforylovaného proteinu dPTH1R (pSer19, pSer40) shrnuje Obrázek 11B na str. 124 [Obšilová 2008]. Síťovací experimenty s EDC mezi NHis14-3-3ζWT a oběma formami TH1R potvrdily v souladu s literaturou [Kleppe 2001] vyšší vazbu dvojitě fosforylované formy dPTH1R na NHis14-3-3ζWT vznikajícími kovalentními dimery NHis14-3-3ζWT:dPTH1R v oblasti 55 kDa (Obrázek 12A, dráha 1, str. 125). Z výsledků elektroforézy je dále patrné, že kromě těchto dimerických produktů vznikají síťovací reakcí s dPTH1R také homodimery NHis14-3-3ζWT (oblast okolo 60 kDa), popsané již dříve jako důsledek nespecifických interakcí N-terminální histidinové značky. Nové experimenty s proteiny bez histidinové značky znovu potvrdily vyšší afinitu dvakrát fosforylované formy dPTH1R ke 14-3-3ζWTΔHis (Obrázek 12B, dráha 1, str. 125).

Výsledky následné **LC-FT-ICR MS analýzy zesíťovaných peptidů heterodimeru 14-3-3ζWTΔHis:dPTH1R** zachycují vazbu dPTH1R do vazebného místa proteinu 14-3-3ζWT v oblasti okolo Lys49 prostřednictvím obou fosforylovaných serinů (Tabulka 4, str. 128). Získaná data neprokázala preferenční vazbu žádného z těchto serinů

a naznačují tak, že pravděpodobně **existují dvě různé orientace, jakými se dPTH1R váže do vazebného místa proteinu 14-3-3ζWT**. Získané výsledky z MS analýzy dále naznačují účast N-terminální a C-terminální domény 14-3-3ζWT na koordinaci dPTH1R.

Kontrolní síťovací reakce mezi monomerním 14-3-3ζS58DΔHis a dPTH1R vedla také ke vzniku kovalentního dimeru 14-3-3ζS58DΔHis:dPTH1R (Obrázek 12B, dráha 6, str. 125). Mutace na pozici 58 tedy nemá vliv na vazbu dvakrát fosforylované dPTH1R na 14-3-3ζS58D. Můžeme tak potvrdit již popsanou skutečnost, že monomerní formy proteinu 14-3-3 jsou schopné vázat některé substráty nezávisle na dimerickém stavu [Woodcock 2003] a to i přesto, že dimerický stav 14-3-3 proteinů jednoznačně převládá *in vivo*. LC-FT-ICR MS analýza dimeru 14-3-3ζS58DΔHis:dPTH1R potvrdila interakce stejných oblastí jako v případě dimeru 14-3-3ζWTΔHis:dPTH1R.

Získané výsledky síťovací reakce s EDC s následnou LC-FT-ICR MS analýzou tedy zachycují vazbu fosforylované regulační domény tyrosinhydroxylasy dPTH1R do vazebného místa 14-3-3ζ a naznačují důležitou úlohu N-koncové i C-koncové oblasti 14-3-3ζ při její správné koordinaci. Ze získaných výsledků nelze usuzovat na preferenci vazby jedné nebo druhé fosforylované skupiny (pSer19 nebo pSer40) dPTH1R v aktivním centru 14-3-3ζ. I přesto tyto výsledky napovídají o terciární struktuře regulační domény tyrosinhydroxylasy, která jako jediná část celé molekuly není zachycena v publikovaném krystalografickém modelu tyrosinhydroxylasy [Goodwill 1998].

Tabulka 4. LC-FT-ICR MS kovalentního heterodimeru14-3-3ζWTΔHis:dPTH1R po reakci s EDC.

Získaná hodnota $[MH]^+$	Chyba (ppm)	Peptid 14-3-3ζWTΔHis	Peptid dPTH1R
2778.3560	0.1	(12-18) LA**E**QA**E**R	(17-33) RVpSELDA**K**QAEAIMSPR
2482.3142	0.6	(42-56) NLLSVAY**K**NVVGARR	(17-24) RVpS**E**L**D**AK
2652.3948	0.5	(42-56) NLLSVAY**K**NVVGARR	(39-46) QpSLI**ED**AR
2822.2302	0.3	(222-245) DNLTLWTSDTQGDEAEEAGEGGEN	(47-49) **K**ER
2389.1853	0.0	(121-127) M**K**DGYYR	(25-37) QA**E**AIMSPRFIGR
3052.5447	0.8	(104-122) FLIPNASQAES**K**VFYL**K**M_{ox}K	(18-24) VpS**E**L**D**AK

Legenda: pS – fosforylovaný serin, M_{ox} – oxidovaný methionin.

Interakce v komplexu membránových proteinů - cytochromu P450 2B4 a cytochromu b_5

Druhým modelem, u kterého jsme použili techniku chemického zesítění s následnou MS identifikací kovalentních dimerů pro studium protein-proteinových interakcí, byl systém dvou **membránových proteinů - cytochromu P450 2B4 (CYP2B4) a cytochromu b_5**. Oba proteiny jsou složkami systému oxygenas se smíšenou funkcí (MFO), který se podílí na metabolismu endogenních látek a xenobiotik. Cytochrom b_5 může zprostředkovat přenos elektronu na CYP2B4 a jeho přítomnost může v závislosti na několika různých faktorech aktivovat ale i inhibovat katalytické působení CYP2B4 [Zhang 2005].

Oba enzymy jsou membránové proteiny a jejich izolace vyžaduje použití speciálních a šetrných přístupů pro získání funkčního enzymu včetně jeho membránové kotvy. V této práci byl izolován cytochrom P450 2B4, cytochrom b_5 a NADPH:cytochrom P450 reduktasa (CPR; jako nezbytná složka MFO systému pro plánované metabolické studie) z jaterního homogenátu králíka domácího po předchozí indukci isoformy CYP2B4 podáním fenobarbitalu [Šulc 2004]. Postup izolace kombinující kroky diferenční centrifugace, solubilizace membránových proteinů za použití ionogeních a neionogeních detergentů, ionexové, afinitní a adsorpční chromatografie shrnuje Obrázek 14 na str. 130 [Šulc 2010].

Přítomnost membránové kotvy u studovaných proteinů CYP2B4 a cytochromu b_5 je velmi důležitá pro studium jejich interakcí v rekonstituovaném systému v lipidových micelách tvořených 1,2-dilauroylfosfatidylcholinem (DLPC), kde zaručuje správnou orientaci proteinů v membráně i vůči sobě navzájem. Dosud publikované výsledky byly získány pro rekombinantní proteiny zkrácené o N-terminální membránovou část molekuly [Im 2011], popř. jako jejich jednobodové mutanty [Bridges 1998], a krystalografické ani *in silico* modely tak nezohledňují důležitou funkci membránové části při koordinaci molekuly. V našem případě ale pracujeme s nativními nezkrácenými proteiny získanými ze zvířecího modelu a síťovací reakce zachycující protein-proteinové interakce probíhaly v podmínkách, které zachovávají nativní strukturu proteinů (v přítomnosti membrány DLPC a ve vodných roztocích).

Pro síťovací reakce s činidlem EDC bylo nutné nejprve **odstranit z finálních proteinů detergenty**, které byly během izolace používány ke stabilizaci membránových proteinů v roztoku, pomocí adsorbce detergentů na silikagel při nízké teplotě a

podmínkách minimalizujících adsorpci proteinů na silikagel [Anzenbacher 1984]. Většina dříve publikovaných prací **předpokládá, že interakce mezi CYP2B4 a cytochromem b_5 je řízena iontovými interakcemi** mezi bazickými aminokyselinami na proximální straně CYP2B4 a komplementární kyselou oblastí na molekule cytochromu b_5 [Bridges 1998]. Pro potvrzení tohoto tvrzení byl zkoumán vliv zvyšující se iontové síly (50 – 500 mM NaCl) na interakci těchto dvou proteinů. Nicméně, ani metabolické studie v rekonstituovaném systému s CPR, ani síťovací reakce s EDC neprokázaly vliv zvyšující se iontové síly na kvalitu a kvantitu vznikajícího dimerického produktu mezi CYP2B4 a cytochromem b_5, který byl na SDS-PAGE stále dobře patrný. Tyto výsledky ukazují, že **kromě iontových interakcí je vazba mezi oběma proteiny řízena také interakcemi hydrofóbními**, které nejsou ovlivňovány přítomností vysoké koncentrace NaCl. Tyto výsledky doplňují již dříve získaná pozorování [Schenkman 2003].

LC-FT-ICR MS analýza kovalentního dimeru CYP2B4:cytochrom b_5 po síťovací reakci s EDC ve čtyřicetinásobném nadbytku odhalila **namísto předpokládaných**

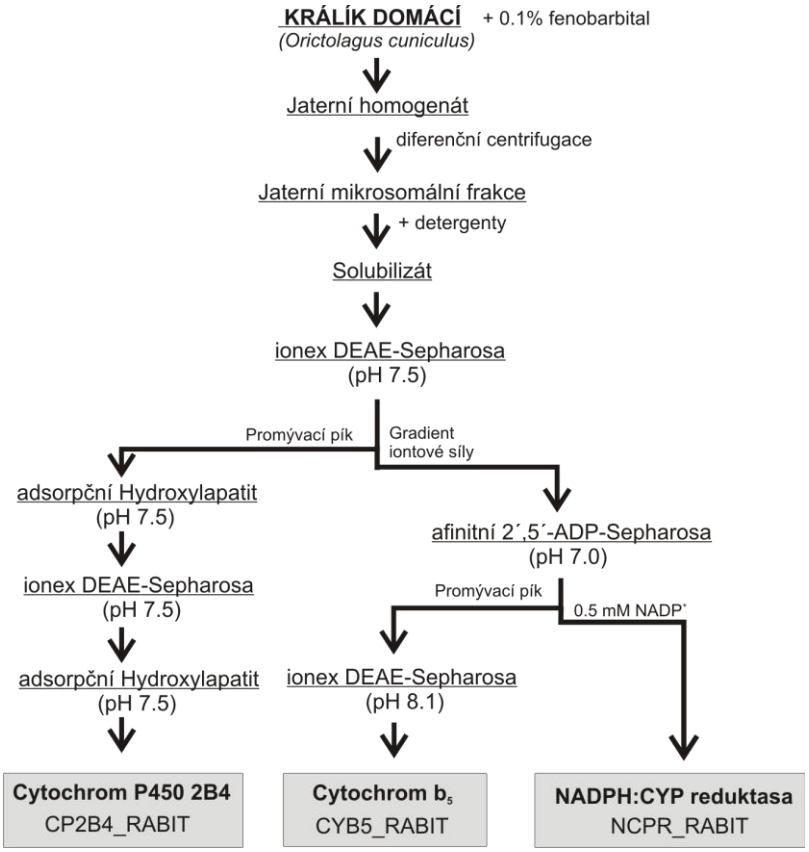

Obrázek 14. Schéma izolace membránových proteinů cytochromu P450 2B4, NADPH:cytochrom P450 reduktasy a cytochromu b_5. Čistota proteinů byla ověřena pomocí SDS-PAGE a PMF MALDI MS, označení proteinů bylo převzato ze Swiss-Prot databáze.

interakcí bazických aminokyselin na proximální straně CYP2B4 interakce hned tří kyselých aminokyselin – Asp134, Glu424 a Glu439, a pouze jediného Lys139. Z toho vyplývá, že na povrchu molekuly cytochromu b_5 jsou kromě popsaných záporně nabitých kyselin i bazické aminokyseliny účastnící se interakce s CYP2B4. Zajímavá je také skutečnost, že aminokyseliny Glu424 a Glu439 na povrchu CYP2B4 zachycené v interakci s cytochromem b_5 se nacházejí ve vzdálené oblasti proximální strany CYP2B4, u které byla předpokládaná interakce výhradně s NADPH:cytochrom P450 reduktasou [Bridges 1998]. Nicméně, naše data jsou v souladu s obdobnými výsledky síťovacích reakcí s EDC na komplexu cytochromu P450 2E1 a cytochromu b_5 [Gao 2006], ve kterých byly identifikovány Lys428 a Lys434 z této vzdálené oblasti proximální strany cytochromu P450 2E1 v interakci s cytochromem b_5. Naše data upřesňují vazbu cytochromu b_5 na CYP2B4 a **rozšiřují vazebné místo na CYP2B4 pro cytochrom b_5 o oblast v okolí sekvence Leu396-Trp452**. Současně prokazují, že **interakce s cytochromem b_5 se účastní také kyselé aminokyseliny CYP2B4**, na rozdíl od všeobecně přijímaného názoru o kladné proximální straně CYP2B4 účastnící se vazby s negativně nabitou oblastí cytochromu b_5.

Na základě získaných dat **byl vytvořen *in silico* model interakcí v komplexu cytochromu CYP2B4 a cytochromu b_5**. Tento model naznačil, jakým způsobem může cytochrom b_5 tak výrazně ovlivňovat katalytické působení CYP2B4. Při zadání parametrů získaných z výsledků síťovacích reakcí na rozhraní interakcí obou molekul, byly nalezeny dvě orientace cytochromu b_5 k molekule CYP2B4: (1) orientace propionátu hemu cytochromu b_5 k proximální straně CYP2B4, a (2) hem cytochromu b_5 odvrácený směrem od CYP2B4. V první popsané orientaci se cytochrom b_5 může účastnit přenosu elektronu, jak potvrzuje objevená interakce **Arg133 z molekuly CYP2B4 s propionátem hemu cytochromu b_5**. Již v dřívější práci [Šulc 2008] byla diskutována interakce této aminokyseliny, která v přítomnosti substrátu/inhibitoru navázaného na CYP2B4 opouští původní pozici při koordinaci hemu CYP2B4 a obrací se na povrch molekuly, kde může interagovat právě s cytochromem b_5. Navíc, pozice této aminokyseliny je velmi konzervovaná, jak bylo zjištěno porovnáním sekvencí čtyř lidských isoforem CYP. Proto předkládáme k dalším diskuzím názor, že právě Arg133 může hrát velmi důležitou úlohu při modulaci aktivity cytochromu P450 působením cytochromu b_5 při přenosu elektronu na cytochromy P450. Druhá popsaná orientace (s hemem cytochromu b_5 odvráceným od CYP2B4) se pravděpodobně neúčastní přenosu druhého elektronu v katalytickém cyklu

CYP2B4. Může ovšem hrát významnou roli v modulaci strukturních změn jak samotné molekuly CYP2B4, tak v uspořádání multimerního komplexu MFO systému. Tuto domněnku potvrzuje i existence trimeru o molekulové hmotnosti 100 kDa (ve složení CYP2B4:cytochrom b_5 v poměru 2:1) na SDS-PAGE po síťovací reakci mezi cytochromem b_5 a CYP2B4 s EDC.

4.2. Charakterizace a identifikace fungálních proteinů a peptidů

Tato část práce byla zaměřena na použití hmotnostní spektrometrie pro mapování proteinových profilů houbových spór. Předmětem studia byly houby rodů *Aspergillus* a *Pseudallescheria*, které patří mezi vřeckovýtrusné houby a byly popsané jako jedny z nejčastějších původců závažných invazivních mykóz se špatnou prognózou např. u imunikopromitovaných pacientů [Lin 2001]. Naší snahou bylo nalézt unikátní diagnostický znak, který by mohl sloužit pro včasnou detekci aspergilóz a scedosporióz. Pro *P. boydii* byl takový metabolit nalezen a charakterizován pomocí hmotnostní spektrometrie a NMR.

Proteinové profily zástupců rodu Aspergillus

Pomocí MALDI-TOF profilování a 1D elektroforézy byly **sestaveny proteinové profily houbových spór 24 kmenů rodu *Aspergillus*** obsahující také klinické izoláty [publikace č. 1]. MALDI-TOF hmotnostně-spektrometrický přístup umožňuje mapování proteinových profilů houbových spór do 20 kDa a elektroforetický přístup zachycuje také proteiny větší než 20 kDa. Obě metody poskytují komplementární informace o stavu proteomu na povrchu spór a mohou přispět k nalezení unikátních znaků pro potřeby včasné detekce aspergilóz. Nicméně, mezi použitými metodikami existují rozdíly v citlivosti a časové náročnosti. Zatímco MALDI MS pracuje s minimálním množstvím 0.3 μg spór (10000 spór) na jednu analýzu, netrvá déle než několik minut a výsledkem je jedinečný profil proteinových signálů, 1D elektroforéza potřebuje více než 1600-krát větší množství materiálu (0.5 mg) a analýza včetně vizualizace elektroforegramu trvá více než 6 hodin. Navíc, výsledné elektroforegramy nebyly schopné vzájemně signifikantně rozlišovat jednotlivé kmeny rodu *Aspergillus* podle rozdílných proteinových profilů.

Po 1D-SDS-PAGE separaci byla dále provedena identifikace proteinů z oblasti 5–25 kDa. Po proteolytickém štěpení trypsinem a extrakci peptidů z gelu byly v klinickém izolátu pomocí LC-MS/MS experimentu nalezeny proteiny, které mohou souviset s virulencí studovaného kmene (hydrofobin, hemolysin, superoxiddismutasa). Přístupem založeným na MALDI-TOF proteinových profilech, kdy byly spóry přímo na terčíku smíchány s MALDI matricí, byly také nalezeny prokazatelné souvislosti mezi proteinovými profily a virulencí druhů, produkcí aflatoxinů či fylogenetickým zařazením jednotlivých kmenů. Použití MALDI MS profilování intaktních spór nebo jejich

proteinových oplachů tak přináší nové možnosti, jak rychle a specificky rozpoznat původce závažných mykóz na základě kombinace několika unikátních proteinových signálů, čehož by mohlo být využito ke zlepšení diagnostiky těchto fungálních onemocnění.

Pseudacykliny jako potenciální „markery“ onemocnění způsobených druhem Pseudallescheria boydii

Další projekt zaměřený na studium fungálních diagnostických znaků pro včasnou detekci invazivních mykóz se zabýval kompletní strukturní charakterizací nalezeného sekundárního metabolitu přítomného v myceliu a na spórách druhu *Pseudallescheria boydii* [publikace č. 2]. U dvou klinických izolátů (lidského a zvířecího původu) byl pomocí ESI-MS identifikován a na základě MS/MS fragmentací a 2D NMR experimentů (Ing. M. Kuzma, PhD., MBÚ AV ČR v.v.i.) charakterizován neribosomální peptid cyklické struktury. Tento **pseudacyklin A** je tvořený cyklickým hexapeptidem ve složení L-Orn, D-Phe, L-Pro, L-Ile, L-Ile, L-Ile (N-acetyl). Úspěšná charakterizace (určení sekvence peptidu, cyklická struktura) byla možná na základě MS/MS fragmentačních spekter měřených na iontové pasti a na FT-ICR hmotnostním spektrometru s vysokým rozlišením. GC-MS experiment napomohl určit D/L formu přítomných aminokyselin.

Kromě majoritního pseudacyklinu A byly pomocí ESI-FT-ICR identifikovány další pseudacykliny (B-E) lišící se od struktury pseudacyklinu A pouze modifikacemi na postranních řetězcích. Díky své unikátnosti a výskytu jak v myceliu tak na spórách by mohly být pseudacykliny **vhodnými diagnostickými znaky pro včasnou detekci mykóz způsobených rody *Pseudallescheria* nebo *Scedosporium*** (anamorf *Pseudallescheria*), které, ač mají podobné symptomy jako aspergilózy, jsou na léčbu Amfotericinem B rezistentní. V současné době se pracuje **na přípravě protilátek proti nalezenému pseudacyklinu A a možnosti zařazení této identifikace do běžných diagnostických ELISA testů**.

4.3. Ostatní proteomické a lipidomické projekty a klinické aplikace

V rámci postgraduálního studia v Laboratoři charakterizace molekulární struktury na MBÚ AV ČR v.v.i. jsem se zapojila také do dalších výzkumných projektů využívajících k identifikaci a charakterizaci biomolekul hmotnostní spektrometrii. Seznámila jsem se tak s dalšími experimentálními přístupy MS i způsoby vyhodnocení MS dat v závislosti na studovaném systému (lidské leukemické buňky, alergeny pšenice s částečně neznámým genomem).

Oxidace během NALDI-TOF MS jako nástroj pro určování polohy dvojných vazeb

Představená metoda přináší zásadní změnu v MS přístupu k **identifikaci polohy dvojné vazby v molekule peptidů nebo lipidů** [publikace č. 3]. MS identifikace byla dodnes možná až po úpravě vzorku derivatizací nebo po provedení MS^3 experimentu[1], který ale umožňují pouze analyzátory typu iontové pasti. Naše řešení přináší možnost elegantního a rychlého určení polohy dvojné vazby na základě výskytu charakteristických *m/z* signálů produktů oxidace dvojné vazby v hmotnostním spektru měřeném na **NALDI terčíku** (komerčně dostupné, Bruker Daltonics) na běžném TOF analyzátoru. Oxidace a následná disociace alifatického řetězce v poloze dvojné vazby je katalyzována výhradně samotným nanopovrchem NALDI terče, (u MALDI experimentů nebyla pozorována) a není způsobena fragmentací vzorku v hmotnostním analyzátoru.

Na příkladu peptidu cyklosporinu A a několika lipidů s nenasycenými mastnými kyselinami jsme prokázali, že k fragmentaci dochází v relativně krátké době a první fragmenty se ve spektru objevují již po 20 minutách po nanesení vzorku na NALDI terčík, v závislosti na analyzovaném vzorku. Úplná fragmentace pak byla pozorována po 24 hodinách. Pozorované fragmenty odpovídají charakteristickým rozštěpením řetězců v místech dvojných vazeb společně s oxidací těchto míst. Na základě alespoň minimální znalosti povahy analyzované látky (peptid, lipid) je možné odvodit, jaké struktuře odpovídá pozorovaná ztráta a v jakém místě byla původní dvojná vazba.

---

[1] Experiment umožňuje postupné fragmentace vybrané molekuly, příp. jejích fragmentů a poskytuje detailní informace o její struktuře. Rozšířenější způsob fragmentace pomocí tandemové hmotnostní spektrometrie (MS/MS nebo MS^2) je schopen prokázat přítomnost dvojné vazby v molekule, ne však přesně určit její polohu.

NALDI-TOF MS představuje rychlý a jednoduchý nástroj pro určování polohy dvojné vazby v molekulách peptidů nebo lipidů. Objasnění mechanismu samovolné oxidace a fragmentace na NALDI povrchu může vysvětlit komplikace, které vznikají při analýze směsí neznámých látek.

Identifikace alergenů v proteomu pšenice

V tomto klinicko-proteomickém projektu (ve spolupráci s RNDr. P. Šotkovským, PhD., MBÚ AV ČR v.v.i.) byla hmotnostní spektrometrie použita jako důležitý nástroj pro **identifikaci nových pšeničných alergenů** [publikace č. 4]. Alergie na pšeničnou mouku postihuje více než 6 % dětské a až 3 % dospělé populace. Současné diagnostické metody jsou bohužel málo specifické a nedostatečně citlivé (symptomy se mohou u pacientů lišit a mohou být ovlivněny dalšími typy alergií). V této práci je publikován postup izolace dostatečného množství nativních pšeničných proteinů pro další testování a charakterizaci, který by mohl urychlit vývoj nových diagnostických postupů.

Z celého proteomu pšenice rozděleného postupně ultrafiltrací, IEF, RP-HPLC a SDS-PAGE bylo na základě pozitivních Western blot reakcí se séry pacientů trpících alergií na pšeničnou mouku vybráno a pomocí MS identifikováno 27 proteinů, z nichž **sedm bylo určeno jako zcela nové alergeny**. MS identifikace byla založena na peptidovém mapování (tryptické štěpení, modifikace cysteinů, popř. odsolení vzorků) technikou MALDI-TOF a prohledávání proti SwissProt nebo TrEMBL databázi rostlinných proteinů pomocí programu Mascot. Jednoznačně byly identifikovány proteiny, u kterých MOWSE skóre[2] překročilo hodnotu 57 (Swiss-Prot), resp. 71 (TrEMBL). Pokud byla hodnota skóre nižší, byla identita proteinů potvrzena MS/MS experimentem.

Proteinový profil leukemických buněk JURL-MK1 v apoptóze

V proteomickém projektu ve spolupráci s kolektivem laboratoře Buněčné biochemie na Ústavu hematologie a krevní transfúze v Praze byly pomocí 2DE a MS charakterizovány změny v proteomu lidských buněk chronické myeloidní leukémie

[2] MOWSE skóre (**MOlecular Weight SEarch)** je statistický údaj, který vyjadřuje správnost určení proteinu na základě změřené peptidové mapy a zadaných parametrů (databáze, organismus, proteasa, povolená chyba MS analýzy).

(JURL-MK1) v apoptóze vyvolané přídavkem léčiva Imatinib [publikace č. 5]. Za tuto formu leukémie je zodpovědný fúzní protein Bcl-Abl, který výrazně ovlivňuje signální dráhy od buněčné adheze až po změny v cytoskeletu, a způsobuje postupné hromadění zralých granulocytů v kostní dřeni a následně i v krvi. Jeden z účinných léčebných postupů je podávání léku obsahujícího imatinib-mesylát, který inhibuje funkce proteinu Bcl-Abl a iniciuje apoptózu leukemických buněk.

Porovnáním 2D elektroforegramů (pI 3-10) proteomu JURL-MK1 buněk před a po působení imatinib-mesylátu bylo vybráno 20 proteinových skvrn se změněnou kvantitou exprese. K jejich identifikaci bylo použito MALDI-TOF peptidové mapování po předchozím tryptickém štěpení proteinů. Tryptické mapy byly prohledány proti SwissProt databázi a u identifikací s MOWSE skóre nižším než 56 byly provedeny doplňující MS/MS experimenty jednoznačně potvrzující proteinové složení každého vzorku. Celkem bylo pomocí MALDI MS a MS/MS experimentů identifikováno 16 proteinů se změněným profilem po působení imatinib-mesylátu, včetně tropomyosinu-alfa, degradovaného F-aktinu nebo fosforylovaného kofilinu ukazující na narušení uspořádání cytoskeletu buněk v apoptóze.

Z výsledků dále vyplynulo, že v důsledku působení imatinib-mesylátu na JURL-MK1 buňky došlo ke **snížení exprese proteinů 14-3-3** (isoformy ε, ζ/δ, β/α), který se hojně účastní interakcí s pro-apoptickými signálními proteiny (Bad, Bax, FOXO). Zároveň byl na 2D gelu pozorován posun skupiny skrvn odpovídajících isoformám proteinu 14-3-3 k nižším molekulovým hmotnostem. Nalezení měnícího se profilu právě tohoto proteinu bylo pro naši skupinu zajímavým výsledkem, protože řešením struktury proteinu 14-3-3 metodami hmotnostní spektrometrie se také zabýváme (viz kap. 3.1.1, str. 31). Pomocí PMF mapování MALDI MS bylo v tomto případě **prokázáno štěpení isoformy theta na C-konci** v důsledku dějů spojených s apoptózou (Obrázek 15, str. 138). Pro zkrácenou formu proteinu 14-3-3ζ byla již dříve v literatuře popsána zvýšená vazba na pro-apoptické proteiny Raf-1 a Bad [Truong 2002]. **C-terminální štěpení a celkový úbytek proteinu 14-3-3 v apoptických buňkách** je pravděpodobně **přirozený důsledek programované buněčné smrti** [Kuželová 2009].

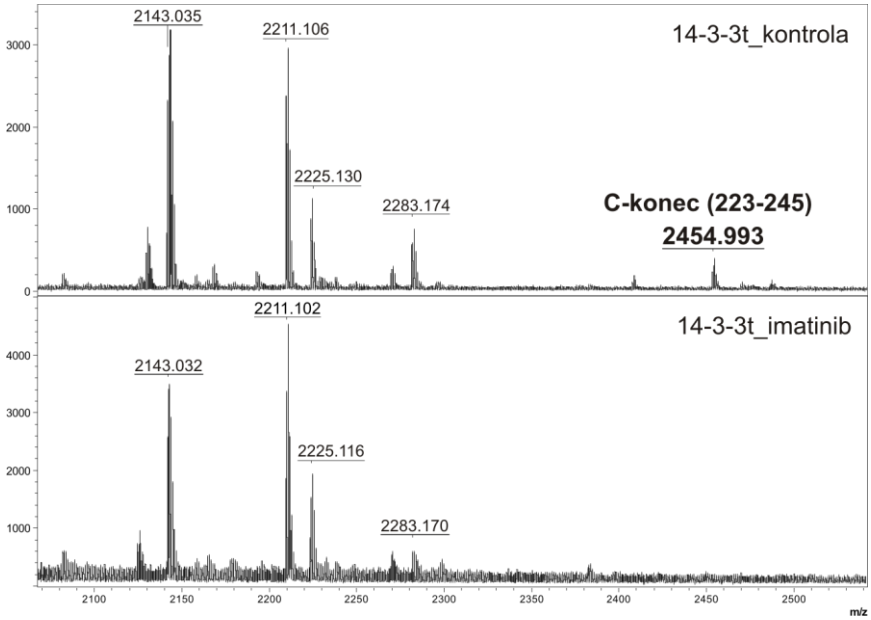

Obrázek 15. PMF MALDI MS spektra (*m/z* 2000 – 2600) proteinu 14-3-3τ v leukemických buňkách JURL-MK1 (A) před a (B) po přídavku imatinib-mesylátu dokazují štěpení tohoto proteinu na C-konci při apoptóze vyvolané přídavkem léčiva.

5. Závěry

Hmotnostní spektrometrie umožňuje studovat nejen primární strukturu proteinů, ale také terciární a kvartérní strukturu proteinových komplexů. Použitá metoda chemického síťování s následnou identifikací modifikovaných produktů pomocí hmotnostní spektrometrie s vysokým rozlišením přinesla důležité informace o interakcích flexibilních oblastí zkoumaných proteinových molekul. Metoda peptidového mapování a MS/MS experimenty umožňily získat unikátní proteinové profily houbových spór a charakterizovat změny v proteomech pšenice a lidských leukemických buněk. Dále byla popsána rychlá a spolehlivá metoda pro určování polohy dvojné vazby ve struktuře peptidů a lipidů pomocí techniky NALDI-TOF.

Ze souboru publikovaných původních prací vyjímám tyto zajímavé výsledky:

- Na proteinových interakcích na rozhraní samovolně vznikajícího dimeru lidského regulačního proteinu 14-3-3ζ se silně podílí zejména N-koncová aminoskupina z popsané N-koncové flexibilní části.
- Rozšířili jsme polohu vazebného místa cytochromu b_5 na proximální straně CYP2B4 a nalezli interakce, které jsou schopny objasnit přenos elektronu na CYP2B4 nebo strukturní modulaci aktivity CYP2B4.
- Sestavili jsme proteinové profily houbových spór 24 kmenů rodu *Aspergillus* a nalezli souvislosti s jejich fylogenezí a virulencí. U dvou zástupců rodu *Pseudallescheria* jsme identifikovali a následně charakterizovali skupinu specifických cyklických peptidů, které mohou být vhodnými diagnostickými znaky pro včasnou detekci závažných invazivních mykóz.
- Popsali jsme rychlou a jednoduchou metodu identifikace polohy dvojných vazeb ve struktuře peptidů nebo lipidů.
- Určili jsme zcela nové lidské alergeny v pšeničné mouce.
- Identifikovali jsme změny v proteomu lidských leukemických buněk JURL-MK1 v apoptóze vyvolané podáním léčiva imatinib-mesylátu, včetně měnícího se profilu a C-koncové fragmentace proteinů 14-3-3.

6. Seznam publikací

[1] Šulc M., **Pešlová K.**, Žabka M., Hajdúch M., Havlíček V.: *Biomarkers of Aspergillus Spores: Strain Typing and Protein Identification.* Int J Mass Spectrom. 280, 162-168 (2009) (IF 2.1)

[2] **Pavlásková K.**, Nedvěd J., Kuzma M., Žabka M., Šulc M., Sklenář J., Novák P., Benada O., Kofroňová O., Hajdúch M., Derrick P.J., Lemr K., Jegorov A., Havlíček V.: *Characterization of Pseudacyclins A-E, a Suite of Cyclic Peptides Produced by Pseudallescheria boydii.* J Nat Prod. 73(6), 1027-1032 (2010) (IF 3.2)

[3] **Pavlásková K.**, Strnadová M., Strohalm M., Havlíček V., Šulc M., Volný M.: *Time-dependent Oxidation during Nano-assisted Laser Desorption Ionization Mass Spectrometry: A Useful Tool for Structure Determination or a Source of Possible Confusion?* Anal Chem. 83(14), 5661-5665 (2011) (IF 5.8)

[4] Šotkovský P., Sklenář J., Halada P., Cinová J., Šetinová I., Kainarová A., Goliáš J., **Pavlásková K.**, Honzová S., Tučková L.: *A New Approach to the Isolation and Characterization of Wheat Flour Allergens.* Clin Exp Allergy. 41, 1031-1043 (2011) (IF 4.1)

[5] Kuželová K., Pluskalová M., Grebeňová D., **Pavlásková K.**, Halada P., Hrkal Z.: *Changes in Cell Adhesivity and Cytoskeleton-related Proteins During Imatinib-Induced Apoptosis of Leukemic JURL-MK1 Cells.* J Cell Biochem. 111(6), 1413-1425 (2010) (IF 2.9)

Manuskripty připravené k odeslání:

[6] **Pavlásková K.**, Mrázek H., Ječmen T., Halada P., Man P., Novák P., Obšil T., Šulc M.: The *Combination of Chemical Cross-linking and H/D Exchange with Mass Spectrometry: Mapping of Human 14-3-3zeta Homodimer Interaction.* (Biochem Biophys Res Commun.)

[7] Šulc M., **Pavlásková K.**, Ječmen T., Novák P., Martínek V., Stiborová M., Hudeček J., Hodek P.: *Mapping of Interaction between Two Membrane Proteins, Cytochrome b5 and P450 2B4 - Enlargement of P450 2B4 Binding Site for Cytochrome b5.* Arch Biochem Biophys. (odesláno do redakce dne 16.7.2011)

7. Použitá literatura

Aebersold R., Mann M.: Nature 422,198-207 (2003).

Aitken A., Baxter H., Dubois T., Clokie S., Mackie S., Mitchell K., Peden A., Zemlickova E.: Biochem Soc Trans. 30(4), 351-360 (2002).

Alexander B.D.: Transpl Infect Dis. 4, 32-37 (2002).

Altman R.B., Dugan J.M. – Defining Bioinformatics and Structural Bioinformatics, v knize Structural Bioinformatics (Bourne P.E., Weissig H. ed.), John Willey and Sons, Inc., New Jersey, str. 3-14 (2003).

Anzenbacher P., Šípal Z., Hodek P.: Biomed Biochim Acta. 43(12), 1343-1349 (1984).

Back J.W., de Jong L., Muijsers A.O., de Koster Ch.G.: J Mol Biol. 331, 303-313 (2003).

Boháč M., Ingendoh A., Fuchser J., Witt M.: Chem Listy 99, 943-951 (2005).

Bridges A., Gruenke L., Chang Y.-T., Vakser I.A., Loew G., Waskell L.: J Biol Chem. 273(27), 17036-17049 (1998).

Cardoso J.C., Serra D., Cardoso R., Reis J.P., Tellechea O., Figueiredo A.: Dermatology Online Journal 15(10),8 (2009).

Coblitz B., Wu M., Shikano S., Li M.: FEBS Lett. 580, 1531-13535 (2006).

Comisarow M.B., Marshall A.G.: Chemical Physics Letters 25, 282 (1974) citováno z http://www.chm.bris.ac.uk/ms/theory/fticr:massspec.html

Coon M.J., Ding X., Pernecky S.J., Vaz A.D.N.: FASEB J. 6, 669-673 (1992).

Daniels R.H., Dikler S., Li E., Stacey C.: J Assoc Lab Automation 13, 314 (2008).

Dass Ch.: Modes of Ionization, v knize Fundamentals of contemporary mass spectrometry, vydalo nakl. John Wiley & Sons, Inc., str. 15-65 (2007a).

Dass Ch.: Mass Analysis and Ion Detection, v knize Fundamentals of contemporary mass spectrometry, vydalo nakl. John Wiley & Sons, Inc., str. 67-117 (2007b).

Dass Ch.: Proteins and Peptides: Structure Determination, v knize Fundamentals of contemporary mass spectrometry, vydalo nakl. John Wiley & Sons, Inc., str. 289-342 (2007c).

Dihazi G.H., Sinz A.: Rapid Commun Mass Spectrom. 17(17), 2005-2014 (2003).

Donnelly J.P.: Clin Infect Dis. 42, 487-789 (2006).

Dunkley P.R., Bobrovskaya L., Graham M.E., Nagi-Felsobuky E.I., Dickson P.W.: J Neurochem. 91, 1025-1043 (2004).

Fenn J.B., Mann M., Meng C.K., Wong S.F., Whitehouse C.M.: Science 246(4926), 64-71 (1989).

Fuller B., Stevens S.M.Jr., Sehnke P.C., Ferl R.J.: Proteomics. 6(10), 3050-3059 (2006).

Gao Q., Deneanu C.E., Shaffer S.A., Asman E.T., Goodlett D.R., Nelson S.D.: J Biol Chem. 281(29), 20404-20417 (2006).

Goodwill K.E., Sabatier Ch., Stevens R.C.: Biochemistry 37, 13437-13445 (1998).

Graves P.R., Haystead T.A.: Microbiol Mol Biol Rev. 66(1), 39-63 (2002).

Henriksson M.L., Francis M.S., Peden A., Aili M., Stefansson K., Palmer R., Aitken A., Hallberg B.: Eur J Biochem. 269, 4921-4929 (2002).

Hermanson G.T.: Functional Targets, v knize Bioconjugate techniques, 2. vydání, vydalo nakl. Elsevier , str. 3-167 (2005).

Hernandez H., Robinson C.V.: J Biol Chem. 276(50), 46685-46688 (2001).

Ichimura T., Isobe T., Okuyama T., Takahashi N., Araki K., Kuwano R., Takahashi Y.: Proc Natl Acad Sci. USA 85, 7084-7088 (1988).

Im S.-C., Waskell L.: Arch Biochem Biophys. 507, 144-153 (2011).

Jinno H., Tanaka-Kagawa T., Ohno A., Makino Y., Matsushima E., Hanioka N., Ando M.: Drug Metab Dispos. 31(4), 398-403 (2003).

Karas M., Hillenkamp F.: Anal Chem. 60, 2299-2301 (1988).

Kleppe R., Toska K., Haavik J.: J Neurochem. 77(4), 1097-1107 (2001).

Kocher T., Superti-Furga G.: Nature Methods 4(10), 807-815 (2007).

Kuželová K., Grebeňová D., Pluskalová M., Kavan D., Halada P., Hrkal Z.: J Cell Biochem. 106, 673-681 (2009).

Kuželová K., Pluskalová M., Grebeňova D., Pavlásková K., Halada P., Hrkal Z.: J Cell Biochem. 111(6), 1413-1425 (2010).

Leitner A., Walzthoeni T., Kahraman A., Herzog F., Rinner O., Beck M., Aebersold R.: Mol Cell Proteomics 9(8), 1634-1649 (2010).

Lin S.J., Schranz J., Teutsch S.M.: Clin Infect Dis. 32, 358-366 (2001).

Liu D., Bienkowska J., Petosa C., Collier R.J., Fu H., Liddington R.: Nature 376(6536), 191-194 (1995).

Mackie S., Aitken A.: FEBS J. 272(16), 4202-4210 (2005).

Molday R.S., Englander S.W., Kallen R.G.: Biochem. 11(2), 150-158 (1972).

Muslin A.J., Xing H.: Cellular Signalling 12, 703-709 (2000).

Nelson D.R., Strobel H.W.: Mol Biol Evol. 4, 572-593 (1987).

Nelson D.R.: Methods Mol Biol.320, 1-10 (2006).

Novák P., Young M.M., Schoeninger J.S., Kruppa G.H.: Eur J Mass Spectrom. 9, 623-631 (2003).

Novák P., Giannakopulos A.E.: Eur J Mass Spectrom. 13, 105-113 (2007).

O'Brian T.A.: Anti Infect Ther Medsurg Nurs. 3, 765-73 (2005).

Obšil T., Ghirlando R., Klein D.C., Ganguly S., Dyda F.: Cell 105, 257-267 (2001).

Obšilová V., Nedbálková E., Šilhán J., Bouřa E., Herman P., Večer J., Šulc M., Teisinger J., Dyda F., Obšil T.: Biochem. 47, 1768-1777 (2008).

Obšilová V., Šilhán J., Bouřa E., Teisinger J., Obšil T.: Physiol Res. 57, S11-S21 (2008).

Pavlásková K., Nedvěd J., Kuzma M., Žabka M., Šulc M., Sklenář J., Novák P., Benada O., Kofroňová O., Hajdúch M., Derrick P.J., Lemr K., Jegorov A., Havlíček V.: J Nat Prod. 73, 1027-1032 (2010).

Pavlásková K, Strnadová M, Strohalm M, Havlíček V, Šulc M, Volný M. : Anal Chem. 83(14), 5661-5665 (2011).

Petosa C., Masters S.C., Bankston L.A., Pohl J., Wang B., Fu H., Liddington R.C.: J Biol Chem. 273, 16305-16310 (1998).

Porter T.D., Coon M.J.: J Biol Chem. 266, 13469-13472 (1991).

Powell D.W., Rane M.J., Joughin B.A., Kalmukova R., Hong J.-H., Tidor B., Dean W.L., Pierce W.M., Klein J.B., Yaffe M.B., McLeish K.R.: Mol Cell Biol. 23(15), 5376-5387 (2003).

Rittinger K., Budman J., Xu J., Volinia S., Cantley L.C., Smerdon S.J., Gamblin S.J., Yaffe M.B.: Mol Cell 4(2), 153-166 (1999).

Santos A.L., Bittencourt V.C., Pinto M.R., Silve B.A., Barreto-Bergter E.: Med Mycol. 47(4), 375-386 (2009).

Sedláček P.: Ambulantná terapia 2, 92-97 (2008).

Schenkman J.B., Jansson I.: Pharmacol Ther. 97, 139-152 (2003).

Singh P., Panchaud A., Goodlett D.R.: Anal Chem. 92, 2636-2642 (2010).

Sinz A.: Mass Spec Rev. 25, 663-682 (2006).

Sinz A.: Chemical Cross-Linking and Mass Spectrometry for Investigation of Protein–Protein Interactions, v knize Mass Spectrometry of Protein Interactions, editor K. Downard, vydalo nakl. John Wiley & Sons (2007).

Stiborová M., Hudeček J., Hodek P., Frei E.: Chem. Listy 93, 229-237 (1999).

Stiborová M., Hudeček J., Páca J. jr., Martínek V., Páca J.: Chem. Listy 98, 876-890 (2004).

Stiborová M., Martínek V., Schmeiser H.H., Frei E.: Neuro Endocrinol Lett. 27(2), 35-39 (2006).

Šilhan J., Obšilová V., Večer J., Herman P., Šulc M., Teisinger J., Obšil T.: J Biol Chem. 279(47), 49113-49119 (2004).

Šotkovský P., Sklenář J., Halada P., Cinová J., Šetinová I., Kainarová A., Goliáš J., Pavlásková K., Honzová S., Tučková L.: Clin Exp Allergy. 41,1031-1043 (2011).

Šulc M., Kubíčková B., Máslová V., Hodek P.: Gen Physiol Biophys. 23, 423-433 (2004).

Šulc M., Hudeček J., Stiborová M., Hodek P.: Neuro Endocrinol Lett. 29, 722-7 (2008).

Šulc M., Pešlová K., Žabka M., Hajdúch M., Havlíček V.: Int J Mass Spectrom. 280, 162-168 (2009).

Šulc M., Hodek P., Stiborová M.: Gen Physiol Biophys. 29, 175-85 (2010).

Tanaka K., Waki H., Ido Y., Akita S., Yoshida Y., Yoshida T.: Rapid Commun Mass Spectrom. 2, 151 (1988).

Thornton C.R.: Clin Vac Immunol. 16,756-764 (2009).

Truong A.B., Masters S.C., Yang H., Fu H.: Proteins 49, 321-325 (2002).

Tzivion G., Avruch J.: J Biol Chem. 277, 3061-3064 (2002).

Vidová V., Novák P., Strohalm M., Pól J., Havlíček V., Volný M.: Anal Chem. 82(12), 4994-4997 (2010).

Walsh T.J., Groll A.H.: Curr Opin Investig Drugs 2, 1366-1367 (2001).

Walsh T.J., Anaissie E.J., Denning D.W., Herbrecht R., Kontoyiannis D.P., Marr K.A., Morrison V.A., Segal B.H., Steinbach W.J., Stevens D.A., van Burik J.-A., Wingard J.R., Patterson T.F.: Clin Infect Dis. 46(3), 327-360 (2008).

Weiss D.D., Kaveti S., Wu Y., Engen J.R.: Probing Protein Interactions Using Hydrogen–Deuterium Exchange Mass Spectrometry, v knize Mass Spectrometry of Protein Interactions, editor K. Downard, vydalo nakl. John Wiley & Sons (2007).

Whitehouse C.M., Dreyer R.N., Yamashita M., Fenn J.B.: Anal Chem. 57, 675-679 (1985).

Wilderman P.R., Shah M.B., Liu T., Li S., Hsu S., Roberts A.G., Goodlett D.R., Zhang Q., Woods V.L. Jr., Stout C.D., Halpert J.R.: J Biol Chem 285(49), 38602-38611 (2010).

Wilker E., Yaffe M.B.: J Mol Cell Cardiol. 37, 633-42 (2004).

Woodcock J.M., Murphy J., Stomski F.C., Berndt M.C., Lopez A.F.: J Biol Chem. 278, 36323-36327 (2003).

Yang X., Lee W.H., Sobott F., Papagrigoriou E., Robinson C.V., Grossmann J.G., Sunstrom M., Doyle D.A., Elkins J.M.: Proc Natl Acad Sci U S A. 103(46), 17237-17242 (2006)

Young M.M., Tang N., Hempel J.C., Oshiro C.M., Taylor E.W., Kuntz I.D., Gibson B.W., Dollinger G.: Proc Natl Acad Sci USA. 97(11), 5802-5806 (2000).

Zhang H., Gruenke L., Arscott D., Shen A., Kasper Ch., Harris D.L., Glavanovich M., Johnson R., Waskell L.: Biochemistry 42(40), 11594-11603 (2003).

Zhang H., Myshkin E., Waskell L.: Biochem Biophys Res Commun. 338, 499-506 (2005).

Zhang H., Im S.-C., Waskell L.: J Biol Chem. 282(41), 29766-29776 (2007).